

PROPAGATION MEASUREMENT BASED STUDY ON RELAY NETWORKS

M. Sc. Aihua Hong

Dissertation zur Erlangung des
akademischen Grades Doktor-Ingenieur (Dr.-Ing.)

Anfertigung im:	Fachgebiet Elektronische Messtechnik Institut für Informationstechnik Fakultät für Elektrotechnik und Informationstechnik
Gutachter:	Prof. Dr.-Ing. habil. Reiner S. Thomä (TU-Ilmenau) Prof. Dr.-Ing. Wolfgang Koch (Universität Erlangen-Nürnberg) Dr.-Ing. Egon Schulz (Huawei Technologies Duesseldorf GmbH)
Vorgelegt am:	31.03.2010
Verteidigt am:	16.12.2010

ABSTRACT

Considering technological bases of next generation wireless systems, it is expected that systems can provide a variety of coverage requirements to support ubiquitous communications. To satisfy the requirements, an innovative idea, integrating network elements with a relaying capability into cellular networks, is one of the most promising solutions.

The main topic of this dissertation is a propagation measurement based study on relay networks. The study includes three parts: channel modeling, performance evaluation, and verification. First of all, an empirical channel model for relay networks is proposed based on statistical analyses of measurement data. Then, advanced techniques for the throughput improvement and interference cancellation are proposed for Multiple Access Relay Networks (MARN) which are used as an example of relay networks. The performance of the considered MARN is evaluated for Rayleigh channels, and then verified for realistic channels, obtained from measurement data and from the experimental relay channel model as well.

For relay channel modeling, the long-term correlation properties between links are of crucial importance due to the meshed-network topology. Although, there is a wide variety of research results for Multiple-Input Multiple-Output (MIMO) channel modeling available, the characterization of correlation properties has been significantly simplified or even completely ignored which motivates this research to be performed. In this dissertation, the experimental results of the correlation properties of Large Scale Parameters (LSP) are presented through the analysis on the real-field measurement data for both the urban and indoor scenarios. Furthermore, the correlation properties have been fully introduced into the WINNER channel Model (WIM) for realistic relay channel simulations.

As a further contribution of this dissertation, various advanced techniques are proposed for MARN in the presence of Unknown Interference (UKIF). Multiple Access Coding (MAC) is introduced as a multiple access technique. The use of MAC provides the signal separability at the receiver and improves throughput. Thereafter, high system resource efficiency can be achieved through relay protocol design. At the receiver, Minimum Mean Square Error (MMSE)-based spatial filtering is used to suppress UKIF while preserving multiple Mobile Station (MS)s' MAC-encoded signal structure. Furthermore, an error detection aided signal selection technique is proposed for diversity increasing.

The theoretical system performance with aforementioned techniques is simulated for Rayleigh channels. Thereafter, realistic channels are exploited for the performance verification. The gap between the theoretical performance and the realistic performance indicates that the assumptions made to the simplified Rayleigh-channels do not fully hold in reality.

For the future relay system design, this work provides valuable information about the performance evaluation of relay networks in consideration of the correlation properties between links.

KURZFASSUNG

Von der nächsten Generation von Mobilfunksystemen erwartet man eine umfassende Versorgung mit breitbandigen Multimediadiensten. Um die dafür erforderliche flächendeckende Versorgung mit hohen Datenraten zu gewährleisten, können Relay-Netzwerke einen wesentlichen Beitrag liefern. Hierbei werden Netzwerkstationen mit Relay-Funktionalität in zellulare Netzwerke integriert.

Diese Dissertation befasst sich mit der Untersuchung Relay-basierter Netzwerke unter Verwendung von Ausbreitungsmessungen. Die Arbeit deckt Fragen zur Kanalmodellierung, Systemevaluierung bis hin zur Systemverifikation ab. - Zunächst wird ein auf Funkkanalmessungen beruhendes experimentelles Kanalmodell für Relay-Netzwerke vorgestellt. Im Weiteren werden technische Verfahren für *Mehrfachzugriffs-Relay-Netzwerke* MARN diskutiert. Die erreichbare Systemleistung wurde unter Verwendung von Rayleigh-Kanälen innerhalb einer Systemsimulation bestimmt und im Anschluss mit realen Kanälen, die sowohl direkt aus Funkkanalmessungen als auch indirekt aus dem bereits erwähnten Kanalmodell abgeleitet wurden, verifiziert.

Bisherige Arbeiten zur Modellierung breitbandiger Multiple-Input Multiple-Output (MIMO) Kanäle berücksichtigen nicht oder nur sehr stark vereinfacht die Langzeitkorrelationseigenschaften zwischen den Links und werden damit der vermaschten und räumlich weit verteilten Topologie von Relay-Netzwerken gerecht. In der vorliegenden Dissertation erfolgte daher eine experimentelle Untersuchung zu den Korrelationseigenschaften von *Large-Scale-Parametern* LSP, die unter Verwendung von Funkkanalmessdaten aus urbanen Umgebungen und aus Innenräumen abgeleitet wurden. Die Ergebnisse hierzu fanden Eingang in das vom WINNER-Projekt entwickelte Kanalmodell. Sie erlauben damit eine realistischere Simulation von Relay-unterstützten Netzen.

Einen weiteren Schwerpunkt dieser Arbeit stellen technische Verfahren dar, die eine Erhöhung der Systemleistung in MARN mit *unbekannter Interferenz* UKIF versprechen. Im Einzelnen handelt es sich um die *Mehrfachzugriffs-Kodierung* MAC - die eine verbesserte Signaltrennung auf der Empfängerseite und eine Erhöhung des Datendurchsatzes erlaubt, den Entwurf eines Relay-Protokolls zur Erhöhung der Systemeffizienz, einen Minimum Mean Square Error (MMSE) Algorithmus zur Unterdrückung unbekannter Interferenzen bei Erhaltung der MAC-Signalstruktur mehrerer *Mobilstationen* MS, und ein fehlererkennungsbasiertes Signalauswahlverfahren zur Diversitätserhöhung.

Die vorgenannten Verfahren werden in einer Systemsimulation zunächst mit Rayleigh-Kanälen evaluiert und demonstrieren die erzielbare theoretische Leistungssteigerung. Die Berücksichtigung realer Funkkanäle innerhalb der Systemsimulation zeigt allerdings, dass die theoretische Systemleistung so in der Realität nicht erreichbar ist. Die Ursache hierfür ist in den idealisierten Annahmen theoretischer Kanäle zu suchen.

Für die Entwicklung künftiger Relay-Netzwerke bieten die in dieser Arbeit aufbereiteten Erkenntnisse hinsichtlich der Langzeitkorrelationseigenschaften zwischen den Links einen wertvollen Beitrag für die Abschätzung ihrer Systemleistung auf der Basis eines verbesserten Kanalmodells.

ACKNOWLEDGMENTS

The valuable discussion with various people has made this dissertation to be completed. First, I want to thank Prof. Dr.-Ing. Reiner S. Thomä, the leader of my lab, for his continuous support and encouragement, both as a supervisor and as a colleague. Further, I want to thank all the colleagues in the lab, Elektronische Messtechnik at Technische Universität Ilmenau, among whom I would like to mention especially Gerd Sommerkorn, Milan Narandžić, Dr. Wim Kotterman, and Marcus Grossmann who helped me both in practical matters, such as preparing, organizing, and performing measurement campaign, and in scientific matters, such as discussion on theoretical stuff.

I am deeply indebted to Prof. Tad Matsumoto from University of Oulu, Finland, not only for fruitful technical discussion, but also for all kinds of support and encouragement in the work. During his stay at Technische Universität Ilmenau and my stay at center for wireless communication of University of Oulu, Finland, many new ideas have been stimulated and the interesting results have been published.

This work has been partially sponsored by the radio system technology department of Nokia-Siemens Networks GmbH & Co. KG in Munich, Germany. My special appreciation is given to Dipl. Wolfgang Zirwas from this department for the valuable discussion and his reviewing of my work.

Furthermore, I would like to thank Prof. Dr.-Ing. Wolfgang Koch from Universität Erlangen-Nürnberg and Dr. Egon Schulz from Huawei Technologies Duesseldorf GmbH for reviewing my thesis.

I also would like to thank Markus Landmann, Giovanni Del Galdo and Jörg Lotze for many useful tips in terms of applying L^AT_EX to write this thesis.

My deepest gratitude goes indeed to my husband, Jian Shen, who always encouraged me to finish my thesis, and to my son, Yuchen Leon Shen, who opens a new chapter in my life.

Finally, I would like to thank all my friends who are a very important part of my life.

CONTENTS

Title	i
Abstract	iii
Kurzfassung	v
Acknowledgments	vii
Contents	ix
List of Figures	xiii
List of Tables	xvii
1. Introduction	1
1.1 Problem statement	4
1.2 Contributions and overview	5
1.2.1 Main contributions	5
1.2.2 Overview	6
2. Channel modeling methodology of relay networks	9
2.1 Background and own contributions	9
2.1.1 Background and state-of-the-art	9
2.1.2 Own contributions	12
2.2 Channel modeling process	12
2.3 MIMO channel modeling approaches	13
2.4 Channel modeling process for relay networks	16
2.4.1 System requirements	16
2.4.2 Comparison among the state-of-the-art MIMO channel models	17
2.4.3 Modeling goals	19
2.5 The definition of Large Scale Parameters (LSP) and their correlation properties	21
2.6 Usage of the correlation models of LSP	28
3. Experimental channel evaluation and modeling	35
3.1 Background and own contributions	35
3.1.1 Background and state-of-the-art	35
3.1.2 Own contributions	36

3.2	Propagation scenarios	37
3.2.1	Urban scenarios	37
3.2.1.1	U1 scenario: urban micro-cell	37
3.2.1.2	U2 scenario: urban macro-cell	37
3.2.2	Indoor scenarios	38
3.2.2.1	I1 scenario: indoor corridor	38
3.3	Relay measurement campaigns	38
3.3.1	Broadband radio channel sounding: technique and equipment	38
3.3.2	Micro-cell to macro-cell urban scenario: U1 and U2	39
3.3.3	Indoor corridor scenario: I1	40
3.4	Extraction procedure of LSP and their correlation properties	43
3.4.1	Extraction procedure of the LSP values	43
3.4.2	Extraction algorithms of the LSP values	46
3.4.3	The impact of the setting parameters on the LSP values	48
3.4.3.1	Different noise cut levels	48
3.4.3.2	Different lengths of a Space Time (ST) averaging window and different overlapping ratios	49
3.4.4	Extraction methodology of the correlation models of LSP	50
3.5	Experimental results	53
3.5.1	Micro-cell to macro-cell urban scenarios (U1 and U2)	54
3.5.1.1	Statistical distribution of LSP	54
3.5.1.2	The intra-site correlation of the transformed LSP	56
3.5.1.3	The inter-sector correlation of the transformed LSP	60
3.5.1.4	The inter-site correlation of the transformed LSP	60
3.5.2	Indoor corridor scenario I1	62
3.5.2.1	Statistical distribution of LSP	62
3.5.2.2	The intra-site correlation of the transformed LSP	62
3.5.2.3	The inter-sector correlation of the transformed LSP	64
3.5.2.4	The inter-site correlation of the transformed LSP	65
3.5.3	Main findings	66
4.	System structure of cooperative Multiple Access Relay Networks (MARN)	71
4.1	Background and own contributions	71
4.1.1	Background and state-of-the-art	71
4.1.2	Own contributions	75
4.1.3	Simulation assumptions	76
4.2	System model of MARN	77
4.3	Forwarding strategies	79
4.3.1	The Amplify-and-Forward (AF) strategy	80
4.3.2	The Decode-and-Forward (DF) strategy	81
4.4	Proposed protocols	82
4.4.1	Relaying protocol design	83

4.4.1.1	Direct transmission without relaying	83
4.4.1.2	Always relaying protocol	83
4.4.1.3	Adaptive relaying protocol with limited feedback	83
4.4.2	Multiple Access Coding (MAC)	84
4.4.3	Symbol-wise super-positioning	86
4.4.4	Re-transmission at the second time-slot	87
4.5	MMSE detection	88
4.5.1	JU MMSE detection	88
4.5.1.1	JU MMSE \mathcal{A} -criterion	88
4.5.1.2	JU MMSE \mathbf{H} -criterion	89
4.5.2	ML detection	90
4.5.3	Error detection aided signal selection	90
4.6	Numerical simulation results of an example scenario	91
4.6.1	MAC for the direct transmission	91
4.6.2	JU MMSE for the interference cancellation	92
4.6.3	The functionality of the RS: the AF relay and the DF relay	93
4.6.4	Error detection aided signal selection	96
4.6.5	Relay protocol with limited feedback	96
5.	Performance verification of cooperative MARN	99
5.1	Background and own contributions	100
5.1.1	Background and state-of-the-art	100
5.1.2	Own contributions	102
5.2	Simulation channels	103
5.2.1	Relay measurement campaign	103
5.2.2	Application of raw measurement data for the performance evaluation	104
5.2.3	Application of the relay channel model for the performance evaluation	106
5.2.4	Simulation scenarios and parameters	108
5.3	Measurement data based performance verification	108
5.3.1	Impacts of the small scale propagation phenomena	109
5.3.1.1	Small Scale Fading (SSF)	109
5.3.1.2	Influence of the antenna element spacing at the Base Station (BS)	111
5.3.2	Impacts of the large scale propagation phenomena	113
5.3.2.1	Large Scale Fading (LSF)	113
5.3.2.2	Path Loss (PL) plus LSF	114
5.3.2.3	Power allocation schemes	117
5.4	Relay channel model based performance verification	119
5.4.1	Positioning of the Relay Station (RS)	119
6.	Conclusions	121
Appendix A. Comparison among the state-of-the-art Multiple-Input Multiple-Output (MIMO) channel models		125

Appendix B. Examples of MAC	127
Appendix C. Solution of the Minimum Mean Square Error (MMSE) criterion	129
Appendix D. Glossary of operators, symbols, and acronyms	131
D.1 Mathematical operators	131
D.2 Acronym	131
D.3 List of frequently used symbols	133
Bibliography	139
Theses	149
Erklärung	151

LIST OF FIGURES

1.1	The relationship of the Signal-to-Noise Ratio (SNR) values between a direct link and a dual-hop relay link, assuming that they provide the same end-to-end Shannon capacity	2
1.2	a) A single-hop cell; b) A two-hop cell for coverage extension; c) A two-hop cell for capacity improvement; d) A two-hop cell for transmit power minimization	3
1.3	A two-hop cell for service provision in a shadowed area	3
1.4	The meshed structure of cluster-wise two-hop relay networks	4
2.1	Channel modeling process	13
2.2	The top-down modeling philosophy of the WINNER channel Model (WIM)	18
2.3	A link level channel modeling over a Local Stationary Area (LSA)	18
2.4	A system level channel modeling	19
2.5	Examples of the inter-site correlation	20
2.6	An example Power Delay Profile (PDP) and the corresponding channel parameters	22
2.7	PDP with a direct Line of Sight (LOS) path and the remaining Multipath Component (MPC)s	23
2.8	The intra-site auto-correlation	25
2.9	The inter-sector correlation	26
2.10	A hand over scenario	27
2.11	Received power difference (in [dB]) from two BSs with different PL exponents	27
2.12	Handover probability	28
2.13	Regeneration process and algorithms based on the correlation models of LSP	29
2.14	Geometric distribution of Mobile Station (MS)s and BSs	31
2.15	Distribution of the LSP values over the whole area with the inter-site correlation ρ_{BS} and the de-correlation distance d_{decorr} as parameters	33
3.1	MIMO channel sounder switching scheme	39
3.2	Antenna arrays used for a high resolution parameter estimation	40
3.3	Ilmenau downtown seen from the 16 [m] BS antenna array	40
3.4	Measurement routes in a 2-dimensional Ilmenau city map	41
3.5	Photos of the Helmholtzbau measurement environment	42
3.6	Measurement routes in the floor plan of the Helmholtzbau	43
3.7	Getting a Channel Transfer Function (CTF) from the raw data	44
3.8	The structure of measurement data (left) and the dimension of a CTF (right)	44
3.9	Snapshot groups over the whole measurement data	45

3.10	The extraction procedure of the LSP values	45
3.11	The first method to derive a PL model and the LSF values	47
3.12	The second method to derive the LSF values	48
3.13	Impact of a noise cut level on the Cumulative Distribution Function (cdf) curves of PL and Delay Spread (DS) in the LOS and None Line of Sight (NLOS) propagations	50
3.14	Impact of a ST averaging window on the cdf curves of PL and DS in the LOS and NLOS propagations	51
3.15	Impact of the overlapping ratio on the cdf curves of PL and DS in the LOS and NLOS propagations	52
3.16	Unified modeling and reproduction procedures	52
3.17	The cdf curves of LSP from the measurement data in the LOS and NLOS propagations with different BS heights	55
3.18	An example to show the transform process of K-factor: the original cdf distribution \rightarrow the transformed cdf distribution \rightarrow the modeled cdf distribution	56
3.19	An example to show the intra-site auto-correlation of the transformed LSF: the original intra-site auto-correlation \rightarrow model with an exponential decaying function with the de-correlation distance being 3.9 [m]	57
3.20	The intra-site auto-correlation of the transformed LSP in the U1 and U2 scenarios in the LOS and NLOS propagations	58
3.21	The dependence of the inter-site correlation of the transformed LSP on $\langle d_{diff}, \theta \rangle$ in the urban U1 and U2 scenarios	63
3.22	The dependence of the inter-site correlation of the transformed LSP on $\langle d_{diff}, \theta, d_{BS} \rangle$ in the I1 scenario	67
4.1	Relay network with various structures	73
4.2	The system structure with N blocked desired MSs having a single antenna, L Unknown Interference (UKIF) MSs having a single antenna, and one BS having n_{Rx} antenna elements.	77
4.3	Relay transmission in two phases	78
4.4	Flow-chart of the relay protocol with Automatic Repeat-reQuest (ARQ).	84
4.5	Achievable capacity region of a 2-MS access channel.	84
4.6	Transmission time schemes of a multiple access channel with/without a half-duplex relaying transmission	86
4.7	Receive structure at the BS with n_{Rx} antenna elements.	89
4.8	The Bit Error Rate (BER) and throughput performances of MAC with <i>a</i>) uncoded with $n_{Rx} = 1$ and $L = 0$, <i>b</i>) MAC-encoded with $n_{Rx} = 1$ and $L = 0$, and <i>c</i>) MAC-encoded with $n_{Rx} = 2$ and $L = 0$	92
4.9	The BER performances of MAC with H -criterion and A -criterion in the case of $n_{Rx} = 2$ and $L = 1$	93
4.10	The BER performances of MS1 and MS2 as well as MS3 with the AF relay and the DF relay	94
4.11	The BER performances of MS1 and MS2 as well as MS3 with the AF relay and the DF relay	95

4.12	The BER performance of MS1 and MS2 as well as MS3 with an error detection aided signal selection technique in the case of the AF relay (left) and the DF relay (right)	97
4.13	The BER performances of MS1 and MS2 (left) as well as MS3 (right) with the re-transmission technique	98
5.1	Relay measurement routes in a 2-dimensional Ilmenau city map	104
5.2	The cdf curves of SSF of the stationary BS-RS link with four polarization pairs	105
5.3	MS's normalized received powers from BS5/BS6/RS2 along route 1 and route 2	106
5.4	The cdf curves of SSF of the stationary BS-RS link based on the relay channel simulations if the RS is located in the middle of the BS and MSs	107
5.5	The cdf curves of the BER performances of MS1 and MS2 (left) as well as MS3 (right) under the assumption that $SNR_{sd} = 0$ [dB] while $SNR_{sr} = SNR_{rd} = 10$ [dB]	110
5.6	The cdf curves of the fading amplitude of the end-to-end channel of a tandem relay link	111
5.7	The cdf curves of the BER performances of MS1 and MS2 as well as MS3 based on the BS5's measurement data (left) and based on the BS6's measurement data (right) with different BS antenna element spacing under the assumption that $SNR_{sd} = 0$ [dB] while $SNR_{sr} = SNR_{rd} = 10$ [dB]	112
5.8	Dependence of the BER performances of MS1 and MS2 as well as MS3 on the LSF value along route 2	114
5.9	The cdf curves of SNR_{sr} and SNR_{sd} as well as SNR_{rd} along route 1 (left) and route 2 (right) based on the BS5's and BS6's measurement data	115
5.10	The cdf curves of the BER performances of MS1 and MS2 as well as MS3 along route 1(left) and route 2(right)	116
5.11	The BER performances of MS1 and MS2 (left) as well as MS3 (right) along route 2 based on the BS6 measurement data	117
5.12	The cdf curves of the BER performances of MS1 and MS2 (left) as well as MS3 (right) with different RS positioning schemes	119

LIST OF TABLES

2.1	Categories of MIMO channel modeling approaches	14
2.2	Hand-over parameter setup	27
3.1	Propagation scenarios for relay network applications	37
3.2	The key technical parameters of the MIMO channel sounder equipments	39
3.3	TU-Ilmenau relay measurement campaigns: U1, U2, and I1	42
3.4	The median value and the variance of the transformed LSP in the U1 and U2 scenarios in the LOS and NLOS propagations	57
3.5	The de-correlation distance of the transformed LSP in the U1 and U2 scenarios in the LOS and NLOS propagations	57
3.6	The intra-site cross-correlation of the transformed LSP in the U1 and U2 scenarios in the LOS and NLOS propagations	59
3.7	The inter-sector correlation of the transformed LSP in the U1 and U2 scenarios	60
3.8	The inter-site correlation of the transformed LSP in the urban U1 and U2 scenarios	61
3.9	The median value and the variance of the transformed LSP in the I1 scenario in the LOS and NLOS propagations	64
3.10	De-correlation distance of the transformed LSP in the I1 scenario in the LOS and NLOS propagations	64
3.11	The intra-site cross-correlation of the transformed LSP in the I1 scenario in the LOS and NLOS propagations	65
3.12	The inter-sector correlation of the transformed LSP in the I1 scenario	65
3.13	The inter-site correlation of the transformed LSP in the I1 scenario	66
4.1	Simulation parameters	91
5.1	Simulation parameters for performance verification	108
B.1	Examples of MAC for 4-MS case after computer searching.	127
B.2	Examples of MAC for 2-MS case and 3-MS case after computer searching.	128

1. INTRODUCTION

To satisfy rapid demands in providing a wide variety of wireless communications, it is of crucial important to support ubiquity in various service requirements such as data rate and coverage while utilizing the frequency spectrum as efficiently as possible. These requirements impose unprecedented challenges to wireless communication engineers who are mainly focusing on single-hop structured networks, both in cellular networks, such as Global System for Mobile Communications (GSM) and Universal Mobile Telecommunications System (UMTS), and in local networks like Wireless Local Area Networks (WLAN). In single-hop networks, a MS communicates directly with a BS or an Access Point (AP) ¹ [13]. This single-hop structure limits the network performance. First of all, with higher operation frequency, the coverage provided by a single BS is limited to the order of several hundred meters because of PL [14] [15] [16]. Furthermore, it happens very often that a transmit signal will be heavily attenuated due to shadowing because of relatively large obstacles like tall buildings, big trees or cars in outdoor scenarios, or like walls and floors in indoor scenarios. Due to these facts, ubiquitous coverage can be achieved by increasing the geographical density of BSs and/or by increasing the transmit power. However, the former solution is too costly (lease BS positions, cabling, and maintain BSs) to be accepted. The latter solution imposes increased system interference which in turn impairs the performance.

An innovative idea, integrating network elements with a relaying capability into conventional single-hop structured networks [17], is one of the most promising solutions. In relay-enabled networks, RSs are introduced into the communication between a BS and a MS having a weak link to the BS or even being blocked from the BS. The RSs receive first a signal from the BS and then forward the signal to the MS and vice versa [18]. Either BS or MS can play the roles of RS, depending on applications. Furthermore, the signal forwarding performed at a RS works in a half-duplex mode due to the self-interference. This indicates, a RS will not perform simultaneous receiving and transmitting at the same frequency/time/code/antenna due to the large difference between the incoming and outgoing signal power levels. Due to the half-duplex operation at a RS, the end-to-end capacity of a relay link is divided by the number of hops n_{hop} . It implies that the link capacity at each hop in relay networks should be at least n_{hop} times as large as the single-hop capacity so that the same end-to-end capacity can be achieved. Figure 1.1 shows the relationship of the SNR values between a direct link and a dual-hop relay link, assuming that they provide the same end-to-end Shannon capacity. The gap between the dashed curve and the solid curve defines the minimal SNR gain that a dual-hop relay link should provide over a direct link. A relay link outperforms a direct link in the area under the solid curve. Otherwise, a direct link is preferable.

Although the end-to-end capacity of a relay link is limited due to the half-duplex operation of a

¹ In this dissertation, there is no clear difference between a BS and an AP. The terminology BS is used throughout this dissertation standing for both BS and AP for the simplicity.

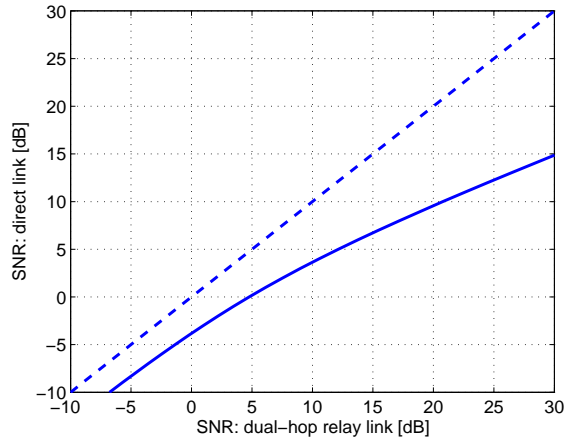


Fig. 1.1: The relationship of the SNR values between a direct link and a dual-hop relay link, assuming that they provide the same end-to-end Shannon capacity

RS, the performance of networks, comprising RSs with a relaying capability, can be improved in the following senses [19] [20].

1. Extend coverage

In future mobile communication systems, the coverage of a single BS becomes smaller due to the fact that a higher carrier frequency is expected to be allocated. As a trade off between providing wide spectrum of services in wide area and avoiding costly expenditure due to the deployment of huge amounts of BSs, RSs will be the most promising solution. At the coverage margin of a BS, several RSs can be deployed to extend the coverage of a single BS as shown in subplot b) in Fig. 1.2. Compared with a single-hop cell, the coverage of a two-hop cell becomes larger. The high link quality between the BS and the RS can be supported by using directional antenna with high antenna gain at the both sides. This type of RS application is especially efficient to the area where coverage is much more crucial than Quality of Services (QoS), for example, suburban and rural area with a low density of population.

2. Capacity improvement

When the coverage is not a crucial issue, the relay concept can be used to improve the system capacity or spectrum efficiency. In a cell, RSs may be deployed in a relatively nearby area around the BS as shown in subplot c) in Fig. 1.2. The coverage of a two-hop cell is as the same as that of a single-hop cell. However, the power distribution in the outer area between them is different. A two-hop cell has high power over the whole cell area. As a consequence, the cell capacity can be improved. Furthermore, the fairness between the MSs having different distance to the BS can be improved. In a single-hop cell, the MSs near to the BS can normally achieve better QoS than the MSs far from the BS due to the fact that the received power is normally decreased with an increasing distance between the MS and the BS. However, in a two-hop cell, MSs can still have a good QoS even in the case that they are not in the near field of a BS. This kind of RS application is especially attractive for the hot spot areas, such as campus and airport as well as center railway station.

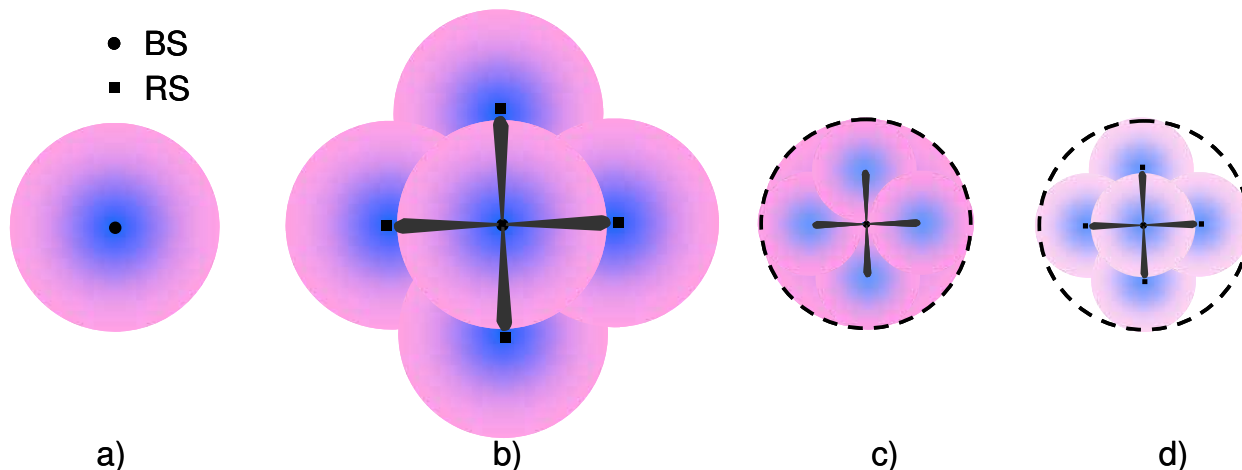


Fig. 1.2: a) A single-hop cell; b) A two-hop cell for coverage extension; c) A two-hop cell for capacity improvement; d) A two-hop cell for transmit power minimization

3. Transmit power reduction

When a system aims neither at coverage extension, nor at capacity increasing, a two-hop cell can be used to minimize the transmit power both at BSs and at MSs as shown in subplot d) in Fig. 1.2. The obvious consequences are, firstly, the life longevity of a battery at MSs will be larger; secondly, the system interference will be reduced.

4. Shadowing Mitigation

In several applications, the receive signal from a BS is significantly attenuated due to shadowing. The shadowed area could be covered by using RSs. In outdoor urban scenarios, for example, the coverage of a BS can be extended to the shadowed area if a RS is deployed around the street corner as shown in Fig. 1.3.

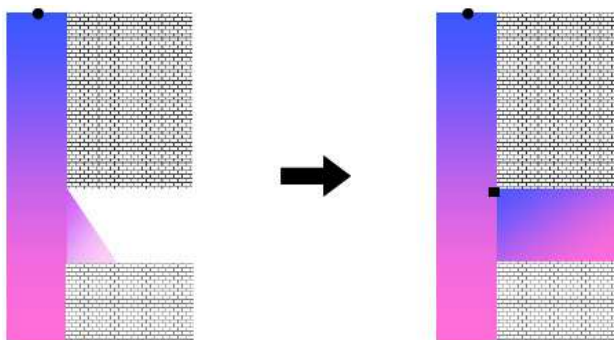


Fig. 1.3: A two-hop cell for service provision in a shadowed area

Furthermore, various advanced techniques, such as cooperative relaying [21] [22] [23] [24] [25] [26] and distributed MIMO [27] as well as bi-directional relaying [28], have been proposed in relay-enabled networks. Significant performance improvement has been observed. These advanced techniques benefit from the meshed network topology of relay-enabled networks which is different from

the star-topology of single-hop networks. Figure 1.4 shows an example of the meshed structure of cluster-wise two-hop relay networks. This system includes three clusters of stations, the BS cluster, the RS cluster, and the MS cluster. A meshed connection among clusters forms a distributed MIMO system even in the case that each station has a single antenna. In this distributed MIMO system, the number of transmit/receive antennas (n_{Tx}/n_{Rx}) is the sum of antennas of all stations within one cluster. The meshed multiple BS-RS-MS system has the potential to take maximum advantage from MIMO techniques [29] [30].

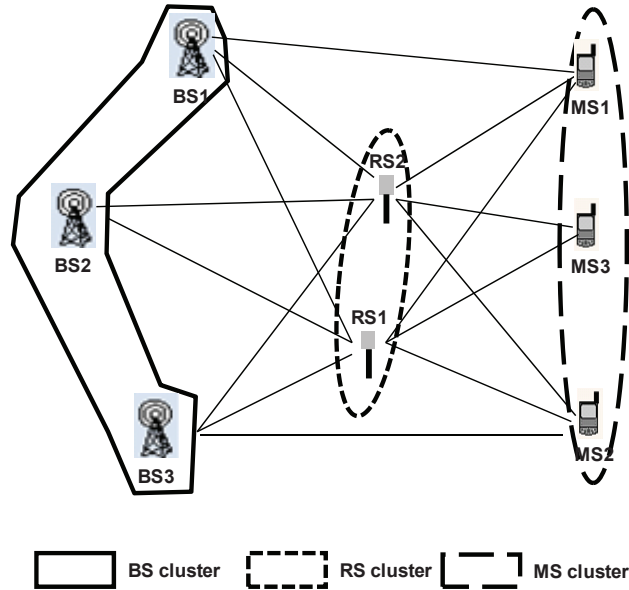


Fig. 1.4: The meshed structure of cluster-wise two-hop relay networks

1.1 Problem statement

In literature [21] [22] [23] [24] [25] [26] [27] [28], it has been stated that relay-enabled networks are one of the most promising techniques for the future wireless communication system design. The cooperative relay concept, based on the meshed network structure of relay-enabled networks, can further improve the system performance.

The performance of cooperative relay networks in a meshed link scenario will heavily depend on the correlation properties between meshed links. That does not only include the pure availability of the links. It will also include statistical space-time parameters and the interdependence of these parameters between different links of meshed relay networks as well as their temporal and spatial properties. However, majority of the current research activities about relay topic are based on analytical channel models [31] [32] [33] or existing channel models [34] [35] [36] [1]. Both the analytical channel models and majority of the existing channel models focus on describing the short-term/long-term wave propagation between two stations. An interesting observation from the literature is that the correlation properties between meshed links are either out of discussions or significantly simplified. Therefore, for the purpose of the accurate performance evaluation of relay networks, the current knowledge about the realistic broadband relay channels is rare and insuffi-

cient. Thus, it is necessary to study the relay channels and then provide the channel models which support more realistic relay network simulations than conventional very simple ones.

Due to the limited knowledge about relay channels, majority of the research works in the performance evaluation of relay networks have been performed under various simplified assumptions on the channel properties. These assumptions include for example, Rayleigh-distributed fading, an exponential PL model without LSF, and the independent channel fading between different distributed links. As a consequence, the simulation results are attractive but unrealistic. Therefore, in order to provide a realistic insight into the performance of future relay networks and to give valuable information to the future relay network deployment, the theoretical performance should be verified based on the realistic relay channels, either from real-field measurement campaigns directly or from the channel model supporting a relay structure.

These topics can be detailed in the following crucial questions:

1. What are the main challenges of the channel modeling for relay networks, comparing with the state-of-the-art channel models?
2. What are the key channel metrics for the relay channel modeling?
3. How can we obtain the experimental results for the relay channel modeling, based on measurement data?
4. What kind of techniques can be proposed to improve the system performance of MARN which are used as an example of relay networks?
5. What is the realistic performance of MARN, both based on measurement data and based on the relay channel model?

1.2 Contributions and overview

1.2.1 Main contributions

The main contributions of this dissertation can be summarized as follows. First of all, the correlation properties of LSP are highlighted as the most important channel metrics for the channel modeling for relay networks. Based on relay measurement campaigns, this dissertation provides the experimental results of these channel metrics and addresses the method of how to acquire the results. Furthermore, based on the WIM, an experimental relay channel model is proposed. Thereafter, various advanced techniques for the throughput improvement and interference cancellation are proposed to an example of relay structure: MARN. The achievable system performance with these techniques is evaluation over the simplified Rayleigh channel model and then verified through realistic channel realizations derived both from raw measurement data and from the aforementioned empirical relay channel model.

1.2.2 Overview

This subsection describes roughly the contributions of this dissertation chapter by chapter and how the dissertation is organized. A detailed description to the contributions of each chapter could be found at the beginning of each chapter.

Both Chapter 2 and Chapter 3 deal with the channel modeling for relay networks. Chapter 2 discusses the channel modeling methodology while Chapter 3 presents the experimental results for both urban and indoor scenarios through the analysis on the measurement data gathered from real-field measurement campaigns.

The author's contributions related to some of the topics of these two chapters have been published in [1] [2] [3] [4] [5] [6] [7] [8] [9].

Chapter 2 describes firstly the general channel modeling process and the MIMO channel modeling approaches. Thereafter, Chapter 2 specifies the channel modeling process of relay networks. In this process, at first, the system requirements of relay networks are analyzed. Then, the state-of-the-art MIMO channel models are compared, by which the WIM is selected as the initial channel model of relay networks. Thereafter, channel modeling goals for a full relay networks support are discussed based on the WIM framework. The main goal is modeling the correlation properties of LSP. At the end of this chapter, the method of how to reproduce relay channel realizations is presented, by using the correlation models of LSP.

Chapter 3 presents the experimental results of the correlation properties of LSP, by statistically analyzing the measurement data gathered from two scenarios: urban micro/macro scenarios and indoor scenario. The detailed information about the measurement campaigns and measurement scenarios is provided at the beginning of this chapter. Thereafter, the extraction procedure of the LSP values and their correlation properties is described. Whereby, the impact of the setting parameters on LSP is investigated. At the end of this chapter, experimental results are presented. The results include the statistical distribution of LSP, the intra-site correlation, the inter-sector correlation, and the inter-site correlation of LSP.

Chapter 4 studies the theoretical performance of MARN which are used as an example of relay networks. First of all, this chapter shows the general system model of MARN in the presence of UKIF. Two different forwarding strategies: an AF relaying and a DF relaying, have been under consideration. Based on this system model, advanced techniques, such as MAC [37], relay protocol design [25] [22], a symbol-wise super-positioning, and the Joint User (JU) MMSE algorithm [38] as well as an error detection aided signal selection technique [22] [39], are proposed for the further system performance improvement. Significant performance enhancement has been shown at the end of this chapter based on the numerical simulations, using the simplified Rayleigh channel model.

Own contributions related to some of the topics of this chapter have been published in [10] [11] [12].

The numerical results of MARN with the proposed advanced techniques have been highlighted in Chapter 4 based on the theoretical channels. However, these results are attractive but unrealistic. Therefore, the performance has been verified in Chapter 5 through realistic channel realizations extracted both from measurement data and from the experimental relay channel model. The method of how to get the realistic channels is described at the beginning of this chapter. Thereafter, for

the measurement data based performance verification, both the impacts of the small scale channel propagation phenomena and the impacts of the large scale propagation phenomena have been investigated. For the relay channel model based performance verification, different positionings of a RS have been studied.

Parts of the results in this chapter have been published in [10].

Finally, Chapter 5 summarizes this dissertation and gives an outlook to the future works.

2. CHANNEL MODELING METHODOLOGY OF RELAY NETWORKS

As discussed in Chapter 1, relay networks are distinguished from single-hop networks in the sense that they have intermediate RSs between a BS and a MS, by which the topology of relay networks becomes mesh-structured. With the mesh topology of relay networks, new technological problems have to be challenged in the channel modeling where the relationship between meshed links becomes to be one of the focus points. The current existing channel models [34] [35] [40] [36] [41] [42] concentrate on the modeling of single links. Even though for some of them it is stated that more sophisticated network structures like ad-hoc networks as well as relay networks are supported [41], the relationship between links is only partially modeled or unrealistically simplified. This chapter discusses comprehensively the requirements which are of crucial importance for the wideband MIMO relay channel modeling. According to these requirements, the most important channel metrics are highlighted, namely, the large scale correlation properties between links. The correlation includes both the intra-site correlation and the inter-site correlation. Furthermore, the methods, how to include the correlation properties of LSP in the whole channel modeling process, are discussed.

The outline of this chapter is as follows. First of all, Section 2.1 summarizes the state-of-the-art research in the channel modeling and summarizes the main contributions of this chapter. Then, Section 2.2 describes the general channel modeling process. Thereafter, various MIMO channel modeling methods are summarized in Section 2.3. In Section 2.4, the existing state-of-the-art channel models are compared and the WIM, which provides the best match to the system requirements of relay networks, is chosen as the initial channel model. Thereafter, three kinds of correlation properties between links are proposed in Section 2.5 as the most important channel metrics of relay networks. Section 2.6 shows the methods of how to include and reproduce these correlation properties.

2.1 Background and own contributions

2.1.1 Background and state-of-the-art

Channel analysis for modeling started at the most beginning for the narrowband channel signal transmission where only the time domain channel variation has been considered, for example, the Rayleigh-fading channel model, the Rice-fading channel model, the Nakagami-fading channel model, and the Suzuki-fading channel model [43] [31] [13].

In the middle of 1990s, the wideband frequency resource is envisaged to be licensed to satisfy the

rapid demand on wireless communications. Thus, channel modeling needed to be expanded to reflect more accurately the wideband channel behaviors including the channel properties both in the time and frequency domains.

At the end of 1990s, Foschini and Telatar published their results about the promising attractive MIMO capacity in [29] [30]. After the recognition of the importance of MIMO techniques, booming research activities have been shifted to MIMO systems. The intensive study on broadband MIMO channel models is one of the research areas where researchers focus on characterizing the MIMO propagation.

The broadband MIMO channel models have been investigated in many communities: 3Generation Partnership Project (GPP) [34], Institute of Electrical and Electronics Engineers (IEEE) [35], European Cooperation in the field of Scientific and Technical Research (COST) [40] [36], and the most recent Wireless World Initiative New Radio (WINNER) project [44]. The classification of MIMO channel modeling approaches is discussed in [45] [46]. Generally speaking, they include the stochastic channel modeling [35] and the deterministic channel modeling [47] [48].

Both approaches described above mainly focus on reproducing the short-term MIMO wave propagation between two stations in a LSA¹, namely a link level channel modeling [5]. The large scale properties, such as the variation of propagation channels along a MS's moving trajectory from a LSA to another neighboring LSA and the correlation between MS's propagation channels to BSs/RSs, are not explicitly included. This indicatively means, the system level channel properties are not a central point of discussions. In [50] the authors modeled the channels of relay networks as a simple interconnection of intermediate links, again without considering the large scale properties. However, for relay networks, the large scale propagation properties are very important. It has been stressed in [51] [52] [39] [22] [53] that the performance of relay networks can be significantly improved by various advanced algorithms, such as cooperative relaying as well as virtual antenna arrays. These algorithms investigated in the literatures rely on both the availability of links and their large scale properties.

To characterize the large scale behaviors of propagation channels, two correlation metrics; the intra-site auto- and cross-correlation and the inter-site correlation, are introduced. By introducing those correlation metrics, system level channel properties can be characterized. Furthermore, networks with a more sophisticated layout, such as relay networks, can be simulated. The intra-site auto- and cross-correlation models enable it to simulate single-cell multi-user applications as well as single-cell ad-hoc networks while the inter-site correlation enables multi-cell simulation like relay networks as well as Service Area (SA) [54]. Using the classical three-station structured relay networks [51] [52] [55] as an example, the intra-site auto- and cross-correlation can describe the similarity between the S-D² link and the S-R link while the inter-site correlation captures the correlation between the S-D link and the R-D link.

In [56] [57], Fraile showed already the impacts of the intra-site auto-correlation properties of LSF on the system performances. It proves that the system-level performances in terms of throughput

¹ The terminology LSA [49] is defined as the area where a channel can be regarded as wide-sense stationary. LSA is similar with the terminology *segment* in the WIM [1], *drop* in the 3GPP SCM [34].

² S-R-D stands for the relay channel in three-station structured relay networks, namely, S-R stands for the channel between the source and the RS, S-D the channel between the source and the destination, R-D the channel between the RS and the destination. The source is one from the MS and the BS, depending on the down-link or up-link transmission.

and Block Error Rate (BLER) are sensitive to the intra-site auto-correlation model of LSF. Furthermore, the importance of the inter-site correlation has been discussed in literature [58] [59] [60] [61] [62] [63] where it has been observed that the inter-site correlation plays a key role in system design like interference management, radio resource allocation, hand-over algorithm, power-control algorithm, cooperative process, and macro-diversity management. The recognition of the importance of these correlation properties pushes the research activities towards channel modeling. The experimental results of the intra-site correlation, based on measurement data, have been shown in [64] [65] [5] [66] [67] in various propagation scenarios. The intra-site cross-correlation were considered already in the WIM [1] [5] and in the 3GPP Spatial Channel Model (SCM) [34]. As an extension to the SCM [34], the WIM included the intra-site auto-correlation in the final deliverable [1] and in the channel simulation software [44]. Compared with the fruitful results of the intra-site analysis, the study to the inter-site correlation is countable. The representative literature about the inter-site correlation is [68] [69] [70] [71] [72]. All of them limit their study to the inter-site correlation of LSF in the macro-cell scenario except [73] due to the following facts:

- In first generation wireless communication systems SNR is the single key indicator when access the system performances. As shown in Eqn. 2.9, SNR is only decided by LSF with a defined PL model, a fixed transmit power, and a fixed transmit and receive antenna gain. This is the reason why LSF is the single LSP which was considered in the modeling of the inter-site correlation.
- Outdoor macro-cell systems with a high-elevated BS antenna were the most interesting application at the beginning of mobile communication since a large area can be covered with a single BS. This is the reason why only macro-cell scenarios were considered in the modeling of the inter-site correlation.
- The measurement equipment used in designing our legacy systems was limited in identifying the parameters related to the inter-site correlation modeling. Majority of the measurement campaigns performed for the purpose of the inter-site correlation modeling were for narrowband measurements. Thus, none of the channel properties in the delay domain can be captured. Furthermore, high resolution antenna arrays are not applied, either. Therefore, it is impossible to get sufficient channel information in the delay and spatial domains.

In [73], the authors considered the inter-site correlation of Angular Spread (AS) and investigated the inter-site correlation properties in indoor scenarios. Regardless of these research activities in the inter-site correlation, a fixed inter-site correlation of LSF, which is typically 0.5, was considered in the simulation studies in [74] and in the 3GPP channel modeling as well [34]. In fact, this value is estimated from a few limited measurements and therefore it may not be useful in the general case. The WIM has investigated the inter-site correlation model theoretically. However, the inter-site correlation of LSP has been set to be 0 in the WIM, and excluded from the final deliverable [1] and from the channel simulation software [44].

2.1.2 Own contributions

Since the correlation properties are crucial for the system level channel modeling in designing relay networks, the major contributions of this chapter were set at studying and investigating the correlation properties of LSP comprehensively. As a final result, a relay channel model will be proposed, based on the WIM.

The main contributions of this chapter are listed as follows.

- A summary of MIMO channel modeling approaches.

After presenting the general MIMO channel modeling process, MIMO channel modeling approaches including the stochastic and deterministic modeling methods are discussed.

- A comprehensive comparison among the state-of-the-art channel models.

the state-of-the-art MIMO channel models, including the 3GPP SCM [34], the IEEE 802.11n channel model [35], and the COST 273 channel model [40] [36] as well as the WIM [44] [1], are compared in terms of modeling approach and model parameters as well as software implementation. According to the system requirements imposed on the relay channel modeling, the WIM is selected as an initial channel model.

- Proposal of the channel model for relay networks, based on the WIM.

According to the system requirements and the network topology of relay networks, the goals of the channel modeling are discussed. Using the WIM as the initial channel model, the key channel metrics for relay networks have been proposed. They are the intra-site correlation and the inter-site correlation. Both of them reflect the long-term correlation properties between meshed links. These correlation properties have been studied for LSP, representing the large scale channel properties in the spatial, temporal, frequency, and power domains.

- Providing method of how to reproduce the channel correlation properties in the whole reproduction process.

If the correlation properties of LSP are available, this chapter provides the methods of how to reproduce these channel metrics and of how to integrate these correlation properties into the whole channel modeling process. An example has been exploited to detail the whole reproduction process.

2.2 Channel modeling process

Channel modeling is a cooperation work between propagation researchers and system designers [75]. The system designers provide the propagation researchers with the information on investigated systems and the requirements on channel models. At the end, the results of propagation modeling are output to the system designers.

The general channel modeling process is shown in Fig. 2.1. The whole process is divided into 3

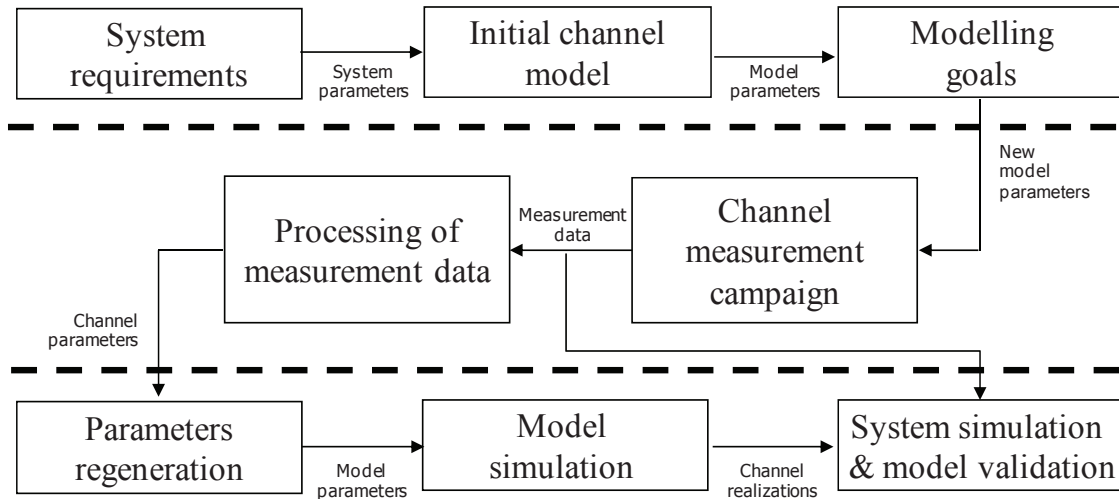


Fig. 2.1: Channel modeling process

phases. The first phase focuses on the initialization of a channel model and the modeling goals. The second phase aims at getting the channel parameters required both for the initial channel model and for the new modeling goals. In the third phase, the model parameters are reproduced and fed to the model to simulate channel realizations.

The first phase starts with system requirements. After studying the investigated radio system, the required system parameters are returned. Based on those system requirements, the channel model, providing the best match to the considered system, is selected from existing channel models as the initial channel model. The model parameters are adopted from the initial channel model. However, the initial channel model can not fulfill all system requirements. Therefore, some new modeling goals are proposed, from which new model parameters are returned. To acquire the new model parameters as well as the initial model parameters, measurement campaigns are planned and then conducted at the second phase. Measurement data, stored in a massive memory disk array, is post-processed, by which the model parameters can be extracted. Those parameters are input to the third phase where according to their statistical properties, the model parameters are reproduced by using a random number generating algorithm and a filtering algorithm. The reproduced model parameters are fed to the modeling algorithm for channel realization simulations. Using the channel realizations, system performance can be predicted. Furthermore, the channel model can be further verified by comparing the simulated channel realizations with those directly from measurement data.

2.3 MIMO channel modeling approaches

For MIMO channel modeling, generally a distinction can be made between the stochastic and deterministic modeling approaches [45] [46]. Table 2.1 gives an overview of the categories.

1. Stochastic channel modeling

stochastic modeling aims to describe the stochastic properties of channel parameters. It does

Tab. 2.1: Categories of MIMO channel modeling approaches

MIMO channel modeling				
Stochastic channel modeling		Deterministic channel modeling		
Correlation based [35]	Geometric scatter based [34]	Ray-tracing based [47]	Measurement based parametric [48]	Stored channels

not depend on the site-specific description. In the stochastic section, two sub-categories are introduced, namely correlation based modeling and geometric scatter based modeling.

(a) Correlation based channel modeling

Under the assumption that the channel coefficients of a MIMO channel matrix \mathbf{H} are complex Gaussian distributed, the first- and second-order moments of the channel coefficients can fully characterize the statistical behavior of a MIMO channel. Several models are developed based on the second-order statistics of a MIMO channel, such as the IEEE 802.11n channel model [35]. Correlation based channel modeling gives a limited insight into the propagation characteristics of a MIMO channel since no physical parameters, such as scatters, are used. The statistical correlation matrix \mathbf{R} [76], expressing the correlation characteristics between any transmit and receive antenna pair, is exploited for the modeling purpose. \mathbf{R} can be computed as

$$\mathbf{R} = E\{vec(\mathbf{H}) \bullet vec(\mathbf{H})^H\}, \quad (2.1)$$

where $E\{\cdot\}$ is the expectation operation, the superscript H denotes the complex conjugate transpose, \mathbf{H} , a MIMO channel matrix, has a dimension of $n_{Tx} \times n_{Rx}$, and vec stands for the operation of stacking all columns of the channel matrix \mathbf{H} into a vector. Using the correlation matrix \mathbf{R} , a MIMO channel can be reproduced by

$$vec(\mathbf{H}) = \mathbf{R}^{\frac{1}{2}}\mathcal{G}, \quad (2.2)$$

where \mathcal{G} is a matrix with its elements being independent and identically distributed (i.i.d) zero mean complex Gaussian random variables. Thus, the correlation matrix \mathbf{R} has a dimension: $n_{Tx}n_{Rx} \times n_{Tx}n_{Rx}$. As the number of antenna elements increases, the extreme large dimension of the correlation matrix makes the calculation more complicated and even impossible. A simplified Kronecker model [77] is proposed under the assumption that the transmit correlation matrix \mathbf{R}_{Tx} and the receive correlation matrix \mathbf{R}_{Rx} are independent, where

$$\mathbf{R}_{Rx} = E\{h_i h_i^H\}, \text{ for } i = 1, \dots, n_{Rx} \quad (2.3)$$

and

$$\mathbf{R}_{Tx} = E\{((h^j)^H)h^j\}, \text{ for } j = 1, \dots, n_{Tx}. \quad (2.4)$$

where h_i stands for the i^{th} column of \mathbf{H} while h^j stands for the j^{th} row of \mathbf{H} , and the superscript T denotes the complex transpose.

The channel correlation matrix \mathbf{R} can be approximated by the Kronecker product of $\mathbf{R}_{\mathbf{T}\mathbf{x}}$ and $\mathbf{R}_{\mathbf{R}\mathbf{x}}$ as

$$\mathbf{R} = \mathbf{R}_{\mathbf{T}\mathbf{x}} \otimes \mathbf{R}_{\mathbf{R}\mathbf{x}}, \quad (2.5)$$

and a MIMO channel can be reproduced by

$$\mathbf{H} = \mathbf{R}_{\mathbf{T}\mathbf{x}}^{\frac{1}{2}} \mathcal{G} \mathbf{R}_{\mathbf{R}\mathbf{x}}^{\frac{T}{2}}. \quad (2.6)$$

The principle of the Kronecker assumption could hold in the scenarios where scatters are uniformly distributed around both stations, for example a two-ring model [76]. However, this assumption often could not hold in realistic propagation. Mostly, the Kronecker model underestimates the correlation. The correlation based models are beneficial when analyzing the MIMO capacity [77].

(b) Geometric scatter based channel modeling

Geometric scatter based channel modeling is based on the locations and properties of individual scatter in a given propagation environment. It is a physical modeling approach. The shape of a scatter area can be defined with respect to the type of scenario, for example, a one-ring model in the case when a BS is assumed to be highly elevated while a MS is surrounded by scatters [76], a two-ring model in the case when both a BS and a MS are surrounded by scatters [76], and an elliptical model [78]. The second variant of the geometric scatter based models describes the channel as a superposition of impinging waves [49]. Channel realizations are based on a tap delay line structure. Each path is a propagation path which is characterized by the spatial scatter distribution.

2. Deterministic channel modeling

Deterministic channel modeling needs a precise description of the specific propagation scenario. Therefore, it is a site-specific channel modeling method. Three approaches are described in the following, namely ray-tracing based, measurement based parametric channel modeling, and stored channels.

(a) Ray-tracing based channel modeling

Ray-tracing based channel modeling is based on geometric optic approximations. An accurate description of the geometric environment and its electro-magnetic properties [47] [79] is required in ray-tracing. The Channel Impulse Response (CIR) at certain position is predicted by summing up the contribution from a large number of paths through the environment. Both the signal strength and the direction of each MPC can be computed. The more accurate the description of the environment, the better the match between a ray-tracing based simulation channel and a realistic channel. However, the computational effort is enormous. More general, there are many simplified ray-tracing based methods, by which the simulation complexity can be significantly reduced while providing a reliable channel simulation [80].

To predict the coverage in a certain environment and to compute the CIRs in an accurately defined environment, ray-tracing is the most popular method.

(b) Measurement based parametric channel modeling

Measurement based parametric channel modeling [81] describes the propagation as a superposition of specular components [48]. First of all, the stored MIMO measurement data is processed by using a high-resolution channel parameter estimation algorithm like Estimation of Signal Parameters via Rotational Invariance Techniques (ESPRIT), Space Alternating Generalized Expectation maximization (SAGE), or Gradient based ML Parameter estimation algorithm (RIMAX) [82]. As a result, the parameters of each MPC can be estimated. The parameters, including the complex channel gain, delay, Angle of Arrival (AOA) and Angle of Departure (AOD) for azimuth and elevation, and Doppler frequency shift, represent the complex multipath CIR in the power, delay/frequency, spatial, and temporal domains. One of the aims of measurement based parametric channel modeling is to separate the influence of the antennas from the radio channel. A MIMO channel can be simulated by integrating the directivity of an antenna array into a multipath channel. Thus, an arbitrary antenna array can be included in synthesized channels.

(c) Stored MIMO channels

The stored MIMO channels from measurement campaigns are often used in the performance simulation for the verification purpose [10] [83] but rarely used to simulate radio channels directly. It is due to the fact that this approach is too site-specific, less flexible, and further measurement antenna array dependent.

In stochastic channel modeling, a large number of random parameters can be a headache for a reliable channel simulation. Thus, several parameters will be fixed to reduce the system simulation complexity meanwhile to provide an acceptable accuracy.

2.4 Channel modeling process for relay networks

The channel modeling for relay networks will be performed according to the process presented in Subsection 2.2. Each step will be described in detail in the following.

2.4.1 System requirements

Nowadays, both wideband and MIMO are standard techniques. Thus, the channel of relay networks would be a wideband MIMO propagation channel. The wideband MIMO channel between any two stations in relay networks can be modeled as what has been conducted for single-hop networks, using the approaches described in Section 2.3. It is called a link level channel modeling where the short-term wave propagation of a single link is characterized and then modeled. However, a link level channel modeling is not sufficient for relay networks. It has been widely discussed and accepted that wireless communication systems benefit from relay concepts not only due to the availability of intermediate RSs, but also due to the meshed network topology. The ideas such as cooperative relaying as well as virtual antenna arrays [51] [52] [39] [22] [53] have been stimulated

from the meshed network topology. Therefore, the channel modeling for relay networks should not only focus on modeling the channel between any two stations for short-term, but also the long-term properties between meshed two-station channels. Using the classical three-station structured relay networks as an example, the task of channel modeling for relay networks should not be limited to model the single S-D, S-R, and R-D channels. The correlation between them is of importance which should be treated as one of the focus points [5] in the channel modeling for relay networks.

2.4.2 Comparison among the state-of-the-art MIMO channel models

To facilitate the channel modeling for relay networks, the state-of-the-art MIMO channel models, including the 3GPP SCM [34], the IEEE 802.11n channel model [35], and the COST 273 channel model [40] [36] as well as the WIM [44] [1], are compared. The one, providing the best match to the system requirements, will be selected as an initial channel model, based on which the channel model of relay networks will be proposed. Some comparisons have been done in Table A in Appendix [84] [41] [42] [44] [85]. It can be observed from Table A that all these channel models are based on the stochastic channel modeling approach. The IEEE 802.11 channel model uses the Kronecker product of two correlation matrices as the modeling approach. The fact that it covers only indoor scenarios limits its application to relay networks. Therefore, it will not be considered as the basis for relay channel modeling. The modeling methodology of the remaining three channel models can be traced back to the COST 259 [40] framework: the ray-based spatial channel modeling. Cluster strategies are introduced which facilitate the channel modeling and reduce the modeling complexity. Both the WIM and the 3GPP SCM are a system level channel modeling and provide a software implementation. Furthermore, the former makes a significant improvement to the latter in terms of scenarios, bandwidth, and channel parameters. Therefore, the WIM is selected as the initial channel model of relay networks.

The WIM has a top-down modeling philosophy where at first the system level propagation and then the link level propagation are reproduced. With this top-down structure as shown in Fig. 2.2, the WIM models firstly the multi-cell case by exploiting the inter-site correlation as a key channel metric. Thereafter, it shifts the focus to the single-cell case where the intra-site correlation is introduced. Thereafter, single-links are modeled by MPCs. Each path in MPCs comprises sub-paths with a sum of sinusoids method. This top-down structure makes the WIM applicable for any kind of networks with various network topologies, for example relay networks.

At the link level, the MPC parameters of a clustered delay line model (as shown in Fig. 2.3) describe the short-term propagation between two stations over a LSA. The parameters of each MPC are called small scale parameters. They include complex polarimetric path gain, departure (from the transmitter) and arrival (to the receiver) angles, and propagation delay. For each channel realization over a LSA, these MPC parameters are chosen randomly according to their Probability Density Function (PDF)s. The sub-paths of each MPC are generated by summing up equal-powered sinusoids [86], having the same delay, fixed AOA and AOD offsets, but different phases. Both in the WIM and in the 3GPP SCM, the small scale parameters are low-level model parameters. They are controlled by LSP which stay the same over a LSA and vary continuously from a LSA to another

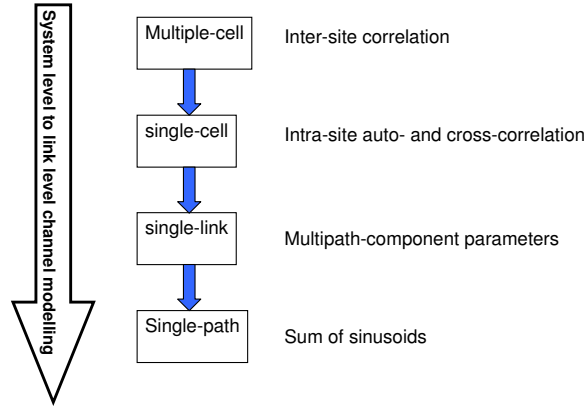


Fig. 2.2: The top-down modeling philosophy of the WIM

neighboring LSA. The parameters, such as DS, AS, LSF, and K-factor, belong to the LSP group in the WIM while the LSP group in the 3GPP SCM includes only DS, AS, and LSF. Since the spatial, temporal, frequency, and power domains of a channel are most probably not independent, the intra-site cross-correlation between different LSP is introduced as a metric to quantify this interdependence. The intra-site cross-correlation has been considered already both in the WIM [1] [5] and in the 3GPP SCM [34].

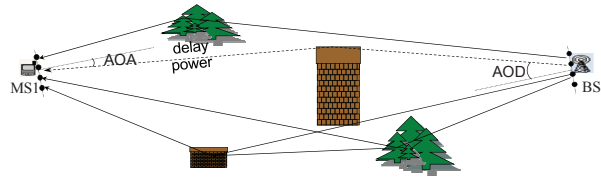


Fig. 2.3: A link level channel modeling over a LSA

Now shifting our observation from the single link short-term propagation illustrated in Fig. 2.3 to the multiple links long-term propagation illustrated in Fig. 2.4, two cases are considered. The one is that two MSs are connected to the same BS as shown in Fig. 2.4(a), the other is that two BSs communicate with the same MS as shown in Fig. 2.4(b). The question is raised: is there any long-term similarity among multiple radio links, between BS1-MS1 and BS1-MS2 or between BS1-MS1 and BS2-MS1, in the spatial, temporal, frequency, and power domains? Due to the existence of common scatters and reflectors among multiple links, the answer is definitively yes. Thereafter, we introduce the measures, the intra-site auto-correlation and the inter-site correlation to quantify those similarities. The intra-site auto-correlation is a channel metric which characterizes the similarity between multiple links from different MSs to the same BS as shown in Fig. 2.4(a) while the inter-site correlation is a channel metric which characterizes the similarity between multiple links from different BSs to the same MS as shown in Fig. 2.4(b). LSP are considered in calculating the two long-term correlations.

By introducing the two correlation metrics: the intra-site auto- and cross-correlation and the inter-site correlation, systems with a more complicated layout can be simulated. The intra-site auto- and cross-correlation allows it to simulate channel realizations for single-cell multi-user applications

and single-cell ad-hoc networks while the inter-site correlation allows a multi-cell simulation like relay networks and SA [54]. In 3GPP channel modeling, both the intra-site cross-correlation and the inter-site correlation have been considered. The intra-site cross-correlation of LSP has been investigated for LSF and DS as well as AS. But the inter-site correlation study is limited to LSF with a fixed correlation coefficient of 0.5. The intra-site auto- and cross-correlation has been proposed and implemented in the WIM. Furthermore, the WIM has investigated the inter-site correlation model theoretically. However, the inter-site correlation of LSP has been set to be 0 and excluded from the final software implementation in the WIM. Therefore, it can be concluded that the WIM supports both the link level and system level channel modeling.

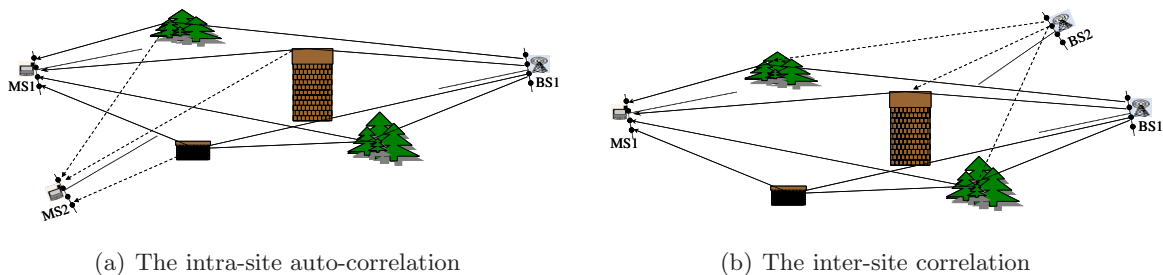


Fig. 2.4: A system level channel modeling

2.4.3 Modeling goals

Although the correlation concepts have been proposed in the WIM, only the intra-site auto- and cross-correlation is included in the final deliverable [1] and implemented in the final channel simulation software [44]. Furthermore, some aspects of the correlation properties are not considered in the final deliverable due to insufficient measurement data. Moreover, the inter-site correlation is only introduced but not implemented in the WIM channel simulation tool. Since these correlations are crucial for the system level relay channel modeling, one of the major contributions of this chapter is to study and to investigate the correlation properties of LSP. As a final result, the channel model of relay networks will be proposed based on the WIM framework.

The investigation includes the following aspects:

1. Except the parameters considered in the WIM, the following channel parameters will be included into the LSP group
 - Cross-polarization Ratio (XPR);
 - MIMO metric such as Normalized Parallel Channel Gain (NPCG) [77], which captures the spatial characteristics of a MIMO channel and gives an insight into the MIMO gain compared with a Single-Input Single-Output (SISO) channel.
2. AS in the elevation domain

The WIM characterized the MIMO space only in the azimuth domain. In this chapter, the elevation domain will be also studied to provide a fully three dimensional description to the

MIMO space.

3. The intra-site auto- and cross-correlation

The intra-site auto- and cross-correlation characterizes the correlation in two cases. The one is the case where two MS have a distance d_{MS} from each other, to the same BS, the other is the case where one MS move a distance d_{MS} , to the same BS [56]. Since both cases are equivalent in terms of the intra-site correlation modeling, only the first one is considered for the simplicity.

The work conducted up to now focuses mostly on the relationship between the intra-site auto- and cross-correlation and the distance between two MSs. A new dimension will be introduced to characterize the intra-site correlation, namely, the BS height.

4. The inter-site correlation

In relay networks, the signals coming from different BSs/RSs are often correlated especially if common dominating scatters exist. For example, the inter-site correlation in the example scenario in Fig. 2.5(a) will be larger than the one in the example scenario in Fig. 2.5(b).

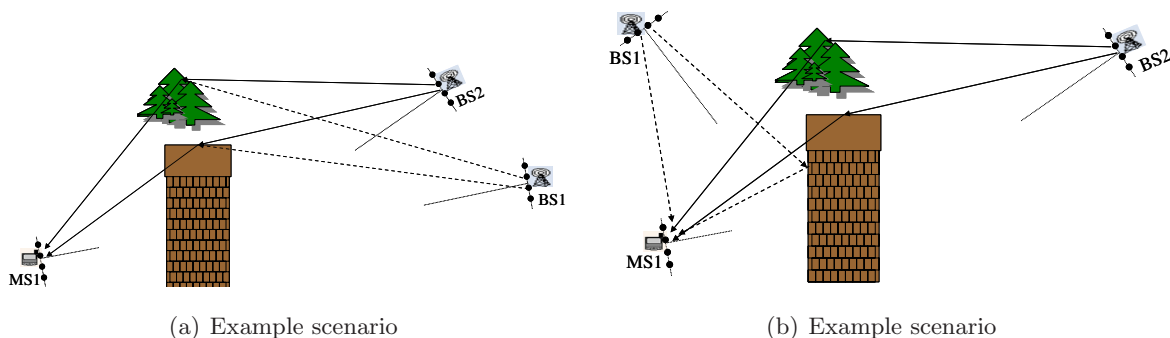


Fig. 2.5: Examples of the inter-site correlation

The first investigations of the inter-site correlation properties have been done only to one LSP, namely, LSF. The results in [71] [72] showed the dependence of the inter-site correlation on the angle seen from a MS to two sites: BSs/RSs. Other experimental studies showed that the inter-site correlation depends on the relative distance between two sites [63]. Besides these two factors, the distance difference between two links and the height difference between two sites will be considered as the impact factors in the inter-site correlation modeling.

The inter-sector correlation, as a special case of the inter-site correlation, will also be investigated.

5. The BS/RS height

The impact of the BS/RS height on PL models has been studied in [15]. But, no work has been done to investigate its impact on LSP. Thus, one of the focuses will study the impact of the BS/RS height on the statistical distributions of LSP and their correlation properties.

2.5 The definition of LSP and their correlation properties

The following channel metrics are considered: Delay Window (DW) and DS as well as coherence bandwidth in the delay/frequency domain; AS @ Receiver (Rx), AS @ Transmitter (Tx), and NPCG in the spatial domain; PL, LSF, XPR, K-factor, and corner loss in the power domain. Those parameters are introduced into the LSP group except corner loss.

1. DW

In a measured PDP, DW is defined as the time delay of multipath with power being larger than a cut level as shown in Fig. 2.6. The cut level is the threshold under which majority of the signal detected is the measurement thermal noise.

2. DS, coherence bandwidth, and AS

In general, a spread is the root of the second central moment of a power spectral density. DS is computed over a delay power spectral density or a PDP while AS is calculated over an angular delay power spectral density or a Power Angle Spectrum (PAS).

The coherence bandwidth is a measure of the frequency difference, at which the frequency correlation coefficient of a power frequency profile falls from 1 to a certain level. The coherence bandwidth, as a duality to DS, expresses the time dispersive properties of multipath channels in a LSA. The coherence bandwidth is inversely proportional to the DS τ_{rms} [87] as:

$$B_c = \frac{1}{c_\tau \cdot \tau_{rms}}, \quad (2.7)$$

where c_τ ranges from 5 to 10 depending on the shape of a PDP [13] [88].

Furthermore, the coherence bandwidth has a lower bound [87]:

$$B_c \geq \arccos(c_B)/2 \cdot \pi \tau_{rms}, \quad (2.8)$$

where c_B stands for a selected coherence level.

In Fig. 2.6, a PDP is shown as an example. In the same figure, DW, DS, mean delay, and noise level as well as a cut level are shown for the selected PDP.

3. PL, LSF, and SSF

The received signal power P_{Rx} in mobile communication is often modeled as a product of four factors (see Eqn. 2.9): the transmit power P_{Tx} (in [dBm]), the distance dependent PL [13] (in [dB]), log-normal distributed LSF (in [dB]) [89], and SSF (in [dB]).

$$P_{Rx} = P_{Tx} - PL + LSF + SSF. \quad (2.9)$$

PL characterizes the dependence of the signal attenuation on the distance between the transmitter and the receiver. The distance is expressed in meters. Note that the antenna gain might be included or excluded from a PL value. PL is often modeled as follows,

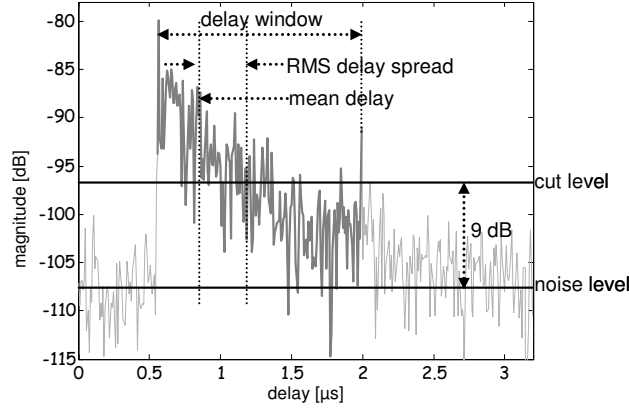


Fig. 2.6: An example PDP and the corresponding channel parameters

$$PL = 10n_{PL} \log_{10} d + B \quad (2.10)$$

where n_{PL} is the PL exponent, d expresses the distance between the transmitter and the receiver in m, and B is the PL value when d is one meter.

As a result of the multiplication of a large number of random attenuating factors along a propagation path, LSF has a log-normal distribution with a zero mean value and a σ^2 variance [89]. The variance σ^2 is expressed in dB.

SSF, characterizing the superposition of multipath propagation, is often modeled as a Rayleigh/Rice distribution. SSF is also called fast fading

The PL model with antenna gains for the free space is given by

$$PL = 10lg \left(\frac{\lambda_{WL}^2 G_{Tx} G_{Rx}}{(4\pi)^2 d^2} \right) = -20lgd + 10lgG_{Tx} + 10lgG_{Rx} + B, \quad (2.11)$$

where λ_{WL} stands for a wave length, G_{Tx} and G_{Rx} stand for the gains of the transmit and receive antennas, respectively.

Without antenna gains the model is given by

$$PL = 10lg \left(\frac{\lambda_{WL}^2}{(4\pi)^2 d^2} \right) = -20lgd + B. \quad (2.12)$$

4. XPR

XPR defines the ratio of the power between the co-polar propagation and the cross-polar propagation.

5. K-factor

K-factor is defined as the ratio between the power of a direct LOS path and the power of the remaining MPCs in a LOS region. In Fig. 2.7, the first path stands for the power of a direct LOS path, while the sum of the rest paths means the power of the remaining MPCs. The ratio between them is computed as the K-factor value.

6. Corner loss [90]

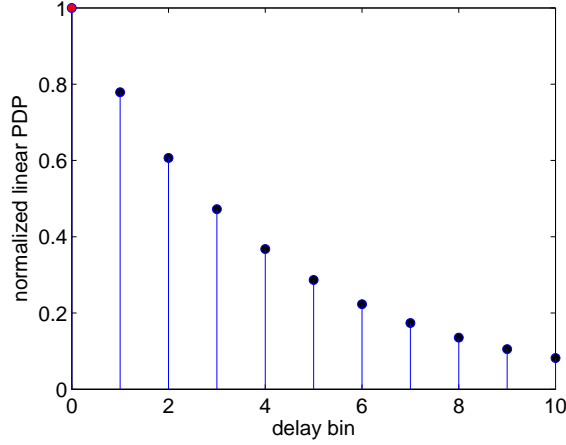


Fig. 2.7: PDP with a direct LOS path and the remaining MPCs

Corner effect in actual urban environments is defined as the sudden decrease in the received power (in [dB]) due to the change from the LOS propagation to the NLOS propagation when a MS turns around a corner.

7. MIMO metrics

(a) Definition of a MIMO channel

MIMO, as one of the significant breakthroughs in modern mobile communications, can improve the system capacity and the frequency efficiency [29] [30]. A MIMO channel, having n_{Rx} receive antenna elements and n_{Tx} transmit antenna elements, can be expressed by a matrix \mathbf{H} with dimension $n_{Tx} \times n_{Rx}$. The system model of a MIMO transmission can be expressed as

$$\begin{pmatrix} r_1 \\ \vdots \\ r_{n_{Rx}} \end{pmatrix} = \begin{pmatrix} h_{1,1} & \cdots & h_{n_{Tx},1} \\ \vdots & h_{ij} & \vdots \\ h_{1,n_{Rx}} & \cdots & h_{n_{Tx},n_{Rx}} \end{pmatrix} \cdot \begin{pmatrix} s_1 \\ \vdots \\ s_{n_{Tx}} \end{pmatrix} + \begin{pmatrix} n_1 \\ \vdots \\ n_{n_{Tx}} \end{pmatrix}, \quad (2.13)$$

where r_i , $1 \leq i \leq n_{Rx}$, is the receive signal; $h_{i,j}$, $1 \leq i \leq n_{Tx}$ and $1 \leq j \leq n_{Rx}$, is the channel efficient; s_i , $1 \leq i \leq n_{Tx}$, is the transmit signal; and n_i , $1 \leq i \leq n_{Tx}$ is the additive white Gaussian noise (AWGN) noise.

With $\mathbf{r} = [r_1, \dots, r_{n_{Rx}}]^T$, $\mathbf{s} = [s_1, \dots, s_{n_{Tx}}]^T$ und $\mathbf{n} = [n_1, \dots, n_{n_{Tx}}]^T$, Eqn. 2.13 can be reformed as

$$\mathbf{r} = \mathbf{H}^T \mathbf{s} + \mathbf{n}. \quad (2.14)$$

(b) Singular values

After performing a singular value decomposition to the channel matrix \mathbf{H}^T , \mathbf{H}^T can be expressed as

$$\mathbf{H}^T = \mathbf{U} \cdot \lambda \cdot \mathbf{V}^H, \quad (2.15)$$

where λ is a $n_{Rx} \times n_{Tx}$ matrix with diagonal elements being $\lambda_1, \dots, \lambda_j, \dots, \lambda_{\min(n_{Tx}, n_{Rx})}$.

These elements are the singular values of the channel matrix \mathbf{H}^T .

(c) The MIMO capacity

Based on the definition of a MIMO channel, the MIMO capacity C_{MIMO} can be calculated as

$$C_{MIMO} = \log_2 \left(\det \left(\mathbf{I}_{n_{Rx}} + \frac{\rho_{SNR} \mathbf{H}^T \mathbf{H}^*}{n_{Tx}} \right) \right). \quad (2.16)$$

where \det stands for a matrix determinant operation, $\mathbf{I}_{n_{Rx}}$ is an identity matrix with a dimension $n_{Rx} \times n_{Rx}$, ρ_{SNR} is the SNR value of a MIMO channel.

By replacing \mathbf{H}^T with Eqn. 2.15, Eqn. 2.16 can be rewritten as

$$\begin{aligned} C_{MIMO} &= \log_2 \left(\det \left(\mathbf{I}_{n_{Rx}} + \frac{\rho_{SNR} \mathbf{U} \cdot \lambda \cdot \mathbf{V}^H \mathbf{V} \cdot \lambda^H \cdot \mathbf{U}^H}{n_{Tx}} \right) \right) \\ &= \log_2 \left(\det \left(\mathbf{U} \left(\mathbf{I}_{\min(n_{Tx}, n_{Rx})} + \frac{\rho_{SNR} \cdot \lambda \cdot \lambda^H}{n_{Tx}} \right) \mathbf{U}^H \right) \right) \\ &= \log_2 \prod_{i=1}^{\min(n_{Tx}, n_{Rx})} \left(1 + \frac{\rho_{SNR}}{n_{Tx}} \lambda_i^2 \right) \\ &= \sum_{i=1}^{\min(n_{Tx}, n_{Rx})} \log_2 \left(1 + \frac{\rho_{SNR}}{n_{Tx}} \lambda_i^2 \right). \end{aligned} \quad (2.17)$$

Eqn. 2.17 indicates that the capacity of a MIMO channel is the sum capacity of $\min(n_{Tx}, n_{Rx})$ parallel SISO channels. $1 + \frac{\rho_{SNR}}{n_{Tx}} \lambda_i^2$ is the channel gain of the i^{th} parallel SISO channel. The key idea of MIMO is to improve the data rate by spatial multiplexing in eigen mode where $\min(n_{Tx}, n_{Rx})$ different data streams can be transmitted over $\min(n_{Tx}, n_{Rx})$ SISO channels. In the best case, $\min(n_{Tx}, n_{Rx})$ times SISO capacity can be achieved.

(d) NPCG

As $\frac{\rho_{SNR}}{n_{Tx}}$ in Eqn. 2.17 becomes larger, $1 + \frac{\rho_{SNR}}{n_{Tx}} \lambda_i^2 \approx \frac{\rho_{SNR}}{n_{Tx}} \lambda_i^2$. Consequently, C_{MIMO} is increased linearly with $\min(n_{Tx}, n_{Rx})$. If $\min(n_{Tx}, n_{Rx})$ is fixed, the MIMO capacity is determined only by the singular value λ_i^2 . To characterize the spread of MIMO singular values, the metric, NPCG, is introduced [36] [91]. NPCG is defined as follows,

$$NPCG = \frac{\sum_{i=1}^{\min(n_{Tx}, n_{Rx})} \lambda_i^2}{\max(\lambda_1^2, \dots, \lambda_{\min(n_{Tx}, n_{Rx})}^2)}. \quad (2.18)$$

Unlike the MIMO capacity, which is a function of the system SNR, NPCG is independent on the system SNR. However, NPCG can still characterize the gain achieved by MIMO. The NPCG value is lower-bounded by 1 and upper-bounded by $\min(n_{Tx}, n_{Rx})$. The upper-bound can be achieved if $\min(n_{Tx}, n_{Rx})$ equal powered parallel SISO channels exist: $\lambda_1^2 = \dots = \lambda_{\min(n_{Tx}, n_{Rx})}^2$.

8. The intra-site correlation properties of LSP

(a) The intra-site auto-correlation of LSP

The intra-site auto-correlation of LSP indicates how fast the LSP values vary along the d_{MS} distance of a MS, alternatively, how large the similarity of the LSP values is between two MSs separated with a distance being d_{MS} as shown in Fig. 2.8. The

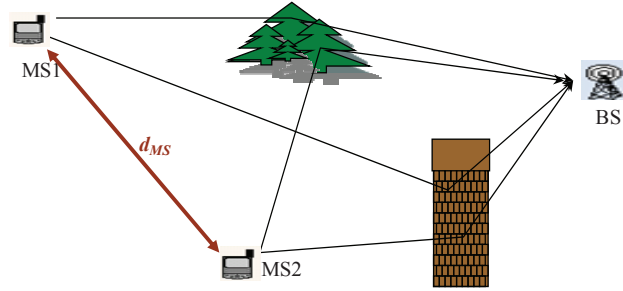


Fig. 2.8: The intra-site auto-correlation

intra-site auto-correlation of LSP can be calculated as,

$$\rho_{MS} = \frac{C_{AB}(d_{MS})}{\sqrt{C_{AA}C_{BB}}}, \quad (2.19)$$

where C_{AB} is the cross-covariance of A and B . A and B are the variables of the same LSP, but between two MSs being separated with a distance being d_{MS} .

As discussed in [64] [65] [5] [66], the spatial variation properties of LSP can be well modeled as an exponential decaying function expressing the change of LSP over the distance d_{MS} ,

$$\rho_{MS} = \exp\left(-\frac{d_{MS}}{d_{decorr}}\right). \quad (2.20)$$

This means, LSP of two links toward the same BS would experience correlations which are proportional to their relative distance d_{MS} . This correlation is quantified by the de-correlation distance d_{decorr} defined as the distance to which the correlation coefficient is dropped to e^{-1} .

(b) The intra-site cross-correlation of LSP

The intra-site cross-correlation is defined as the correlation properties among LSP. It characterizes the correlation between various domains, such as the spatial, temporal, frequency, and power domains. The intra-site cross-correlation coefficients can be expressed with a correlation matrix [5] [67]. Each entity in the matrix is computed as,

$$\rho_{AB} = \frac{C_{AB}}{\sqrt{C_{AA}C_{BB}}}, \quad (2.21)$$

where C_{AB} is the cross-covariance of two LSP, A and B , of the same MS. Since $\rho_{AB} = \rho_{BA}$, the cross-correlation matrix is symmetric.

9. The inter-sector correlation properties of LSP ³

³ If a channel model is antenna-independent, the inter-sector correlation is equal 1. If each sector of a BS is treated as a single BS, the inter-sector correlation merges into a special case of the inter-site correlation, where two BSs are the two sectors of the same BS.

The inter-sector correlation is defined as the correlation of the LSP of a MS which can get signal from two different sectors of the same BS. Let's define the 3-dB main beam widths of sector 1 and sector 2 to be θ_{s1} and θ_{s2} (as shown in Fig. 2.9), respectively. The inter-sector correlation of LSP is divided into two classes. The one is the correlation in the overlapped main beam area θ_{OL} where a MS is in the main beams of two sectors, namely,

$$\theta_{OL} = \theta_{s1} \cap \theta_{s2}; \quad (2.22)$$

the other is the correlation in the $\overline{\theta_{s1}} \cap \theta_{s2}$ area or in the $\theta_{s1} \cap \overline{\theta_{s2}}$ area where a MS is in the main beam of one sector but in the side beam of another sector.

The inter-sector correlation can be expressed as,

$$\rho_{AB} = \frac{C_{AB}}{\sqrt{C_{AA}C_{BB}}}, \quad (2.23)$$

where C_{AB} is the cross-covariance of A and B . A and B are the variables of the same LSP, but from two sectors of the same BS.

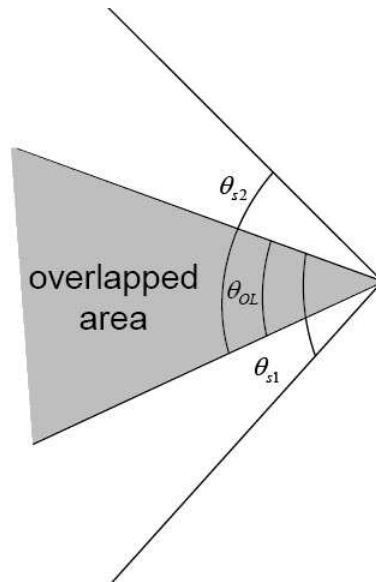


Fig. 2.9: The inter-sector correlation

10. The inter-site correlation properties of LSP ⁴

First of all, an simple example will be provided as follows to show the impact of the inter-site correlation of LSF on the system hand-over management.

Handover rule: a MS communicates with the BS which provides a larger received power.

Ignoring SSF, the received power can be calculated according to Eqn. 2.9. With the parameters defined in Table 2.2, the difference in the received power at a MS from two BSs is shown in Fig. 2.11 where only the PL model is considered. The larger the k_d value, the larger the difference in the received power between two links. Under the hand-over assumption, the

⁴ Only the correlation of the same LSP from two links is considered.

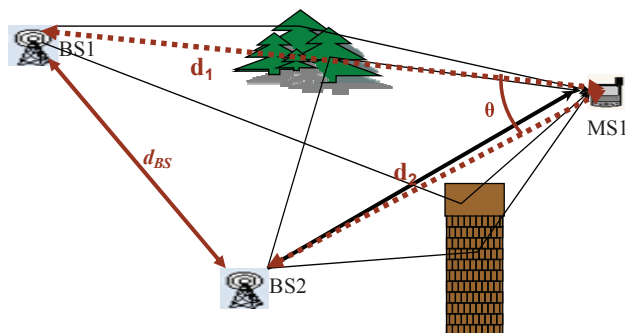


Fig. 2.10: A hand over scenario

Tab. 2.2: Hand-over parameter setup

n_{PL}	3.5
B	38.4
σ	8 dB
d_1 and d_2	$d_2 = k_d d_1$ d_1, d_2 in [km]

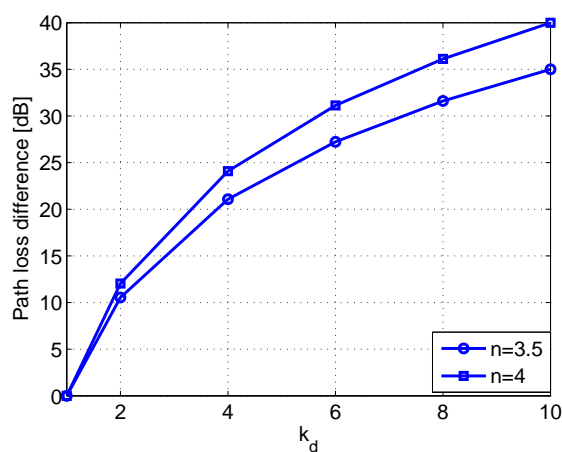


Fig. 2.11: Received power difference (in [dB]) from two BSs with different PL exponents

probability of hand-over is shown in Fig. 2.12 with the inter-site LSF correlation coefficient as a parameter. The inter-site LSF correlation coefficient varies from 0 to 0.8 with a step of 0.2. When a MS has the same distance to two BSs, the probability of handover at the MS is 50 %,

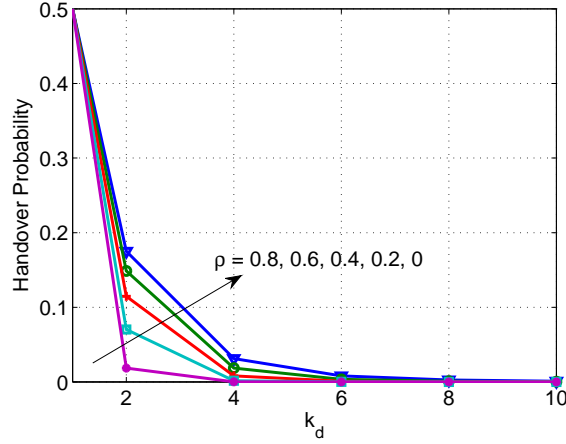


Fig. 2.12: Handover probability

Based on the studies conducted to the inter-site correlation of LSF, it is proposed that the inter-site correlation of LSP can be expressed as,

$$\rho_{BS} = f(d_{diff}, \theta, d_{BS}, h_{diff}), \quad (2.24)$$

where $d_{diff} = 10 \log_{10} \frac{\min(d_1, d_2)}{\max(d_1, d_2)}$ (ref. Fig. 2.10) stands for the distance difference between two links, θ is the angle of arrival difference from two BSs/RSs to the same MS, namely the angle seen from a MS to two BSs/RSs, d_{BS} means the distance between two BSs/RSs, and h_{diff} is the height difference between two BSs/RSs. The proposed new model includes and summarizes the ideas in [92] [71] [72] [63]. Additionally, two new parameters, d_{BS} and h_{diff} , have been introduced.

2.6 Usage of the correlation models of LSP

Under the assumption that the experimental models of the correlation properties of LSP are available, it is important to accurately regenerate the correlation properties in the relay channel modeling process. The method will be addressed in this section. Recall the top-down modeling philosophy of the WIM presented in Fig. 2.2 in Subsection 2.4.2, the channel modeling for relay networks should focus on the first two parts: multi-cell and single-cell. The rest parts stay the same.

The regeneration process is shown in Fig 2.13. First of all, an algorithm, called weighted sums of independent Gaussian random processes, is used to represent the inter-site correlation of LSP. Then, a two-dimensional filter based method [93] will be used to introduce the intra-site auto-correlation.

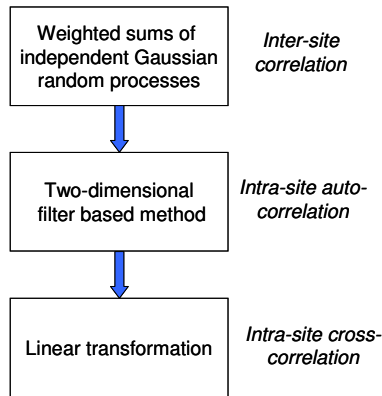


Fig. 2.13: Regeneration process and algorithms based on the correlation models of LSP

Finally, a linear transformation is conducted to reproduce the intra-site cross-correlation. By doing this, the WIM can be adapted for a full relay network support. Furthermore, the WIM and the relay channel model are compatible. This is the case since LAYOUTPAR is one of the input parameters to start channel simulations in the WIM. This parameter provides two-dimensional coordinate informations of BSs/RSs and MSs [1].

The regeneration process is described in detail as follows. Assume that there are n_{BS} one-sector BSs, n_{MS} MSs, each of which has connection to $n_l(i)$ BSs ($1 \leq i \leq n_{MS}$), and n_{LSP} LSP. The geometric area where all BSs and MSs locate has the dimension $m_x \times m_y$ with a resolution of 1 [m].

1. Generate random Gaussian processes

$n_{LSP} \times (\sum_{i=1}^{n_{MS}} n_l(i))$ random Gaussian matrices with a zero mean value and a unit variance are generated. Each matrix has a dimension $m_x \times m_y$. Each MS-BS link has n_{LSP} matrices.

2. The inter-site correlation

Since the geometric structure of the simulation system is known, the inter-site correlation coefficient ρ_{BS} of each LSP can be calculated according to Eqn. 2.24. To each MS, the inter-site correlation of each LSP can be expressed as a $n_l(i) \times n_l(i)$ symmetric matrix. Then, performing Cholesky decomposition to the inter-site correlation matrix, a lower triangular matrix will be returned. By weighting $n_l(i) \times m_x \times m_y$ independent Gaussian random matrix with this lower triangular matrix, the inter-site correlation is introduced to one LSP. Using the same method, the inter-site correlation of the rest LSP and the rest MSs can be introduced.

3. The intra-site auto-correlation

In literature, several design methodologies have been reported to simulate the intra-site auto-correlation properties. The majority of these methods can be classified into one of the following three categories [94] [95].

- (a) The Sum-Of-Sinusoids method

This method is based on the fact that a Gaussian random process can be expressed as an infinite Sum-Of-Sinusoids with random phases and properly selected frequencies. In practice, a finite number of sinusoids can be used to approximate the Gaussian process so that the computational complexity can be reduced while keeping the final results comparable. This method is frequently used to simulate a correlated fast-fading process [86] [43] [31]. As mentioned in Subsection 2.4.2, Sum-Of-Sinusoids method has been used to model each MPC.

(b) The filter-based method

With this method, channel parameters are generated by means of filtering a zero-mean white Gaussian noise process. The frequency response of the filter is the square root of the Power Spectral Density (PSD) of a Gaussian process [94].

(c) Markov processes based method

This method is often used to model radio link quality, such as the SNR and the BER, instead of being used to characterize a physical propagation.

Due to the fact that the two-dimensional coordinate information is provided in the WIM, it is convenient to use a two-dimensional filter based method to reproduce the intra-site auto-correlation in the channel simulation.

Recall the intra-site auto-correlation model proposed in Eqn. 2.20 in Section 2.5, the parameter d_{MS} is defined as the distance between two MSs. Due to the fact that

$$d_{MS} = \sqrt{d_x^2 + d_y^2} = \sqrt{(x_1 - x_2)^2 + (y_1 - y_2)^2} \quad (2.25)$$

where (x_1, y_1) and (x_2, y_2) are the positions of two MSs in a two-dimensional Cartesian coordinate system, Eqn. 2.20 can be rewritten as

$$\rho_{MS} = \exp\left(-\frac{d_{MS}}{d_{decorr}}\right) = \exp\left(-\frac{\sqrt{(x_1 - x_2)^2 + (y_1 - y_2)^2}}{d_{decorr}}\right). \quad (2.26)$$

Now the intra-site auto-correlation model is extended to a two-dimensional coordinate system. To extract the two-dimensional filter function from the intra-site auto-correlation model, following steps are conducted based on the theory that the Fourier transform of an auto-correlation function is the same as the square of the Fourier transform of the related CIR,

- (a) generate a two-dimensional $m_x \times m_y$ matrix $\rho_{\mathbf{MS}}$ to describe the intra-site auto-correlation in a coordinate system, the point with a correlation coefficient being 1 is in the middle of the map.
- (b) Perform a two-dimensional discrete Fourier transformation to $\rho_{\mathbf{MS}}$: $fft(\rho_{\mathbf{MS}})$.
- (c) Get the root square: $\sqrt{fft(\rho_{\mathbf{MS}})}$
- (d) Perform a two-dimensional inverse discrete Fourier transformation $ifft(\sqrt{fft(\rho_{\mathbf{MS}})})$. Note that a proper normalization should be performed to keep the variance to be one.

then a two-dimensional filtering function $\mathbf{f}(\mathbf{x}, \mathbf{y})$ is returned. The output at the second

step is filtered with this two-dimensional filter to introduce the exponential intra-site auto-correlation.

4. The intra-site cross-correlation

After filtering, the LSP values at the MSs' positions are selected for the current channel simulation while the values over the whole map can be saved as a look-up table for the coming channel simulation with the same setup. Now each MS-BS link has n_{LSP} LSP values ζ . The intra-site cross-correlation is generated for each MS-BS link by a linear transformation,

$$\hat{\zeta} = \sqrt{\rho_{\mathbf{AB}}}\zeta, \quad (2.27)$$

where $\rho_{\mathbf{AB}}$ is the symmetric intra-site cross-correlation matrix described in Eqn. 2.21 in Section 2.5.

Now we use an example scenario to illustrate the process described above. In the example scenario, $n_{BS} = 2$, $n_{MS} = 2$, $n_{LSP} = 2$, $m_x = m_y = 400$, MS1 communicates both with BS1 and with BS2 while MS2 communicates only with BS2. The geometric distribution of MSs and BSs in a two-dimensional map is shown in Fig. 2.14.

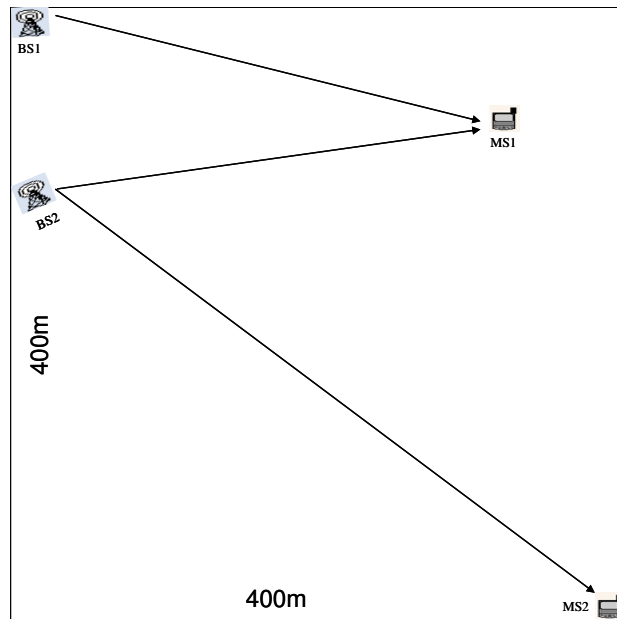


Fig. 2.14: Geometric distribution of MSs and BSs

1. Generate 6 400×400 matrices with a random Gaussian distribution, of which the mean value is zero and the variance is one. Each LSP matrix of the MS1-BS1 link and the MS1-BS2 link \mathbf{g}_i ($1 \leq i \leq 2$) has the dimension $2 \times 400 \times 400$ where 2 stands for two BSs.
2. From the geometric map, the inter-site correlation coefficients between the MS1-BS1 link and the MS1-BS2 link are for example 0.3 and 0.8 for LSP1 and LSP2, respectively. Correspondingly, the inter-site correlation matrices can be expressed as $\begin{vmatrix} 1 & 0.3 \\ 0.3 & 1 \end{vmatrix}$ and $\begin{vmatrix} 1 & 0.8 \\ 0.8 & 1 \end{vmatrix}$ for

LSP1 and LSP2, respectively. After performing Cholesky decomposition to these two matrices, $\begin{vmatrix} 1 & 0 \\ 0.3 & 0.95 \end{vmatrix}$ and $\begin{vmatrix} 1 & 0 \\ 0.8 & 0.6 \end{vmatrix}$ are returned. Weighting \mathbf{g}_1 with the first matrix and \mathbf{g}_2 with the second matrix, the inter-site correlation is introduced to LSP1 and LSP2.

3. Let's assume that LSP1 and LSP2 have, respectively, a de-correlation distance of 10 [m] and 50 [m]. Two 400×400 two-dimensional matrices are generated to represent the intra-site auto-correlation. Using the steps addressed above, the filtering function $\mathbf{f}(\mathbf{x}, \mathbf{y})$ can be extracted from the exponential intra-site auto-correlation functions. Convolution of the filter with the LSP matrices, we can get the LSP values for each MS-BS link.
4. Selecting the LSP values at each MS position and saving the values over the whole map, we can get a vector with n_{LSP} values for each BS-MS link. Vectors ζ_{11} , ζ_{21} , and ζ_{22} are returned. Let's assume the intra-site cross-correlation between LSP1 and LSP2 is 0.4. Then the final LSP values at the MS position for each MS-BS link $\hat{\zeta}_{11}$, $\hat{\zeta}_{21}$, and $\hat{\zeta}_{22}$ can be calculated as

$$\hat{\zeta} = \begin{vmatrix} 1 & 0.4 \\ 0.4 & 1 \end{vmatrix}^{\frac{1}{2}} \zeta. \quad (2.28)$$

These LSP are fixed at each LSA. Their change from one LSA to a neighboring LSA can be observed from the intra-site auto-correlation. Figure 2.15 shows the change of one LSP over the whole area with the inter-site correlation ρ_{BS} and the de-correlation distance d_{decorr} as parameters. Three cases are compared in Fig. 2.15: 2.15(a) $\rho_{BS} = 0.8$ and $d_{decorr} = 50$ [m]; 2.15(b) $\rho_{BS} = 0$ and $d_{decorr} = 50$ [m]; 2.15(c) $\rho_{BS} = 0$ and $d_{decorr} = 100$ [m]. The similarity between two subplots in 2.15(a) is obvious due to the 0.8 inter-site correlation. Whereas, there is almost no similarity between two subplots in 2.15(b) and 2.15(c) where $\rho_{BS} = 0$. Comparing 2.15(b) and 2.15(c), it is observed that the larger the intra-site auto-correlation, the slower the LSP values change over distance.

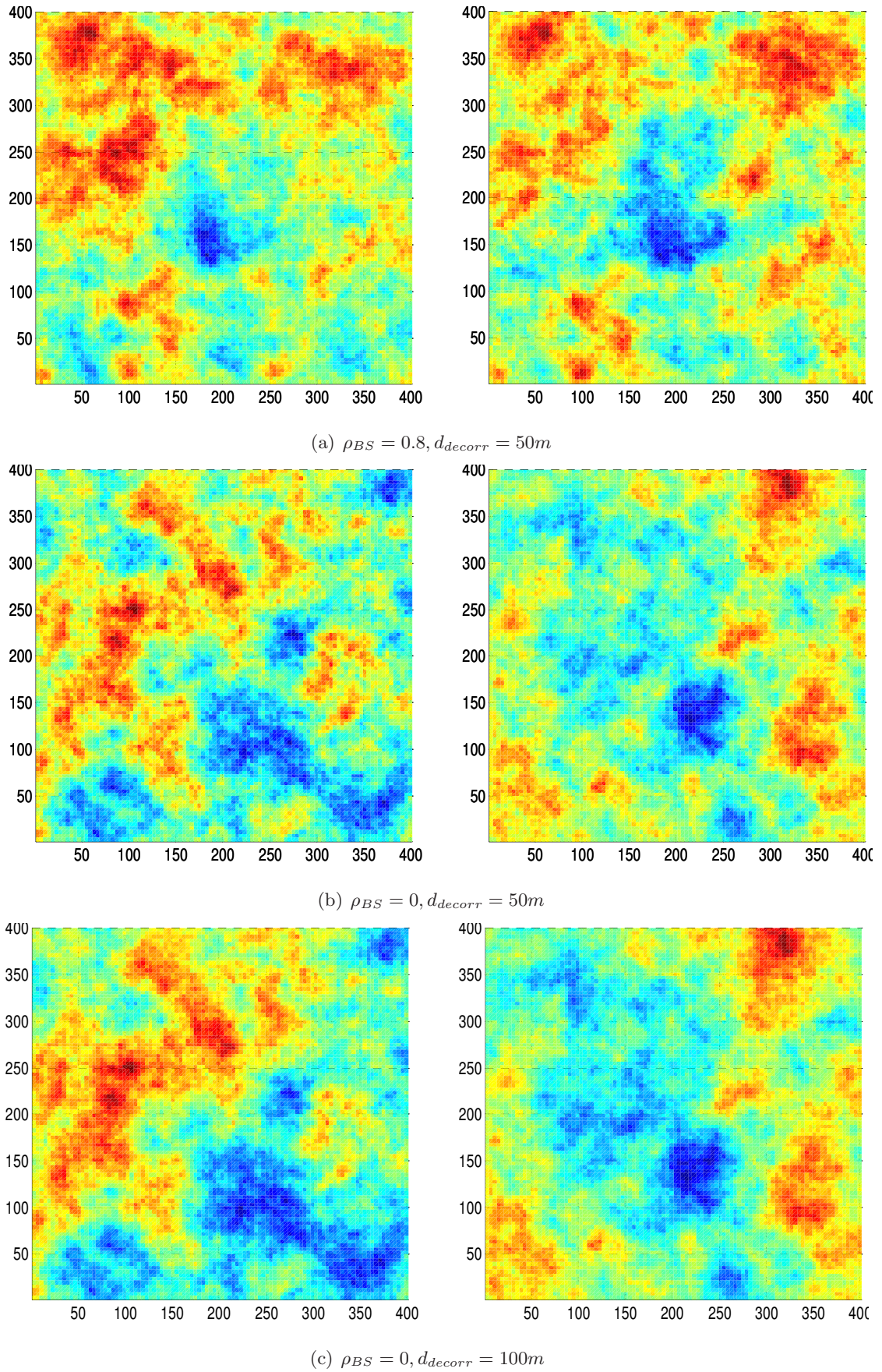


Fig. 2.15: Distribution of the LSP values over the whole area with the inter-site correlation ρ_{BS} and the de-correlation distance d_{decorr} as parameters

3. EXPERIMENTAL CHANNEL EVALUATION AND MODELING

Recall the channel modeling process shown in Fig. 2.1 in Section 2.2, the first and the third phases have been discussed in Chapter 2. This chapter focuses on the second phase: channel measurement campaigns and measurement data post-processing. This phase aims at extracting the channel parameters from measurement data for the relay channel modeling. Both the extraction algorithms and the processing procedure are presented. However, with the same algorithms and procedure, the experimental results may be different. The reason is that the setting parameters during post-processing could be different. To obtain reasonable experimental results, the impacts of the setting parameters on channel parameters are investigated. Appropriate values of the setting parameters are selected for the final measurement data analysis. The LSP values and their correlation properties are highlighted for both the urban and indoor scenarios.

This chapter is structured as follows. First of all, Section 3.1 gives firstly an outlook to the state-of-the-art research activities in the channel modeling for relay networks and summarizes the main contributions of this chapter. Thereafter, Section 3.2 introduces the scenarios which suit for relay applications. The relay measurement campaigns performed in two scenarios: indoor and outdoor urban, are described in Section 3.3. The same section provides a short description to the working principle of the channel sounder used. The extraction procedure and algorithms of the channel parameters are presented in Section 3.4 while Section 3.5 shows the experimental results of the LSP values and their correlation properties.

3.1 Background and own contributions

3.1.1 Background and state-of-the-art

Gudmundson proposed in [92] to model the intra-site auto-correlation function of LSF as an exponential decaying function, where the correlation coefficient is a function of the distance between two MSs. This model has been confirmed many times by the experimental results based on measurements [72] [64] [65] [3] [6]. As an extension, the authors in [64] [3] have investigated the intra-site correlation of LSF and DS as well as AS. The experimental decaying model is extensively used in mobile communications testbeds and simulation studies [96] [74].

Compared with the fruitful results for the intra-site correlation modeling, there is still no commonly acceptable model for the inter-site correlation. In 1978, Graziano published his experimental results of the inter-site correlation of LSF based on 900MHz channel measurements [68]. In his paper, he showed that the inter-site LSF correlation tends to be a function of the angle of arrival difference (θ)

in Fig. 2.10); the smaller the angle, the larger the correlation. After his work, Mawira proposed in 1992 that the inter-site LSF correlation can be modeled as a linear function of the angle of arrival difference [69] which is in line with the experimental observation in [68]. In 1999, Sorensen confirmed Mawira's and Graziano's observation in [70] that the inter-site LSF correlation depends on the angle of arrival difference θ . In his paper he proposed to model the correlation as a piecewise function of θ . However, Perahia et. al observed that no association between the inter-site LSF correlation and θ has been found and the correlation is relatively low both in rural and in suburban environments [71]. Thereafter, Weitzen et. al doubted the conclusion drawn by Graziano with the argument that no enough data sets were available in the measurements used in [68]. Based on Weitzen's relatively massive data sets, he observed in his paper [72] that the average correlation coefficient is smaller than 0.2 even when the angle of arrival difference θ is small. The reason is that the distance difference between two links (d_1 and d_2) is very large. In the case of a large distance difference while small θ , the common objects causing shadowing between two links are still very rare. As a consequence, a MS experiences no similar LSF from two BSs. This means that both the distance difference between two links and the angle of arrival difference are decisive factors in the modeling of the inter-site correlation.

The first investigation of the inter-site correlation properties has been done only to one LSP, namely LSF. The results in [71] [72] showed the dependence of the inter-site correlation on the angle seen from a MS to two sites: BSs/RSs. Experimental studies in [63] showed that the inter-site correlation depends on the relative distance between two sites. The results are estimated from a few limited measurements and therefore it may not be useful in a general case. The first results of the inter-site correlation in indoor scenarios have been presented by Jalden and Hong in [6]. The results showed that in the indoor case, the inter-site correlation is rather high for one measurement route but quite low for another route [6]. The WIM has investigated the inter-site correlation model theoretically. However, the inter-site correlation of LSP has been set to be 0 and excluded from the final software implementation in the WIM.

3.1.2 Own contributions

Through the analysis on measurement data gathered from the urban and indoor scenarios, the experimental results of the statistical distributions of LSP and their correlation properties are presented in this chapter. The main contributions of this chapter is listed as follows:

- Except LSF, DS, and K-factor as well as AS, the channel parameters such as XPR and the MIMO metric NPCG, have been considered as LSP.
- Investigating the dependence of the LSP and their intra-site correlation properties on the BS height [7].

The intra-site correlation properties have been normally modeled as a function of the distance between two MSs. During the urban measurement campaign, the BS antenna has been set to two heights: 10 [m] and 16 [m], representing an urban micro- and macro-cell scenario,

Tab. 3.1: Propagation scenarios for relay network applications

Scenario	Definition	v_{MS}	h_{BS}	h_{RS}	h_{MS}
		[km/h]	[m]	[m]	[m]
U1	Micro-cell urban	1 – 50	below rooftop	3	1.5
U2	Macro-cell urban	1 – 50	above rooftop	3	1.5
I1	Indoor corridor	1 – 5	3	3	1.5

respectively. Therefore, the impact of the BS/RS height on the statistical distributions of LSP and their intra-site correlation properties can be studied.

- Experimental results on the correlation behaviors between two sectors of a BS.

Both in the urban measurement campaign and in the indoor measurement campaign, the BS antenna array has been set to two orientations, angle of which is 90 [deg.] and 180 [deg.], respectively. A high inter-sector correlation can be observed in the overlapped main beam area.

- Experimental model of the inter-site correlation.

The dependence of the inter-site correlation properties of LSP on the following parameters has been studied based on measurement data, distance difference between two links, angle of arrival difference from two BSs/RSs to a MS, the distance between two BSs/RSs, and the height difference between two BSs/RSs.

3.2 Propagation scenarios

The propagation scenarios defined for relay network applications are summarized in Table 3.1. A description of each scenario is provided in the following subsections.

3.2.1 Urban scenarios

3.2.1.1 U1 scenario: urban micro-cell

U1 scenario defines the environments where both a BS antenna array and a RS antenna array are deployed lower than surrounding buildings. The BS antenna array is normally placed at the main street while the RS antenna array is located at the crossroad to provide coverage to a shadowed street, being perpendicular to the main street. This scenario covers both LOS and NLOS propagation conditions. The environment is defined as a Manhattan-like grid scenario, one of the most promising relay application scenarios [17].

3.2.1.2 U2 scenario: urban macro-cell

U2 scenario is distinguished from U1 scenario because the BS antenna array is above surrounding buildings. In this scenario, the BS antenna array provides a relatively large coverage due to its

height. The RS antenna array is expected to extend coverage or to provide coverage to a shadowed area. Both LOS and NLOS propagation conditions are considered.

3.2.2 Indoor scenarios

3.2.2.1 I1 scenario: indoor corridor

I1 scenario represents a typical office environment. The BS antenna array is assumed to be in corridor. Thus, it is a LOS propagation in the corridor where the BS is located while a NLOS propagation in the perpendicular corridors. Both the BS and RS antenna arrays have the same height.

3.3 Relay measurement campaigns

Relay measurement campaigns aim to capture the correlation properties of LSP. The scenarios defined in Section 3.2, U1, U2, and I1, are considered in measurement campaigns. Before going detailed to each measurement campaign in Subsection 3.3.2 and Subsection 3.3.3, Subsection 3.3.1 gives a short introduction to the working principle of the channel sounder equipment used [97].

3.3.1 Broadband radio channel sounding: technique and equipment

The channel sounder used [98] [97] measures MIMO CIRs between n_{Tx} transmit antenna elements and n_{Rx} receive antenna elements. $n_{Tx} \times n_{Rx}$ MIMO sub-channels are measured sequentially by the synchronous switching of the transmit and receive antenna elements. Figure 3.1 shows the switching time frame of the sequential MIMO channel sounding with a 3×4 -antenna configuration. A SISO measurement has been conducted at each measurement time by sending a "periodic multi-sine" excitation signal [98]. This approach is well known from the frequency domain system identification in measurement engineering. In communication engineering this signal may be called Multi-Carrier Spread Spectrum Signal (MCSSS). Given the time length of a SISO CIR to be τ_{max} , the total time length of a MIMO snapshot is $24\tau_{max}$ (i.e. $2n_{Tx}n_{Rx}\tau_{max}$). The factor 2 comes from the fact that a guard time is inserted after each SISO measurement to avoid switching transients. During measurements, the SISO CIR length τ_{max} is adjustable, depending on measurement environments and on the distance between the transmitter and the receiver. The larger the distance, the larger the value τ_{max} should be. Normally, τ_{max} is larger in outdoor scenarios than in indoor scenarios. Two MIMO channel sounders, ATM sounder and HyEff sounder, are manufactured by the MEDAV GmbH, Germany [99]. The key technical parameters of these two sounders are summarized in Table 3.2 [98].

The high resolution antenna arrays used in measurements are optimized to estimate the spatial dimension of a MIMO CIR with high resolution estimation algorithms, e.g. RIMAX [82] [98] [100]. Figure 3.2 summarizes the measurement antenna arrays for the high resolution parameter estimation, of which a Polarimetric Uniform Linear Array (PULA) is used as the BS/RS antenna array while either a Polarimetric Uniform Circular Patch Array (PUCPA) or a Stacked Polarimetric

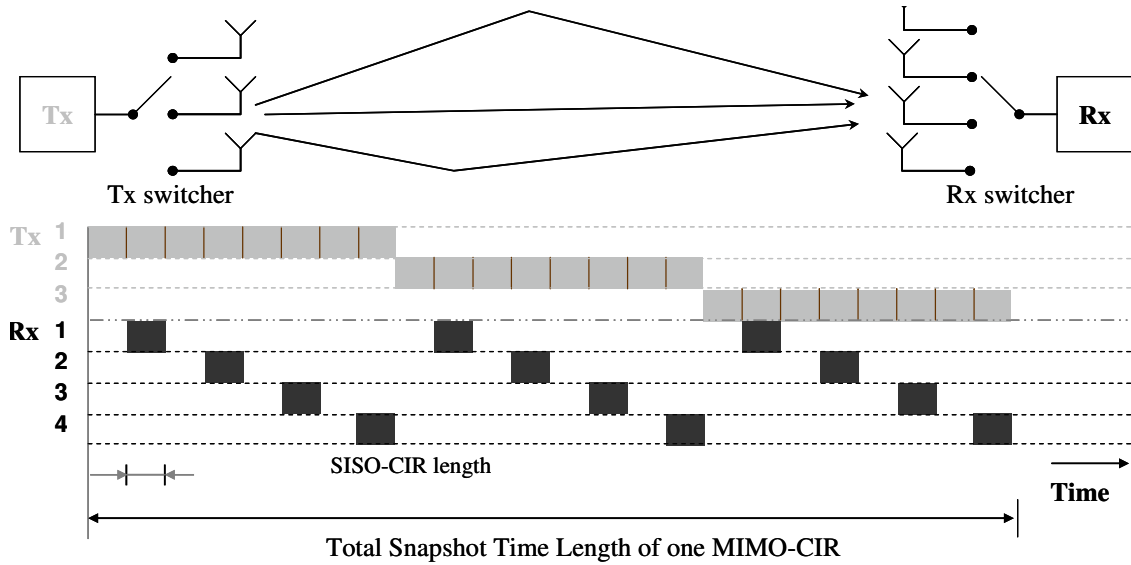


Fig. 3.1: MIMO channel sounder switching scheme

Tab. 3.2: The key technical parameters of the MIMO channel sounder equipments

Name	Carrier frequency	Bandwidth	τ_{max}	Tx power	RF sensitivity
	GHz	[MHz]	$[\mu s]$	[W]	[dBm]
HyEff	5.2	240	0.8-25.6	2	-80
ATM	4.5/5.2	120	0.8-12.6	0.5/2/10	-92

Uniform Circular Patch Array (SPUCPA) is used as the MS antenna array. A detailed 3-Dimension (3D) description to the antenna pattern of these antenna arrays is given in [98].

3.3.2 Micro-cell to macro-cell urban scenario: U1 and U2

The urban measurement campaign has been performed, using the HyEff channel sounder, in Aug. 2006 in the center of Ilmenau, Germany. The measurement area can be characterized as a canonical small urban scenario with 1-3 storeys stone buildings at the both sides of streets. Figure 3.3 shows the environment seen from BS3 and BS6, 16 [m]elevated from the ground [7] [8]. The average roof-top level is estimated to be between 12-15 [m]. Street widths do not exceed the roof-top heights. The positions of the RS and BS antenna arrays, PULA, have been shown in Fig. 3.3. The dashed curves in Fig. 3.3 stand for the moving routes of the MS, SPUCPA. Note that only part of the measurement routes are shown in Fig. 3.3. All measurement routes and the BS/RS positions have been shown in Fig. 3.4 in a 2-dimensional Ilmenau city map. The black circles in Fig. 3.4 stand for the positions of the BS/RS while the dashed curves are the moving routes of the MS. The arrows \rightarrow in Fig. 3.4 show the orientation of the BS/RS. The BS antenna array has two orientations: BS2/BS3 and BS5/BS6, the angle of which is 90 [deg.], $\theta_{OL} = 90$ [deg.]. Furthermore, the BS antenna array has been set to two different heights, 10 [m] (BS2/BS5) and 16 [m] (BS3/BS6) with the help of a lifting ramp while the height of the RS antenna array is fixed to 3 [m]. Increasing




Name	Directivity	No. of elements	Inter-element space	Polar.	Picture
BS/RS					
PULA	120°	8	$0.49\lambda_{WL}$	V H	
MS					
PUCPA	360°	24	$0.49\lambda_{WL}$	V H	
SPUCPA	360°	4 x 24	$0.49\lambda_{WL}$	V H	

Fig. 3.2: Antenna arrays used for a high resolution parameter estimation



Fig. 3.3: Ilmenau downtown seen from the 16 [m] BS antenna array

the BS antenna height from 10 [m] to 16 [m], both the U1 and U2 scenarios are covered in the campaign.

The detailed setup information of the channel sounder and of the transmit and receive antenna arrays is given in Table 3.3.

3.3.3 Indoor corridor scenario: I1

The indoor measurement campaign has been performed in Feb. 2006 inside the Helmholtz building, at the university campus of TU-Ilmenau, Germany. Measurements were conducted with 8 different BS positions. At two BS positions, two different antenna broadside orientations are used, $\langle BS2, BS3 \rangle$ and $\langle BS7, BS8 \rangle$, the angle of which is 180 [deg.] as shown in Fig. 3.6, $\theta_{OL} = 0$ [deg.]. The BSs were placed 2.4 m above floor ground. Most of the BSs are located in the corridor area except BS5/BS6.

Measurements routes have been chosen along corridors and in two seminar rooms (shown as dashed curves in Fig. 3.6). The black circles in Fig. 3.6 stand for the positions of the BSs. The arrows \rightarrow show the orientation of the BSs.

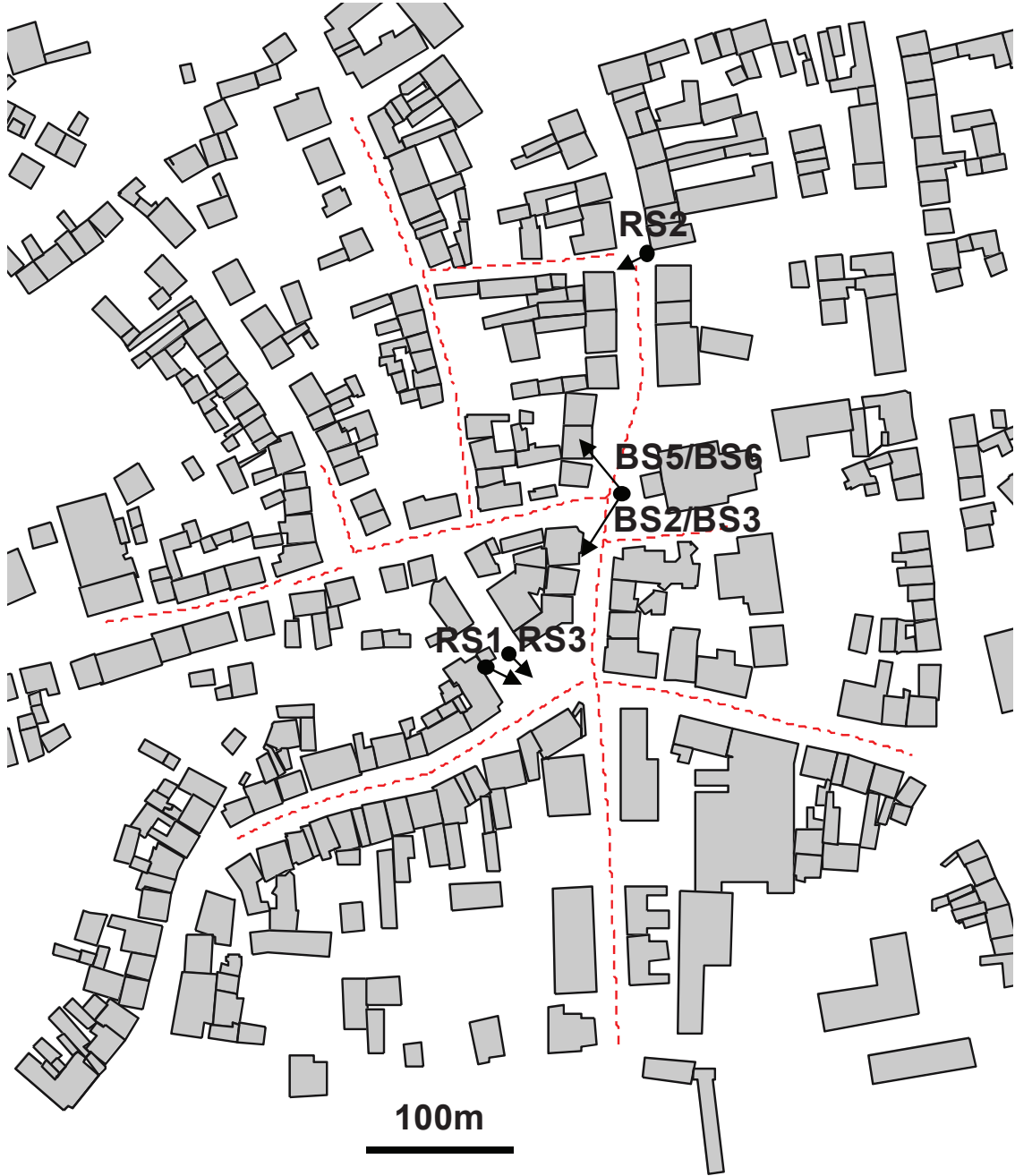
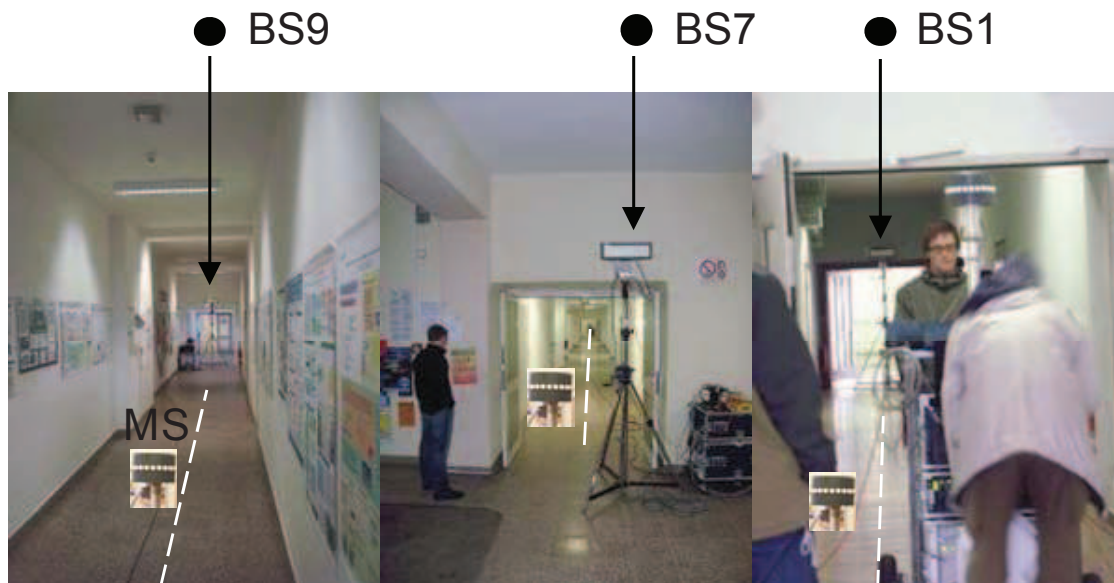


Fig. 3.4: Measurement routes in a 2-dimensional Ilmenau city map

Tab. 3.3: TU-Ilmenau relay measurement campaigns: U1, U2, and I1

Measurement campaign			
Institution		TU-Ilmenau	
Scenario		U1, U2	I1
Location		Ilmenau downtown	Helmholtzbau, TU-Ilmenau campus
Date/Time		Aug. 2006	Feb. 2006
Measurement setup		MIMO	
Channel sounder			
Type		RUSK HyEff [97]	RUSK HyEff [97]
center frequency	[GHz]	5.2	5.2
Bandwidth	[MHz]	120	120
CIR length	[μ s]	3.2	1.6
No. of sub-channels		3088	784
Transmit antenna array (BS/RS)			
Name (type)		PULA	PULA
Height	[m]	3,10,16	2.4
Azimuth	[deg.]	120	120
Tilt	[deg.]	-5 at the BS only	0
Mobility	[km/h]	0	0
Receive antenna array (MS)			
Name(type)		SPUCPA	PUCPA
Height	[m]	1.9	1.7
Tilt	[deg.]	0	0
Mobility	[km/h]	\approx 5	\approx 3

**Fig. 3.5:** Photos of the Helmholtzbau measurement environment

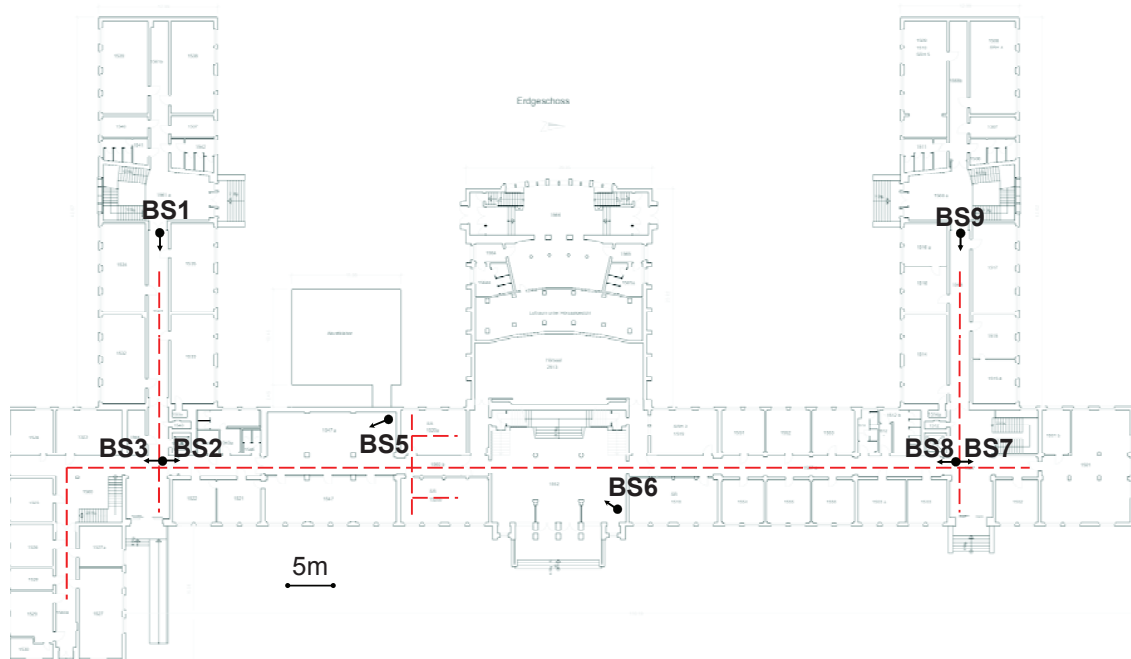


Fig. 3.6: Measurement routes in the floor plan of the Helmholtzbau

Measurements were performed with the RUSK HyEff channel sounder. The detailed settings of the channel sounder as well as the type of the transmit and receive antenna arrays, are given in Table 3.3.

3.4 Extraction procedure of LSP and their correlation properties

After performing measurement campaigns, measurement data has been stored in a massive memory disk array. This section deals with the post-processing of measurement data. Subsection 3.4.1 and Subsection 3.4.2 focus on the extraction procedure and algorithms, respectively. During the extracting procedure, the setting parameters, like noise cut level as well as the length of a ST averaging window, are introduced. Subsection 3.4.3 presents the influence of these setting parameters on the LSP values. Subsection 3.4.4 deals with the method of how to acquire the correlation models of LSP from measurement data.

3.4.1 Extraction procedure of the LSP values

To raw measurement data, the following steps are performed to get the LSP values:

- Reading raw measurement data;
- Grouping snapshots belonging to the same LSA;
- Selecting the valid snapshots within a LSA;
- Extracting the LSP values.

At first to step 1, reading raw measurement data. Since the format of the recorded raw measurement data can not be used directly for a further post-processing, an import filter will be needed to read information from the recorded raw measurement data as shown in Fig. 3.7. The information includes the antenna switching scheme and the measurement setup as well as the MIMO CTF \mathbf{H} . The structure of a CTF is shown in Fig. 3.8. A set of measurement data has in total ss_n snapshots

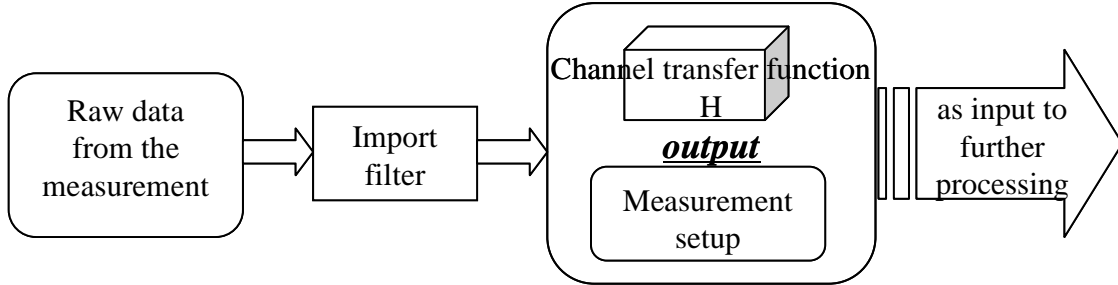


Fig. 3.7: Getting a CTF from the raw data

and has a dimensions $ss_n \times n_{Tx} \times n_{Rx} \times n_f$ as shown in the left subplot in Fig. 3.8. n_f is the number of frequency bins and corresponds to τ_{max} in the delay domain after performing an Inverse Fast Fourier Transformation (ifft) operation. Each MIMO snapshot has a dimension $n_{Tx} \times n_{Rx} \times n_f$ as shown in the right subplot in Fig. 3.8. The output of the import filter is the basic input for the further processing.

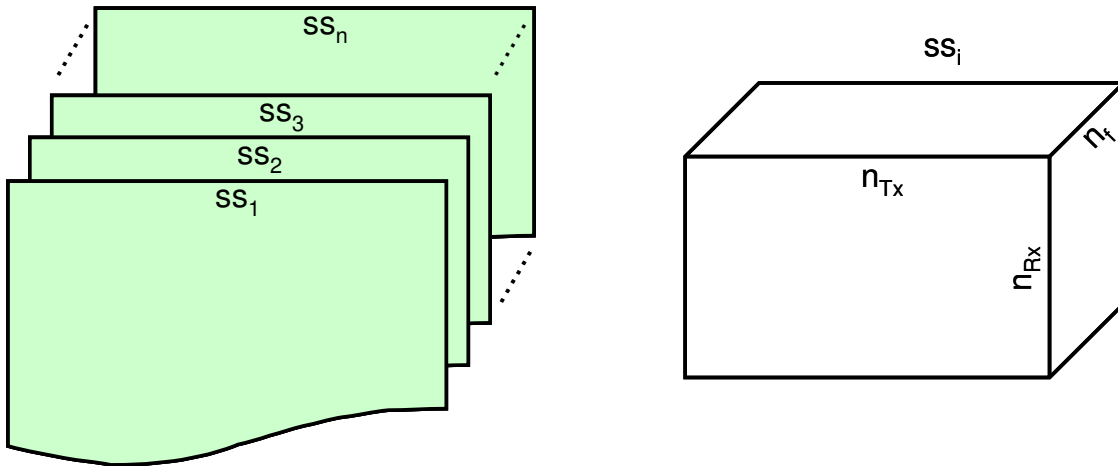


Fig. 3.8: The structure of measurement data (left) and the dimension of a CTF (right)

Then go to step 2, grouping snapshots belonging to the same LSA. Recall the explanation in Section 2.2 that LSP are constant over a LSA. This means that LSP are the channel metrics which should be extracted for each LSA. Hence, the whole measurement data will be divided into snapshots groups, each of which the temporal and spatial spans can be regarded as a LSA. The span of a LSA is in the order of $10\lambda_{WL}$ [79], depending on scenarios. Figure 3.9 shows an example of grouping snapshots within a LSA over the whole measurement data. The whole data can be divided into LSA_n groups, each of which corresponds to a LSA. LSA_1 includes 3 MIMO snapshots while LSA_2 includes 4 MIMO snapshots. The chunk of the CTFs over each LSA has a dimension

of $n_{ss} \times n_{Tx} \times n_{Rx} \times n_f$.

After step 2, valid snapshots within a LSA are selected. Within each LSA, the snapshots comprising only measurement noise are called invalid snapshots. In this dissertation, a snapshot is valid if and only if it has at least one SISO sub-channel with the peak power being 20 [dB] larger than the noise level. Invalid snapshots will be excluded from further processing. Then, the dimension of the valid chunk of the CTFs over each LSA is reduced to $\tilde{n}_{ss} \times n_{Tx} \times n_{Rx} \times n_f$ with $\tilde{n}_{ss} \leq n_{ss}$. In Fig. 3.9 ss_5 is an invalid snapshot within LSA_2 .

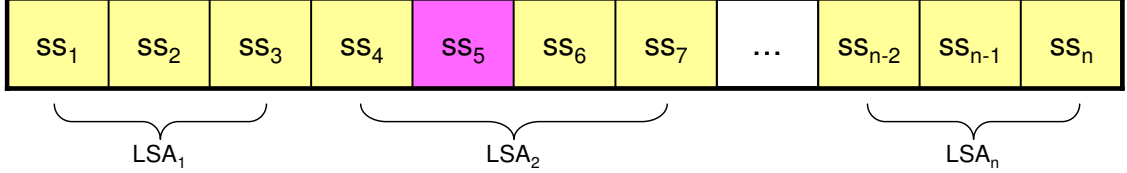


Fig. 3.9: Snapshot groups over the whole measurement data

Now the valid snapshots within a LSA are ready for the further processing. The extraction procedure of the LSP values from $\mathbf{H}_{\tilde{n}_{ss} \times n_{Tx} \times n_{Rx} \times n_f}$ is shown in Fig. 3.10. LSP defined in Subsection

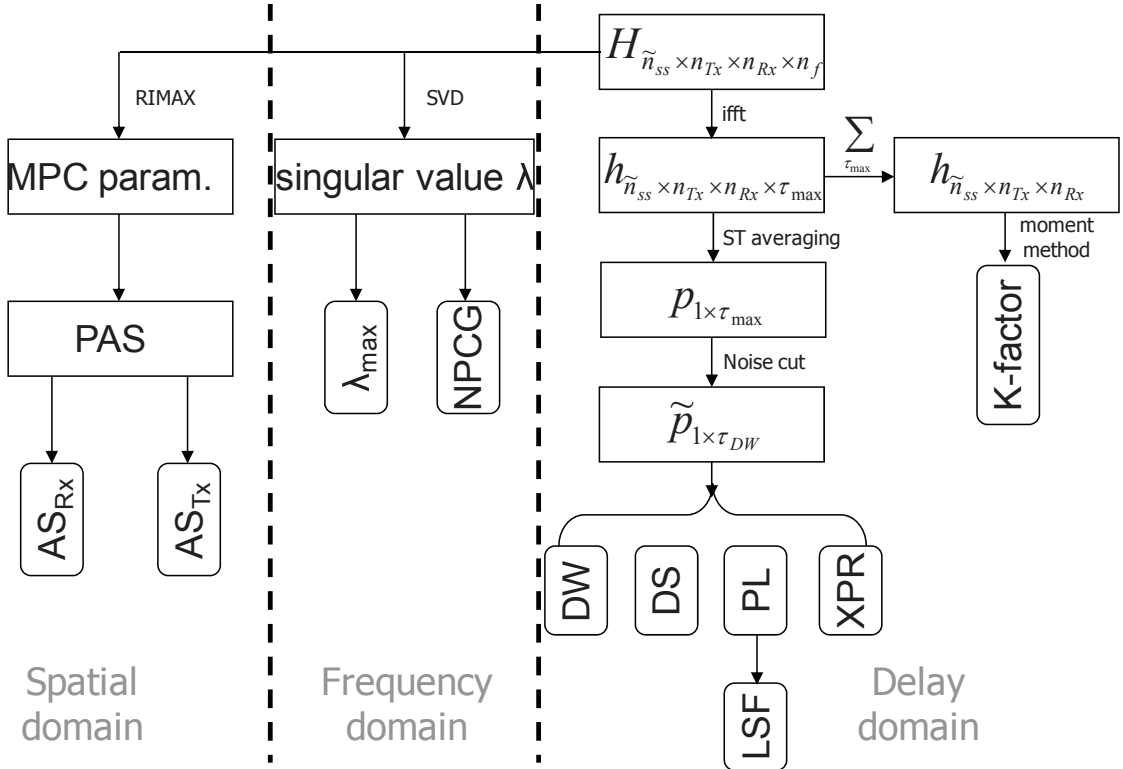


Fig. 3.10: The extraction procedure of the LSP values

2.5 can be extracted from a chunk of MIMO channel matrices: parameters, AS_{Tx} and AS_{Rx} , from the spatial domain; MIMO parameters, λ_{max} and $NPCG$, from the frequency domain; parameters, DW, DS, LSF, XPR, and K-factor, from the delay domain.

3.4.2 Extraction algorithms of the LSP values

- AS_{Tx} and AS_{Rx}

The parameters AS_{Tx} and AS_{Rx} are derived from the high resolution estimation results [82] [98] where a radio propagation channel is described as a superposition of specular components and dense path components. The specular components comprise 10 structural parameters: a 2×2 matrix with complex polarimetric path gain, Direction of Departure (DoD) (azimuth and co-elevation), Direction of Arrival (DoA) (azimuth and co-elevation), Time Delay of Arrival (TDoA), and Doppler shift. AS_{Tx} and AS_{Rx} are the root of the second central moment of the mean PAS which is the mean specular components over \widetilde{n}_{ss} . Since the beam pattern of a measurement antenna array is subtracted from the high resolution estimation results, LSP from the spatial domain are independent on the measurement antenna arrays used.

- λ_{max} and $NPCG$

The parameters λ_{max} and $NPCG$ are calculated from the MIMO CTFs over a LSA. The λ_{max} and $NPCG$ values are returned after performing a Single Value Decomposition (SVD) operation to each MIMO CTF, $\mathbf{H}_{n_{Tx} \times n_{Rx}}$. The mean value of $\widetilde{n}_{ss} \times n_f$ samples is used as the final λ_{max} and $NPCG$ values.

- DW and DS

After a Fast Fourier Transformation (fft) operation to $\mathbf{H}_{\widetilde{n}_{ss} \times n_{Tx} \times n_{Rx} \times n_f}$, CIR $\mathbf{h}_{\widetilde{n}_{ss} \times n_{Tx} \times n_{Rx} \times \tau_{max}}$ is returned. LSP from the delay domain are based on this CIR. First of all, a ST averaging is performed to the PDP, square of a CIR, to remove the small scale effect. Then, the measurement noise is removed from the averaged PDP. The value of the averaged PDP at the delay bin will be set to zero if it is smaller than the defined noise cut level. The length of the delay bins of PDP $\widetilde{p}_{1 \times \tau_{DW}}$ is called DW. DS, the root of the second central moment of $\widetilde{p}_{1 \times \tau_{DW}}$, can be calculated as,

$$DS = \sqrt{\frac{\int_1^{\tau_{DW}} (\tau - \bar{\tau})^2 \widetilde{p}_{1 \times \tau_{DW}} d\tau}{\int_1^{\tau_{DW}} \widetilde{p}_{1 \times \tau_{DW}} d\tau}}, \quad (3.1)$$

where

$$\bar{\tau} = \frac{\int_1^{\tau_{DW}} \tau \widetilde{p}_{1 \times \tau_{DW}} d\tau}{\int_1^{\tau_{DW}} \widetilde{p}_{1 \times \tau_{DW}} d\tau}. \quad (3.2)$$

- PL and LSF

The PL value over a LSA is computed by summing up the power of $\widetilde{p}_{1 \times \tau_{DW}}$ over τ_{DW} . There are two common methods to get a PL model and LSF from the PL values. The most common one is to exploit a Least Mean Square Error (LMSE) algorithm, the other is to use different ST averaging lengths. The first method is especially useful if the distance information between the transmitter and the receiver for each LSA is available and the measurement campaign has been conducted over a large range of the transmitter-receiver distance. Otherwise, the second method is preferable.

In the first method, the empirical PL formulas as shown in Eqn. 2.10, including a PL exponent n_{PL} and B , are returned after performing a LMSE fitting between the PL values and $\log_{10} d$. Figure 3.11(a) gives an example to get a PL model from the PL values. The points are the PL values while the straight curve stands for the PL model after performing a LMSE algorithm [4].

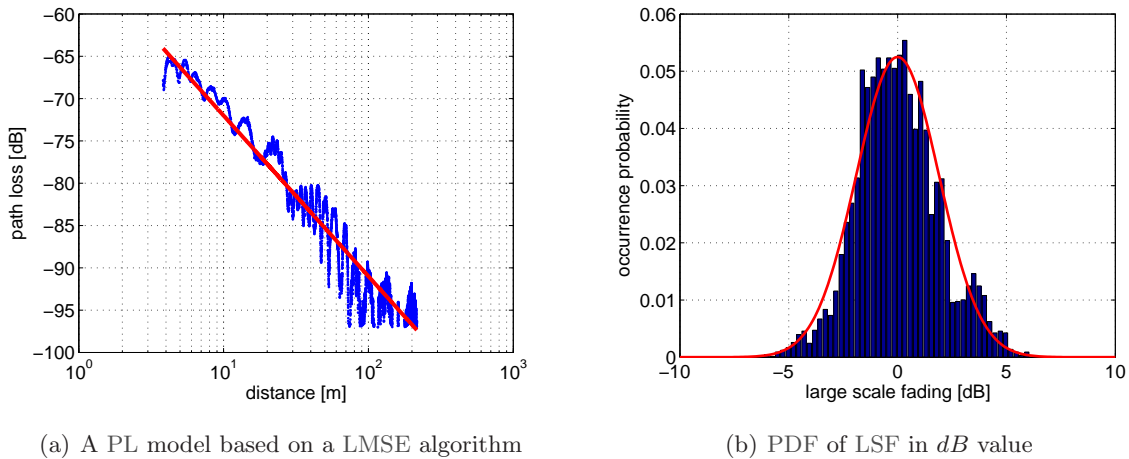


Fig. 3.11: The first method to derive a PL model and the LSF values

Removing the distance dependent PL values from the measured PL values, the remaining is the LSF values. Normally, LSF follows a log-normal distribution in linear value and a normal distribution in dB value [13] [89]. Figure 3.11(b) shows the PDF of LSF in dB value. In the same figure, a normal distribution with the same variance is plotted. A good agreement between them can be observed.

The second way to derive a PL model and the LSF values is based on the different lengths of a ST averaging window. The basic principle of this method is similar with the idea that SSF can be removed by a ST averaging. As expressed in Eqn. 2.9, the PL values from measurement data comprise three factors: the PL model values, LSF, and SSF. After removing of SSF, the rest PL values include the PL model values and LSF. after performing a ST averaging to the rest PL values, LSF can be removed and the PL model values are left [101] [72] [102]. Differed from the first method, no explicit PL model will be returned. This method is specially useful for indoor scenarios. Figure 3.12 shows the LSF results based on a set of example measurement data by using the second method. In Fig. 3.12(a), the points show the measured PL values after a ST averaging, while the gray curve stands for the explicit PL model values after an 8 [m] averaging. The 8 [m] averaging window is identical as 500 snapshots in snapshot sense, and $140\lambda_{WL}$ in wave sense [72] [101] [6] [3]. After removing the PL model values from the measured PL values, LSF is left. Figure 3.12(b) shows the distribution of the LSF values in dB value. A good agreement between a normal distribution and the distribution of the LSF values can be observed.

- XPR

According to the definition of XPR in Subsection 2.5, three values can be computed: XPR_H , the power ratio between the HH co-polar and the HV cross-polar, XPR_V , the power ratio

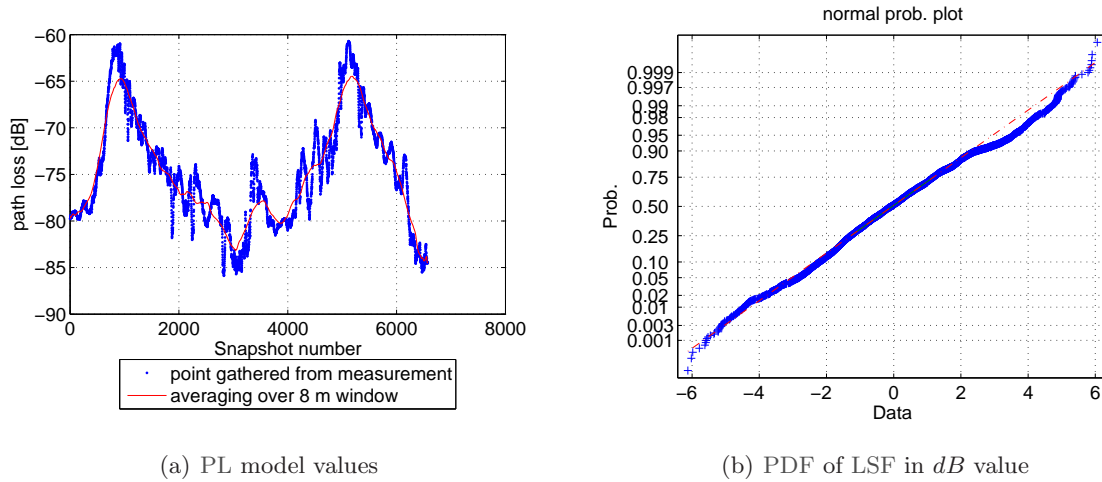


Fig. 3.12: The second method to derive the LSF values

between the VV co-polar and the VH cross-polar, and XPR , the power ratio between the $HH + VV$ co-polars and the $HV + VH$ cross-polars. All these three XPR values can be computed from the measured PL values [36]. The last one is used in this dissertation.

- K-factor

A wideband CIR is at first summed up in the delay domain to get a narrowband time varying CIR. Thereafter, the K-factor value can be derived by using the moment method introduced in [103].

Since the antenna beam pattern is embedded in both $\mathbf{H}_{\widetilde{n_{ss} \times n_{Tx} \times n_{Rx} \times n_f}}$ and $\mathbf{h}_{\widetilde{n_{ss} \times n_{Tx} \times n_{Rx} \times \tau_{max}}}$, the parameters from the frequency domain and from the delay domain depend on the beam pattern of the measurement antenna arrays used.

3.4.3 The impact of the setting parameters on the LSP values

As shown in Fig. 3.10, the LSP values are extracted from the mean PDP which is the product after a ST averaging and after removing measurement noise. Therefore, the mean PDP varies, depending on two setting parameters: the length of a LSA and a noise cut level. As a consequence, the channel parameters extracted from the mean PDP may change. In detail, the setting parameters include different noise cut levels, different lengths of a LSA, and different overlapping ratios of the ST averaging windows. Their impacts on the LSP values are studied both for a LOS propagation condition and a NLOS propagation condition because different propagation environments may have different spans of a LSA. Two of the defined LSP, PL and DS, are exploited as example parameters. Both LOS and NLOS propagation conditions are selected from the measurement campaign with a 10 [m] BS height in Ilmenau city, being detailed described in Subsection 3.3.2.

3.4.3.1 Different noise cut levels

As shown in Fig. 2.6, a cut level, together with an estimated measurement noise level, will be considered as the threshold to distinguish real propagation signals from noise signals. The noise

cut level selected varies from 3 [dB] to 12 [dB] with a step of 3 [dB].

The cdf curves of PL and DS with different noise cut levels in a LOS propagation condition and in a NLOS propagation condition are shown in Fig. 3.13(a) and in Fig. 3.13(b), respectively. It is observed from Fig. 3.13(a) and Fig. 3.13(b) that different noise cut levels have only an impact on PL in the NLOS propagation. In the NLOS propagation, the larger the noise cut level, the larger the PL values. The difference between the LOS propagation and the NLOS propagation comes from a LOS path. In a LOS scenario, the LOS path has a more significant contribution to the PL value than the rest MPCs. Even though increasing noise cut level leads to removing some real MPCs, having small power, their contribution to the total PL is too small to be included. Therefore, the PL value stays almost the same due to the strong LOS path. In a NLOS scenario, the PL values will increase if a noise cut level increases. The reason is that, due to the disappearance of a LOS path, the possibility is very high that the noise signal could be considered as MPCs in the case of a high noise cut level. It is found both in Fig. 3.13(a) and in Fig. 3.13(b) that increasing noise cut level results in a parallel shifting of the cdf curve of DS. The larger the noise cut level, the smaller the DS values are. The reason is that DS is a power weighted delay variable. Thus, it depends both on the delay and on the power of MPCs. Normally the MPCs with a small power have a large delay. As noise cut level increases, more MPCs, having small power, are treated as noise. However, these MPCs usually have a large delay. Therefore, removing these MPCs leads to a reduction of the DS value.

Based on these observations, it is reasonable to choose 9 [dB] as a noise cut level both for LOS and NLOS propagations in the further processing.

3.4.3.2 Different lengths of a ST averaging window and different overlapping ratios

As discussed in [49], a LSA is defined as the absolute area of the movement of a MS, where the local stationarity of propagation channels holds the same. Within one LSA, a channel shows a small scale propagation phenomenon. Averaging over a LSA can remove the small scale effect and meantime keep large scale characteristics. The length of a LSA varies, depending on propagation environments and propagation conditions (LOS and NLOS). Different lengths of a ST averaging window ($0, 10\lambda_{WL}, 20\lambda_{WL}, 30\lambda_{WL}, 40\lambda_{WL}$) with different overlapping ratios (0, 0.25, 0.5, 0.75) are considered in the processing of measurement data in the LOS and NLOS propagations.

- Different ST averaging windows

Figure 3.14(a) shows the cdf results of PL and DS with different ST averaging windows but without overlapping for the LOS propagation while Fig. 3.14(b) depicts the results for the NLOS propagation. The results show that the cdf results of PL and DS in the LOS and NLOS propagations are similar even though different ST averaging windows are used. The reason is that a spatial averaging over all MIMO sub-channels has been performed before a ST averaging. As shown in Table 3.3, one MIMO snapshot includes 3088 sub-channels in the U1/U2 measurement campaign and 784 sub-channels in the I1 measurement campaign. This means, a spatial averaging over sub-channels within one snapshot can remove majority of the small scale effect. The single impact is that the smaller the averaging window, the more PL/DS values can be returned, and consequently, the smoother the cdf curves are.

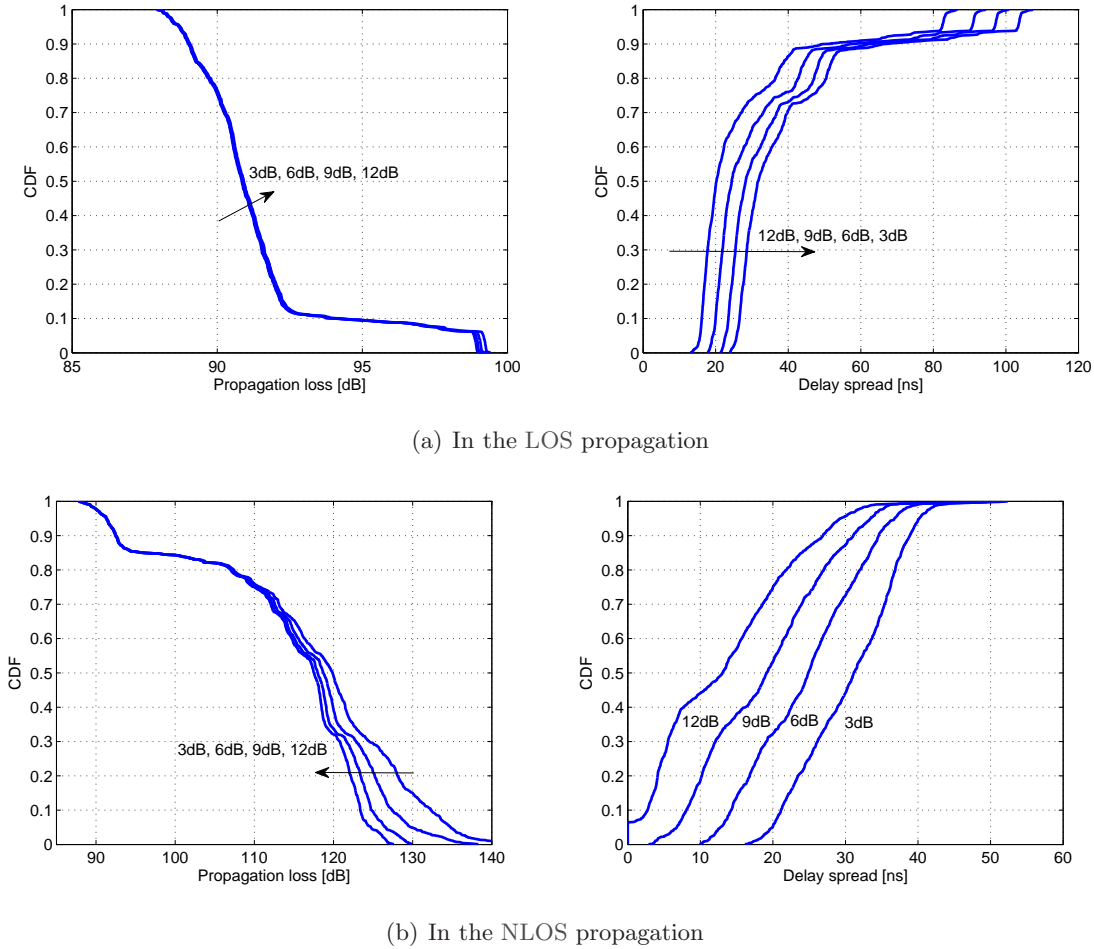


Fig. 3.13: Impact of a noise cut level on the cdf curves of PL and DS in the LOS and NLOS propagations

- Different overlapping ratios

Figure 3.15(a) shows the cdf results of PL and DS with different overlapping ratios in the LOS propagation, while Fig. 3.15(b) presents the results in the NLOS propagation. The length of a ST averaging window is $20\lambda_{WL}$. The results show that the cdf curves of PL and DS in the LOS and NLOS propagations are very similar even though different overlapping ratios are used. The single impact is that the larger the overlapping ratio, the more values can be returned, and consequently, the smoother the cdf curves are.

The above observation indicates that the small scale propagation effect can be significantly removed after a spatial averaging over all MIMO sub-channels within one snapshot. Thus, an averaging length $10\lambda_{WL}$ without overlapping is used in the further processing.

3.4.4 Extraction methodology of the correlation models of LSP

By using the methods described in Subsection 3.4 and the parameters defined in Subsection 3.4.3, the LSP values can be calculated from measurement data. The simplest way is to use Eqn. 2.19 and Eqn. 2.21 in Subsection 2.5 to get the correlation models. Based on the correlation models, the LSP

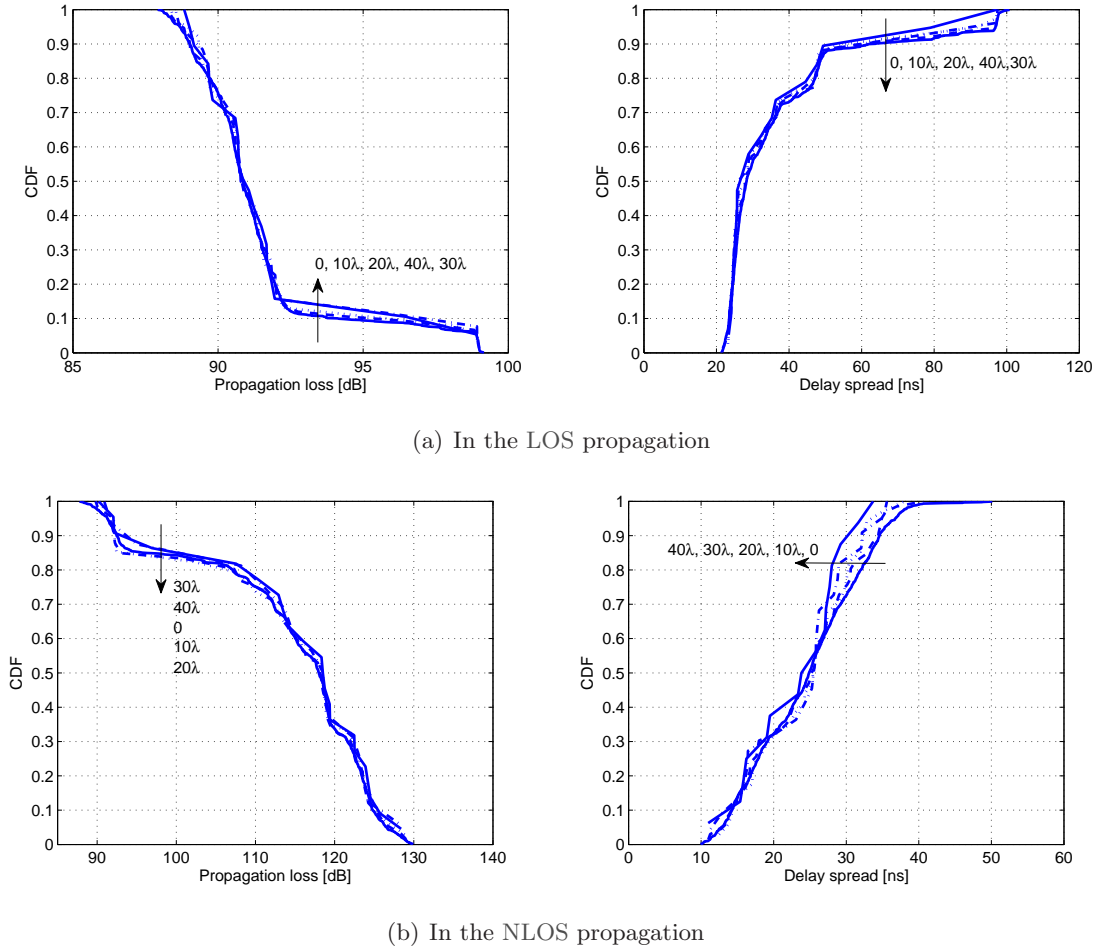
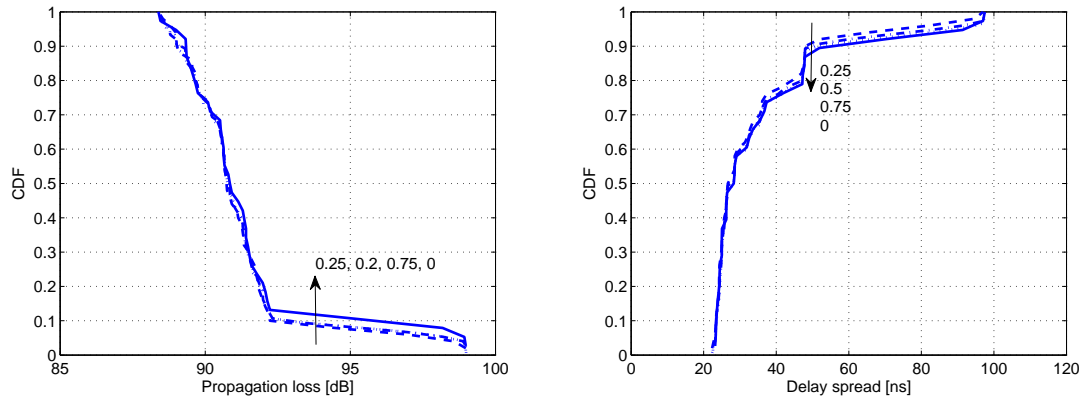


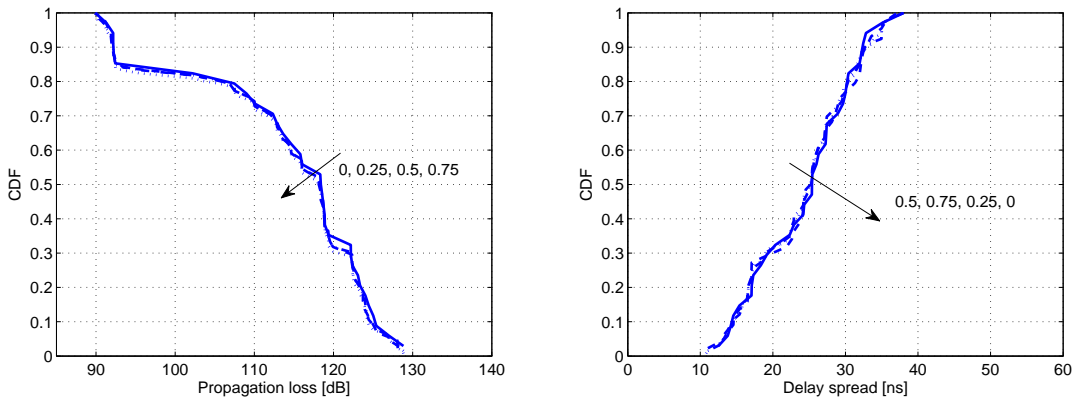
Fig. 3.14: Impact of a ST averaging window on the cdf curves of PL and DS in the LOS and NLOS propagations

values can be reproduced in a channel simulation procedure. Section 2.6 has stated the reproduction algorithms. The reproduction procedure is shown in Fig. 3.16 which is based on i.i.d Gaussian variables with a zero mean value and a unit standard variance. Because introducing correlation in the i.i.d Gaussian variables will not change the first-order statistical property of LSP, the final LSP values in the reproduction procedure are the colored Gaussian variables with a zero mean value and a unit standard variance. These reproduced LSP are expected to have the same statistical properties as the LSP computed from measurement data. However, LSP from measurement data may not be Gaussian-distributed variables with a zero mean value and a unit standard variance. To bridge the gap between the modeling procedure and the reproduction procedure, two key steps, transformed Gaussian distributed LSP and then normalized Gaussian distributed LSP, are introduced into the modeling procedure as shown in Fig. 3.16.

Through the step, transformed Gaussian distributed LSP, the LSP values extracted directly from measurement data are transformed to be Gaussian distributed values. Therefore, it is crucial in the modeling procedure to find a mathematic function $f(LSP)$ which can map the original values of each LSP to Gaussian distributed values. Furthermore, $f(LSP)$ should be a one-to-one mapping function due to the bi-directionality between the modeling procedure and the reproduction



(a) In the LOS propagation



(b) In the NLOS propagation

Fig. 3.15: Impact of the overlapping ratio on the cdf curves of PL and DS in the LOS and NLOS propagations

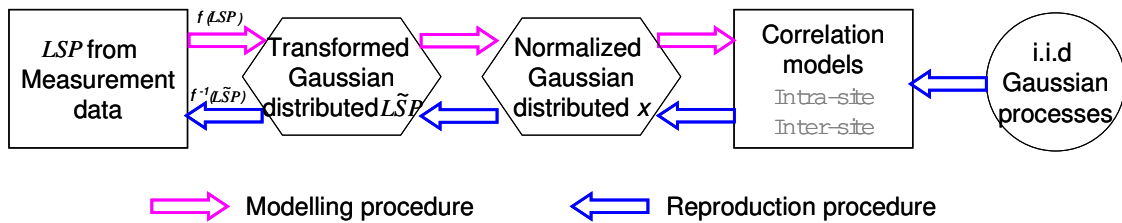


Fig. 3.16: Unified modeling and reproduction procedures

procedure. The step, transformed Gaussian distributed LSP, outputs Gaussian distributed values of each LSP are returned. The next step is normalized Gaussian distributed LSP values. This step aims at transforming the outputs of the previous step to be normalized Gaussian values. After the second step, the values of each LSP are Gaussian distributed with a zero mean value and a unit standard variance. These outputs statistically agree with the outputs of the reproduction procedure: colored Gaussian variables with a zero mean value and a unit standard variance.

In the reproduction procedure, the same steps will be conducted with an inverse function to the modeling procedure as shown in Fig. 3.16. The process described in Section 2.6 outputs the colored Gaussian distributed LSP values with a zero mean value and a unit standard variance. Then, the experimental mean value and standard variance are introduced. Thereafter, the output is mapped to the original values from measurement data by the inverse function $f^{-1}(LSP)$.

In the following, an example is exploited to explain the method described above in detail. LSF is used as the example LSP. The LSF values from measurement data are usually log-normal distributed. Thus, the function

$$f(LSF) = 10 \log_{10}(LSF) \quad (3.3)$$

is used to map the LSF values from a log-normal distribution to a Gaussian distribution in the modeling procedure. Furthermore, $f(LSF)$ is a one-to-one mapping function. After using $f(LSF)$ to each LSF value, a Gaussian-distributed \widetilde{LSF} , having a mean value $\mu_{\widetilde{LSF}}$ and a variance $\sigma_{\widetilde{LSF}}^2$, will be returned. It can be expressed as

$$\widetilde{LSF} = \sigma_{\widetilde{LSF}} \times x + \mu_{\widetilde{LSF}}, \quad (3.4)$$

where x is a Gaussian distributed variable with a zero mean value and a unit standard variance. Therefore, the following function

$$f(\widetilde{LSF}) = \frac{\widetilde{LSF} - \mu_{\widetilde{LSF}}}{\sigma_{\widetilde{LSF}}} \quad (3.5)$$

is used to transform \widetilde{LSF} to be a Gaussian distribution with a zero mean value and a unit standard variance. The normalized Gaussian distributed values x are fed to Eqn. 2.19 and Eqn. 2.21 as inputs for the further correlation modeling.

In the reproduction procedure, the process described in Section 2.6 outputs x values after filtering. The x values are then transformed to the original values from measurement data by using at first the inverse functions

$$\widetilde{LSF} = \sigma_{\widetilde{LSF}} \times x + \mu_{\widetilde{LSF}}, \quad (3.6)$$

and then the inverse function

$$LSF = f^{-1}(\widetilde{LSF}) = 10^{\frac{\widetilde{LSF}}{10}}. \quad (3.7)$$

3.5 Experimental results

By using the extraction methodology addressed in Subsection 3.4, the experimental results of LSP are obtained from the measurement data of different measurement campaigns. The experimental

stochastic properties of LSP are presented in this Section. Subsection 3.5.1 deals with the results for the urban scenarios (U1 and U2) while Subsections 3.5.2 highlights the results for the indoor corridor scenario I1.

3.5.1 Micro-cell to macro-cell urban scenarios (U1 and U2)

This Subsection focuses on the statistical experimental results of LSP both in the LOS propagation and in the NLOS propagation. Sub-subsection 3.5.1.1 shows the statistical distribution of LSP and their transform functions; Sub-subsection 3.5.1.2 deals with the intra-site auto- and cross-correlation; Sub-subsection 3.5.1.3 highlights on the inter-sector correlation properties; and Sub-subsection 3.5.1.4 presents the results of the inter-site correlation properties.

3.5.1.1 Statistical distribution of LSP

Figure 3.17 shows the cdf curves of LSP based on measurement data in the LOS and NLOS propagations. As stated in Subsection 3.3.2 that the height of the BS antenna array varies from 10 [m] to 16 [m] during the measurement campaign. As a consequence, the scenario changes from U1 to U2. Therefore, Fig. 3.17 reveals the dependence of the LSP distributions on the BS height.

It is observed from Fig. 3.17 that, in the LOS propagation, the higher the BS antenna array, the higher the LSF, DS, AS_{MS} , and ES_{MS} values, whereas, the lower the K-factor, XPR, NPCG, and AS_{BS} values. In the NLOS propagation, the higher the BS antenna array, the higher the LSF, DS, NPCG, AS_{MS} , and ES_{MS} values, whereas, the lower the XPR values. However, the height of the BS antenna array has almost no impact on the DW values both in the LOS and NLOS propagations and has a minor impact on the AS_{BS} values in the NLOS scenario. The reason is that the propagation between a BS and a MS varies from a two-ring or ellipse model to a one-ring model [104] [76] ifn the BS antenna array goes from below rooftop to above rooftop. As the BS antenna array is below rooftop, both the BS and the MS are surrounded by local objects like buildings, and traffic lights. The wave propagation between the MS and the BS interacts with these objects. Then, a two-ring or ellipse model is formed with the BS and the MS being two centers of two rings or two foci of the ellipse. The geometric range of the two-ring or ellipse model is limited by the local objects. As the BS height increases, the number of the local objects around the BS decreases. In an extreme case, there is no object around the BS if the BS is highly elevated. However, the MS is surrounded by objects which interact with propagation waves. Furthermore, more objects are involved into the propagation even including some far objects. Thus, the propagation between the MS and the BS is a one-ring model with the MS being the center of the ring. The geometric range of the ring goes from the local objects to the far objects. Therefore, the propagation between the BS and the MS includes the MPCs with a long propagation delay. It can not happen in a two-ring or ellipse model. As a consequence, the LSF, DS, AS_{MS} , and ES_{MS} values are increased with an increasing BS height and their cdf curves shift to the right hand side. Simultaneously, the additional MPCs with a long propagation delay lead to the reduction of the K-factor and XPR values.

As stated in Sub-section 3.4.4, a transform function f is required during the modeling procedure, by which the none-Gaussian distributed LSP values extracted directly from measurement data can

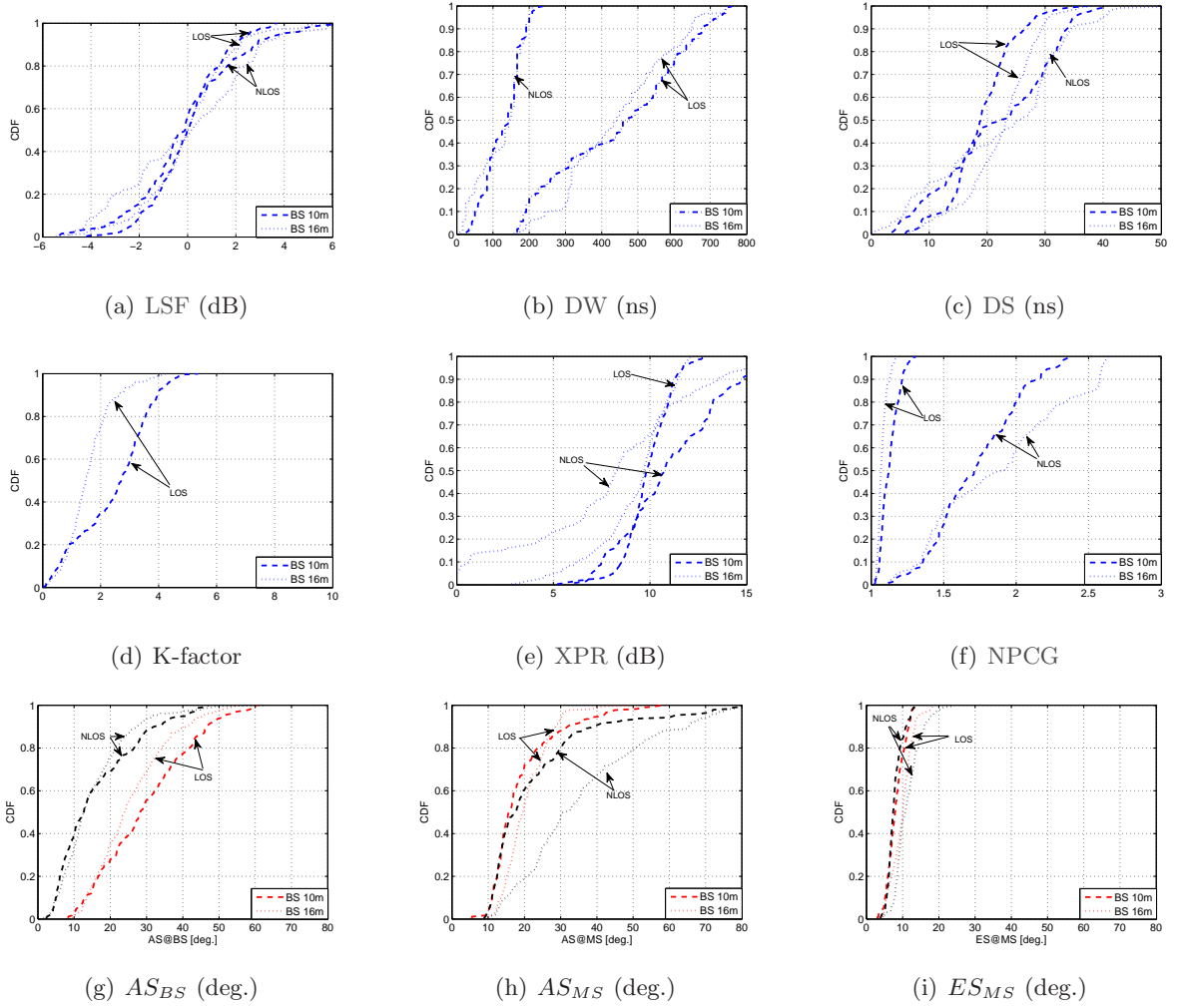


Fig. 3.17: The cdf curves of LSP from the measurement data in the LOS and NLOS propagations with different BS heights

be transformed to be Gaussian-distributed. Figure 3.18 shows the transform process by using K-factor with the BS height being 16 [m] as an example. The dotted curve shows the cdf distribution of the original K-factor values after the post-processing of measurement data. Obviously, the original K-factor values are not Gaussian distributed. After introducing the transform function $f = 10 \log_{10} LSP_K$, the original K-factor values are mapped to the new values, the cdf distribution of which is shown as the dashed curve in Fig. 3.18. The transformed K-factor values can be modeled as a normal distribution with a median value ¹ $\mu = 1.5$ and a variance $\sigma^2 = 3.6^2$. The cdf curve of the modeled normal distribution is shown in Fig. 3.18 as the solid curve. A good agreement can be observed between the transformed cdf curve and the modeled cdf curve. The transformed K-factor values will be used for the further modeling of the correlation properties of LSP. The transform functions f of the rest LSP are shown in Table 3.4. Note that no transformation has been done to two LSP: NPCG and DW, due to the fact that they are not the parameters for the channel modeling purpose but the parameters for the performance assessment purpose.

¹ The median value is defined as the value separating the higher 50% probability distribution and the lower 50% probability.

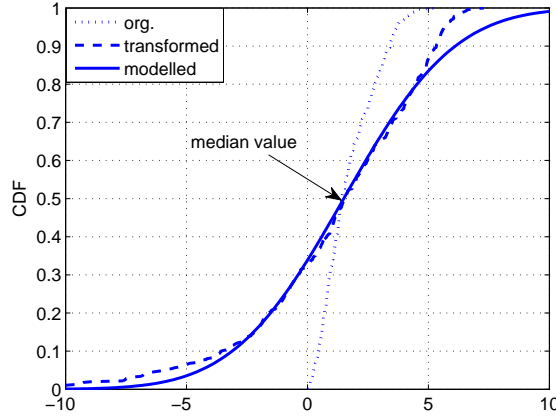


Fig. 3.18: An example to show the transform process of K-factor: the original cdf distribution \rightarrow the transformed cdf distribution \rightarrow the modeled cdf distribution

The median value and the variance of the transformed LSP in the LOS and NLOS propagations are presented in Table 3.4². It is observed in Table 3.4 that the variance of LSF is smaller than what has been reported in literature where the variance of LSF varies from 2 [dB] to 10 [dB] [105] [71] [106]. The reason is that the variance of LSF depends on the size of a measurement area [105]. In a small area, a channel experiences less large scale variation. Therefore, in the investigated small measurement area, smaller variance values can be calculated. Furthermore, it is found from Table 3.4 that the variances of LSF, DS, XPR, NPCG, AS_{BS} , AS_{MS} , and ES_{MS} are larger in the NLOS propagation scenario than in the LOS propagation scenario. However, the variance of DW is smaller in the NLOS propagation. It is due to the disappearance of a LOS path in the NLOS scenario. In the LOS propagation, the LOS path dominates the propagation phenomenon. Even though the rest MPCs change, their influence on the LSP values is not significant. However, in a NLOS propagation, the change of the rest MPCs leads to the change of the LSP values due to the disappearance of a LOS path. Therefore, the variance of LSP is smaller in the LOS propagation than in the NLOS propagation.

3.5.1.2 The intra-site correlation of the transformed LSP

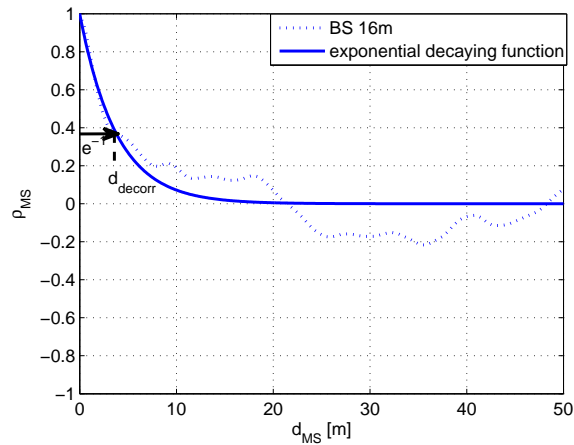
As discussed in Section 2.5, the intra-site auto-correlation of LSP can be modeled as an exponential decaying function of the distance between two MSs. Figure 3.19 shows the intra-site auto-correlation of LSF in the LOS scenario with the 16 [m] BS height. An exponential decaying function is plotted in the same figure. A good agreement between them can be observed. The de-correlation distance introduced in Section 2.5 is used as the key coefficient characterizing the intra-site auto-correlation. The de-correlation distance of the transformed LSF is 3.9 [m] in Fig. 3.19.

Table 3.5 summarizes the de-correlation distance of the transformed LSP in the U1 and U2 scenarios in the LOS and NLOS propagations. The corresponding intra-site auto-correlation curves of the transformed LSP are presented in Fig. 3.20.

² n.a. in Table 3.4 stands for not available. K-factor is a specific channel metric for a LOS propagation according to its definition in Section 2.5. Therefore, the K-factor values are only available for the LOS propagation.

Tab. 3.4: The median value and the variance of the transformed LSP in the U1 and U2 scenarios in the LOS and NLOS propagations

		LSF	DW	DS	K	XPR	NPCG	AS_{BS}	AS_{MS}	ES_{MS}	
		[dB]	[ns]	[ns]	[dB]	[dB]		[deg.]	[deg.]	[deg.]	
Transform func.		no	no	\log_{10}	no	no	no	\log_{10}	\log_{10}	\log_{10}	
Distribution		Norm.	Unif.	Norm.	Norm.	Norm.	Rayl.	Norm.	Norm.	Norm.	
U1	LOS	μ	0	475	1.3	4.3	9.5	1.1	1.45	1.29	0.9
		σ	1.5	184	0.15	4.1	1.5	0.06	0.2	0.12	0.13
	NLOS	μ	0	142	1.4	n.a.	10.8	1.7	1.1	1.25	0.87
		σ	2.3	53	0.3	n.a.	3	0.3	0.38	0.38	0.1
U2	LOS	μ	0	441	1.4	1.7	9.2	1.1	1.38	1.2	1
		σ	1.7	145	0.15	1.8	2.2	0.03	0.18	0.2	0.1
	NLOS	μ	0	150	1.4	n.a.	8.3	1.9	1.1	1.5	1.03
		σ	2.7	67	0.4	n.a.	4.7	0.5	0.28	0.23	0.13

**Fig. 3.19:** An example to show the intra-site auto-correlation of the transformed LSP: the original intra-site auto-correlation \rightarrow model with an exponential decaying function with the de-correlation distance being 3.9 [m]**Tab. 3.5:** The de-correlation distance of the transformed LSP in the U1 and U2 scenarios in the LOS and NLOS propagations

	d_{decorr} [m]	LSF	DW	$\log_{10}(DS)$	K	XPR	NPCG	AS_{BS}	AS_{MS}	ES_{MS}
U1	LOS	2	23	8	20.1	2	6.6	1	3.8	2.5
	NLOS	1	8.3	8.5	n.a.	4	5.4	2.2	9.6	1
U2	LOS	3.9	29.6	31	2.8	2.4	6.6	1	1	3.5
	NLOS	4.4	6.6	7.5	n.a.	4	7.4	3.5	1	3.5

It is observed both from Table 3.5 and from Fig. 3.20 that the higher the BS antenna array, the larger the de-correlation distances of the transformed LSP except K-factor and AS_{MS} . This means that increasing the BS height leads to a higher similarity between the radio channels of two MSs belonging to the same BS. The reason is that more common scatters are involved in the propagation as the BS becomes higher. As a consequence, there are more common paths between propagation links from two MSs to the same BS. Thereafter, the intra-site auto-correlation is increased.

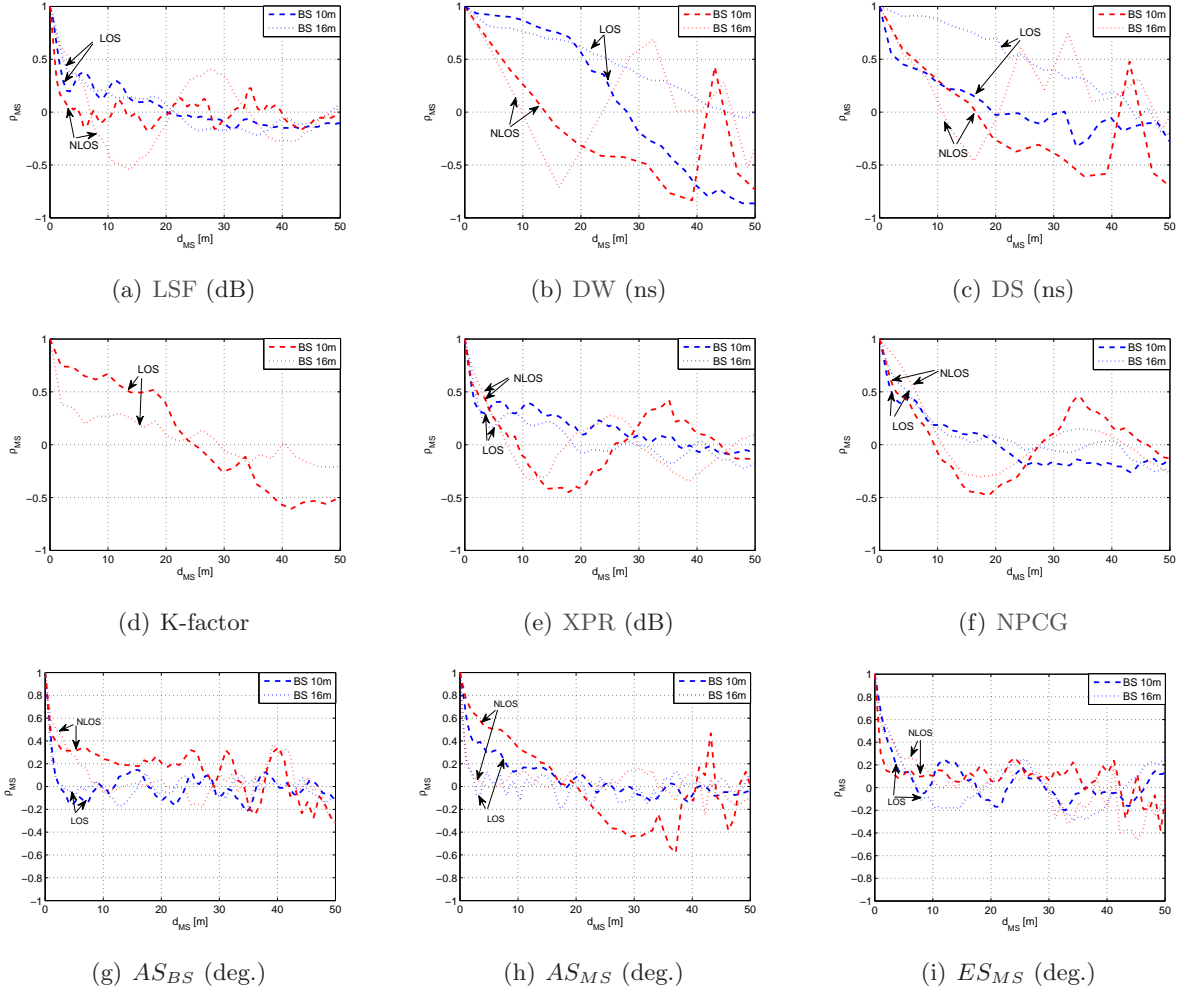


Fig. 3.20: The intra-site auto-correlation of the transformed LSP in the U1 and U2 scenarios in the LOS and NLOS propagations

After the discussion of the intra-site auto-correlation of the transformed LSP, Table 3.6 shows the intra-site cross-correlation of the transformed LSP in the U1 and U2 scenarios in the LOS and NLOS propagations. It is observed from Table 3.6 that in the LOS scenario, LSF has a positive correlation with XPR but a negative correlation with DW, DS, NPCG, and AS_{MS} . In the NLOS scenario, DW and DS have a positive correlation with LSF and AS_{MS} , but a negative correlation with XPR, NPCG, AS_{BS} , and ES_{MS} . The reason is that in the LOS scenario, as the LSF value increases, it means that the LOS path becomes to be the dominating path compared with the rest MPCs. Then, more energy will be transmitted over the co-polarized LOS path. As a consequence, the XPR values increase while the DW, DS, NPCG, and AS_{MS} values decrease. In the NLOS scenario, the multipath components become more important due to the disappearance of a LOS path. When

Tab. 3.6: The intra-site cross-correlation of the transformed LSP in the U1 and U2 scenarios in the LOS and NLOS propagations

LSP pair	Scenario			
	LOS		NLOS	
	U1	U2	U1	U2
LSF& DW	0.1	0	0	0.24
LSF& DS	-0.2	-0.14	-0.3	0
LSF& K	0.22	0	n.a.	n.a.
LSF& XPR	0.67	0.69	-0.18	-0.46
LSF& NPCG	-0.3	-0.43	-0.38	-0.3
LSF& AS_{BS}	0	0	0.16	-0.51
LSF& AS_{MS}	-0.2	-0.1	0.1	0.1
LSF& ES_{MS}	0.32	0.27	-0.1	-0.52
DW & DS	0.32	0.87	0.86	0.85
DW & K	0.8	0.33	n.a.	n.a.
DW & XPR	0	-0.43	-0.58	0.22
DW & NPCG	0.54	0.17	-0.77	-0.88
DW& AS_{BS}	0	-0.12	-0.19	-0.28
DW& AS_{MS}	-0.26	0.12	0.6	0.23
DW& ES_{MS}	0.59	0.4	-0.19	-0.42
DS & K	0.19	0.37	n.a.	n.a.
DS & XPR	-0.4	-0.47	-0.4	0.42
DS & NPCG	0.57	0.32	-0.57	-0.69
DS& AS_{BS}	0	-0.18	-0.29	-0.1
DS& AS_{MS}	0.31	0.29	0.55	0.32
DS& ES_{MS}	0.28	0.27	-0.13	-0.29
K & XPR	0	-0.19	n.a.	n.a.
K & NPCG	0.37	0.37	n.a.	n.a.
XPR& NPCG	-0.47	-0.36	0.6	-0.25
XPR& AS_{BS}	-0.1	0	-0.1	0.17
XPR& AS_{MS}	-0.22	-0.17	-0.3	-0.13
XPR& ES_{MS}	0.1	-0.12	0	-0.12
NPCG& AS_{BS}	0	0	0.22	0.55
NPCG& AS_{MS}	0.16	0.26	-0.55	-0.14
NPCG& ES_{MS}	0.36	0.26	0.27	0.49
AS_{BS} & AS_{MS}	-0.28	-0.15	-0.25	0.24
AS_{BS} & ES_{MS}	-0.15	-0.26	0.31	0.17
AS_{MS} & ES_{MS}	0	0.35	0	0.15

the LSF values increase, more MPCs are involved in the propagation. As a consequence, the DW, DS, and AS_{MS} values increase. However, due to the reflection/diffraction/refraction propagation phenomena of the MPCs, there exist many cross-polarized paths. Then, the XPR, AS_{BS} , and ES_{MS} values decrease.

From Table 3.6 it has been observed that the intra-site cross-correlation of the transformed LSP shows no obvious dependence on the BS height.

Tab. 3.7: The inter-sector correlation of the transformed LSP in the U1 and U2 scenarios

BS param.	h_{BS}	Angle	LSF	DW	DS	XPR	NPCG	AS_{BS}	AS_{MS}	ES_{MS}
	[m]	[deg.]	[dB]	[ns]		[dB]				
$\langle BS2, BS5 \rangle$	10	$\theta_{BS2} \cap \theta_{BS5}$	0.49	0.72	0.12	-0.42	0.8	n.a.	n.a.	n.a.
$\langle BS2, BS5 \rangle$	10	$\theta_{BS2} \cap \theta_{BS5}$	0.81	0.97	0.78	0.84	0.88	0	0.15	0.55
$\langle BS3, BS6 \rangle$	16	$\theta_{BS3} \cap \theta_{BS6}$	0.27	0.35	0.29	0.28	0.8	n.a.	n.a.	n.a.
$\langle BS3, BS6 \rangle$	16	$\theta_{BS6} \cap \theta_{BS3}$	0.24	0.78	0.48	-0.28	-0.33	0.37	0.18	0.56
$\langle BS3, BS6 \rangle$	16	$\theta_{BS3} \cap \theta_{BS6}$	0.85	0.95	0.84	0.88	0.91	-0.15	0.26	0.51

3.5.1.3 The inter-sector correlation of the transformed LSP

As explained in Subsection 3.3.2 that the BS antenna array at the same position has been set to two orientations, of which the angle of the overlapped area is 90 [deg.], $\theta_{OL} = 90$ [deg.].

Table 3.7 shows the experimental results of the inter-sector correlation. The sector pair $\langle BS2, BS5 \rangle$ has a 10 [m] BS height while the sector pair $\langle BS3, BS6 \rangle$ has a 16 [m] BS height. It is found in Table 3.7 that the transformed LSP except AS_{BS} and AS_{MS} are highly correlated with correlation coefficient around 0.8 in the overlapped area. Furthermore, in the overlapped area, the inter-sector correlation of the transformed LSP with a 16 [m] BS height is a little bit higher than that with a 10 [m] BS height. The reason is that more common scatters will be involved in the propagation as the BS antenna array becomes higher. As a consequence, the similarity in the propagation from two different sectors in the overlapped area is increased. However, the inter-sector correlation could not be one, even though in the overlapped area where two sectors have main beam. The fact is that a MS can still receive the signal coming from one sector's main beam but outside the overlapped area by reflection/diffraction/refraction. This signal reflected/diffracted/refracted by the objects outside the overlapped main beam area leads to the reduction of the inter-sector correlation. The larger the ratio of the overlapped main beam area to the whole main beam width of two sectors, namely $\frac{\theta_{OL}}{\theta_{s1}}$ assuming $\theta_{s1} = \theta_{s2}$, the larger the inter-sector correlation. The inter-sector correlation could be one if and only if two sectors are fully overlapped to each other.

In the areas where only one sector has the main beam: $\theta_{BS2} \cap \overline{\theta_{BS5}}$, $\theta_{BS3} \cap \overline{\theta_{BS6}}$, and $\theta_{BS6} \cap \overline{\theta_{BS3}}$, the inter-sector correlation of the transformed LSP is around 0.3. Some of the transformed LSP have even a negative inter-sector correlation.

3.5.1.4 The inter-site correlation of the transformed LSP

Rit is proposed that the inter-site correlation is a function of d_{diff} (the distance difference between two links), θ (the angle of arrival difference from two BSs/RSs to the same MS), d_{BS} (the distance between two BSs/RSs), and h_{diff} (the height difference between two BSs/RSs). The experimental results of the inter-site correlation of the transformed LSP³ between pairs of BSs/RSs has been summarized in Table 3.8. It can be observed that:

- High inter-site correlation of the transformed LSP can be observed between RS1 and RS3.

³ The values of K-factor, AS_{BS} , AS_{MS} , and ES_{MS} are not included in the investigation of the inter-site correlation

Tab. 3.8: The inter-site correlation of the transformed LSP in the urban U1 and U2 scenarios

BS param.	d_{BS}	$\min(d_{1,2})$	$\max(d_{1,2})$	d_{diff}	θ	LSF	DW	DS	XPR	NPCG
	[m]	[m]	[m]	[dB]	[deg.]					
$\langle RS1, RS3 \rangle$	6	22	107	[-0.7 0]	[0 16]	0.37	0.94	0.59	0.68	0.85
$\langle RS1, BS3 \rangle$	77	16	154	[-7 0]	[4 140]	0.12	-0.1	-0.1	0.27	0.1
$\langle RS3, BS3 \rangle$	73	16	177	[-7 0]	[4 140]	0.16	-0.2	-0.3	0	0.1
$\langle RS2, BS5 \rangle$	83	9	87	[-10 0]	[60 180]	0.43	-0.8	0.63	0.1	-0.2
$\langle RS2, BS6 \rangle$	83	9	100	[-10 0]	[55 170]	0.38	-0.28	0.56	0.18	-0.2

As shown in Fig. 3.4 and in Table 3.8, RS1 and RS3 are near to each other with $d_{BS} = 6$ [m] $< \min(d_{1,2})$ ⁴. Furthermore, θ is smaller than 16 [deg.] and h_{diff} is zero. This means that both RS1 and RS3 see a very similar propagation environment to the MS. Thus, it is not surprising that they have a high inter-site correlation;

- The transformed LSP, LSF, DW, and DS, are highly correlated for the BS pairs $\langle RS2, BS5 \rangle$ and $\langle RS2, BS6 \rangle$. The small change of the inter-site correlation from the BS pair $\langle RS2, BS5 \rangle$ to the BS pair $\langle RS2, BS6 \rangle$ indicates that the inter-site correlation depends on the height difference between two BSs/RSs, namely h_{diff} . The larger the height difference, the smaller the inter-site correlation is. The reason is that two BSs will see different scatters in wave propagations if they have different heights. As a consequence, two inter-site links have different large scale propagation phenomenon and the inter-site correlation decreases;
- There is almost no correlation for the BS pairs $\langle RS1, BS3 \rangle$ and $\langle RS3, BS3 \rangle$ even though θ is as small as 4 [deg.] for some MS routes. It is due to the height difference between two BSs/RSs, namely h_{diff} . As presented in Subsection 3.3.2, the height of BS3 is 16 [m] while the heights of RS1 and RS3 are 3 [m]. The propagation between the BS3 and the MS is a macro-cell propagation where some far objects may be involved. However, the propagation between the RS1/RS3 and the MS is a micro-cell propagation where only local objects are involved;

Based on these observations it can be concluded that a high inter-site correlation can happen in two cases:

1. $d_{diff} \rightarrow 0$, $\theta \rightarrow 0$, $d_{BS} < \min(d_{1,2})$, and $h_{diff} \rightarrow 0$;
2. $\theta \rightarrow 180$, $d_{BS} > \max(d_{1,2})$, and $h_{diff} \rightarrow 0$. If θ approaches 180, the inter-site correlation of DW is negative.

It means that the DW values of one BS/RS decrease while the DW values of another BS/RS increase as a MS moves from one BS/RS to another BS/RS. In other case, the inter-site correlation of the transformed LSP is very small and can be almost ignored in the modeling procedure.

After a rough discussion about the BS-wise inter-site correlation of the transformed LSP based on the results in Table 3.8, following we focus on the detailed dependence of ρ_{BS} on $\langle d_{diff}, \theta \rangle$ ⁵ by

⁴ $d_{1,2}$ stands for d_1, d_2

⁵ h_{diff} and d_{BS} are not included due to the lack of statistical values of d_{BS} and h_{diff} since only 3 h_{diff} values and 4 d_{BS} values are available.

gathering data from all BS pairs. Figure 3.21 shows the experimental results. Weitzen doubt in his paper [72] the experimental results of the inter-site correlation of LSF in the previous work [68]. In his paper he argued that the experimental results in [68] is not plausible because no enough data has been used for the modeling purpose. Therefore, a large number of data is the prerequisite for a reliable modeling of the inter-site correlation properties of the transformed LSP. To show the plausibility of the experimental results in Fig. 3.21, Fig. 3.21(a) shows the number of samples for each $\langle d_{diff}, \theta \rangle$ grid point. The smallest number of samples is 63 at the grid point $\langle d_{diff} = -6, \theta = 38 \rangle$ while the grid point $\langle d_{diff} = -0.4, \theta = 5 \rangle$ has the largest number of samples (= 579). Comparing Fig. 3.21(b), 3.21(c), 3.21(d), 3.21(e), and 3.21(f), it is found that the grid point $\langle d_{diff} = -0.4, \theta = 5 \rangle$ has the largest inter-site correlation coefficient for all transformed LSP. If the d_{diff} value is fixed, the inter-site correlation coefficient of DW decreases monotonously with an increasing θ . Furthermore, the inter-site correlation coefficient of other transformed LSP tends to decrease, but not monotonously. Generally speaking, a large θ value results in a small inter-site correlation coefficient of the transformed LSP. If the θ value is fixed, no clear change tendency of the inter-site correlation coefficient has been observed for all LSP with an increasing d_{diff} . This means that the inter-site correlation is independent on the d_{diff} value.

3.5.2 Indoor corridor scenario I1

The experimental results of the indoor corridor measurement campaign are shown in this Subsection [2] [3]. Sub-subsection 3.5.2.1 addresses the statistical distributions of LSP; Sub-subsection 3.5.2.2 deals with the intra-site auto- and cross-correlation; Sub-subsection 3.5.2.3 highlights the results of the inter-sector correlation; and finally Sub-subsection 3.5.2.4 presents the results of the inter-site correlation properties.

3.5.2.1 Statistical distribution of LSP

Table 3.9 summarizes the media value and the variance of the transformed LSP in the I1 indoor corridor scenario for the LOS and NLOS propagations. Note that the second method described in Section 3.4 has been used to derive the LSF values from the I1 measurement data. It is observed from the table that the mean value of K-factor is larger in the indoor LOS scenario than in the urban U1 and U2 LOS scenarios by comparing Table 3.9 with Table 3.4. This is due to the rich MPCs in an urban scenario. In the indoor corridor scenario, the number of scatters is limited due to the building layout. As a consequence, the number of the MPCs is limited. Furthermore, it is found in Table 3.9 that LSP including LSF, DS, and XPR as well as NPCG, have a larger variance in the NLOS propagation than in the LOS propagation. It is due to the disappearance of a LOS path in the NLOS propagation.

3.5.2.2 The intra-site correlation of the transformed LSP

Table 3.10 shows the de-correlation distance of the transformed LSP in the indoor corridor LOS and NLOS scenarios. It is found that the de-correlation distance of the transformed LSP is in the

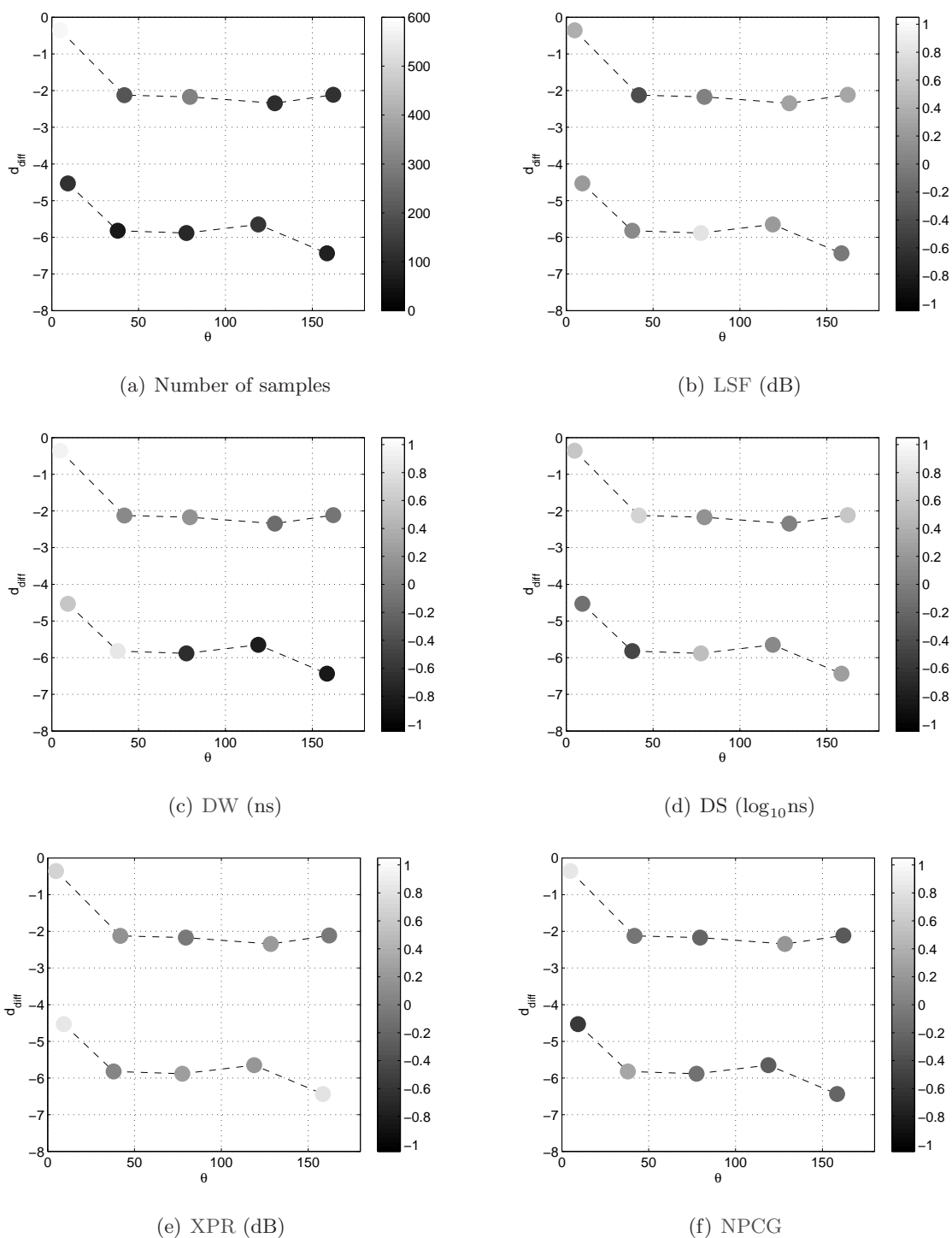


Fig. 3.21: The dependence of the inter-site correlation of the transformed LSP on $\langle d_{diff}, \theta \rangle$ in the urban U1 and U2 scenarios

Tab. 3.9: The median value and the variance of the transformed LSP in the I1 scenario in the LOS and NLOS propagations

	LSF	DW	$\log_{10}(\text{DS})$	K	XPR	NPCG	
	[dB]	[ns]	[ns]	[dB]	[dB]		
Distribution	Normal	Uniform	Normal	Normal	Normal	Rayleigh	
LOS	μ	0	200	1.15	5	11	1.2
	σ	2.6	67	0.17	2.3	1.3	0.1
NLOS	μ	0	99	1.19	n.a.	10	1.7
	σ	4.6	46	0.28	n.a.	2.6	0.4

Tab. 3.10: De-correlation distance of the transformed LSP in the I1 scenario in the LOS and NLOS propagations

d_{decorr} [m]	LSF	DW	$\log_{10}(\text{DS})$	K	XPR	NPCG
LOS	0.8	2.1	1.2	0.5	2.7	3.2
NLOS	3	5.6	4.5	n.a.	1.6	3.3

oder of few meters, which is in line with the results presented in [2] [3]. The small de-correlation distance indicates that LSP change very fast as a MS moves. This means that the LSP values can be treated to be uncorrelated if the distance between two MSs is larger than 3 [m].

Table 3.11 shows the intra-site cross-correlation of the transformed LSP in the indoor corridor LOS and NLOS scenarios. It is observed from the table that there exists a high negative correlation between LSF and DS in the LOS propagation. Furthermore, it is observed that in the I1 LOS scenario, LSF has a negative correlation with DW, DS, and NPCG, but a positive correlation with XPR and K-factor. In the I1 NLOS scenario, LSF has a positive correlation with DW and DS, but a negative correlation with XPR and NPCG.

3.5.2.3 The inter-sector correlation of the transformed LSP

Table 3.12 shows the experimental results of the sector pair $\langle BS2, BS3 \rangle$ and the sector pair $\langle BS7, BS8 \rangle$. It is found that the correlation properties between $\theta_{BS2} \cap \overline{\theta_{BS3}}$ and $\theta_{BS8} \cap \overline{\theta_{BS7}}$, between $\theta_{BS2} \cap \theta_{BS3}$ and $\theta_{BS7} \cap \theta_{BS8}$, are very similar. It is due to the symmetric layout of the building as shown in Fig. 3.6. In the overlapped area, it is found that LSP except DW are almost un-correlated. The reason is that the overlapped area is out of the main beam of both sectors. Furthermore, a high correlation of DW, DS, and XPR has been observed to the area where only one BS from BS2 and BS3 has main beam. The reason is that in the area where only one sector for example BS2 has main beam while BS3 points to the opposite direction, a MS can still get strong signal from BS3 due to the reflection. In the direction where BS3 points, there exist several metallic room signs. These objects will reflect BS3's signal back to the corridor where BS2 points with main beam. Therefore, seen from the MS, both BS2 and BS3 are similar. The high inter-sector correlation reflects this similarity.

Tab. 3.11: The intra-site cross-correlation of the transformed LSP in the I1 scenario in the LOS and NLOS propagations

LSP pair	LOS	NLOS
LSF& DW	-0.1	0.51
LSF& DS	-0.76	0.6
LSF& K	0.56	n.a.
LSF& XPR	0.55	-0.1
LSF& NPCG	-0.28	-0.44
DW& DS	0.46	0.84
DW& K	0.12	n.a.
DW& XPR	-0.38	-0.38
DW& NPCG	0.1	-0.32
DS& K	-0.4	n.a.
DS& XPR	-0.64	-0.25
DS& NPCG	0.37	-0.12
K& XPR	0.31	n.a.
K& NPCG	-0.14	n.a.
XPR& NPCG	-0.59	0.23

Tab. 3.12: The inter-sector correlation of the transformed LSP in the I1 scenario

BS param.	Angle[deg.]	LSF	DW	DS	XPR	NPCG
$\langle BS2, BS3 \rangle$	$\theta_{BS2} \cap \theta_{BS3}$	-0.1	0.7	-0.5	0.64	0.3
$\langle BS2, BS3 \rangle$	$\theta_{BS2} \cap \theta_{BS3}$	0	0.65	0.1	0.35	0.1
$\langle BS2, BS3 \rangle$	$\theta_{BS3} \cap \theta_{BS2}$	0.75	0.92	0.54	0.2	0.86
$\langle BS7, BS8 \rangle$	$\theta_{BS8} \cap \theta_{BS7}$	-0.27	0.5	-0.46	0.81	-0.1
$\langle BS7, BS8 \rangle$	$\theta_{BS7} \cap \theta_{BS8}$	0.3	0.87	0.18	0.1	0.1

3.5.2.4 The inter-site correlation of the transformed LSP

The inter-site correlation between BS pairs is summarized in Table 3.13. It has been observed that:

- Comparing the inter-site correlation results of the BS pair $\langle BS1, BS3 \rangle$ and the BS pair $\langle BS3, BS7 \rangle$, it is found that LSP except NPCG are negative correlated as a MS moves between two BSs, namely, $d_{BS} \geq \max(d_{1,2})$ and $160 [\text{deg.}] \leq \theta \leq 180 [\text{deg.}]$.
- Relatively high inter-site correlation of the transformed LSP can be found for the BS pair $\langle BS5, BS7 \rangle$ with $20 [\text{deg.}] \leq \theta \leq 90 [\text{deg.}]$ and the BS pair $\langle BS6, BS7 \rangle$ with $15 [\text{deg.}] \leq \theta \leq 90 [\text{deg.}]$. The inter-site correlation coefficients are very similar between these two BS pairs because of the similar propagation mechanism: a MS has a LOS connection to one BS (BS5/BS6) and a NLOS connection to another BS (BS7).
- The transformed LSP except DS are highly correlated for the BS pair $\langle BS5, BS6 \rangle$ with $110 [\text{deg.}] \leq \theta \leq 170 [\text{deg.}]$. It corresponds to the measurement routes in two seminar rooms. Even though both BSs are looking from different sides of the rooms, their channels are similar. The reason is that the wave from both BSs arrives at a MS from the same door or by penetrating the similar walls.

Tab. 3.13: The inter-site correlation of the transformed LSP in the I1 scenario

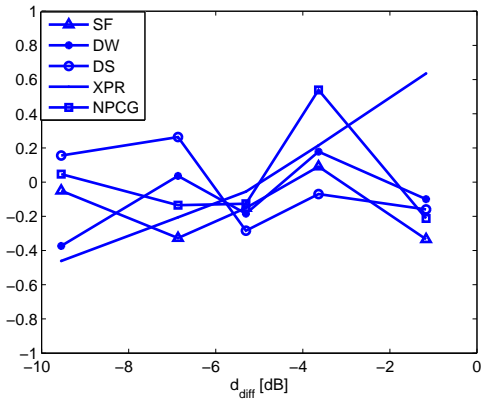
BS param.	d_{BS}	$\min(d_{1,2})$	$\max(d_{1,2})$	d_{diff}	θ	LSF	DW	DS	XPR	NPCG
	[m]	[m]	[m]	[dB]	[deg.]					
$\langle BS1, BS3 \rangle$	25.4	4.2	21.3	[-7 -0.1]	[165 175]	-0.2	-0.8	0.14	-0.13	0.1
$\langle BS3, BS5 \rangle$	25	5.2	24.5	[-7 0]	[90 160]	-0.48	-0.32	-0.1	-0.1	-0.44
$\langle BS3, BS5 \rangle$	25	5.2	36.8	[-7 -4.5]	[20 90]	0	-0.25	-0.61	0	0.33
$\langle BS3, BS6 \rangle$	50	16	34.3	[-3.5 0]	[165 175]	-0.35	0	0	0	0
$\langle BS3, BS6 \rangle$	50	4.5	49.1	[-10 -7]	[90 165]	0.13	0.1	-0.66	-0.48	0
$\langle BS3, BS7 \rangle$	87	4	83	[-13.5 0]	[165 180]	-0.19	-0.41	-0.21	-0.5	0.1
$\langle BS5, BS6 \rangle$	26.8	5.2	30.6	[-7 0]	[50 175]	-0.36	-0.87	0.6	-0.1	-0.68
$\langle BS5, BS6 \rangle$	26.8	3.8	24.3	[-9.5 -4]	[130 170]	-0.7	0.27	0	-0.1	0.67
$\langle BS5, BS6 \rangle$	26.8	6	22.7	[-6 -3]	[110 130]	0.73	0.6	0	-0.1	0.87
$\langle BS5, BS7 \rangle$	62.5	15.8	91.1	[-7 -5]	[8 20]	-0.15	-0.45	0.1	0.35	0.78
$\langle BS5, BS7 \rangle$	62.5	5.2	76.6	[-11 -7]	[20 90]	0.64	0.17	-0.52	-0.35	0.21
$\langle BS5, BS7 \rangle$	62.5	5.2	62	[-11 -6]	[90 155]	-0.28	0.2	-0.2	-0.43	0.63
$\langle BS6, BS7 \rangle$	37.6	17	67.5	[-5 -3.5]	[8 15]	0.24	-0.3	-0.2	-0.25	-0.52
$\langle BS6, BS7 \rangle$	37.6	4.7	52.3	[-9.5 -5]	[15 90]	-0.63	0.23	-0.62	-0.44	-0.45
$\langle BS6, BS7 \rangle$	37.6	4.5	37.4	[-9.5 -2.5]	[90 160]	-0.12	-0.17	0.27	-0.33	0.22

Figure 3.22(a), Fig. 3.22(c), and Fig. 3.22(e) show the dependence of the inter-site correlation of the transformed LSP on d_{diff} , θ , and d_{BS} , respectively. For each $d_{diff}/\theta/d_{BS}$ value, the number of samples is shown in Fig. 3.22(b), Fig. 3.22(d), and Fig. 3.22(f), respectively. It has been observed in Fig. 3.22 that the inter-site correlation of XPR has a linear dependence on d_{diff} and a piecewise dependence on θ . Furthermore, increasing d_{BS} leads to a negative inter-site correlation. The inter-site correlation of the other transformed LSP shows no obvious dependence on d_{diff} and θ .

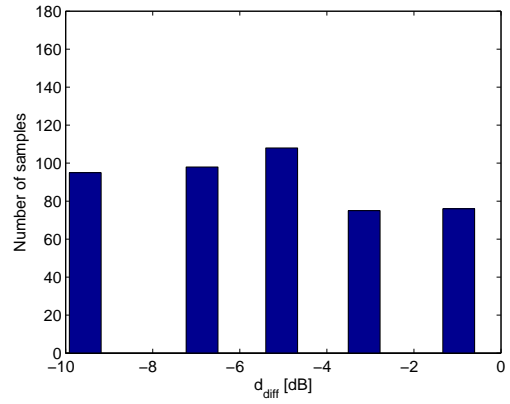
3.5.3 Main findings

The previous two Subsections 3.5.1 and 3.5.2 presented the experimental results of the statistical distribution of LSP and their correlation properties in the urban and indoor scenarios, respectively. This section makes a short summary on the main findings.

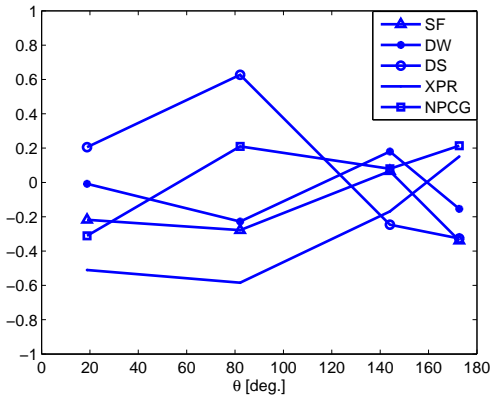
- Statistical distribution of LSP
 - Both in the U1, U2, and I1 scenarios, LSF, K-factor, and XPR are log-normal distributed while $\log_{10}DS$ is normal distributed. Furthermore, DW and NPCG have a uniform distribution and a Rayleigh distribution, respectively.
 - In the outdoor urban LOS propagation, the higher the BS antenna array, the higher the LSF and DS values, whereas, the lower the K-factor, XPR, and NPCG values. In the NLOS propagation, the higher the BS antenna array, the higher the LSF, DS, and NPCG values, whereas, the lower the XPR values. Furthermore, the height of BS antenna array has almost no impact on the DW values both in the LOS and NLOS propagations.
 - Both in the U1, U2, and I1 scenarios, LSP including LSF, DS, and XPR as well as NPCG have a larger variance in the NLOS propagation than in the LOS propagation.



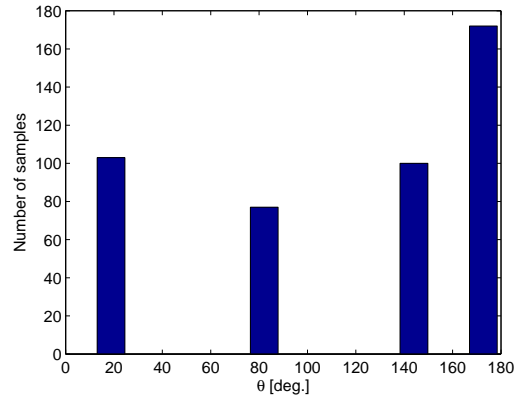
(a) Dependence of the inter-site correlation on d_{diff}



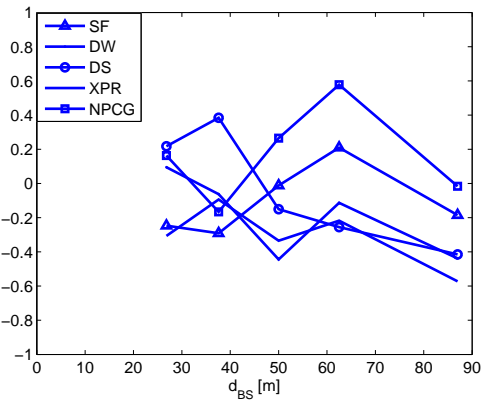
(b) Number of points for each d_{diff}



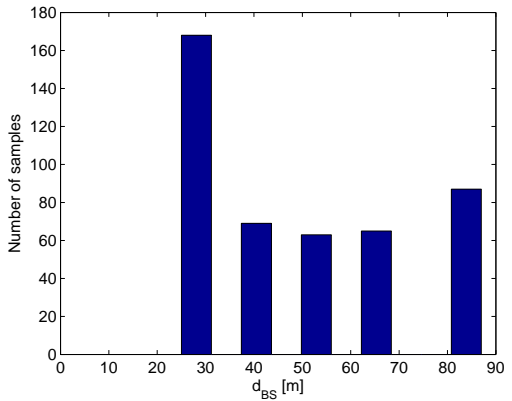
(c) Dependence of the inter-site correlation on θ



(d) Number of points for each θ



(e) Dependence of the inter-site correlation on d_{BS}



(f) Number of points for each d_{BS}

Fig. 3.22: The dependence of the inter-site correlation of the transformed LSP on $\langle d_{diff}, \theta, d_{BS} \rangle$ in the I1 scenario

- The intra-site auto-correlation of the transformed LSP
 - In the urban scenario, the de-correlation distances of LSP except XPR are larger in the LOS propagation than in the NLOS propagation.
 - In the urban scenario, the higher the BS antenna array, the larger the de-correlation distance of the transformed LSP except K-factor.
 - In the indoor scenario, the LSP values can be treated to be uncorrelated if the distance between two MSs is larger than 3 [m].

- The intra-site cross-correlation of the transformed LSP

By analyzing the results in Table 3.6 and in Table 3.11, the following tendency can be observed for the U1, U2, and I1 scenarios:

- In the LOS urban and indoor scenarios, DW has a positive correlation with DS and NPCG, but has a negative correlation with LSF, XPR, and K-factor;
- In the NLOS urban and indoor scenarios, DW has a positive correlation with DS and LSF, but has a negative correlation with XPR and NPCG.

- The inter-sector correlation of the transformed LSP

From the results in Table 3.7 and in Table 3.12, it can be concluded that:

- High inter-sector correlation can be observed only in the overlapped area where two sectors have main beam. However, the inter-sector correlation could not be one. The correlation depends on the ratio of the overlapped main beam width to the 3-dB beam width of sectors, namely $\frac{\theta_{OL}}{\theta_{s1}}$ assuming $\theta_{s1} = \theta_{s2}$. The larger the ratio, the larger the inter-sector correlation. The inter-sector correlation could be one only if two sectors are fully overlapped to each other;
- In the area where one sector has main beam and the other sector has side beam, the inter-sector correlation could be still high if there exist several strong reflectors. With the help of these reflectors, the signal can be reflected from the main beam of a sector into the side beam where the other sector has main beam. Otherwise, the correlation in this area is low.

- The inter-site correlation of the transformed LSP

- In the urban scenario, the inter-site correlation of LSP is high if the distance between two BSs approaches 0, the angle of arrival difference from two BSs/RSs to a MS is very small, the distance between two BSs/RSs is smaller than each link distance, and the height difference between two BSs/RSs approaches 0;
- In the urban scenario, the inter-site correlation depends on the height difference between two BSs/RSs h_{diff} . The larger the height difference, the smaller the inter-site correlation;
- In the urban scenario, the inter-site correlation of DW is negative if angle of arrival difference from two BSs/RSs to a MS approaches 180°;

-
- In the indoor scenario, the inter-site correlation of XPR shows a linear dependence on the distance difference between two links and shows a piecewise dependence on the angle of arrival difference from two BSs/RSs to a MS. However, the inter-site correlation of the other transformed LSP has no obvious dependence on these two parameters;
 - In the indoor scenario, the inter-site correlation of the transformed LSP tends to be negative if the distance between two BSs/RSs increases.
-

4. SYSTEM STRUCTURE OF COOPERATIVE MARN

As shown in Fig. 2.1 in Chapter 2, channel realizations can be simulated by using the experimental channel models. The last step of the channel modeling process, system simulation and model validation, can be performed by using the simulated channels. In this chapter, a cooperative multiple access relay system will be introduced as an example of the relay system for system simulation. This system is used both for the purpose of performance evaluation and further for the purpose of performance verification.

The performance of wireless networks can be improved by introducing a station, acting as a RS for blocked MSs [51] [22] [27] [53]. Further performance improvement can be expected if the RS can aid not just a single MS, but a couple of MSs simultaneously. The terminology, multiple access relay channel, has been proposed by Kramer in [107] for the relay networks where a dedicated RS is used for the forwarding of the signals to/from several blocked MSs. MARN are especially attractive for the cellular network applications where a cooperation between MSs is not allowed [108]. In this chapter, advanced techniques, such as MAC [37], protocol design [25] [22], symbol-wise super-positioning, and JU MMSE [38] as well as an error detection aided signal selection technique [22] [39], are proposed. A significant performance enhancement can be observed based on numerical simulations, using simplified Rayleigh channel realizations. A reality check of the performance improvement will be conducted in the coming Chapter 5.

This chapter is organized as follows: Section 4.1 provides firstly a survey to the state-of-the-art research activities in relay networks. In the same section, the main contributions of this chapter are summarized and the simulation assumptions made throughout this chapter are listed. Thereafter, Section 4.2 provides a detailed description to the system model of MARN in the presence of UKIF. Two forwarding strategies, the AF strategy and the DF strategy, are presented in Section 4.3 from the information theory point of view. In Section 4.4, advanced techniques, such as relay protocol design and MAC as well as symbol-wise super-positioning, are proposed. Section 4.5 addresses two JU MMSE criteria for the interference cancellation while preserving the MAC-encoded structure. Finally, Section 4.6 exploits an example scenario to evaluate the system performance with the proposed techniques over simplified Rayleigh channels.

4.1 Background and own contributions

4.1.1 Background and state-of-the-art

In 1971, van der Meulen has proposed in [51] the relaying method, of which a RS has been introduced between a source and a destination to form a S-R-D three-station structured relay network. Thereafter, Cover has performed an information theoretical study on the three-station structured

relay network in 1979 in [52] and a more detailed description can be found in his book [55]. In his work, the maximum achievable capacity has been derived for different channel conditions. They include a degraded relay Gaussian channel, a reversely degraded relay Gaussian channel, an arbitrary relay Gaussian channel with feedback, and a general relay Gaussian channel. The degraded relay Gaussian channel stands for the case that the destination's output is a degraded version of the RS's output. The reversely degraded relay Gaussian channel stands for the case where the RS's output is a degraded version of the destination's output. This case is less interesting since the sense of using relaying technique disappears. The arbitrary relay Gaussian channel with feedback means a source and a RS get a causal feedback from a RS and a destination. These four kinds of channels cover all possibilities of relay channels, of which the general relay Gaussian channel has been frequently considered in the research work [22] [27] [53] [109].

In the middle of the 90s, the idea of using relaying has been revised to extend the coverage of a BS to remote MSs or to provide service to the MSs located in a shadowed area [17]. Since then, the booming research works have been done to the relay topic [110] [111] [22] [112] [25] [27] [53] [109] both in the academia and in the industries. Most of them are based on the Cover's theoretical study. The research activities can be classified into the following four main directions.

- Various relay network structures.

Relay networks include the classical three-station structured relay networks as studied in [51] [52] [55]; the multiple-hop (stage) relay networks discussed by Herhold in [39]; the multiple access (uplink) or broadcast (downlink) relay networks firstly proposed by Kramer in [107]; the multi-RS networks introduced by Gallager in [113]. Subplots 4.1(a), 4.1(b), 4.1(c), and 4.1(d) in Fig. 4.1 represent these four types of relay networks, respectively. Any other sophisticated relay networks, such as multi-MS multi-RS networks in [27], are the results of combing the aforementioned basic structures. Different structures represent different network topologies. As a consequence, different techniques have been discussed. For example, a bi-directional relaying concept is based on the duality of the downlink and uplink transmission structures [28]; resource reuse algorithms in multiple-hop (stage) relay networks; a coded cooperation in MARN; RS selection techniques or distributed cooperative space-time coding techniques in multi-RS networks; and a virtual antenna array concept in multi-MS multi-RS networks.

- Two kinds of cooperative stations: MS cooperation (generally speaking, user cooperation) and relay cooperation.

In the MS cooperation case, MSs, having their own signal to transmit, can serve as a RS for each other. The milestones of the MS cooperation concept have been contributed by Sendonaris in [110] [111] where the frame of a MS's transmission is divided into two parts. At the first part, the MS transmits only its own signal while at the second part, the MS transmits a combined version of its own signal together with the signal from its neighboring MS. His work has been extended to a general case of the MS cooperation through coding by Hunter [23] [24]. In Hunter's work, he considered a two-user case with a cooperation rate $\frac{N_2}{N_1+N_2}$. The transmission of one frame, having a bit length $N_1 + N_2$, will be partitioned into two parts with a bit length being N_1 and N_2 , respectively. Each MS transmits N_1 its own

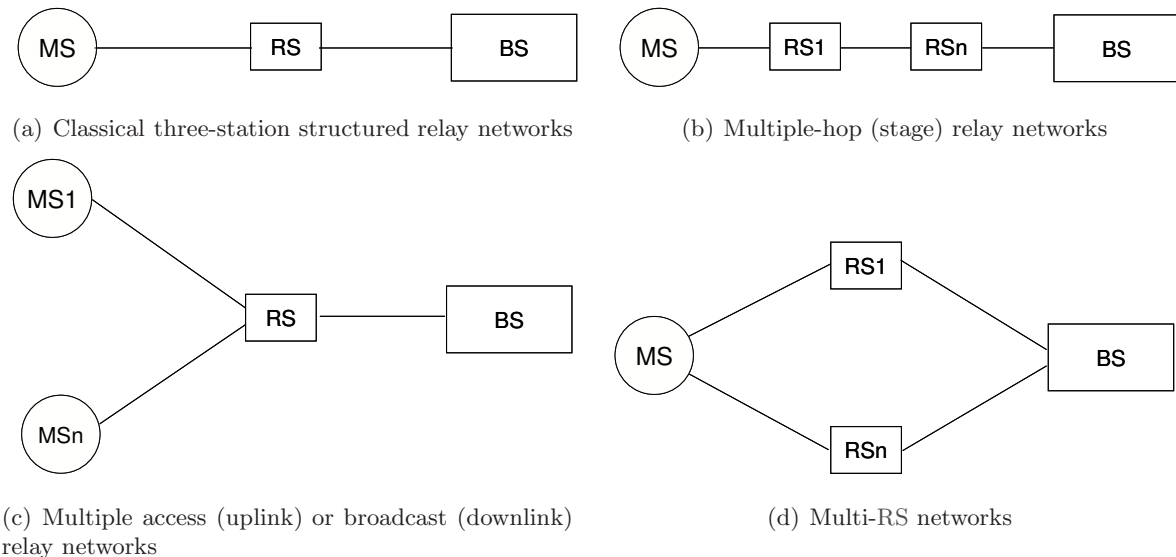


Fig. 4.1: Relay network with various structures

bits while N_2 bits from the other MS.

In the relay cooperation case, a dedicated RS is introduced as an extra network element to serve as a relay which has no own data to transmit. The classical three-station structured relay networks proposed in [51] [52] [55] are one example of this case.

The comparison between the MS cooperation and the relay cooperation has been performed by Sankaranarayanan in [109], using the total transmitting and processing power as a cost function. The results indicate that the relay cooperation is more energy efficient than the MS cooperation when accounting for the energy costs of cooperation.

- Various forwarding strategies: AF relaying and DF relaying as well as compress-and-forward relaying.

A RS with an AF functionality amplifies the received signal and then forwards it. The AF relaying results in the enhancement of a noise floor.

In the concept of a DF relaying, three different re-encoding strategies have been discussed in literature, depending on the re-encoding functionality of a RS.

When a RS decodes the received signal and re-encodes it with the same codebook as the codebook of the received signal, the RS is called a repetition-re-encoded RS. However, the RS can re-encode the received signal with a different codebook, by which an additional code gain can be achieved [114]. Zhao proposed in [115] the idea of a distributed turbo coding where a RS transmits the redundancy of a turbo code which is different from the direct transmission by interleaving the received signal. In this case, a conventional iterative turbo algorithm can be performed at the destination for decoding [116]. Hausl extended Zhao's work to the multiple-access relay networks in [117]. In his paper, a distributed channel coding is used together with a symbol-wise superpositioning algorithm, by which the RS can transmit the signals from different MSs jointly [118]. The result shows that a joint network-channel coding idea outperforms a distributed turbo-code idea due to the introduction of a network-coding technique.

When an error occurs in one of the intermediate relaying links, the wrong message will be propagated to the following transmissions. This phenomenon is termed as error propagation. Due to this phenomenon, Azarian proposed a dynamic-decode-forward relaying concept in [119], where a RS tries to receive the information from a MS as much as the instantaneous S-R channel maximally allows, namely the instantaneous S-R channel mutual information. According to the Shannon theory, the average error probability at the RS for a Gaussian code can be arbitrary small. This means, no error happens to the S-R transmission. Consequently, no error propagation happens. It is observed in [119] that a dynamic-decode-forward relaying outperforms an AF relaying in terms of the diversity-multiplexing tradeoff metric proposed by Zheng in [120].

A compress-and-forward relaying utilizes the correlation between the message received by a RS and the original message transmitted by a MS/BS. The message received by the RS is a degraded version of the original message transmitted by the MS/BS. Their correlation depends on the link quality of the S-R channel. The better the S-R channel, the higher the correlation between the message received by the RS and the original message transmitted by the MS. Using the Wyner-Ziv coding technique [121] which generalizes the Slepian-Wolf theory [122] by introducing rate distortion, the RS can compress the received message by a joint source and channel coding technique. In [123] [124], Li implemented the compress-and-forward relaying concept which exploits the distributed source coding technology based on the Slepian-Wolf theory.

- Multi-MS ST code design.

The research work on MIMO techniques is boomed since the landmark papers published by Foschini [29] and by Telatar [30]. In 1998, Alamouti proposed a very appealing transmit diversity scheme for the two transmit antenna elements case in [125]. Tarokh improved Alamouti's work by his paper [126] where the important properties of ST block codes are discussed. The advantages of the ST codes have been exploited in relay networks even though the stations may have only a single antenna element. In relay networks, a half-duplex RS transmission introduces an additional redundancy, by which distributed virtual MIMO/ Single-Input Multiple-Output (SIMO)/ Multiple-Input Single-Output (MISO) structures can be formed [127] [22] [25] [27] [128] [129] [114] [10] among single antenna MSs/RSs. A ST code can be constructed to all types of relay network structures. In [130], Yang discussed the ST code construction criterion for AF relay networks with a receive collision at the destination. The receive collision concept, firstly proposed by Nabar in [25], differs from the orthogonal concept in the classical relay networks [51] [52] [55] [22] where the source station does not transmit when a RS forwards the source station's signal to the destination. In [25] Nabar proposed that the source station transmits its signal to the destination as the RS performs forwarding. The results reveal that a non-orthogonal relaying technique yields higher capacity than an orthogonal relaying technique at the expense of a receive collision. Further, Yang confirmed in his paper that an optimal diversity-multiplexing tradeoff can be achieved by some examples of ST codes with a non-orthogonal relaying.

4.1.2 Own contributions

This chapter deals with the cooperative MARN where multiple MSs communicate with a BS with the help of dedicated RSs. The dedicated RS deployment may be suitable for the infrastructure based networks [131], where both RSs and the BSs are deployed and managed by service providers. Even though a dedicated RS incurs additional infrastructure costs, it is reasonable and acceptable to introduce a common RS shared by multiple blocked desired MSs. The reason is that the cost coming from an extra RS can be taken by multiple desired MSs.

The main contributions of this chapter are listed as follows:

1. MAC has been proposed to cooperative MARN [10] [11] [12].

Allowing for the beneficial point of a multiple access channel, MACs are designed so that the signal separability can be achieved at the receiver side. Despite the redundancy incurred by the MAC scheme, throughput gain can be achieved due to the increased number of codewords. In 1976, Kasami proposed a class of MACs in [37] for Binary Phase-Shifted Keying (BPSK)-modulation in AWGN channels. The code proposed in [37] has been extended in this dissertation to the system using a Quadrature Phase Shift Keying (QPSK)-modulation in the frequency-flat Rayleigh fading channels, of which the codewords can be uniquely decoded at the receiver side. Simultaneously, the total throughput can be increased.

2. Protocol design to improve the system resource efficiency [22] [39].

Even though the introduction of intermediate RSs enables the communication between MSs and a BS, the end-to-end capacity of relay networks is divided by the number of the intermediate RSs n_{hop} due to the half-duplex operation of a RS as explained in Chapter 1. Therefore, the introduction of a RS can improve the system performance if and only if the relay transmission outperforms the direct transmission. To make more efficient use of the system resource, the system should operate adaptively between a direct transmission or a relay transmission, depending on the superiority of their performances. For this purpose, an ARQ based protocol is proposed in this chapter, by which a RS can decide when to forward and MSs can decide when to retransmit. This means that the MSs retransmit the signal when the RS forwards the same signal which is termed as a non-orthogonal relaying transmission. Unlike the classical orthogonal relaying transmission where the RS forwards while the MSs are in an "idle" status, an additional gain can be expected with the non-orthogonal relaying transmission at the price of receive collisions [25].

3. A JU MMSE algorithm is introduced for the UKIF cancellation while keeping the multiple MSs' MAC-encoded signal structure [12] [11].

Due to the fact that the final end-to-end capacity of a relay link is divided by the factor of the number of intermediate RSs, Zirwas proposed in [21] the "SIMU" concept, where the spatially separated relay links work simultaneously. The "SIMU" concept increases the overall capacity with a time/space resource reuse technique. However, it introduces additional system interference. Therefore, it is necessary that a BS will be equipped with multiple receive antenna elements to suppress interference since the BS's operational environment requires

resistance against the unknown co-channel interference. This chapter assumes that the interfering MSs have the same spectrum bandwidth and allocation as the desired MSs. In many cases, such scenario assumption should apply to the co-channel interference environments. Then, the primary role of the BS, using multiple antenna elements, is to detect the multiple MSs' MAC-encoded signals while suppressing the interfering components. With the assumption mentioned above, it is also reasonable to further assume that the BS uses an interference suppression technique based on the JU MMSE criterion, by which the multiple MSs' MAC-encoded signal structure can be preserved.

Furthermore, two JU MMSE criteria are compared with each other [11] [12]. One is to minimize the Mean Square Error (MSE) between the spatial filter output and the *actually* received *composite* signal comprising the *desired* MAC-encoded signals [132] [133], which is referred to as **H**-Criterion in this dissertation, where **H** represents the actual channel matrix of the desired MSs. The other is to minimize the MSE also between two terms, but the desired signal term should not necessarily be the *actually* received *composite* signal [38], referred to as **A**-Criterion, where **A** represents an equivalent channel matrix of the desired MSs.

4. Two forwarding strategies at the RS are compared: an AF versus a DF.

Two kinds of functionality at the RS are considered in this dissertation. The one is the AF relaying; the other is the DF relaying. For the latter one, the RS is a repetition re-encoder, of which the same codebook as the received signal is used. Furthermore, the decoded symbols from the desired MSs are symbol-wise super-positioned due to the unique separability and decodability property of MAC.

5. Error detection aided signal selection [10].

After the Maximum Likelihood (ML) detection, each desired MS's transmitted signal is identified from two transmissions: the direct transmission and the relay transmission. Even though the direct link of each desired MS is significantly attenuated, the contribution from the direct link should not be ignored. In this chapter, the detected signals from the direct transmission and from the relay transmission are jointly detected at the BS. This means that an error message is returned for the desired MS if and only if an error occurs at the same received symbol position, both from the direct transmission and from the relay transmission. Otherwise, the signal could be recovered without any error.

4.1.3 Simulation assumptions

The general simulation assumptions used throughout this chapter are stated as follows and the specific assumptions will be given at the related place.

1. All channels are assumed to be a frequency-flat Rayleigh-fading channel and stay the same over one frame (= block fading). Furthermore, the channel gains are mutually complex independent with a variance being unity.
-

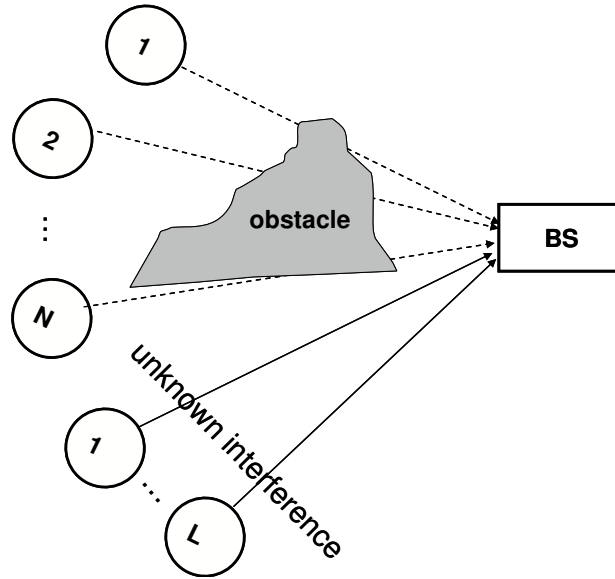


Fig. 4.2: The system structure with N blocked desired MSs having a single antenna, L UKIF MSs having a single antenna, and one BS having n_{Rx} antenna elements.

2. The additive noises at different stations are zero-mean, mutually independent, circularly symmetric, and white complex Gaussian.
3. All stations except the BS have a single antenna and operate synchronously. Only the receive stations (RS or BS) have the Channel State Information (CSI) while the transmit stations (MSs or RS) have no CSI.

4.2 System model of MARN

Consider a communication system with $N + L$ MSs, transmitting signals to their BSs, as shown in Fig. 4.2. The BS has n_{Rx} ($n_{Rx} \geq L + 1$) antenna elements while each MS has only one antenna element. Of the $N + L$ MSs, N are the desired MSs and the L UKIF MSs. Due to the battery's life longevity requirement of MSs, each MS's transmit power is limited. Hence, it may happen quite often that one or some of the desired MSs are blocked from the BS due to obstacles as shown in Fig. 4.2. In this dissertation, all of the N desired MSs are assumed to be blocked from the BS. With the help of a dedicated RS, the signals from the desired MSs can be relayed by the dedicated RS and finally delivered to the BS. A simple example is the case where the transmission of the blocked desired MSs is divided into two phases: at the first transmission phase, all the N desired MSs broadcast their signals. N MSs' signals are received both by the RS and by the BS as shown in Fig. 4.3(a). The second transmission phase is for the relaying of the blocked desired MSs' signals at the RS. Simultaneously, also the L UKIF MSs transmit their signals to their destinations, and their signals may reach the receive antenna elements of the desired MSs' BS at the first and second phases. At the first time-slot, the received signals at the BS $\mathbf{Y}_{s,d}^{(1)}$ and at the RS $y_{s,r}^{(1)}$ can be

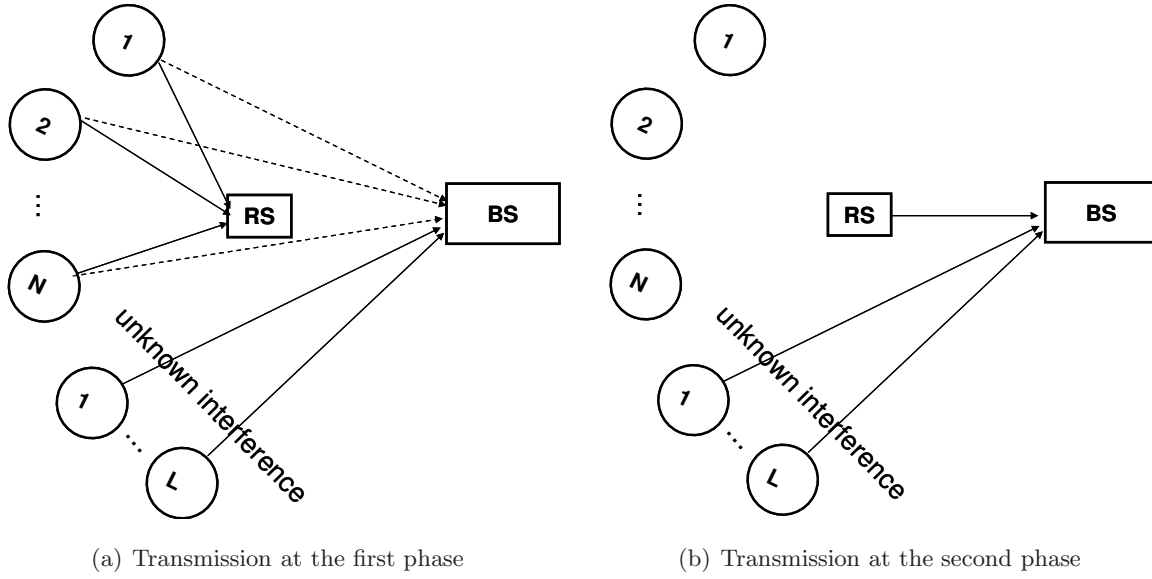


Fig. 4.3: Relay transmission in two phases

expressed, respectively, as

$$\mathbf{Y}_{s,d}^{(1)} = \underbrace{\mathbf{H}_{s,d}^{(1)} \sqrt{\mathbf{P}_{s,d}^{(1)}} \mathbf{X}^{(1)}}_{\text{desired}} + \underbrace{\mathbf{H}_{u,d}^{(1)} \sqrt{\mathbf{P}_{u,d}^{(1)}} \mathbf{S}^{(1)}}_{\text{UKIF}} + \underbrace{\mathbf{n}^{(1)}}_{\text{noise}} \quad (4.1)$$

and

$$\begin{aligned} y_{s,r}^{(1)} &= \mathbf{H}_{s,r}^{(1)} \sqrt{\mathbf{P}_{s,r}^{(1)}} \mathbf{X}^{(1)} + \mathbf{n}_{s,r}^{(1)} \\ &= \begin{vmatrix} h_{1,r}^{(1)} & \cdots & h_{N,r}^{(1)} \end{vmatrix} \begin{vmatrix} p_{1,r}^{(1)} \cdots 0 \\ \vdots \vdots \vdots \\ 0 \cdots p_{N,r}^{(1)} \end{vmatrix}^{\frac{1}{2}} \begin{vmatrix} x_1^{(1)} \\ \vdots \\ x_N^{(1)} \end{vmatrix} + n_{s,r}^{(1)}. \end{aligned} \quad (4.2)$$

Eqn. 4.1 can be detailed expressed as

$$\begin{aligned} \begin{vmatrix} y_1^{(1)} \\ \vdots \\ y_{n_{Rx}}^{(1)} \end{vmatrix} &= \underbrace{\begin{vmatrix} h_{1,1}^{(1)} & \cdots & h_{1,N}^{(1)} \\ \vdots & \ddots & \vdots \\ h_{n_{Rx},1}^{(1)} & \cdots & h_{n_{Rx},N}^{(1)} \end{vmatrix} \begin{vmatrix} p_{1,d}^{(1)} \cdots 0 \\ \vdots \vdots \vdots \\ 0 \cdots p_{N,d}^{(1)} \end{vmatrix}^{\frac{1}{2}} \begin{vmatrix} x_1^{(1)} \\ \vdots \\ x_N^{(1)} \end{vmatrix}}_{\text{desired}} + \cdots \\ &\quad \underbrace{\begin{vmatrix} h_{1,1}^{(1)} & \cdots & h_{1,L}^{(1)} \\ \vdots & \ddots & \vdots \\ h_{n_{Rx},1}^{(1)} & \cdots & h_{n_{Rx},L}^{(1)} \end{vmatrix} \begin{vmatrix} p_{1,d}^{(1)} \cdots 0 \\ \vdots \vdots \vdots \\ 0 \cdots p_{L,d}^{(1)} \end{vmatrix}^{\frac{1}{2}} \begin{vmatrix} s_1^{(1)} \\ \vdots \\ s_L^{(1)} \end{vmatrix}}_{\text{UKIF}} + \underbrace{\begin{vmatrix} n_1^{(1)} \\ \vdots \\ n_{n_{Rx}}^{(1)} \end{vmatrix}}_{\text{noise}} \end{aligned} \quad (4.3)$$

In Eqn. 4.1 and Eqn. 4.2, $\mathbf{H}_{s,d}^{(1)}$, $\mathbf{H}_{u,d}^{(1)}$, and $\mathbf{H}_{s,r}^{(1)}$ stand for, respectively, the complex channel gain between the desired MSs and the BS, between the UKIF MSs and the BS, and between the desired MSs and the RS at the first time-slot. The mean value of the complex channel gain is zero while

the variance is unity.

The received signal $\mathbf{Y}_{r,d}^{(2)}$ at the BS at the second time-slot can be expressed as

$$\begin{aligned} \mathbf{Y}_{r,d}^{(2)} &= \underbrace{\mathbf{H}_{r,d}^{(2)} \sqrt{P_{r,d}^{(2)}} x_{r,d}^{(2)}}_{\text{desired}} + \underbrace{\mathbf{H}_{u,d}^{(2)} \sqrt{\mathbf{P}_{u,d}^{(2)}} \mathbf{S}^{(2)}}_{UKIF} + \underbrace{\mathbf{n}^{(2)}}_{\text{noise}} \\ &= \underbrace{\begin{bmatrix} h_{r,1}^{(1)} & \cdots & h_{r,n_{Rx}}^{(1)} \end{bmatrix}^T \sqrt{P_{r,d}^{(2)}} x_{r,d}^{(2)}}_{\text{desired}} + \underbrace{\mathbf{H}_{u,d}^{(2)} \sqrt{\mathbf{P}_{u,d}^{(2)}} \mathbf{S}^{(2)}}_{UKIF} + \underbrace{\mathbf{n}^{(2)}}_{\text{noise}} \end{aligned} \quad (4.4)$$

The definitions of $\mathbf{H}_{u,d}^{(2)}$, $\sqrt{\mathbf{P}_{u,d}^{(2)}}$, $\mathbf{S}^{(2)}$, and $\mathbf{n}^{(2)}$ are akin to the definitions in Eqn. 4.3, but with superscript $^{(2)}$ indexing the second time-slot. In Eqn. 4.1, Eqn. 4.2, and Eqn. 4.4, $\mathbf{P}_{s,d}^{(1)}/\mathbf{P}_{u,d}^{(1)}$, $P_{s,r}^{(1)}$, and $\mathbf{P}_{r,d}^{(2)}/\mathbf{P}_{u,d}^{(2)}$ are diagonal matrices. The elements along the diagonal stand for the transmit power from different transmitters (MSs/RS). For example, $p_{i,d}^{(1)}$, $1 \leq i \leq N$ in Eqn. 4.3 stands for the transmit power between the desired MS i and the BS at the first time-slot. The losses due to LSF and PL are already included in the transmit power matrices which can be calculated by Eqn. 2.9 in Section 2.5. $\mathbf{X}^{(1)}$, $x_{r,d}^{(2)}$, and $\mathbf{S}^{(i)}$ with $1 \leq i \leq 2$, are the transmitted signals from the N blocked desired MSs at the first time-slot, from the RS at the second time-slot, and from the L UKIF MSs at the first and second time-slots, respectively. The transmitted signals have unit expectational values.

Since $x_{r,d}^{(2)}$ is the output of the RS while $y_{s,r}^{(1)}$ is the input of the RS, $x_{r,d}^{(2)}$ can be expressed as a function of $y_{s,r}^{(1)}$, depending on the forwarding strategy at the RS. $\mathbf{n}^{(i)}$, $1 \leq i \leq 2$, are the AWGN vectors at the BS at the first and second time-slots, respectively, sorting up the noise components with the n_{Rx} BS antenna elements, each being assumed to have a power $\sigma_{n,d}^2$. $n_{s,r}^{(i)}$ is the AWGN signal at the RS at the first time-slot, being assumed to have a power $\sigma_{n,r}^2$.

At the first time-slot, signal to interference power ratio $SIR^{(1)}$ is defined as the power ratio between the blocked desired MS having the largest power and the total power from the L UKIF MSs, namely

$$SIR^{(1)} = \frac{\max \left(p_{1,d}^{(1)} \cdots p_{N,d}^{(1)} \right)}{\sum_{i=1}^L p_i^{(1)}}. \quad (4.5)$$

At the second time-slot, $SIR^{(2)}$ is defined as the power ratio between the RS's power and the total power from the L UKIF MSs, namely

$$SIR^{(2)} = \frac{p_{r,d}^{(2)}}{\sum_{i=1}^L p_i^{(2)}}. \quad (4.6)$$

4.3 Forwarding strategies

In Section 4.2, it has been mentioned that the output of the RS $x_{r,d}^{(2)}$ at the second time-slot can be expressed as a function of $y_{s,r}^{(1)}$ due to the operational causality. The function between $x_{r,d}^{(2)}$ and $y_{s,r}^{(1)}$ depends on the forwarding strategy at the RS. This dissertation focuses on two common relaying

strategies: an AF relaying strategy and a DF relaying strategy with a repetition coding. These two forwarding strategies at the RS are stressed in this section. According to the forwarding strategy, the final output at the BS is highlighted, combining the output from the first and second time-slots.

4.3.1 The AF strategy

For the AF relay transmission, the RS amplifies its received signal $y_{s,r}^{(1)}$ by a factor β as follows

$$x_{r,d}^{(2)} = \beta y_{s,r}^{(1)}. \quad (4.7)$$

Since it is assumed in Section 4.2 that the transmitted signals have unit expectational values, the amplify factor β should satisfy

$$\left| \beta y_{s,r}^{(1)} \right|^2 = 1. \quad (4.8)$$

This means

$$\beta = \frac{1}{\left| y_{s,r}^{(1)} \right|^2} = \frac{1}{\sqrt{\sum_{i=1}^N p_{i,r}^{(1)} |h_{i,r}^{(1)}|^2 + \sigma_{n,r}^2}}. \quad (4.9)$$

Substituting Eqn. 4.7 into Eqn. 4.4, it turns out

$$\begin{aligned} \mathbf{Y}_{r,d}^{(2)} &= \mathbf{H}_{r,d}^{(2)} \sqrt{P_{r,d}^{(2)}} \beta y_{s,r}^{(1)} + \mathbf{H}_{u,d}^{(2)} \sqrt{\mathbf{P}_{u,d}^{(2)}} \mathbf{S}^{(2)} + \mathbf{n}^{(2)} \\ &= \beta \mathbf{H}_{r,d}^{(2)} \sqrt{P_{r,d}^{(2)}} \left(\mathbf{H}_{s,r}^{(1)} \sqrt{\mathbf{P}_{s,r}^{(1)}} \mathbf{X}^{(1)} + n_{s,r}^{(1)} \right) + \mathbf{H}_{u,d}^{(2)} \sqrt{\mathbf{P}_{u,d}^{(2)}} \mathbf{S}^{(2)} + \mathbf{n}^{(2)} \\ &= \underbrace{\beta \mathbf{H}_{r,d}^{(2)} \mathbf{H}_{s,r}^{(1)} \sqrt{P_{r,d}^{(2)} \mathbf{P}_{s,r}^{(1)}} \mathbf{X}^{(1)}}_{\text{desired}} + \underbrace{\mathbf{H}_{u,d}^{(2)} \sqrt{\mathbf{P}_{u,d}^{(2)}} \mathbf{S}^{(2)}}_{\text{UKIF}} + \underbrace{\beta \mathbf{H}_{r,d}^{(2)} \sqrt{P_{r,d}^{(2)}} n_{s,r}^{(1)} + \mathbf{n}^{(2)}}_{\text{noise}}. \end{aligned} \quad (4.10)$$

The part in Eqn. 4.10 $\beta \mathbf{H}_{r,d}^{(2)} \sqrt{P_{r,d}^{(2)}} n_{s,r}^{(1)}$ indicates that the noise at the RS is amplified together with the desired signal. As a consequence, the noise floor in $\mathbf{Y}_{r,d}^{(2)}$ is increased. Combining $\mathbf{Y}_{s,d}^{(1)}$ at the first time-slot and $\mathbf{Y}_{r,d}^{(2)}$ at the second time-slot, the final output at the BS can be expressed as

$$\begin{aligned} \begin{bmatrix} \mathbf{Y}_{s,d}^{(1)} \\ \mathbf{Y}_{r,d}^{(2)} \end{bmatrix} &= \underbrace{\begin{bmatrix} \mathbf{H}_{s,d}^{(1)} \sqrt{\mathbf{P}_{s,d}^{(1)}} \\ \beta \mathbf{H}_{r,d}^{(2)} \mathbf{H}_{s,r}^{(1)} \sqrt{P_{r,d}^{(2)} \mathbf{P}_{s,r}^{(1)}} \end{bmatrix} \mathbf{X}^{(1)}}_{\text{desired}} + \underbrace{\begin{bmatrix} \mathbf{H}_{u,d}^{(1)} \sqrt{\mathbf{P}_{u,d}^{(1)}} \mathbf{S}^{(1)} \\ \mathbf{H}_{u,d}^{(2)} \sqrt{\mathbf{P}_{u,d}^{(2)}} \mathbf{S}^{(2)} \end{bmatrix}}_{\text{UKIF}} + \underbrace{\begin{bmatrix} \mathbf{n}^{(1)} \\ \beta \mathbf{H}_{r,d}^{(2)} \sqrt{P_{r,d}^{(2)}} n_{s,r}^{(1)} + \mathbf{n}^{(2)} \end{bmatrix}}_{\text{noise}} \end{aligned} \quad (4.11)$$

The final output of the AF relaying can be simplified as

$$\mathbf{Y}_d^{AF} = \mathbf{H}_d^{AF} \mathbf{X}^{(1)} + \mathbf{H}_u^{AF} \mathbf{S}^{AF} + \mathbf{n}^{AF}. \quad (4.12)$$

An AF RS produces an equivalent N -input, 2-group of n_{Rx} -output channel with 2-group of L UKIFs and different noise levels in the output. The channel is a multiple-access channel. The maximum mutual information I^{AF} between $\mathbf{X}^{(1)}$ and \mathbf{Y}_d^{AF} is given by

$$I^{AF} = \frac{1}{2} I \left(\mathbf{X}^{(1)}; \mathbf{Y}_d^{AF} \right) = \frac{1}{2} \log \det \left| \mathbf{I} + \frac{\mathbf{H}_d^{AF} (\mathbf{H}_d^{AF})^H}{(\mathbf{H}_u^{AF} \mathbf{S}^{AF} + \mathbf{n}^{AF}) (\mathbf{H}_u^{AF} \mathbf{S}^{AF} + \mathbf{n}^{AF})^H} \right|, \quad (4.13)$$

where \mathbf{I} is an identity matrix. The factor $\frac{1}{2}$ comes from the fact that two time-slots are required for the relaying transmission due to the RS's half-duplex operation. The capacity region of the multiple-access AF relay channel is a closure of the set of the rates

$$I^{AF} = I\left(\mathbb{X}^{(1)}; \mathbf{Y}_d^{AF} / \overline{\mathbb{X}}^{(1)}\right), \quad (4.14)$$

where $\mathbb{X}^{(1)}$ is a subset of $\left[x_1^{(1)} \ \dots \ x_N^{(1)} \right]$ while $\overline{\mathbb{X}}^{(1)}$ is the complement of $\mathbb{X}^{(1)}$ in $\left[x_1^{(1)} \ \dots \ x_N^{(1)} \right]$.

4.3.2 The DF strategy

Unlike the AF relaying, a RS with a DF functionality decodes the received signal $y_{s,r}^{(1)}$, re-encodes and forwards the signal to the BS in the form of either an incremental redundancy [115] [117] or a repetition coding as explained in Sub-section 4.1.1. It is assumed in the dissertation that the RS transmits the messages from the N blocked desired MSs with a repetition re-encoding. After the signal is decoded by the RS and then re-encoded using the same codebook as used in the first transmission, using the first MS as an example, Eqn. 4.4 can be expressed as

$$\mathbf{Y}_{r,d}^{(2)}(1) = \mathbf{H}_{r,d}^{(2)} \sqrt{P_{r,d}^{(2)}} \hat{x}_1^{(1)} + \mathbf{H}_{u,d}^{(2)} \sqrt{\mathbf{P}_{u,d}^{(2)}} \mathbf{S}^{(2)} + \mathbf{n}^{(2)}, \quad (4.15)$$

where \hat{x}_1 is the detected signal of x_1 at the RS. With the similar method, the DF relaying outputs of the other blocked desired MSs can be derived. It is observed from Eqn. 4.15 that unlike the AF strategy, no enhancement of the noise floor happens to the DF strategy.

In the case when the RS can decode the signals from the MSs correctly, namely,

$$\hat{\mathbf{X}}^{(2)} = \mathbf{X}^{(1)}, \quad (4.16)$$

combining $\mathbf{Y}_{s,d}^{(1)}$ at the first time-slot and $\mathbf{Y}_{r,d}^{(2)}$ at the second time-slot, the final output at the BS can be expressed as

$$\begin{array}{c} \left| \begin{array}{c} \mathbf{Y}_{s,d}^{(1)} \\ \mathbf{Y}_{r,d}^{(2)} \end{array} \right| \\ \left| \begin{array}{c} \mathbf{H}_{s,d}^{(1)} \sqrt{\mathbf{P}_{s,d}^{(1)}} \\ \mathbf{H}_{r,d}^{(2)}(1) \ \dots \ \mathbf{H}_{r,d}^{(2)}(N) \end{array} \right| \sqrt{P_{r,d}^{(2)}} \mathbf{X}^{(1)} + \underbrace{\left| \begin{array}{c} \mathbf{H}_{u,d}^{(1)} \sqrt{\mathbf{P}_{u,d}^{(1)}} \mathbf{S}^{(1)} \\ \mathbf{H}_{u,d}^{(2)} \sqrt{\mathbf{P}_{u,d}^{(2)}} \mathbf{S}^{(2)} \end{array} \right|}_{UKIF} + \underbrace{\left| \begin{array}{c} \mathbf{n}^{(1)} \\ \mathbf{n}^{(2)} \end{array} \right|}_{noise}. \end{array} \quad (4.17)$$

The final output of the DF relaying can be simplified as

$$\mathbf{Y}_d^{DF} = \mathbf{H}_d^{DF} \mathbf{X}^{(1)} + \mathbf{H}_u^{DF} \mathbf{S}^{DF} + \mathbf{n}^{DF}. \quad (4.18)$$

The above expression is valid if and only if the RS can decode the messages from the blocked desired MSs correctly. In the case when the RS can not decode correctly, namely,

$$\hat{\mathbf{X}}^{(2)} \neq \mathbf{X}^{(1)}, \quad (4.19)$$

the error occurring at the S-R transmission will be propagated to the R-D transmission. With the assumption that $\hat{\mathbf{X}}^{(2)}$ stands for the detected signal of $\hat{\mathbf{X}}^{(2)}$ at the BS at the second time-slot, the

end-to-end BER of the relay transmission, using the first MS as an example, can be computed

$$\begin{aligned}
p(\hat{x}^{(2)} \neq x_1) &= 1 - p(\hat{x}^{(2)} = x_1) \\
&= 1 - p(\hat{x}^{(2)} = \hat{x}^{(2)}) \times p(\hat{x}^{(2)} = x_1) \\
&= 1 - (1 - p(\hat{x}^{(2)} \neq \hat{x}^{(2)})) \times (1 - p(\hat{x}^{(2)} \neq x_1)) \\
&= p(\hat{x}^{(2)} \neq x_1) \times (1 - p(\hat{x}^{(2)} \neq \hat{x}^{(2)})) + p(\hat{x}^{(2)} \neq \hat{x}^{(2)}). \tag{4.20}
\end{aligned}$$

Eqn. 4.20 reveals that the final end-to-end BER is the sum of two cases. The one is that an error happens at the first hop while no error happens at the second hop, the other is that an error happens at the second hop. The first part of Eqn. 4.20 indicates that the error, occurring at the first hop, would propagate to the second hop, namely, error propagation. Therefore, both the S-R link and the R-D link play a important role to the final performance of a relay transmission observed at the BS.

At the first time-slot, the blocked desired MSs broadcast their signals to the BS and the RS. For each blocked desired MS, it is a broadcast channel from the MS to the BS and to the RS. Due to the statement that the S-R link quality should be better than the S-D link quality, $\mathbf{Y}_{s,d}^{(1)}$ is a degraded version of $\mathbf{Y}_{s,r}^{(1)}$ (Theorem 1 in [52]) [55]. At the second time-slot, $\mathbf{Y}_{r,d}^{(2)}$ is a degraded version of $\mathbf{Y}_{s,r}^{(1)}$ due to the UKIF and AWGN noise (Theorem 1 in [52]) [55]. Across the N blocked desired MSs, it is a multiple access channel to the BS and to the RS. The maximum mutual information I^{DF} of MARN [134] with a DF relay is given by

$$I^{DF} = \frac{1}{2} \min \left(\underbrace{I \left(\mathbb{X}^{(1)}; y_{s,r}^{(1)}, \mathbf{Y}_d^{DF} / \overline{\mathbb{X}}^{(1)}, x_{r,d}^{(2)} \right)}_{\text{broadcasting}}, \underbrace{I \left(\mathbb{X}^{(1)}, x_{r,d}^{(2)}; \mathbf{Y}_d^{DF} / \overline{\mathbb{X}}^{(1)} \right)}_{\text{multiple access}} \right). \tag{4.21}$$

It is observed from Eqn. 4.21 that I^{DF} is limited by the minimal capacity at the first and second time-slots, namely, the capacity of the broadcasting channel at the first time-slot and the capacity of the multiple access channel at the second time-slot. The definitions of $\mathbb{X}^{(1)}$ and $\overline{\mathbb{X}}^{(1)}$ are the same as the definitions for the AF relay in Eqn. 4.14.

4.4 Proposed protocols

According to the system model introduced in Section 4.2, novel cooperative multiple access relay protocols are proposed in this section. First of all, a relay protocol with a limited feedback is proposed which enables MARN switch adaptively between the direct transmission and the relay transmission, depending on the ARQ feedback message from the BS. Furthermore, MAC is proposed at the first time-slot (see Fig. 4.2) for the separability of the signals from the blocked desired MSs at the receiver and for the total throughput enhancement; symbol-wise super-positioning [26] is proposed at the RS to minimize the amount of the forwarding signals to the destination in one transmission.

4.4.1 Relaying protocol design

4.4.1.1 Direct transmission without relaying

For the comparison purpose, the direct transmission without relaying is used as the baseline. The capacity of the direct transmission can be expressed as

$$I^{Direct} = I(\mathbb{X}; \mathbf{Y}_{s,d}/\overline{\mathbb{X}}). \quad (4.22)$$

The definitions of \mathbb{X} and $\overline{\mathbb{X}}$ are the same as the definitions for the AF relay in Eqn. 4.14.

4.4.1.2 Always relaying protocol

Always relaying protocol stands for the case where the signals from the desired MSs are always forwarded by the RS to the BS, regardless of the transmission quality of the direct transmission. As a consequence, the final end-to-end capacity will be always halved due to the half-duplex operation of the RS as shown in Eqn. 4.14 and Eqn. 4.21. Therefore, the performance improvement because of relaying is limited.

4.4.1.3 Adaptive relaying protocol with limited feedback

By comparing Eqn. 4.22 with Eqn. 4.14 and Eqn. 4.21, it can be found that the capacity difference between the direct transmission and the relay transmission comes from the factor $\frac{1}{2}$. An always relaying protocol can be helpful if and only if the final end-to-end capacity of the relay link is larger than the capacity of the direct transmission. Therefore, the system should make an adaptation between the relay transmission and the direct transmission. Based on this observation, the following protocol as shown in Fig. 4.4 is proposed. First of all, the N blocked MSs broadcast their signals to the RS and to the BS. The BS checks the received signals by the Cyclic Redundancy Check (CRC) information. If the BS finds that it can not detect the signals from the blocked MSs correctly, it will broadcast a Negative Acknowledgment (NAK) message to the MSs and to the RS. It is assumed that the NAK message can be detected reliably both by the MSs and by the RS. At the second time-slot, the MSs will re-transmit their signals to the BS. Simultaneously, the RS will forward the signals received at the first time-slot to the BS. The transmissions from the MSs and from the RS as well can be combined constructively at the BS, of which an additional diversity gain can be achieved at the expense of a receive collision [25]. If the BS can detect the signals from the blocked desired MSs correctly, it will send an Acknowledgment (ACK) message to the MSs and to the RS. Thereafter, the blocked desired MSs start a new transmission. At the same time, the RS stays in an "idle" status. This protocol can make efficiently use of the system resources since the RS works only on demand. The system switches between the direct transmission and the relay transmission based on the ARQ knowledge. Furthermore, this protocol is reasonable for the practical applications where it is the common sense that the MSs are not aware of the existence of the RS. The complexity of the signal processing is taken over by the BS which sounds also reasonable. Normally, the BS is envisaged to be able to perform a complicated signal

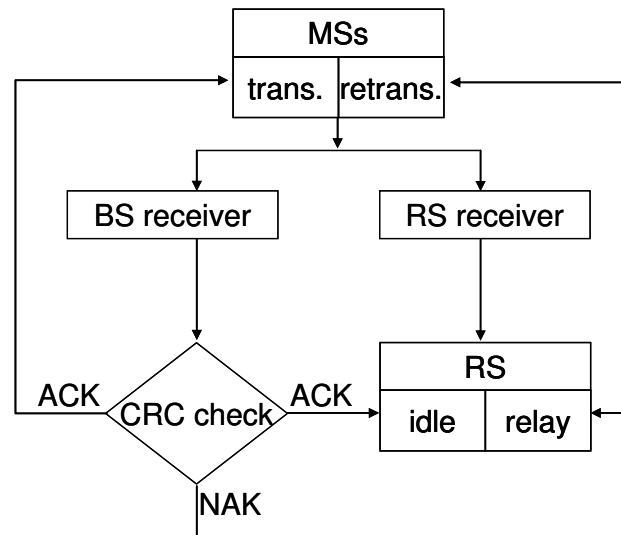


Fig. 4.4: Flow-chart of the relay protocol with ARQ.

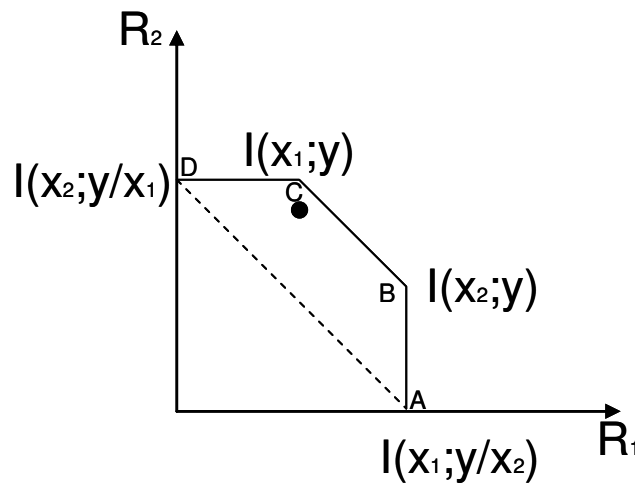


Fig. 4.5: Achievable capacity region of a 2-MS access channel.

processing since it has more redundancy than the MSs in the space and in the dimension during the deployment.

4.4.2 MAC

It is shown in [55] that the capacity of a multiple access channel is the closure of the convex hull of n -tuple rates, where n stands for the number of accessing users. Figure 4.5 shows the achievable capacity margin of a 2-MS access channel with x_1 , x_2 being the inputs of MS₁ and MS₂, respectively, and y being the channel output. The capacity margin is a closure form of the individual rates and the sum of two rates. For example, the line A-B and the line C-D in Fig. 4.5 mean, respectively, the individual rate between x_1 and y conditioned by given x_2 and the individual rate between x_2 and y conditioned by given x_1 . The curve B-C shows the sum rate between (x_1, x_2) and y . In Fig. 4.5, point A at the margin stands for the maximum achievable capacity if MS₁ transmits with full rate while MS₂ transmits nothing. The dashed curve stands for the achievable capacities of

MS₁ and MS₂ when they transmit with orthogonal resource (time/frequency/code/space). Subplot 4.6(a) and Subplot 4.6(b) in Fig. 4.6 show, respectively, the orthogonal Time Division Multiple Access (TDMA) transmission scheme of a multiple access channel and of a two-hop multiple access channel. Point *B* corresponds to the MS₂'s maximum achievable capacity if MS₁ transmits with full rate. The gap between the dashed curve and the A-B-C-D convex shows the gain between the capacity achieved by an orthogonal resource allocation and the maximum capacity.

To approach the capacity margin of a multiple access channel, Kasami proposed MAC in [37] by time-sharing between MSs. The code he proposed guarantees the signal separability while increasing the total throughput for a binary signal transmission over the real-valued channels. The *N*-MS Kasami code has *N* codebooks, denoted as \mathcal{C}_i with $1 \leq i \leq N$, each having ξ_i codewords. Each codeword spans over *N* symbol timings with code rate $\frac{1}{N}$. Subplot 4.6(c) in Fig. 4.6 shows the transmission time scheme of a two-hop multiple access channel with MAC. The transmitted vector $\mathbf{X}^{(1)}$ in Eqn. 4.1 and Eqn. 4.2 collects the symbols in the transmitted codewords from the *N* MSs at each symbol timing. Assume that the MS *i* uses the codebook \mathcal{C}_i , the matrix $\mathbf{X}^{(1)}$, containing the codewords transmitted from the *N* MSs, is then denoted as $\mathbf{X}^{(1)} = [\mathbf{x}_1^{(1)}, \mathbf{x}_2^{(1)}, \dots, \mathbf{x}_N^{(1)}]^T$ with $\mathbf{x}_i^{(1)} \in \mathcal{C}_i$ and $\mathbf{x}_i^{(1)} = [x_i^{(1)}(1), x_i^{(1)}(2), \dots, x_i^{(1)}(N)]^T$ with $1 \leq i \leq N$. Thus, $\mathbf{X}^{(1)}$ is given by

$$\mathbf{X}^{(1)} = [\mathbf{X}^{(1)}(1), \mathbf{X}^{(1)}(2), \dots, \mathbf{X}^{(1)}(N)]. \quad (4.23)$$

Eqn. 4.23 indicates that $\mathbf{X}^{(1)}$ is a column of $\mathbf{X}^{(1)}$. Namely, $\mathbf{X}^{(1)}$ is an enumeration of $\mathbf{X}^{(1)}$ over *N* symbol timings. The set \mathcal{X} , comprising all combinations of $\mathbf{X}^{(1)}$, has $\prod_{i=1}^N \xi_i$ elements in total. Even though all MSs transmit their signals at the same time using the same frequency, their signal can be uniquely decoded and identified without ambiguity at the receiver if and only if, for any matrix $\mathbf{A}, \mathbf{B} \in \mathcal{X}$, no $\mathbf{A} (\mathbf{A} \neq \mathbf{B})$ exists, such that

$$\sum_{j=1}^N \sqrt{P_j} h_j (A(j) - B(j)) = 0. \quad (4.24)$$

where $\sqrt{P_j} h_j$ is the complex channel gain multiplied with the root of the power. They are element from $\mathbf{H}_{s,d}^{(1)} \sqrt{\mathbf{P}_{s,d}^{(1)}}$ (ref. Eqn. 4.1) and $\mathbf{H}_{s,r}^{(1)} \sqrt{\mathbf{P}_{s,r}^{(1)}}$ (ref. Eqn. 4.2), respectively.

The Kasami code, originally designed for the binary transmission over the real-valued channels, can be extended to the transmission over the complex-valued channels. In this dissertation symbols in the codewords are defined over the Galois field (GF)(4) corresponding to QPSK. An example of 2-MS MAC obtained through computer searching is shown in Table B.2 in Appendix B. With orthogonal signaling, the total throughput of a two-MS system is 4 bits/symbol with QPSK. Whereas, with the 2-MS MAC, the total signaling throughput is 5.17 bits/symbol. Therefore, the 2-MS MAC can achieve a 1.17 bits/symbol throughput gain over the orthogonal signaling. The position of the black point in Fig. 4.5 shows the rate of the 2-MS MAC which is near to the capacity region of a 2-MS access channel.

According to the unique decodability definition given by Eqn. 4.24, the signals from different MSs can be separated and uniquely identified at the BS and at the RS. The examples of MAC obtained through a computer searching for the *N*-MS's case, $2 \leq N \leq 4$, can be found in Table B.2 in Appendix B.

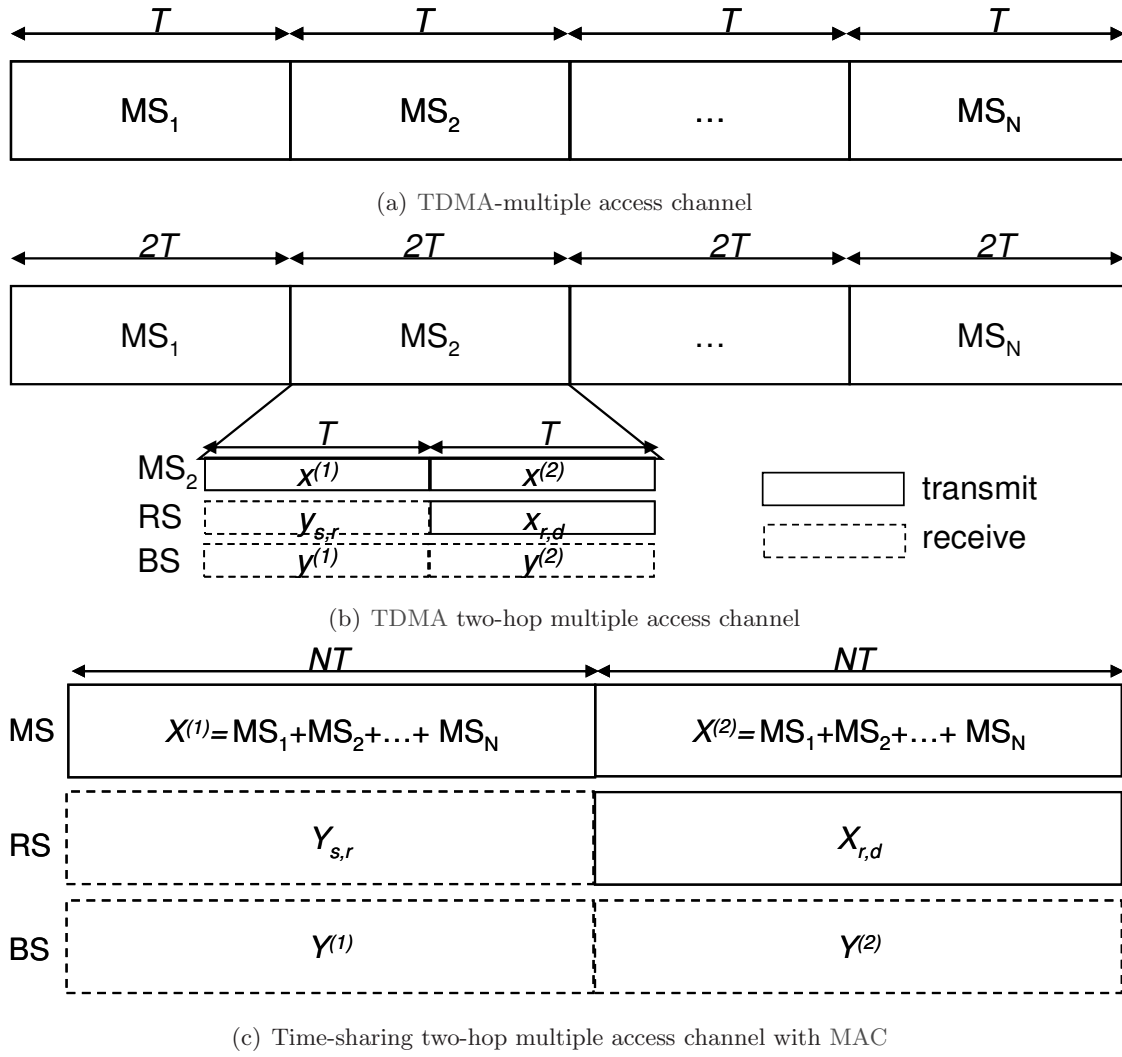


Fig. 4.6: Transmission time schemes of a multiple access channel with/without a half-duplex relaying transmission

4.4.3 Symbol-wise super-positioning

At the first time-slot, the RS receives the signals from the N desired MSs. For the AF relaying, the received message is simply amplified and then retransmitted at the second time-slot by the RS. If the RS has a DF functionality, the received message is firstly decoded, re-encoded, and then re-transmitted to the BS at the second time-slot. In this dissertation, it is assumed that the RS decodes the received message and re-transmits it symbol-wise to the BS at the second time-slot. After decoding the N MAC-encoded transmitted signals by the RS, the RS performs a symbol-level super-positioning by summing up the symbols, obtained as the results of the MAC decoding. As stated that the RS decodes the signals from the desired MSs as $\hat{\mathbf{X}}^{(2)}$, $x_{r,d}^{(2)}$ can be expressed as

$$x_{r,d}^{(2)} = \sum_{i=1}^N \hat{x}_i^{(2)} \quad (4.25)$$

where i stands for the i^{th} MS. Based on the received signal at the destination at the second time-slot, the signals of the desired MSs can be recovered by exploiting, again, the MAC signal separability property.

4.4.4 Re-transmission at the second time-slot

In Sub-subsection 4.4.1.3, it is proposed that the MSs will re-transmit their signals to the BS at the second time-slot if they receive a NAK message correctly. The MSs will re-transmit the same signals, which have been transmitted at the first time-slot. Therefore, the Eqn. 4.4 can be extended as

$$\mathbf{Y}_{r,d}^{(2)} = \underbrace{\mathbf{H}_{r,d}^{(2)}\sqrt{P_{r,d}^{(2)}}x_{r,d}^{(2)} + \mathbf{H}_{s,d}^{(2)}\sqrt{\mathbf{P}_{s,d}^{(2)}}\mathbf{X}^{(1)}}_{desired} + \underbrace{\mathbf{H}_{u,d}^{(2)}\sqrt{\mathbf{P}_{u,d}^{(2)}}\mathbf{S}^{(2)}}_{UKIF} + \underbrace{\mathbf{n}^{(2)}}_{noise} \quad (4.26)$$

Based on the above proposed protocol, the system model of the AF relay at the first time-slot can be summarized as

$$\mathbf{Y}_{final}^{AF(1)} = \underbrace{\mathbf{H}_{s,d}^{(1)}\sqrt{\mathbf{P}_{s,d}^{(1)}}\mathbf{X}^{(1)}}_{desired} + \underbrace{\mathbf{H}_{u,d}^{(1)}\sqrt{\mathbf{P}_{u,d}^{(1)}}\mathbf{S}^{(1)}}_{UKIF} + \underbrace{\mathbf{n}^{(1)}}_{noise} \quad (4.27)$$

while the system model of the AF relay at the second time-slot can be summarized as

$$\mathbf{Y}_{final}^{AF(2)} = \begin{cases} \underbrace{\left(\beta\mathbf{H}_{r,d}^{(2)}\mathbf{H}_{s,r}^{(1)}\sqrt{P_{r,d}^{(2)}}\mathbf{P}_{s,r}^{(1)} + \mathbf{H}_{s,d}^{(2)}\sqrt{\mathbf{P}_{s,d}^{(2)}}\right)\mathbf{X}^{(1)}}_{desired} + \underbrace{\mathbf{H}_{u,d}^{(2)}\sqrt{\mathbf{P}_{u,d}^{(2)}}\mathbf{S}^{(2)}}_{UKIF} + \underbrace{\beta\mathbf{H}_{r,d}^{(2)}\sqrt{P_{r,d}^{(2)}}n_{s,r}^{(1)} + \mathbf{n}^{(2)}}_{noise} & NAK \\ \underbrace{\mathbf{H}_{s,d}^{(2)}\sqrt{\mathbf{P}_{s,d}^{(2)}}\mathbf{X}^{(2)}}_{desired} + \underbrace{\mathbf{H}_{u,d}^{(2)}\sqrt{\mathbf{P}_{u,d}^{(2)}}\mathbf{S}^{(2)}}_{UKIF} + \underbrace{\mathbf{n}^{(2)}}_{noise} & ACK \end{cases} \quad (4.28)$$

The system model of the DF relay at the first time-slot can be expressed exactly the same as that of the AF relay at the first time-slot in Eqn. 4.27. Similarly, the system model of the DF relay at the second time-slot can be summarized as

$$\mathbf{Y}_{final}^{DF(2)} = \begin{cases} \underbrace{\left(\left|\begin{array}{ccc} \mathbf{H}_{r,d}^{(2)} & \cdots & \mathbf{H}_{r,d}^{(2)} \end{array}\right| \sqrt{P_{r,d}^{(2)}} + \mathbf{H}_{s,d}^{(2)}\sqrt{\mathbf{P}_{s,d}^{(2)}}\right)\mathbf{X}^{(1)}}_{desired} + \underbrace{\mathbf{H}_{u,d}^{(2)}\sqrt{\mathbf{P}_{u,d}^{(2)}}\mathbf{S}^{(2)}}_{UKIF} + \underbrace{\mathbf{n}^{(2)}}_{noise} & NAK \\ \underbrace{\mathbf{H}_{s,d}^{(2)}\sqrt{\mathbf{P}_{s,d}^{(2)}}\mathbf{X}^{(2)}}_{desired} + \underbrace{\mathbf{H}_{u,d}^{(2)}\sqrt{\mathbf{P}_{u,d}^{(2)}}\mathbf{S}^{(2)}}_{UKIF} + \underbrace{\mathbf{n}^{(2)}}_{noise} & ACK \end{cases} \quad (4.29)$$

Both in Eqn. 4.28 and in Eqn. 4.29, the first part describes the relay transmission with a NAK feedback message from the BS while the second part presents the direct transmission with an ACK feedback message. The first part includes two transmissions with a receive collision at the BS at the second time-slot. The one is the N MSs' re-transmission, the other is the RS's forwarding transmission. For the notation simplification, Eqn. 4.27, Eqn. 4.28, and Eqn. 4.29 can be generalized to the following form

$$\mathbf{Y} = \mathbf{H}_d\mathbf{X}_d + \mathbf{H}_u\mathbf{S}_u + \mathbf{n} = \left| \begin{array}{cc} \mathbf{H}_d & \mathbf{H}_u \end{array} \right| \left| \begin{array}{c} \mathbf{X}_d \\ \mathbf{S}_u \end{array} \right| + \mathbf{n} = \mathfrak{H}\mathfrak{X} + \mathbf{n}, \quad (4.30)$$

where

$$\begin{aligned} \mathfrak{H} &= \begin{vmatrix} \mathbf{H}_{s,d}^{(1)}\sqrt{\mathbf{P}_{s,d}^{(1)}} & \mathbf{H}_{u,d}^{(1)}\sqrt{\mathbf{P}_{u,d}^{(1)}} \end{vmatrix}, \\ \mathfrak{X} &= \begin{vmatrix} \mathbf{X}^{(1)} \\ \mathbf{S}^{(1)} \end{vmatrix} \end{aligned} \quad (4.31)$$

at the first time-slot while at the second time-slot

$$\begin{aligned} \mathfrak{H} &= \begin{vmatrix} \beta\mathbf{H}_{r,d}^{(2)}\mathbf{H}_{s,r}^{(1)}\sqrt{P_{r,d}^{(2)}\mathbf{P}_{s,r}^{(1)}} + \mathbf{H}_{s,d}^{(2)}\sqrt{\mathbf{P}_{s,d}^{(2)}} & \mathbf{H}_{u,d}^{(2)}\sqrt{\mathbf{P}_{u,d}^{(2)}} \end{vmatrix} \\ \text{or} \\ \mathfrak{H} &= \begin{vmatrix} \mathbf{H}_{r,d}^{(2)} & \cdots & \mathbf{H}_{r,d}^{(2)} \end{vmatrix} \begin{vmatrix} \sqrt{P_{r,d}^{(2)}} + \mathbf{H}_{s,d}^{(2)}\sqrt{\mathbf{P}_{s,d}^{(2)}} & \mathbf{H}_{u,d}^{(2)}\sqrt{\mathbf{P}_{u,d}^{(2)}} \end{vmatrix} \\ \mathfrak{X} &= \begin{vmatrix} \mathbf{X}^{(1)} \\ \mathbf{S}^{(2)} \end{vmatrix} \end{aligned} \quad (4.32)$$

for the AF relay and for the DF relay, respectively. The variance of the final noise \mathbf{n} is σ_n^2 at the first time-slot transmission and at the second time-slot transmission in the case of a DF relay. The variance of the final noise \mathbf{n} will be changed to $\left(\beta\left|\mathbf{H}_{r,d}^{(2)}\right|\sqrt{P_{r,d}^{(2)}} + 1\right)\sigma_n$ at the second time-slot transmission in the case of an AF relay due to the noise floor enhancement. In the following, superscripts ⁽¹⁾ and ⁽²⁾ can be added to Eqn. 4.30, distinguishing two time-slots.

4.5 MMSE detection

As stated in Section 4.2, L UKIF MSs' signals arrive at the BS at both time-slots. At the BS, a spatial filtering using a MMSE algorithm takes place to jointly detect the received *composite signal* comprising the N desired MSs' transmitted signals [132] [38] [135] [11], while suppressing L UKIFs. The algorithm is referred to as JU MMSE for convenience [11]. At the both time-slots, a ML detection follows the MMSE spatial filtering to separate each MS's transmitted MAC codeword as shown in Fig. 4.7. After the detection at the first and second time-slots, an error detection aided signal selection technique is proposed to combine the detected signals at both time-slots constructively.

4.5.1 JU MMSE detection

The key idea behind the JU MMSE technique is that UKIFs are suppressed, while preserving the MAC-encoded *composite signal* structure. Two JU MMSE criteria [11], \mathcal{A} -criterion [38] [135] and \mathbf{H} -criterion [133], are presented in this sub-section.

4.5.1.1 JU MMSE \mathcal{A} -criterion

The JU MMSE detector determines the spatial filtering weights $\mathcal{W}_{\mathcal{A}}$ and \mathcal{A} according to the error cost function $e_{\mathcal{A}}$,

$$\arg \min_{\mathcal{W}_{\mathcal{A}}, \mathcal{A}} E \left\{ \|e_{\mathcal{A}}\|^2 \right\} = \arg \min_{\mathcal{W}_{\mathcal{A}}, \mathcal{A}} E \left\{ \|\mathcal{W}_{\mathcal{A}}^H \mathbf{Y} - \mathcal{A}^H \mathbf{X}_d\|^2 \right\}, \quad (4.33)$$

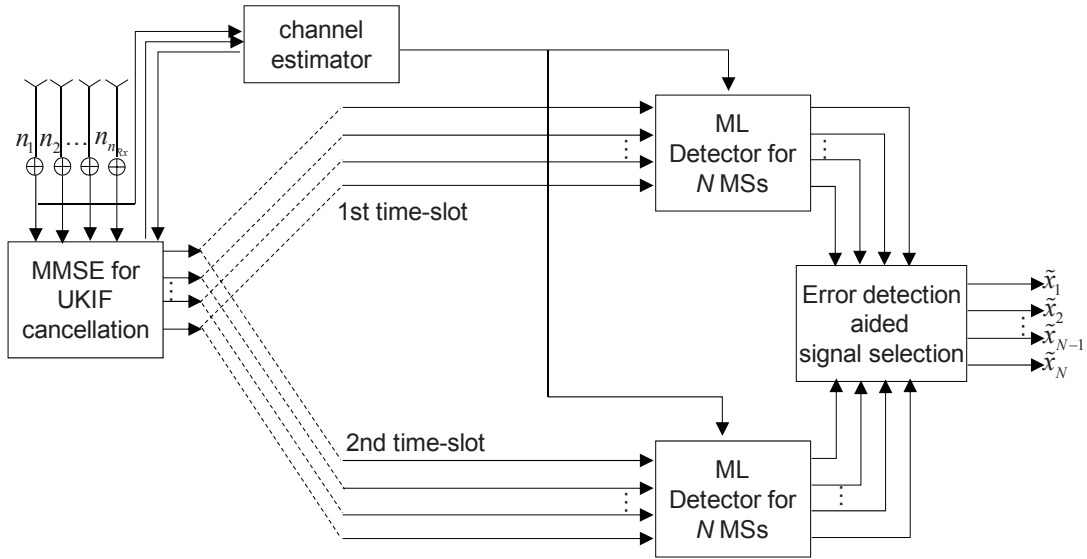


Fig. 4.7: Receive structure at the BS with n_{Rx} antenna elements.

where matrices \mathcal{W}_A and \mathcal{A} are subjected to an appropriate constraint in order to avoid the trivial solution $[\mathcal{W}_A, \mathcal{A}] = [\mathbf{0}, \mathbf{0}]$. At the both time-slots, each MS's signal is not separated with JU MMSE but is separated by the MAC ML detector, because the signal separability is still maintained at the JU MMSE output.

For the reception of the N MSs' received *composite signal*, it is shown in Appendix C that the i^{th} column of the optimal solution \mathcal{W} [11] to Eqn. 4.33 under the constraint $\mathcal{A}_{i,i} = 1$, $1 \leq i \leq n_{Rx}$, is given by

$$\mathcal{W}_i = \left(\mathbf{M} - \sum_{j=1, j \neq i}^N \mathbf{h}_j (\mathbf{h}_j)^H \right)^{-1} \mathbf{h}_i \quad (4.34)$$

where

$$\mathbf{M} = \mathfrak{H} (\mathfrak{H})^H + \sigma_n^2 \mathbf{I} \quad (4.35)$$

and \mathbf{h}_j is the j^{th} column of \mathbf{H}_d .

4.5.1.2 JU MMSE H-criterion

Instead of using $\mathcal{A}^H \mathbf{X}_d$ in Eqn. 4.33, the received *composite signal* comprising the desired signal components alone, $\mathbf{H}_d \mathbf{X}_d$, is used as the reference signal for the JU MMSE detection with the **H**-criterion. The cost function $e_{\mathbf{H}}$ can then be given as

$$\arg \min_{\mathcal{W}_{\mathbf{H}}} E \left\{ \|e_{\mathbf{H}}\|^2 \right\} = \arg \min_{\mathcal{W}_{\mathbf{H}}} E \left\{ \left\| \mathcal{W}_{\mathbf{H}}^H \mathbf{Y} - \mathbf{H}_d \mathbf{X}_d \right\|^2 \right\}. \quad (4.36)$$

The optimal spatial filtering weight vector $\mathcal{W}_{\mathbf{H}}$ is given by [133]

$$\mathcal{W}_{\mathbf{H}}^H = \mathbf{H}_d \mathbf{H}_d^H \mathbf{M}^{-1}. \quad (4.37)$$

H-criterion uses the actual channel matrix \mathbf{H} when finding the weight matrix, by which an additional constraint is imposed. However, with **A**-criterion, both \mathcal{A} and $\mathcal{W}_{\mathcal{A}}$ are variables. Therefore, **H**-criterion will return a local optimum solution while **A**-criterion provides a global solution.

After the JU MMSE detection with either **A**- or **H**-criterion¹, assuming that the contribution of the residual UKIF components is equivalent to noise, the output of the JU MMSE detector $\hat{\mathbf{Y}}$ can be expressed as

$$\hat{\mathbf{Y}} = (\mathcal{W})^H \mathbf{H}_d \mathbf{X}_d + \hat{\mathbf{n}} = \hat{\mathbf{H}}_d \mathbf{X}_d + \hat{\mathbf{n}} \quad (4.38)$$

where $\hat{\mathbf{H}}_d$ is the equivalent channel matrix observed from the output of JU MMSE. The covariance matrix of the equivalent noise $\hat{\mathbf{n}}$ is given by

$$\mathbf{R}_{\hat{\mathbf{n}}} = E \left\{ \hat{\mathbf{n}} (\hat{\mathbf{n}})^H \right\} = (\mathcal{W})^H \mathcal{R}_{cov} \mathcal{W}, \quad (4.39)$$

where \mathcal{R}_{cov} is the covariance matrix of UKIF-plus-noise. Note that the BS is assumed to have a perfect knowledge about the channel matrix \mathbf{H}_d . In practice, training sequences have to be transmitted to estimate the channel matrix \mathbf{H}_d and the covariance matrix of the UKIF-plus-noise component. Adaptive algorithms may be used for this purpose [136] [133]. However, the adaptive implementation of the proposed algorithm is out of the scope of this dissertation.

4.5.2 ML detection

As stated in Subsection 4.4.2, MAC spreads across N timings. Therefore, for the reception of the signal transmitted at the both time-slots, the N MMSE output vectors $\hat{\mathbf{Y}}$ with a dimension of $n_{Rx} \times 1$, taken over N symbol timings, are at first sorted in an $n_{Rx} \times N$ matrix $\hat{\mathcal{Y}}$ and then input to the MAC ML detector. At the MAC ML detector, each MS's signal is separated by utilizing the signal separability supported by MAC. The MAC ML detector finds the codeword matrix $\hat{\mathbf{X}}^{(1)}$ that satisfies

$$\hat{\mathbf{X}}^{(1)} = \arg \min_{\mathbf{X}^{(1)} \in \mathcal{X}} \left| \hat{\mathcal{Y}} - \hat{\mathbf{H}}_d \mathbf{X}^{(1)} \right|^2. \quad (4.40)$$

There are $\prod_{i=1}^N \xi_i$ possible combinations of the codewords that have to be tested for the MAC ML detection at the first and second time-slot.

4.5.3 Error detection aided signal selection

After the ML detection, the N MSs' transmitted signals are identified at both time-slots. However, even though the direct links of the MSs are significantly attenuated, the contribution from the direct links should not be ignored. Now, these two detected vectors of the MSs, $\hat{\mathbf{X}}^{(1)}$ and $\hat{\mathbf{X}}^{(2)}$, are jointly detected. An error message is returned if and only if both the direct and relayed signals are received in error. Otherwise, signals, received without errors either at the first or at the second

¹ When not explicit explanation, we use \mathcal{W} as the general weight matrix of the JU MMSE detector

Modulation	QPSK
Coding	MAC
Frame symbol length	3072
Number of antenna	MS: 1, RS: 1, BS: 2
Number of interference	1
Signal-to-Interference Ratio (SIR)	$SIR^{(1)} = SIR^{(2)} = 0$
SNR	$SNR_1 = SNR_2 = SNR_3$
Channel estimation	perfect

Tab. 4.1: Simulation parameters

time-slots, can finally be selected correctly.

4.6 Numerical simulation results of an example scenario

We exploit an example scenario to assess the performance of a cooperative multiple access relay system with the proposed protocols. In the example scenario, there are 3 ($N = 3$) desired MSs, one interference MS ($L = 1$), and one RS. These three desired MSs are blocked from the BS and their signals are forwarded by the RS to the BS. The BS has 2 ($n_{Rx} = 2$) receive antenna elements, of which the channel gains are independent. It is assumed that the coded symbols are transmitted in frames, each having 3072 symbols. It is also assumed throughout this section that $SIR^{(1)} = SIR^{(2)} = 0$ [dB] and the transmit powers of three MSs are the same. Namely, $SNR_1 = SNR_2 = SNR_3$. We evaluate the total throughput and the average BER as performance measures. Table 4.1 summarizes the major simulation parameters.

4.6.1 MAC for the direct transmission

A 3-MS MAC that has 3 codebooks, having 4, 4, and 36 codewords, respectively, was used in the simulations. The codewords of the 3-MS MAC used are presented in Table B.2 in Appendix B. It improves the total throughput over the orthogonal 3-MS transmission by 3.17 bits/symbol at the expense of an increased complexity for the ML detection. We assign the codebook with the largest number (=36) of codewords to the blocked MS3. The 2 other MSs use the rest of codebooks, each having 4 codewords.

The BER and throughput performances with the 3-MS MAC are presented in Fig. 4.8(a) and Fig. 4.8(b), respectively. As a reference, the BER and the throughput curves with uncoded transmission are also presented in the same figures. There are three cases for the comparison in Figs. 4.8(a) and 4.8(b): *a*) uncoded with $n_{Rx} = 1$ and $L = 0$ (without UKIF) [10]; *b*) coded with $n_{Rx} = 1$ and $L = 0$; *c*) coded with $n_{Rx} = 2$ and $L = 0$. It is found that the BER curves with *a*) and *b*) have the same decay, indicating that the signal separability and the throughput enhancement make a parallel shift in the curves only. In the case of *c*), we can clearly observe the increase in the diversity order. This is simply because all the available Degree of Freedom (DoF) can be used to detect the desired *composite signal* received by the 2 antenna elements at the BS, and the ML

detector combines them, MS by MS, to achieve the diversity gain.

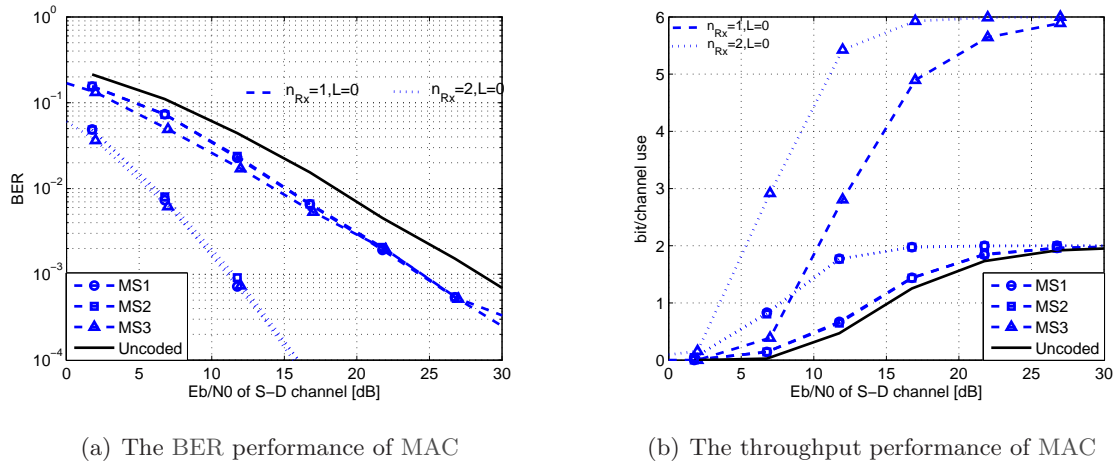


Fig. 4.8: The BER and throughput performances of MAC with *a)* uncoded with $n_{Rx} = 1$ and $L = 0$, *b)* MAC-encoded with $n_{Rx} = 1$ and $L = 0$, and *c)* MAC-encoded with $n_{Rx} = 2$ and $L = 0$.

In Fig. 4.8(b), it is observed that the total throughput with MAC is larger than that of uncoded transmission over the entire range of E_b/N_0 . Furthermore, it is found that the throughput with MS3 is always higher than those of MS1 and MS2 with $n_{Rx} = 1$ due to the fact that MS3 has a larger number of the codewords than MS1 and MS2.

4.6.2 JU MMSE for the interference cancellation

Figure 4.9 provides a comparative result of the performances of two JU MMSE criteria: the \mathcal{A} -criterion and the \mathbf{H} -criterion. It is observed in Fig. 4.9 that a floor is placed to the BER curves with the \mathbf{H} -criterion as the SNR value becomes large while the curves with the \mathcal{A} -criterion tend to have a constant slope. Even though the signal separability is not the objective of a JU MMSE spatial filtering, but the objective of a MAC-ML decoder, a floor happens to the \mathbf{H} -criterion. The reason for this is because the \mathbf{H} -criterion imposes additional constraints to preserve the MAC-encoded signal structure at the spatial filter output. To satisfy the requirement for the constraints, the available DoF has to be wasted; If the BS does not have enough DoF, an error floor is placed. On the contrary, with the \mathcal{A} -criterion, no additional constraints are imposed, resulting in no error floor placed.

It is also found from the MS3's BER curves of both criteria that MS3 has always worse performance than MS1 and MS2 in the presence of UKIF with the same SNR value. This is because the smaller Euclidean distance of MS3's codewords. Both in Fig. 4.8 and in Fig. 4.9, it can be observed that the BER curve of MS1 is overlapped with the BER curve of MS2 in all cases. This means that MS1 and MS2 have the same performance. The reason is that MS1 and MS2 have the same number of codewords and the same Euclidean distance among codewords. In the following, MS1's and MS2's performances will be shown together as one curve.

Compared the BER curves in Fig. 4.9 with the curves in Fig. 4.8(a), it is found that the BER curves in Fig. 4.9 have the same decay as *a)* and *b)*, even though the case in Fig. 4.9 assumes 2

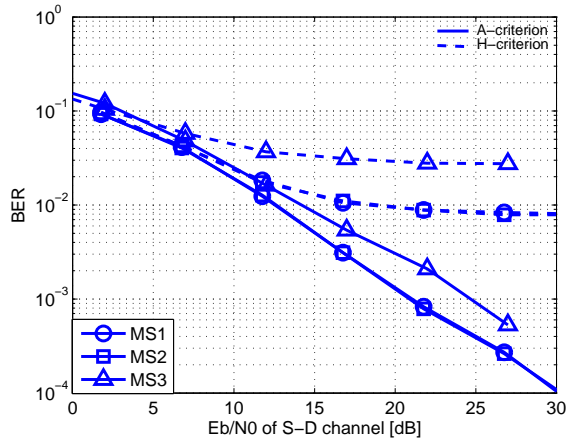


Fig. 4.9: The BER performances of MAC with \mathbf{H} -criterion and \mathcal{A} -criterion in the case of $n_{Rx} = 2$ and $L = 1$.

BS antenna elements. This is because UKIF is canceled by JU MMSE, for which the DoF with the $n_{Rx} = 2$ antenna setting has to be used. By comparing the curves of $c)$ with the curves of the \mathcal{A} -criterion, it can be concluded that the curves of $c)$ approach the curves of the \mathcal{A} -criterion as the SIR value decreases. It indicates that the system performance varies, dependent both on the SNR value and on the SIR value.

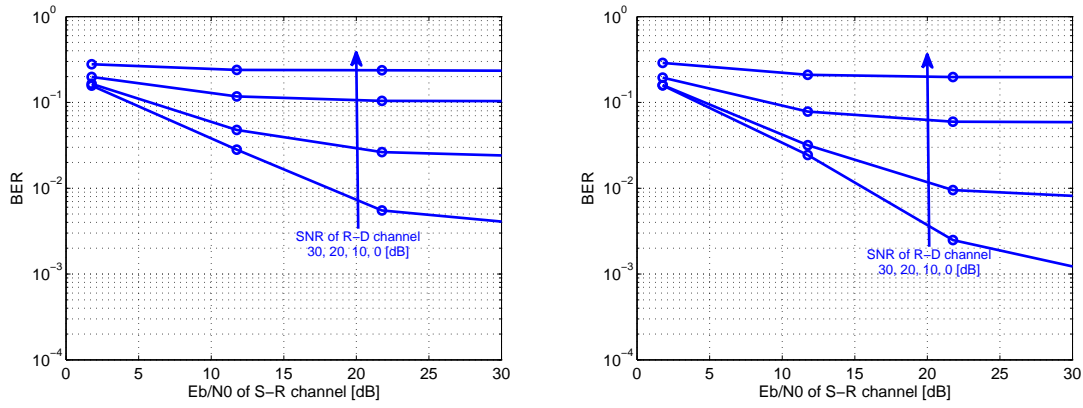
It should be emphasized that with the \mathcal{A} -criterion even though $N > n_{Rx}$ ($3 > 2$), still the multiple MSs' symbols can be well separated. This is because the signal separation is NOT the objective of JU MMSE, but the objective of the MAC ML detector. Therefore, since L antenna elements are required to suppress the L UKIFs, the number of the antenna elements required to detect the multiple MSs' *composite signal* is $L+1$ with the JU MMSE \mathcal{A} -criterion. However, the number of the elements required to detect the multiple MSs' *composite signal* is $L+N$ with the JU MMSE \mathbf{H} -criterion.

In the following simulations when it is not specified, a JU MMSE detector with the \mathcal{A} -criterion is used due to its superiority in the BER performance.

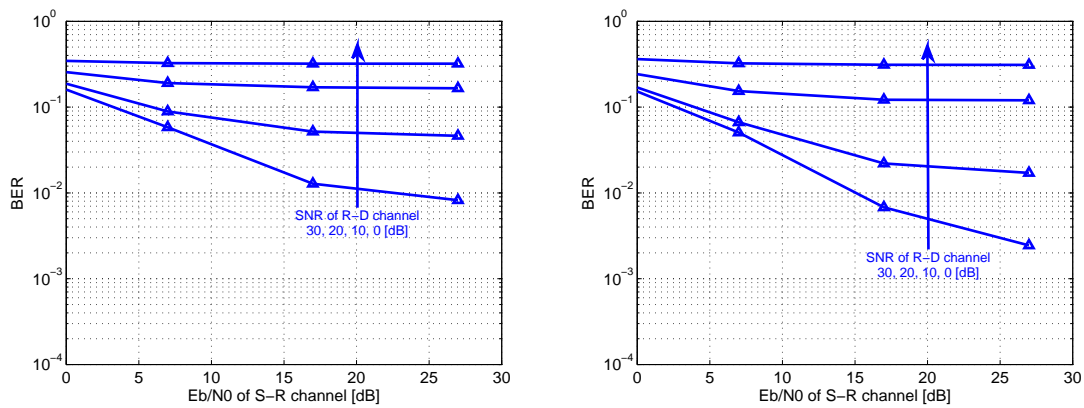
4.6.3 The functionality of the RS: the AF relay and the DF relay

Figure 4.10 provides the BER performances of MS1 and MS2 as well as MS3. The BER performances with two relaying strategies, the AF relay and the DF relay, correspond to the left subplot and the right subplot, respectively.

Each subplot in Fig. 4.10 includes a group of four curves, showing the dependence of the BER performance on the SNR value of the R-D channel. The SNR value of the R-D channel varies from 0 to 30 [dB] with a step of 10 [dB]. With the variable SNR value of the R-D channel, it is observed in all subplots in Fig. 4.10 that a floor is placed to the BER curve if the SNR value of the S-R channel is larger than the SNR value of the R-D channel. For example, when the SNR value of the R-D channel is fixed to 20 [dB] as shown in subplot. 4.10(a), the further increment of the SNR value of the S-R channel, larger than 20 [dB], yields only marginal improvement of the BER performance. A floor is placed after the 20 [dB] threshold. The same observation can be found to the rest SNR



(a) The BER performances of MS1 and MS2 with the AF relay (left) and the DF relay (right)

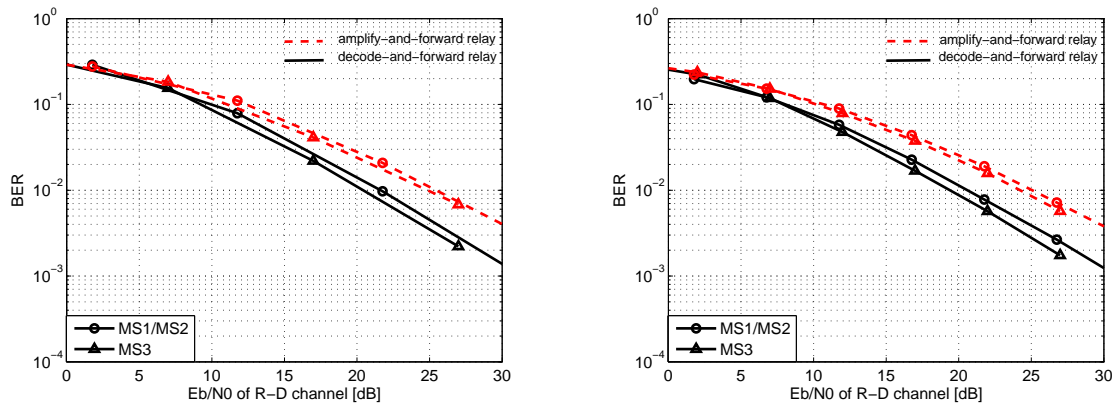


(b) BER performance of MS3 with the AF relay (left) and the DF relay (right)

Fig. 4.10: The BER performances of MS1 and MS2 as well as MS3 with the AF relay and the DF relay

values of the R-D channel, but with different threshold to the floor. The same behavior can be observed to the other MSs, regardless of the difference in the codebooks. It indicates that the final end-to-end performance of a relay channel is determined by the worst intermediate channel among the tandem relay chains, regardless of the relaying strategies. For the AF relay, the floor results from the noise enhancement while the floor of the DF relay stems from the error propagation. This observation agrees with the degraded relay channel argument in [52] [55].

Figure 4.11(a) shows the BER performance of MS1 and MS2 as well as MS3 when the S-R channel and the R-D channel have the same SNR value while Fig. 4.11(b) shows their BER performance when the S-R channel is free of noise. The group of the dashed curves stands for the BER performance of the AF relay while the group of the solid curves shows the performance of the DF relay. Compared the results in Fig. 4.11(a) with the results in Fig. 4.11(b), it is found that the assumption that the S-R channel is free of noise results in a parallel shift of the BER curve to left hand side both for the AF relay and for the DF relay. This observation is reasonable since either the noise enhancement limitation introduced by the AF relay or the error propagation limitation introduced by the DF relay disappears if the S-R channel is free of noise. No noise is enhanced for the the AF relay while no error is propagated to the R-D channel for the the DF relay.



(a) The BER performances of MS1 and MS2 as well as MS3 when the S-R channel and the R-D channel have the same SNR value

(b) The BER performances of MS1 and MS2 as well as MS3 when the S-R channel is free of noise

Fig. 4.11: The BER performances of MS1 and MS2 as well as MS3 with the AF relay and the DF relay

By comparing the BER performances of the AF relay with those of the DF relay, it is found that the DF relay outperforms the AF relay, but not at a remarkable degree. This observation is in line with Meng's observation in [137] where Meng evaluated the relative metrics of the AF relay and the DF relay with a distributed turbo code technique in user cooperation networks. The superiority of the DF relay comes from the fact that the errors occurring at the S-R channel due to noise can be partially detected and recovered by the decoding functionality of the RS. Whereas, the AF relay simply amplifies both the desired signal and the noise. Error detection and correction are only performed at the BS. As discussed in Section 4.3, a symbol-level decoding is performed at the RS for the DF relay while the AF relay needs only a RF front end and a low noise amplifier. Therefore, the DF relay returns in slight superiority in the BER performance at the expense of an additional signal processing complexity at the RS and a higher delay.

Furthermore, it is observed from Fig. 4.11 that MS1 and MS2 as well as MS3 have almost the same BER performance both in the case of the DF relay and the AF relay. This observation is distinguished from the observation in Fig. 4.9 in Sub-section 4.6.2, where the BER performance of MS3 is worse than those of MS1 and MS2 due to the smaller Euclidean distance of MS3's code-words. However, the observation in Fig. 4.11 has a similarity with the observation in Fig. 4.8(a) in Sub-section 4.6.1 where MS1 and MS2 as well as MS3 have almost the same BER performance. The reason is that the signals from all three desired MSs are mixed up at the RS both for the DF relay and the AF relay. The mixed signal is treated as one signal which undergoes the same R-D channel. As a consequence, the performances of MS1 and MS2 as well as MS3 are similar.

Even though there is a similarity between the BER performances shown in Fig. 4.11 and in Fig. 4.8(a) in Sub-section 4.6.1, it is observed that the group of curves in Fig. 4.11 tends to have the same decay as the curves in *b*) case, but is shifted to the right hand side compared with the curves in *b*) case in Fig. 4.8(a). This is due to the error propagation incurred by the DF relay and due to the noise floor enhancement incurred by the AF relay. As stated in Fig. 1.1 in Chapter 1, the S-R-D channel should have a higher SNR value than the direct transmission so that the relay transmission

achieves the same performance as the direct transmission. The observation in Fig. 4.11 verifies this statement. For example, compared Fig. 4.11 with Fig. 4.8(a) in Sub-section 4.6.1, the BER of the S-R-D relaying transmission at $Eb/N0 = 20$ [dB] is almost the same as that of the direct transmission at $Eb/N0 = 10$ [dB]. This observation is in line with the SNR relationship shown in Fig. 1.1 in Chapter 1.

4.6.4 Error detection aided signal selection

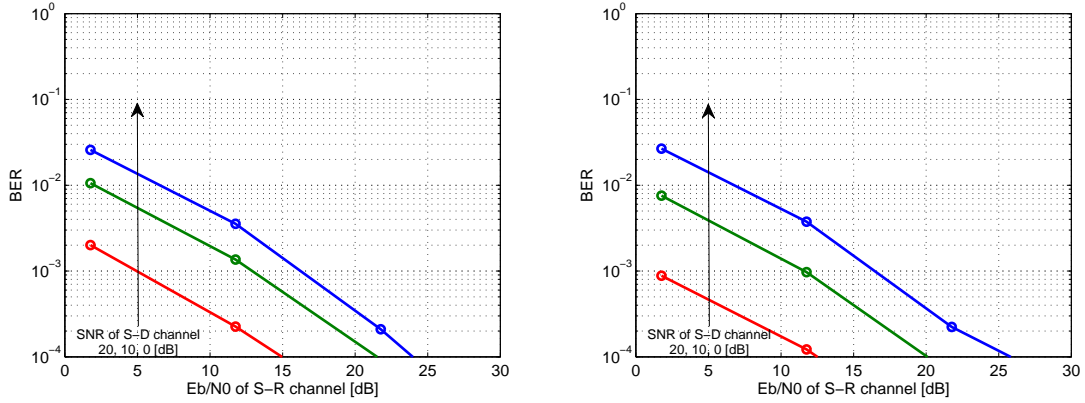
Due to the observation in Sub-section 4.6.3 that the final end-to-end performance of the relay channel is determined by the worst intermediate channel among the tandem relay chains, we set the S-R channel and the R-D channel have the same SNR value in this sub-section.

Figure 4.12 provides the BER performances of MS1 and MS2 as well as MS3. The BER performances with two relaying strategies, the AF relay and the DF relay, correspond to the left subplot and the right subplot, respectively. Each subplot in Fig. 4.12 includes a group of four curves, showing the dependence of the BER performance on the SNR value of the S-D channel, which varies from 0 to 30 [dB] with a step of 10 [dB]. It is observed in Fig. 4.12 that an error detection aided signal selection leads to a parallel shifting of the BER curve. As the SNR value of the S-D channel increases with a constant step of 10 [dB], the BER curves shift down with a variable step but tending to be constant. This observation agrees with the behavior observed in Fig. 4.9 in Sub-section 4.6.2 where the BER curve of MAC tends to have a constant decaying as the SNR value is higher than 10 [dB].

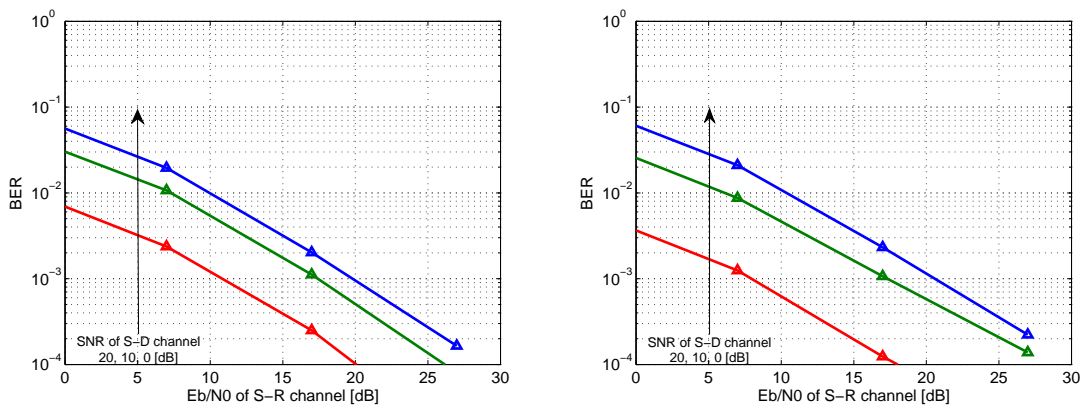
Comparing the BER performances of MS1 and MS2 with that of MS3, it has been found that MS1 and MS2 have better performances than MS3. This is due to the worse BER performance of MS3 during the direct transmission in the presence of UKIF. As discussed in Sub-section 4.6.2, during the direct transmission the BER performance of MS3 is worse than that of MS1 and MS2. Furthermore, by comparing the BER performances of the AF relay and that of the DF relay, it is found in all of the subplots 4.12(a) and 4.12(b) that the DF relay outperforms the AF relay. The higher the SNR value of the S-D channel, the more obvious the superiority of the performance of the DF relay is to the performance of the AF relay. This means, the DF relay provides superiority in the BER performance at the expense of an additional signal processing complexity at the RS.

4.6.5 Relay protocol with limited feedback

In Sub-subsection 4.4.1.3, it is proposed that the desired MSs re-transmit their original signals to the BS at the second time-slot, if they receive a "NAK" message from the BS. Simultaneously, the RS relays the signal from the desired MSs to the BS. Although a receive collision happens at the BS due to the simultaneous relay transmission and re-transmission, a performance gain can be still expected. The re-transmitted signals can be constructively combined with the relayed signal, similar with the error detection aided signal selection technique between the direct transmission and the relay transmission.



(a) The BER performances of MS1 and MS2



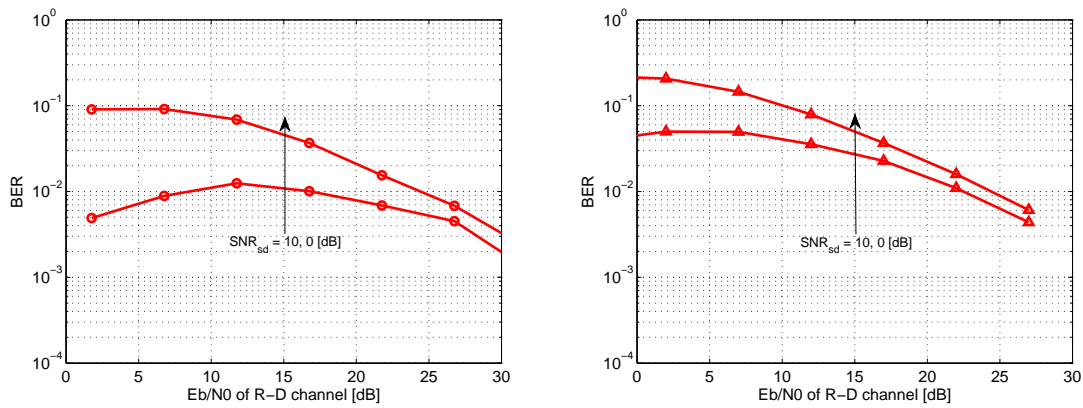
(b) The BER performance of MS3

Fig. 4.12: The BER performance of MS1 and MS2 as well as MS3 with an error detection aided signal selection technique in the case of the AF relay (left) and the DF relay (right)

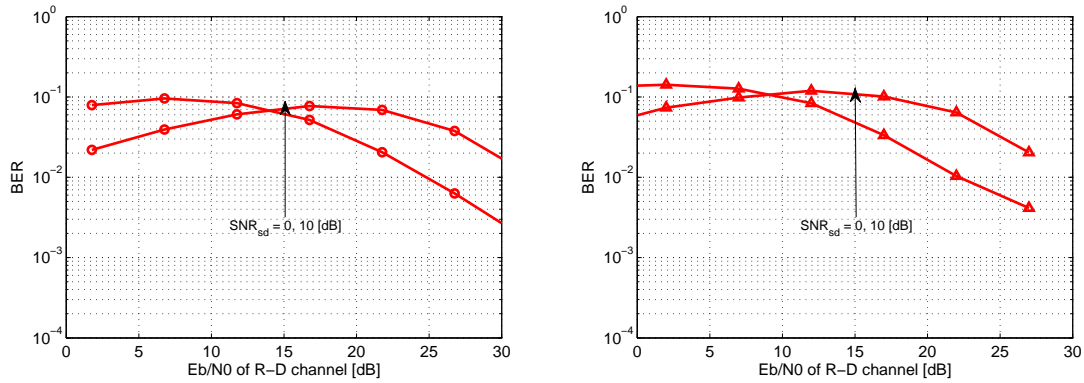
Figure 4.13 shows the BER performances of MS1 and MS2 (left) as well as MS3 (right) with the re-transmission technique, of which Fig. 4.13(a) presents the results in the case of the AF relay while Fig. 4.13(b) shows the results in the case of the DF relay. It is found in Fig. 4.13 that at the low E_b/N_0 range, the BER performance does not monotonously increase with the increasing E_b/N_0 value of the R-D channel². This is due to the change of SIR value when re-transmission. As concluded in Sub-section 4.6.2, the system performance depends both on the SNR value and on the SIR value. It has been stated at the beginning of Section 4.6 that $SIR^{(2)} = 0$ [dB]. This means that the UKIF MS has always the same power as the RS at the second time-slot. When the desired MSs' power is fixed, the final SIR value of the re-transmission increases as the SNR value of the R-D channel increases. However, the final SIR value of the re-transmission does not increase monotonously with the increasing SNR value of the R-D channel. Using the case $SNR_{sd} = 10$ [dB] as an example, both the final SIR value and the final SNR value are 10 [dB] if $SNR_{rd} = 1$ [dB]. As the SNR_{rd} increases to 10 [dB], the final SNR value is 13 [dB] while the final SIR value is 3 [dB]. This means that increasing the SNR value of the R-D channel may lead to the reduction of the final SIR value, depending on the SNR balance between the S-D channel and the

² It is assumed that the S-D channel has the same SNR value as the R-D channel

R-D channel. As a consequence, the BER performance may not show the monotonousness at the low E_b/N_0 range. However, the performance tends to decrease monotonously with the increasing E_b/N_0 value of the R-D channel as the E_b/N_0 becomes large. The reason is that the contribution of the direct transmission becomes minor compared with the contribution of the relay transmission. Both in the case of the AF relay and in the case of the DF relay, two curves, indicating different SNR_{sd} values, are parallel with each other as the E_b/N_0 becomes large. The gap between them is due to the different contribution of the direct transmission. It is observed by comparing Fig. 4.13(a) with Fig. 4.13(b) that the gap between different SNR_{sd} values is larger in the case of the DF relay than in the case of the AF relay. This is due the error propagation introduced by the the DF relay.



(a) The BER performances with the re-transmission technique in the case of the AF relay



(b) The BER performances with the re-transmission technique in the case of the DF relay

Fig. 4.13: The BER performances of MS1 and MS2 (left) as well as MS3 (right) with the re-transmission technique

5. PERFORMANCE VERIFICATION OF COOPERATIVE MARN

In Chapter 4, advanced techniques have been proposed to cooperative MARN for the performance improvement. By exploiting an example scenario, numerical results have been highlighted in Section 4.6 based on the simulation assumptions listed in Sub-section 4.1.3. However, the assumptions made to channels may not hold in realistic propagation environments. For example, channel fading may not be Rayleigh-distributed; independent channel gains between two BS antenna elements happen seldom. Furthermore, the received powers of three MSs can only be the same if they are placed at the same location or if an ideal power control algorithm is assumed. Due to these unrealistic simulation assumptions, it is necessary to verify the performance of cooperative MARN with realistic channels. Therefore, this chapter provides a reality check to the performance of cooperative MARN.

Performance verification can be done in two ways. One way is to plug the channel realizations, direct from raw measurement data, into the simulation chain. This is referred to as measurement data-based performance verification. This method gives the most realistic results since the channel realizations are obtained from real-field measurement data directly. However, this method is hardly applicable for a general evaluation since it is too site-specific and configuration-specific. The results, based on measurement data, are valid only in the environment where the measurement campaign is performed, with the antenna configuration used. If either the environment or the configuration is changed, the results may change too. Therefore, a large amount of measurement data with various environments and configurations should be prerequisite for a general statistical study. However, satisfying this prerequisite may be impractical. Therefore, as a compromise between the accuracy and the complexity, it is preferable to use the experimental channel model, parameterized from measurement data. This is called channel model-based performance verification. This method allows a statistical performance evaluation. Nevertheless, this method can be more conveniently used since it only requires the model structure and the parameters required in the model. by using the experimental results presented in Chapter 3, channel realizations can be reproduced. Exploiting the example multiple access relay system in Chapter 4, the performance verification is performed in this chapter, both based on raw measurement data and based on the experimental channel model. This chapter is organized as follows: Section 5.1 provides firstly a short overview to the state-of-the-art research activities in the performance evaluation of relay networks. In the same section, the main contributions of this chapter are summarized. Thereafter, the method of how to extract channel realizations both from measurement data and from the experimental channel model is given in Section 4.2. The realistic performance of the example cooperative multiple access relay system will be examined in Section 5.3 and in Section 5.4, based on raw measurement data and based on the experimental channel model, respectively. In Section 5.3, both the impacts of the small scale

channel propagation phenomena and the impacts of the large scale propagation phenomena are considered while Section 5.4 focuses on the relay channel model based performance verification.

5.1 Background and own contributions

5.1.1 Background and state-of-the-art

The whole history of the performance evaluation of relay networks can be divided into three stages: the Gaussian-channel based simulation stage in the 1970s; PL + Rayleigh-fading channel based simulation stage since the 1990s; and nowadays the measurement data based simulation stage since Kyritsi's work [138].

Von der Meulen und Cover are the representative persons for the first stage. The information theoretical relay research has been introduced by van der Meulen [51] and has been studied extensively by Cover [52] [55] in various communication scenarios. This analysis was performed only for the Gaussian communication channels. Neither the wireless channel fading (SSF) nor the power gains due to distances as shown in Eqn. 2.9 in Chapter 2 have been explicitly considered for the analysis. Therefore, Cover's work has been extended to the wireless Rayleigh fading channels since the recognition of the value of the relaying technique in the middle of the 1990s. Since then, the second stage is started. The remarkable publications are [110] [111] [112] [22] [25] [27] [53] [109]. Furthermore, the impact of PL on the performance has been introduced to relay networks due to the piecewise shorter relaying propagation distances. The representative work has been contributed by Sendonaris [110] [111], by Gupta [112], and by Herhold [39]. The authors in [139] made a minor progress to the second stage where the independent LSF has been considered as well. In [134] Sanka examined the sum rate of MARN, depending on the relay strategies and on the location of a RS. Even though a significant progress has been achieved in the performance evaluation of relay networks, majority of the aforementioned theoretical works have been performed under the simplified assumptions on the channel properties, such as the Rayleigh-distributed fading, the exponential PL model without LSF, and the independent channel fading between various links. These simplified assumptions make the simulation results attractive but unrealistic due to the following reasons:

- The channel fading may not be Rayleigh-distributed.

Besides Rayleigh distributed channel fading, channel fading can be also modeled as a double-Rayleigh distribution [32], a Rice-distribution, a Nakagami-distribution, and a Suzuki-distribution [33]. Furthermore, it is also possible that the statistical distribution of channel fading based on measurement data matches none of these distributions.

- SSF together with a distance dependent PL model does not cover all parts of channel gain.

As shown in Eqn. 2.9 in Chapter 2, the channel gain is determined by a distance dependent PL model and SSF as well as LSF. Even though SSF as well as the distance dependent PL model has been considered in the second stage, LSF is either out of discussion or considered to be independent. However, the impact of LSF and its correlation properties can not be ignored. It has been reported in [105] [71] [106] that the variance of LSF varies from 2 [dB] to 10 [dB]. Therefore, the channel gain may change 0-20 [dB] when a MS moves from one LSA

to an adjacent LSA due to LSF, depending on the correlation properties of LSF. When the LSF values are highly correlated within two adjacent LSAs, they will stay the same. On the contrary, the LSF values will change randomly from one LSA to an adjacent LSA and their difference ranges between 0 and 20 [dB]. A LSA corresponds to couple of meters, depending on the carrier frequency and propagation environments. Whereas, the channel gain due to a PL model changes only 20-40 [dB] when a MS moves from 10^n [m] to the 10^{n+1} [m] with n being a non-negative integer, for example, from 100 [m] to 1000 [m]. This means, together with a PL model, the correlation properties of LSF between two MSs have also a significant influence on the long-term variation of the channel gain.

- It is not the normal case in reality that the channel fading between different links is independent.

Two kinds of fading can be considered under the concept of independent channel fading: SSF and LSF. Both of them could not be necessarily independent. It is reasonable to assume that SSF between different MSs is independent when the MSs are apart from each other in the order of meters. However, when a MS/BS/RS has multiple antenna elements, it happens very often that the links among different antenna elements are not independent due to the fact that the antenna element spacing at the MS/BS/RS, in many cases of deployment, can not be made larger than meter because of the space limitation for the antenna mounting.

Furthermore, LSF may not be necessarily independent from one LSA to an adjacent LSA due to the existence of common scatters as explained in Sub-section 2.5. The experimental results in Chapter 3 confirm again this argument by showing that the de-decorrelation distance of LSF in the urban scenario is in the order of meters. In [73] [72], the author found that LSF between two MSs, with a distance being 50-150 [m], is still correlated. An exception to the dependent LSF from one LSA to a neighboring LSA is the indoor scenario, where LSF can be treated as uncorrelated from one LSA to a neighboring LSA as shown in Chapter 3 and in publications [73] [6] [3]. The correlation properties of LSF have to be considered in relay networks due to their effects on the system performance. In a relay system, MS cooperation has been often discussed [110] [111] [23] [24]. In [137], Meng concluded that a MS should probably partner with the one that is as close as possible. However, in this case, the MSs can not help each other significantly from the channel gain point of view since both MSs undergo the same PL and the same LSF due to the correlation properties of LSF.

Due to these reasons, Kyritsi predicted the performance of the classical three-station structured relay networks by using the measurement data gathered in an indoor environment [138]. Since then, the third stage of the performance prediction of relay networks has been started. In [138], Kyritsi investigated the impacts of the following channel factors on the performance of relay networks, the power allocation factor between a RS and a MS, an antenna elements selection technique at a RS, using the final end-to-end capacity as a measure. Using the same measurement data, Kyritsi studied the impact of other channel factors on the performance of relay systems in [140]. At first, Kyritsi found that the assumption of a Rayleigh-fading channel is in practice violated. Instead of a Rayleigh-fading channel, a double Rayleigh behavior has been observed, by which the improvement of the system performance by relaying can only be observed at the high SNR

range. Another representative work toward the realistic performance prediction of relay networks has been performed by Haneda in [141] based on outdoor to indoor measurement data. In [141], Haneda exploited the diversity order and the channel gain as the measures to examine the gain-diversity tradeoff both for an AF relay and for a DF relay. The authors in [10] confirmed again that significant performance improvement can be achieved by exploiting mobile relays based on the measurement data collected in an area considered most feasible for relay network applications.

5.1.2 Own contributions

By exploiting the example scenario of MARN with an AF relay used in Section 4.6, performance verification has been done in this chapter using the relay measurements described in Sub-section 3.3.2. The main contributions of this chapter are listed as follows:

- Both the impacts of small scale propagation phenomena and the impacts of large scale propagation phenomena on the realistic performance are discussed based on raw measurement data.

The small scale propagation phenomena include the distribution of SSF [10] and the antenna element spacing at the BS while the large scale propagation phenomena include LSF and further PL plus LSF. Furthermore, various power allocation schemes between the MSs and the RS have been discussed. The main findings are:

- Using the channels within a LSA, the impact of the distribution of SSF on the BER performances can be investigated. It is found that simplified Rayleigh channel-based simulation results overestimate the system performance due to the independent Rayleigh fading assumption. Furthermore, it is observed that *case: re-trans.+signal selection*) provides the best performance which is followed sequentially by *case: relay+signal selection*), *case: re-trans.*), and *case: relay*). Their cdf curves have almost the same standard variance which is larger than the variance of the cdf curve of *case: direct*) having a standard Rayleigh distribution. It is due to the multiplication of the concatenated Rayleigh channels of a tandem relay link as shown in Eqn. 4.10 in Chapter 4.
- By varying the antenna element spacing at the BS from $\frac{1}{2}\lambda_{WL}$ to $\frac{7}{2}\lambda_{WL}$ with a step of $\frac{1}{2}\lambda_{WL}$, the results, achieved by using channels within a LSA, indicate that no further performance improvement can be expected in the practical applications under similar environments considered, by the excessive use of space for the BS antenna mounting larger than $\frac{3}{2}\lambda_{WL}$.
- After removing the PL value from the received power, the BER performances of MSs are determined by LSF. The higher the LSF value, the worse the BER performance. Furthermore, the continuous variation of LSF indicates a same continuous variation tendency of the BER performance.
- When considering both PL and LSF in the received power, along route 1, the BER performance of the direct link is always better than that of the relay link. However, along route 2, only *case: relay*) is possible since the direct transmission is too weak

to contribute anything to the system performance. This means, the relay transmission is of crucial importance in the case when the direct transmission is blocked. As far as the direct transmission is available, the relay transmission can outperform the direct transmission at the price of equivalent SNR_{sr} and SNR_{rd} values which should be higher than the SNR_{sd} value.

- The power allocation schemes can improve the system performance in some sense. However, the performance of the relay transmission is still limited by the R-D channel. Therefore, keeping the balance between the tandem links of a relay channel is crucial for the relay system design.
- Three RS positioning schemes, being near to a BS and being in the middle of a BS and MSs as well as being near to MSs, have been checked based on the relay channel model. The simulation results show that positioning the RS near to the BS provides better BER performance than the other two positioning schemes. This observation indicates that for the realistic deployment, a careful selection of the RS position can further improve the system performance.

5.2 Simulation channels

This section deals with the method and the process how to acquire channel realizations for the performance verification purpose. The channel realizations are obtained in two ways. The one is based on the raw measurement data gathered from channel measurement campaigns, the other is based on the experimental channel model, where the model parameters are extracted from the same raw measurement data. Chapter 3 described two propagation environments for the channel modeling for relay networks: the urban environment and the indoor environment. The relay measurement data from the urban environment, used as an example, is selected for the performance verification purpose. The same method and procedure can be performed to the indoor environment. A detailed description to the urban measurement campaign has been provided in Section 3.3.2. Some additional information will be provided in Sub-section 5.2.1. In the same Sub-section, the experimental results of some basic channel parameters are presented, such as the normalized received power and the statistical distribution of SSF. Thereafter, Sub-section 5.2.2 addresses the way how to extract channel realizations from raw data while Sub-section 5.2.3 focuses on the way how to simulate channel realizations based on the relay channel model.

5.2.1 Relay measurement campaign

Relay measurements have been performed as part of the measurement campaign described in Sub-section 3.3.2. Figure 5.1 provides a detailed view to the relay measurement routes in a 2-dimensional Ilmenau city map, which is actually the upper part of the whole measurement area provided in Fig. 3.4 in Chapter 3. The relay measurements have been conducted over two routes, route 1 and route 2. Along route 1, the MS has LOS propagation to BS5/BS6/RS2 while along route 2, the MS

has LOS propagation only to RS2 but NLOS or obstructed LOS propagation to BS5/BS6. At each position of the two routes, both the BS-MS channel and the RS-MS channel are measured consequently which represent a direct transmission and a relay transmission, respectively. The BS antenna array has been adjusted to two heights, 10 [m] and 16 [m], with the name BS5 and BS6 in Fig. 5.1, respectively. The height of the RS antenna array stays 3 [m] with the name RS2 in Fig. 5.1 while the height of the MS is 1.9 [m], the same as what is provided in Table 3.3 in Chapter 3. A detailed description about the antenna arrays used can be found in Sub-section 3.3.2.

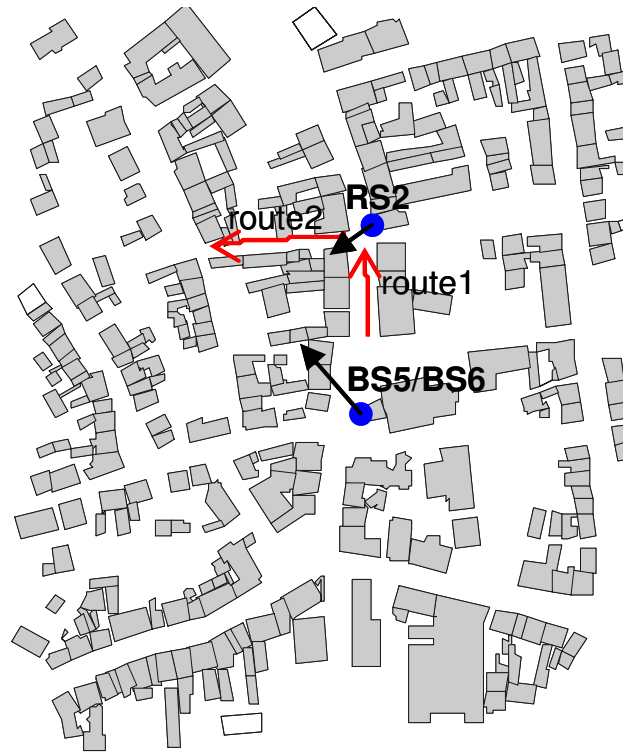


Fig. 5.1: Relay measurement routes in a 2-dimensional Ilmenau city map

5.2.2 Application of raw measurement data for the performance evaluation

In the relay measurements, no measurement has been conducted for the stationary BS-RS link where both the BS and the RS do not move and LOS propagation exists between them. These propagation features make the BS-RS channel less interesting. However, channels of the BS-RS link are required for simulations. The experimental results provided in Sub-subsection 3.5.1.2 indicate that a propagation channel holds to be stationary within couple of meters. This indicates the channel of the BS-RS link has the same stationary properties as the BS-MS channel if a MS is in the couple of meters from a RS. Because the end point of route 1 is around 7 [m] from RS2, the BS-MS channels, measured at the end of route 1, have the same stationary propagation as the BS-MS channels. Therefore, they can be used as the measurement of the BS-RS link.

The cdf curves of SSF of the stationary BS-RS link are plotted in Fig. 5.2, with the polarization

pair ¹ as a parameter. In the same figure, the cdf curve of Rayleigh fading channels is plotted as a reference. It can be observed from Fig. 5.2 that none of the BS-RS channels has a perfect Rayleigh distributed SSF [142] [143] [32]. The cdf curves of the co-polar channels shift clearly to the left hand side of the standard Rayleigh distribution while the cdf curves of the cross-polar channels show a slight difference from the standard Rayleigh distribution. This is due to the LOS path. As stated in Sub-section 5.2.1, the MS has LOS propagation to BS5/BS6/RS2 along route 1. This means that a LOS path exists in the BS-RS channel. Due to XPR, the LOS path affects the cdf curves of the co-polar channels more significantly than those of the cross-polar channels. In the following, only one ring of the BS/RS antenna array and the HH co-polar channel are considered when not explicitly stated.

A frequency segment of 60 [MHz] around the carrier frequency is used in the simulations out of the

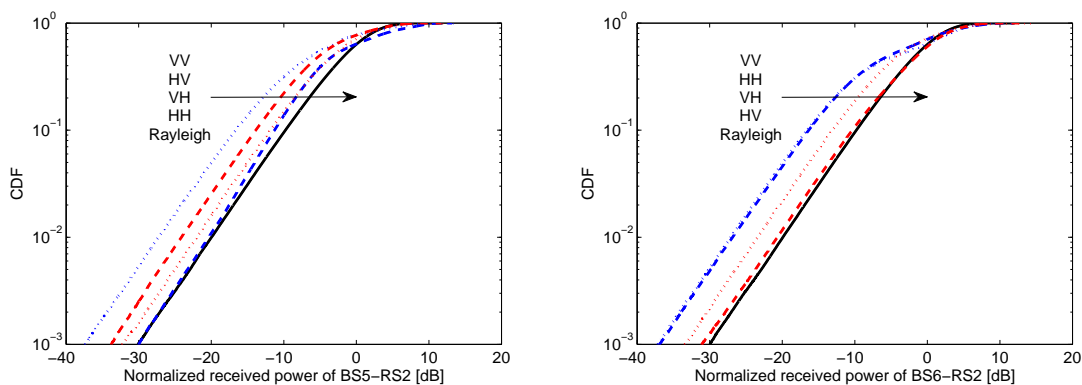


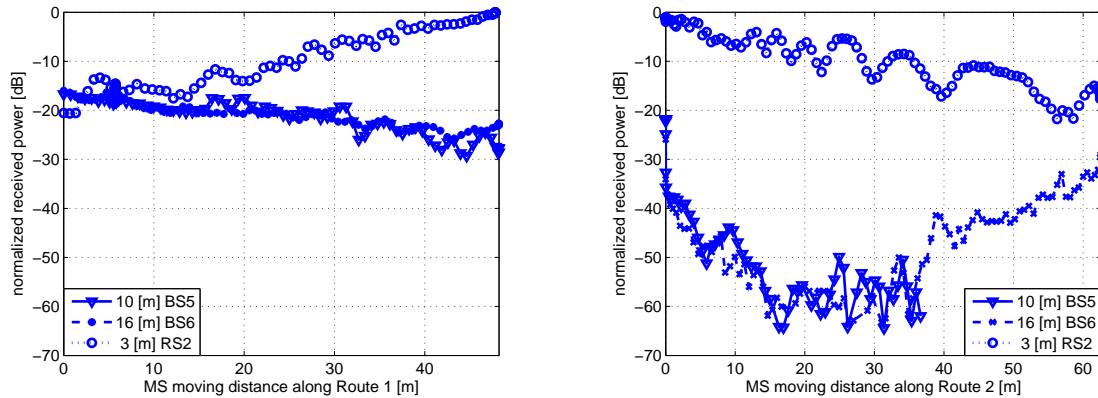
Fig. 5.2: The cdf curves of SSF of the stationary BS-RS link with four polarization pairs

120 [MHz] total measurement bandwidth. It corresponds to 192 frequency bins. The sub-carrier distance is 312.5 [KHz] which matches with the chunk size defined for the metropolitan area in the WINNER project [144]. The channels from chunk to chunk suffer from independent frequency-flat fading. Before using CTFs from raw measurement data, the step, removing the measurement noise, should be performed. Based on the observation in Sub-subsection 3.4.3.1, it is reasonable to choose 9 [dB] as the noise cut level. The measurement noise is removed from each CIR by padding zeros to the delay bins if their amplitudes are smaller than the noise cut level. Therefore, each snapshot has around 37,000 samples of frequency-flat CTFs. The number of the samples is the multiplication result of $8 \times 24 \times 192$ ($n_{Tx} \times n_{Rx} \times n_f$).

Figure 5.3(a) and Fig. 5.3(b) show the MS's normalized received power from BS5/BS6/RS2 along route 1 and route 2, respectively. The normalized power of the BS5-RS2 channel and of the BS6-RS2 channel is -28 [dB] and -23 [dB], respectively. It can be observed from Fig. 5.3(a) that at the beginning of route 1, the MS receives more power from BS5/BS6 than from RS2. As the MS moves towards RS2, it receives more power from RS2 than from BS5/BS6 due to the shorter propagation distance to RS2 than to BS5/BS6. The height of the BS has almost no impact on the received power at the MS. At the beginning of route 2, the MS turns around the corner and undergoes around 20 [dB] corner loss. As the MS goes away from RS2, the MS's received power from BS5/BS6/RS2

¹ Since the antenna arrays of both stations are V/H dual-polarized, four polarization pairs (VV, VH, HV, HH) are returned

decreases simultaneously till the MS moves around 35 [m]. After this point, the MS's received power from BS6 starts increasing while the MS receives almost nothing from BS5. It is due to the different heights of BS5 and BS6. As mentioned in Sub-section 5.2.1, BS5 is 10 [m] high while BS6 is 16 [m] high. Since BS5 is below rooftop, the propagation from BS5 to route 2 comes from the diffraction of the street corners around the cross road, by which virtual sources are created. The wave from the virtual sources is so weak that it can not propagate to far distance. However, BS6 is above rooftop, the MS can get signal from BS6 by street corners' diffraction and by buildings' diffraction from above rooftop to below rooftop. Based on the diffraction theory, the latter one is too weak to contribute anything [63]. At the first 35 [m] along route 2, BS6 experiences the same propagation phenomenon as BS5. As the MS goes further along route 2, the MS can also get diffracted signal from the street corner of the other side of route 2 from BS6. It can be observed from Fig. 3.3 that BS6 has a LOS view to the cross road of the other side of route 2. Because BS5 is below rooftop, BS5 has a NLOS view to this cross road. This is the reason why the received power from BS6 starts increasing while the MS receives almost nothing from BS5. This observation indicates that the system benefits more from a relay solution in the BS5 case than in the BS6 case, which stand for the urban micro-cell and macro-cell scenarios, respectively. In the urban macro-cell scenario, a highly elevated BS can provide enough coverage. Therefore, the relay solution can provide some complementary coverage.



(a) MS's normalized received power along route 1 (b) MS's normalized received power along route 2

Fig. 5.3: MS's normalized received powers from BS5/BS6/RS2 along route 1 and route 2

5.2.3 Application of the relay channel model for the performance evaluation

It has been pointed out that the channel model of relay networks can be proposed based on the WIM framework. The most important feature of the relay channel model is modeling the intra-site and inter-site correlation properties of LSP. Therefore, the algorithms, described in Section 2.6, are used to reproduce the correlation properties of LSP. Furthermore, the modeling algorithms will be parameterized by the experimental results, presented in Subsection 3.5.1 for the U1 and U2 scenarios.

After presenting the relay channel model, channel realizations in different scenarios can be simulated. In this chapter, an urban micro-cell scenario with the following parameter settings, is

considered as an example scenario for the performance verification purpose. The same method can be applied to the other scenarios.

1. The system center frequency is 5.25 [GHz] and the bandwidth is 100 [MHz];
2. Both the BS and the RS are below rooftop level and have LOS propagation with MSs. The RS has also LOS propagation with the BS. MSs, nearby to each other in the same LSA, are at street level;
3. The BS has a 2-element Uniform Linear Array (ULA) while both the RS and MSs have a single-element omni-directional antenna;
4. The distance between the BS and MSs is fixed to 500 [m] while the RS is positioned between them. Furthermore, all stations stay in a line;
5. The experimental results of the inter-site correlation of LSP for $\langle RS2, BS5 \rangle$ in Table 3.8 in Chapter 3 are used for channel simulations;
6. The rest channel parameters are taken from [1] for the B1 scenario with LOS propagation.

By using the relay channel model, the CIRs of the S-D, S-R, and R-D channels can be simulated. Figure 5.4 shows the cdf curve of SSF of the stationary BS-RS link when the RS is located in the middle of the BS and MSs. As a reference, the cdf curve of a standard Rayleigh fading channel is shown in the same figure. It can be observed that the simulated SSF does not match the Rayleigh distribution.

The simulated system has a 100 [MHz] bandwidth. A frequency segment of 60 [MHz] around center

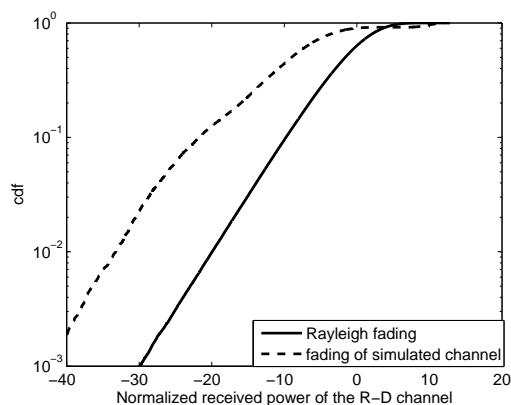


Fig. 5.4: The cdf curves of SSF of the stationary BS-RS link based on the relay channel simulations if the RS is located in the middle of the BS and MSs

frequency is used in the simulation. The same chunk size as used for raw measurement data in Subsection 5.2.2 is considered to the experimental channel model based channel realizations.

Since the distance between the BS and MSs is fixed to 500 [m] and the RS is positioned somewhere in between, the received power is normalized so that the SNR_{sd} value is 0 [dB]. The SNR_{sr} and

Modulation	QPSK
Coding	MAC
Frame symbol length	3072
Bandwidth	60 MHZ
Multiplexing	OFDM
Number of sub-carrier	192
Number of antenna	MS: 1, RS: 1, BS: 2
Number of interference	1
SIR	$SIR^{(1)} = SIR^{(2)} = 0$
Channel estimation	perfect

Tab. 5.1: Simulation parameters for performance verification

SNR_{rd} values vary, depending on the position of the RS. An equal power allocation scheme between the RS and MSs is considered.

5.2.4 Simulation scenarios and parameters

It has been stated in Sub-section 4.6.3 that a DF relay returns slight superiority in the BER performance compared with an AF relay, at the expense of an additional signal processing complexity at the RS. As a compromise between the signal processing complexity and the performance improvement, the AF forwarding strategy is considered in this Chapter for the purpose of performance verification. Throughout this chapter $SIR^{(1)} = SIR^{(2)} = 0$ [dB] when it is not explicitly explained. The example scenario used in Section 4.6 is exploited. Furthermore, the following five cases are considered in the simulation:

case: direct) the direct transmission with MAC;

case: relay) the relay transmission with an AF relay;

case: relay+signal selection) constructive combining the direct transmission with the relay transmission with an error detection aided signal selection technique;

case: re-trans.) MSs re-transmit their signals to the BS when the RS performs forwarding at the second time-slot;

case: re-trans.+signal selection) constructive combining the direct transmission with the transmission stated in *case: re-trans.*) with an error detection aided signal selection technique.

Table 5.1 summarizes the major simulation parameters.

5.3 Measurement data based performance verification

Measurement data based performance verification will be done by considering two levels of propagation. The one is the small scale propagation, the other is the large scale propagation. Sub-section 5.3.1 and Sub-section 5.3.2 deal with these two levels, respectively.

5.3.1 Impacts of the small scale propagation phenomena

Both SSF and the element spacing at the BS are considered in studying the impact of the small scale propagation phenomena. Sub-subsection 5.3.1.1 deals with the impacts of SSF while Sub-subsection 5.3.1.2 highlights the impacts of the element spacing at the BS.

Both in Sub-subsection 5.3.1.1 and in Sub-subsection 5.3.1.2, measurement data within a LSA is selected. The selected LSA is located in the vicinity of the start point of route 1. Within this LSA, the LSF and PL values are removed from the received power to keep the SNR value of each link. The following parameter set is assumed during the simulation: $SNR_{sd} = 0$ [dB] while $SNR_{sr} = SNR_{rd} = 10$ [dB].

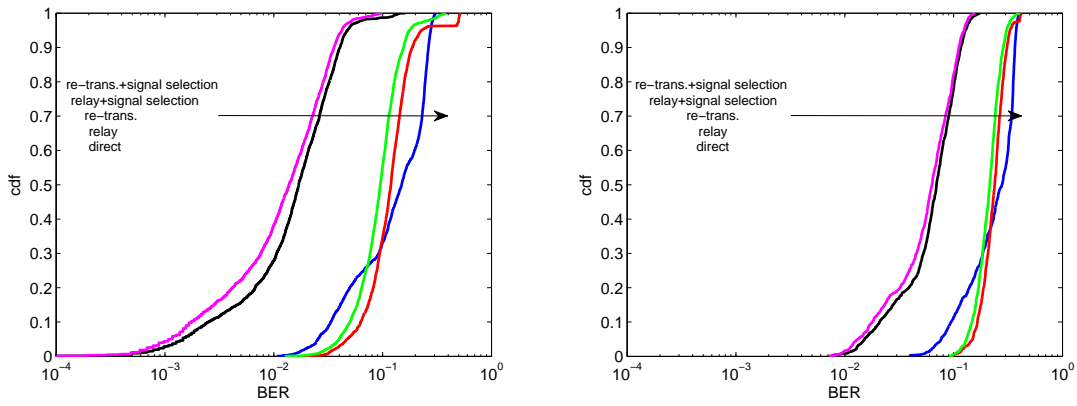
5.3.1.1 SSF

The BS antenna array has 8 antenna elements, two of which, having the largest element spacing being $\frac{7}{2}\lambda_{WL}$, are selected for the simulation. The cdf curves of the BER performances of MS1 and MS2 as well as MS3 are shown in Fig. 5.5. As a comparison, three kinds of channels are considered. They are channels from the BS5's measurement data, from the BS6's measurement data, and from the simplified Rayleigh channel model.

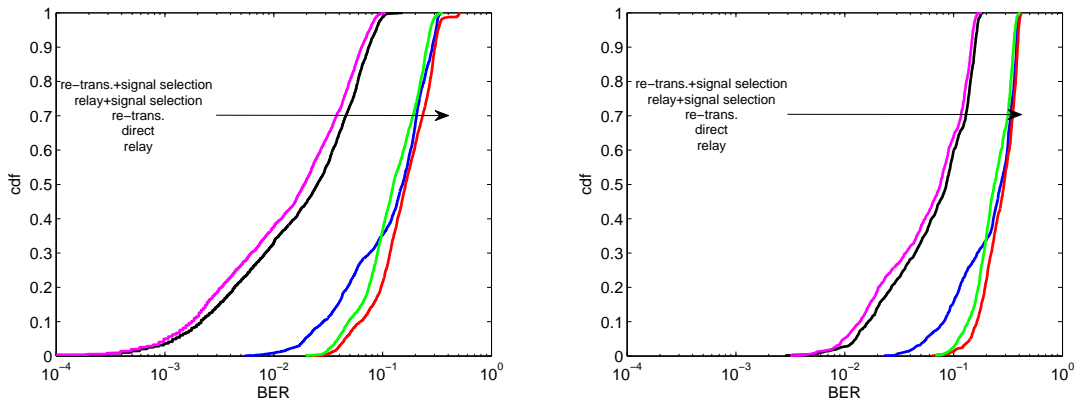
It is found in Fig. 5.5 that MS3 has worse performance than MS1 and MS2 even though all of the three MSs have the same SNR value. This is due to the fact that MS3 transmits more bits than MS1 and MS2 within one MAC-encoded symbol having the same energy.

Observing the cdf curves of the BER performances based on simplified Rayleigh channels, it is found that the cdf curves of *case: relay*), *case: re-trans.*), *case: relay+signal selection*), and *case: re-trans.+signal selection*) are parallel shifted to the left sequentially. They have almost the same standard variance which is larger than the variance of the cdf curve of *case: direct*). It is due to the multiplication of the concatenated channels of a tandem relay link as shown in Eqn. 4.10 in Chapter 4. Even though each channel of a tandem relay link has a Rayleigh distribution, the multiplication of two Rayleigh distributed channels results in a end-to-end channel which has a larger standard variance than that of a Rayleigh channel. In Fig. 5.6, the dashed curves show the cdf curves of the fading amplitudes of the end-to-end channel of a tandem relay link. As a reference, the fading amplitude of a single Rayleigh channel is depicted in the same figure by a solid curve. The observation in Fig. 5.6 confirms the argument that the fading amplitude of a tandem relay link has a larger standard variance than that of a single Rayleigh channel. The cdf curves of the fading amplitude of a tandem relay link include a group of 6 curves, showing the dependence on the correlation coefficient between the single Rayleigh-distributed channels. It is observed from the group of the dashed curves that the larger the fading correlation coefficient, the larger the standard variance of a tandem relay link.

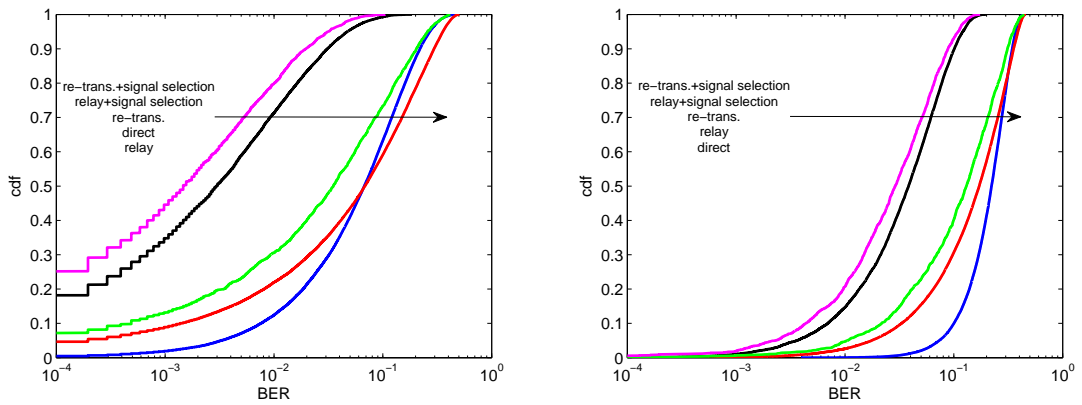
By comparing the cdf curves based on measurement data with the curves based on the simplified Rayleigh channels, it is found that the former are shifted to the right hand side compared with the latter. It reveals that the simplified Rayleigh channel model-based simulation results tend to overestimate the system performance. This means that the promising performance provided by the theoretical study can not be achieved in reality. There are two reasons: the first one is due to



(a) Based on the BS5's measurement data



(b) Based on the BS6's measurement data



(c) based on the simplified Rayleigh channels

Fig. 5.5: The cdf curves of the BER performances of MS1 and MS2 (left) as well as MS3 (right) under the assumption that $SNR_{sd} = 0$ [dB] while $SNR_{sr} = SNR_{rd} = 10$ [dB]

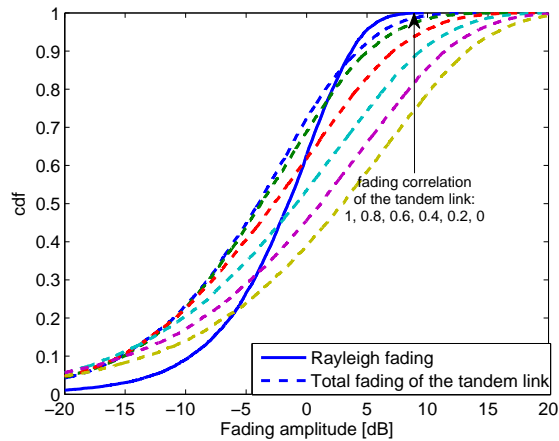


Fig. 5.6: The cdf curves of the fading amplitude of the end-to-end channel of a tandem relay link

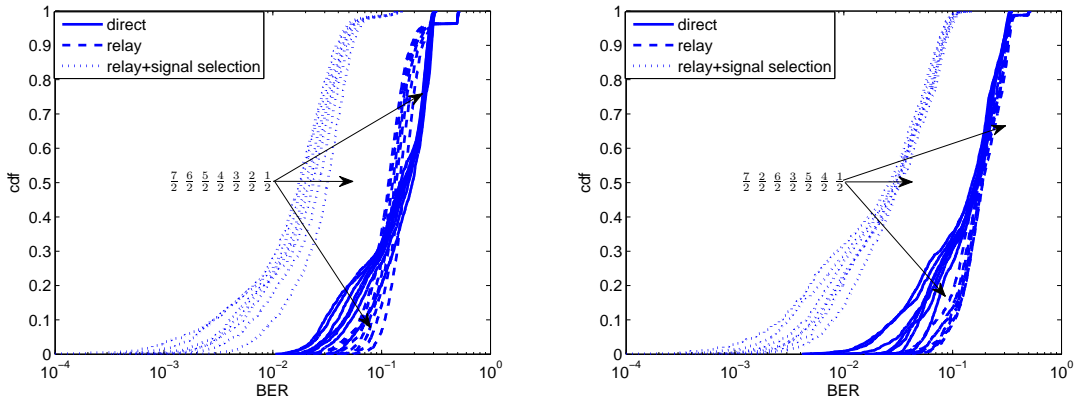
the unrealistic assumption that the channels among the BS antenna elements are independent; the second one is because of the Rayleigh fading assumption. Due to the space limitation for the antenna mounting, the spacing between the antenna elements at the BS in many cases of deployment, can not be made larger than required. Therefore, it happens seldom that the spatial correlation among the BS antenna elements approaches zero, which stands for the case of independent BS channels. As a result, the predicted theoretical performance is impaired by the introduction of the spatial correlation among the BS antenna elements. Furthermore, as already shown in Fig. 5.2, none of the cdf curves of SSF matches a Rayleigh distribution which in turn impacts the predicted performance. By comparing the cdf curves based on the BS5's and BS6's measurement data, it is found that the cdf curves based on the BS5's measurement data have a smaller standard variance than the variance of the curves based on the BS6's measurement data, but not at a remarkable level. This observation is consistent with the observation in Fig. 5.2 where SSF of the HH polarization from the BS6's measurement data has a larger variance than the variance from the BS5's measurement data.

5.3.1.2 Influence of the antenna element spacing at the BS

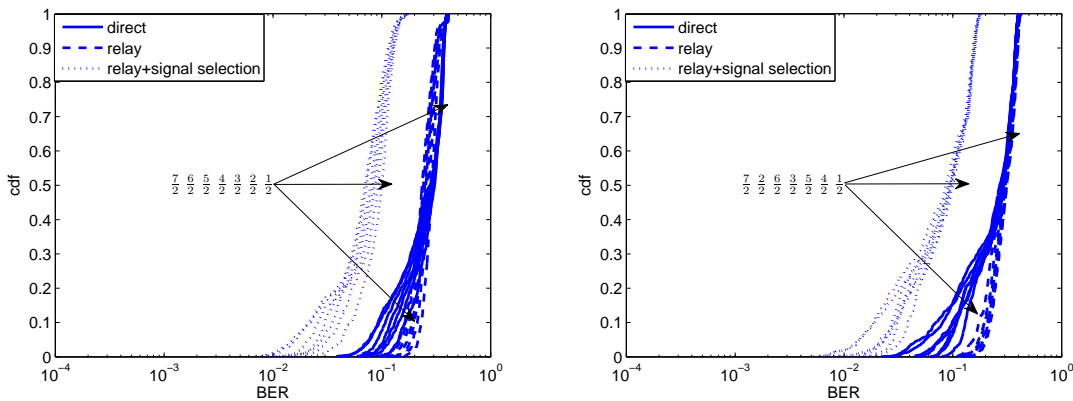
As stated in Sub-subsection 5.3.1.1 that the spatial correlation among the BS antenna elements has a significant influence on the system performance. The spatial correlation among the BS antenna elements varies, depending on the element spacing. Therefore, the two-element antenna subsets at the BS are selected from 8 antenna elements, according to the antenna element spacing. From the 8 BS antenna elements, 7 groups, with spacing $\frac{1}{2}\lambda_{WL}$, $\frac{2}{2}\lambda_{WL}$, $\frac{3}{2}\lambda_{WL}$, $\frac{4}{2}\lambda_{WL}$, $\frac{5}{2}\lambda_{WL}$, $\frac{6}{2}\lambda_{WL}$, and $\frac{7}{2}\lambda_{WL}$, are considered in the simulations. In each group, antenna elements have the same spacing. Since the re-transmission at the second time-slot results in a slight parallel shifting in the cdf curves compared with the cdf curves of *case: relay*) and *case: relay+signal selection*) as shown in Fig. 5.5, three cases are considered in this Sub-subsection. They are *case: direct*), *case: relay*), and *case: relay+signal selection*).

Figure 5.7 shows the cdf curves of the BER performances of MS1 and MS2 as well as MS3, with the BS height and the BS antenna element spacing as parameters. Figure 5.7(a) shows the results

of MS1 and MS2 while Fig. 5.7(b) shows the results of MS3. The left subplot depicts the results based on the BS5's measurement data while the right subplot shows the results based on the BS6's measurement data. It is observed from Fig. 5.7 that the BS antenna element spacing has an obvious impact on the BER results based on the BS5's measurement data. However, it makes only a minor influence on the results based on the BS6's measurement data. Observing the results based on the BS5's measurement data, it is found that the cdf curves of three MSs are shifted to the left sequentially with an increasing BS element spacing. The reason is that the spatial correlation between two BS antenna elements decreases with an increasing element spacing. However, the BER improvement of three MSs becomes smaller as the element spacing is larger than $\frac{3}{2}\lambda_{WL}$. It indicates that in the practical applications under similar environments, the excessive use of space for BS antenna mounting, necessary to make antenna element spacing larger than $\frac{3}{2}\lambda_{WL}$, can not be paid off. Observing the results based on the BS6's measurement data, it is found that the BS antenna element spacing has only a minor impact on the BER performances of three MSs at the low BER range which occurs with around 0.2 probability. From the 0.2 probability threshold, the cdf curves with variable antenna element spacing are overlapped almost with each other.



(a) The cdf curves of the BER performances of MS1 and MS2



(b) The cdf curves of the BER performances of MS3

Fig. 5.7: The cdf curves of the BER performances of MS1 and MS2 as well as MS3 based on the BS5's measurement data (left) and based on the BS6's measurement data (right) with different BS antenna element spacing under the assumption that $SNR_{sd} = 0$ [dB] while $SNR_{sr} = SNR_{rd} = 10$ [dB]

5.3.2 Impacts of the large scale propagation phenomena

Both LSF and PL are considered in the large scale propagation phenomena. The measurement data is selected, not limited to a LSA, but from a long measurement route (route 1 and/or route 2 in Fig. 5.1) comprising many LSAs². The mean BER value within a LSA is considered as the final result of this LSA. In Sub-subsection 5.3.2.1, the dependence of the system performance on LSF will be discussed. Sub-subsection 5.3.2.2 deals with the influence of the whole loss including both PL and LSF. Thereafter, various power allocation schemes between the MSs and the RS are highlighted in Sub-subsection 5.3.2.3.

5.3.2.1 LSF

To study the impact of LSF on the system performance of the example cooperative multiple access relay system, the whole measurement track along route 2, having 2432 snapshots, has been applied. The PL value along route 2 is removed from the received power, by which only the LSF value is left for each snapshot. Since the direct transmission between the MSs and the BS is blocked at the most time along route 2, we consider only *case: relay*) in this sub-subsection. For each simulation instant, MS1, MS2, and MS3 are randomly located in route 2. All together, 800 simulation instants are chosen of each MS. The SNR_{sr} value at each simulation instant is determined by the LSF value. Because the mean value of LSF is zero, an additional 3 [dB] has been added to the LSF value which is defined as the final SNR_{sr} value. BS6, as an example, is selected as the final receive station. For each simulation instant, the channel between the RS and BS6 has been randomly selected with SNR_{rd} being 10 [dB]³ while $SIR^{(2)}$ being 0 [dB]. Two BS antenna elements, having the largest element spacing, are selected from BS6 as the receive antenna elements.

The BER performances of MS1 and MS2 as well as MS3 along route 2 are shown in Fig. 5.8. As a comparison, SNR_{sr} along route 2, which is 3 [dB] larger than the LSF value, is shown in the same figure. It is observed by comparing the upper subplot with the middle subplot that MS3 has worse BER performance than MS1 and MS2 even though all of the three MSs have the same SNR_{sr} at the same position along route 2. This is due to the fact that MS3 transmits more bits than MS1 and MS2 within one MAC-encoded symbol having the same energy.

Despite the superiority of the MS1's and MS2's performances to the MS3's performance, there exists a similarity in the performance tendency along route 2 between the upper subplot and the middle subplot. It can be found that along route 2, the BER performances of MS1 and MS2 as well as MS3 become simultaneously good/bad at the same snapshot position. This tendency is in line with the variation tendency of $-SNR_{sr}$. Four dashed lines are plotted among the upper, middle, and lower subplots to provide a better comparison view between the BER performances and $-SNR_{sr}$. It can be observed that the BER performances of three MSs are highly correlated with $-SNR_{sr}$, indirectly with LSF along route 2. This means, the BER performances are determined

² The span of one snapshot is treated as a LSA

³ It has been concluded in Sub-subsection 4.6.3 that the final end-to-end performance of a relay channel is determined by the worst intermediate channel among the tandem relay chain. Since this Sub-subsection focuses on the impact of LSF of the S-R link on the performance, SNR_{rd} should be set larger than SNR_{sr} having the largest value being 9.5 [dB].

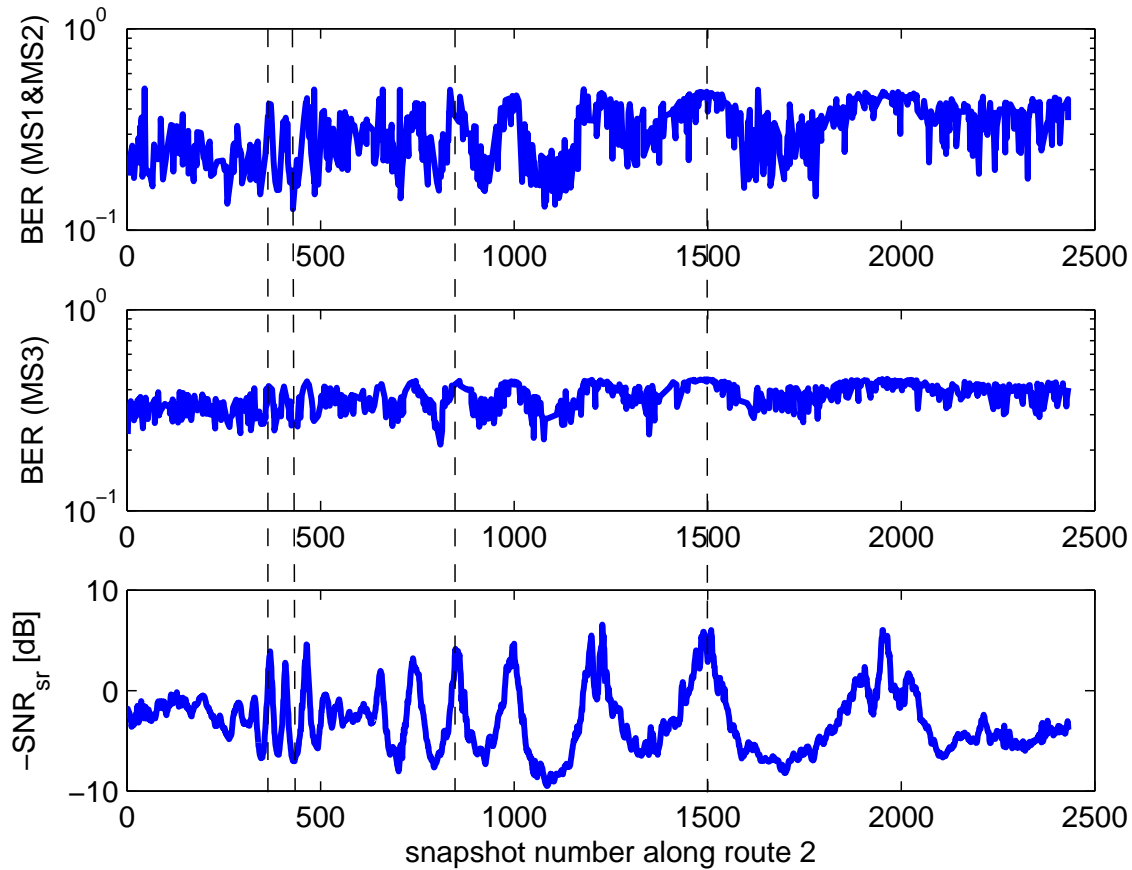


Fig. 5.8: Dependence of the BER performances of MS1 and MS2 as well as MS3 on the LSF value along route 2

by LSF along route 2. The higher the LSF value, the worse the BER performances. Furthermore, the continuous variation of LSF indicates a same continuous variation tendency of the BER performances. The BER curves do not have the same smooth tendency as the LSF curve due to the fact that the BER performance depends not only on SNR_{sr} but also on the effective SIR. Since three MS3 are randomly located along route 2, they have different SNR_{sr} values. However, the total transmit power at the RS is scaled to 1. This means that, based on the SIR definition at the second time-slot, the MS, having the largest SNR_{sr} value, has larger effective SIR than the other two MSs. As a consequence, there is a minor difference in the performances of three MSs.

5.3.2.2 PL plus LSF

The simulation results in Sub-subsection 5.3.2.1 show the dependence of the BER performance on LSF along route 2 after removing PL from the received power. In this Sub-subsection, the system performance will be investigated, considering both PL and LSF in the received power. Furthermore, the total transmit power from the MSs and the RS for the relay transmission is limited to the same as the transmit power from the MSs for the direct transmission only. By doing this, the

fairness can be kept in the performance comparison between the direct transmission and the relay transmission. Otherwise, the argument will be raised that the relay transmission can improve the system performance at the price of additional transmit power at the RS. It is assumed an equal power allocation between the MSs and the RS. Therefore, both the MSs and the RS have half of the transmit power of the direct transmission. This means, the normalized received power curves of the 3 [m] RS along route 1 and route 2 shown in Fig. 5.3 should be shifted down for 3 [dB] due to the reduction of the transmit power. In this Sub-section, the received powers is normalized so that the maximal value among SNR_{sr} and SNR_{sd} as well as SNR_{rd} along route 1 and route 2 will be 30 [dB]. Figure 5.9 depicts the cdf curves of SNR_{sr} and SNR_{sd} as well as SNR_{rd} along

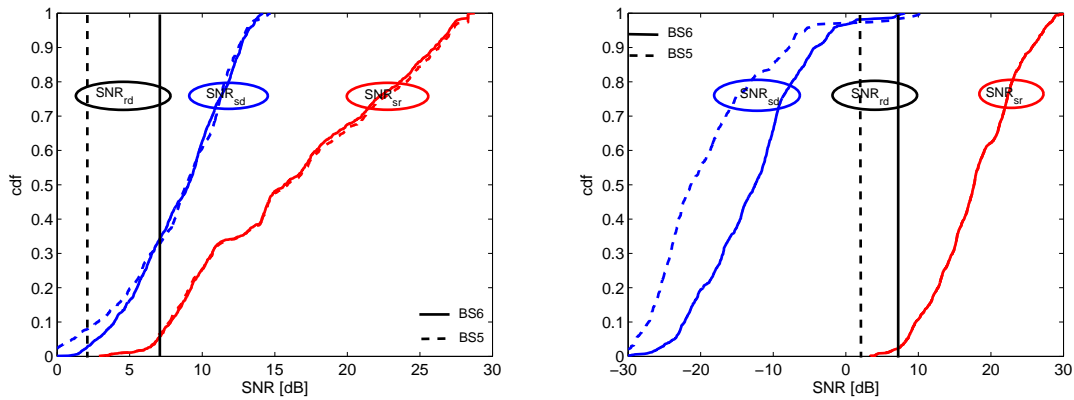
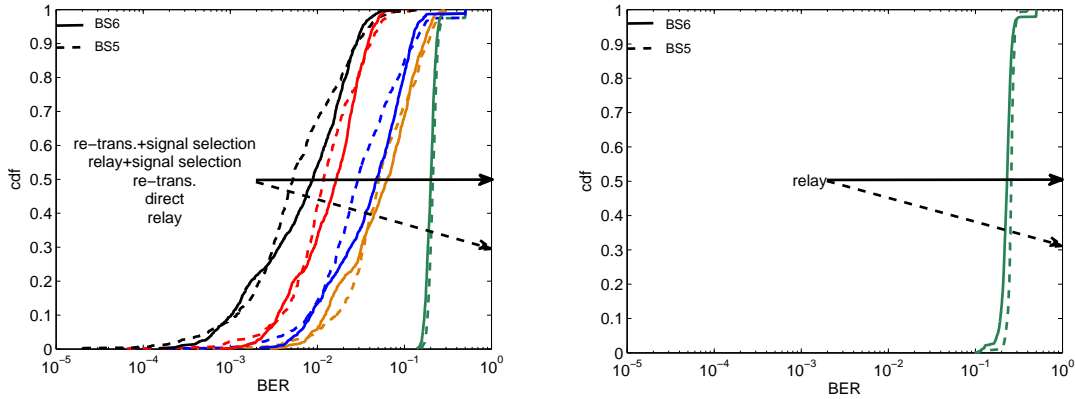


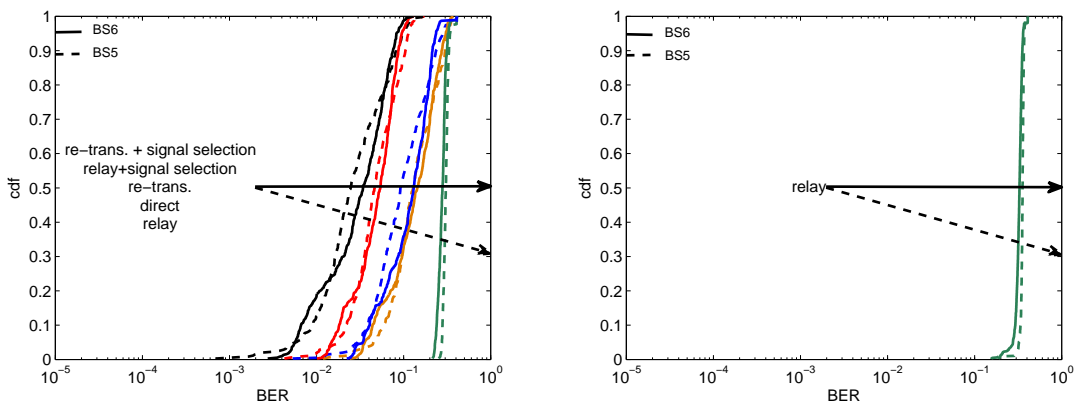
Fig. 5.9: The cdf curves of SNR_{sr} and SNR_{sd} as well as SNR_{rd} along route 1 (left) and route 2 (right) based on the BS5's and BS6's measurement data

route 1 and route 2 based on the BS5's and BS6's measurement data. The maximal SNR value, limited to 30 [dB], occurs along route 2 for the SNR_{sr} value. It can be observed from Fig. 5.9 that at least in 70 % case SNR_{sd} along route 2 is smaller than -10 [dB]. Therefore, only *case: relay*) is considered for the performance investigation along route 2. However, all 5 cases: *case: direct*), *case: relay*), *case: relay+signal selection*), *case: re-trans.*), and *case: re-trans.+signal selection*), are considered during the simulation along route 1 because of the comparable SNR_{sd} , SNR_{sr} , and SNR_{rd} values. For each simulation instant, MS1, MS2, and MS3 are located within three adjacent snapshots.

The BER performances of MS1 and MS2 as well as MS3 along route 1 and route 2 based on the BS5's and BS6's measurement data have been shown in Fig. 5.10. It can be observed from Fig. 5.10 that for all three MSs along route 1, the BER performance of the direct link is always better than that of the relay link. The reasons are as follows. First of all, SNR_{sd} of the existing direct transmission along route 1 is only a little bit worse than SNR_{sr} of the relay transmission which can be observed from the left subplot in Fig. 5.9. Secondly, the performance of the relay transmission is limited by the SNR_{rd} value which is lower than SNR_{sr} at the most time. Furthermore, it can be found that for all three MSs along route 1, the *case: re-trans.+signal selection*) has the best BER performance which is followed sequentially by *case: relay+signal selection*), *case: re-trans.*), *case: direct*), and *case: relay*). However, for all three MSs along route 2, only *case: relay*) is possible since the direct transmission is too weak to contribute anything to the system performance. This



(a) The BER performances of MS1 and MS2 based on the BS5's and BS6's measurement data



(b) The BER performance of MS3 based on the BS5's and BS6's measurement data

Fig. 5.10: The cdf curves of the BER performances of MS1 and MS2 as well as MS3 along route 1(left) and route 2(right)

means, the relay transmission is especially important in the case when the direct transmission is blocked. As far as the direct transmission is available, the relay transmission can outperform the direct transmission at the price of equivalent SNR_{sr} and SNR_{rd} values which should be higher than the SNR_{sd} value. This observation is consistent with the argument shown in Fig. 1.1 in Chapter 1 and stated again in Sub-subsection 4.6.3. To achieve the same performance between the direct transmission and the relay transmission, the comparable SNR_{sd} value and SNR_{sr}/SNR_{rd} values can be found in Fig. 1.1 in Chapter 1. By comparing the BER performances based on the BS5's and BS6's measurement data along route 1 it can be observed that the results of *case: re-trans.+signal selection*), *case: relay+signal selection*), *case: re-trans.*), and *case: direct*) based on the BS5's measurement data are slightly better than the results based on the BS6's measurement data at the 50% cdf position. The reason is that the SNR_{sd} value based on the BS5's measurement data is a little bit better than that based on the BS6's measurement data at the 50% cdf position which can be observed from the left subplot in Fig. 5.9. However, for all three MSs along both route 1 and route 2, the result of the relay transmission based on the BS6's measurement data is better than that based on the BS5's measurement data. The reason is that the SNR_{rd} value based on the BS6's measurement data is higher than that based on the BS5's measurement data.

Both along route 1 and along route 2, the SNR_{sr} value is larger than the SNR_{rd} value at the most time. As discussed in Sub-subsection 4.6.3, the final end-to-end performance of a relay transmission is determined by the worst intermediate channel among the tandem relay chain. Therefore, the performance of the relay transmission is limited by the SNR_{rd} value. The higher the SNR_{rd} value, the better the BER performance. Even though the SNR_{sr} value varies between 5 [dB] and 30 [dB] along route 1 and between 10 [dB] and 30 [dB] along route 2, the BER curves of the relay transmission in Fig. 5.10 have almost no variance due to the low SNR_{rd} value. This means that no further performance improvement can be expected by further increasing SNR_{sr} in the case of the SNR_{sr} value being higher than SNR_{rd} .

5.3.2.3 Power allocation schemes

In Sub-subsection 5.3.2.2, it has been observed that with an equal power allocation between the MSs and the RS, the end-to-end performance of the relay transmission is limited by the small SNR_{rd} value. Therefore, further performance improvement can be expected if different power allocation schemes are utilized. This Sub-subsection focuses on the power allocation schemes and their influence on the final end-to-end performance of the relay transmission.

Based on the observation in Sub-subsection 5.3.2.2, more power should be allocated to the R-D link to improve the SNR_{rd} value. Therefore, three power allocation schemes are considered. They are $[\frac{1}{4} \frac{3}{4}]$, $[\frac{1}{8} \frac{7}{8}]$, and an adaptive power allocation. The first two schemes have a fix power allocation ratio while the last one is adaptive. An adaptive power allocation aims at providing equal SNR_{sr} and SNR_{rd} values for each snapshot. For each simulation instant, MS1, MS2, and MS3 are located within 3 adjacent snapshots. Therefore, three MSs have different SNR_{sr} values. The adaptive power allocation scheme targets at balancing SNR_{rd} and the minimum SNR_{sr} value of three MSs. The relay transmission along route 2 together with two antenna elements from BS6, having the largest element spacing, is under consideration with these power allocation schemes.

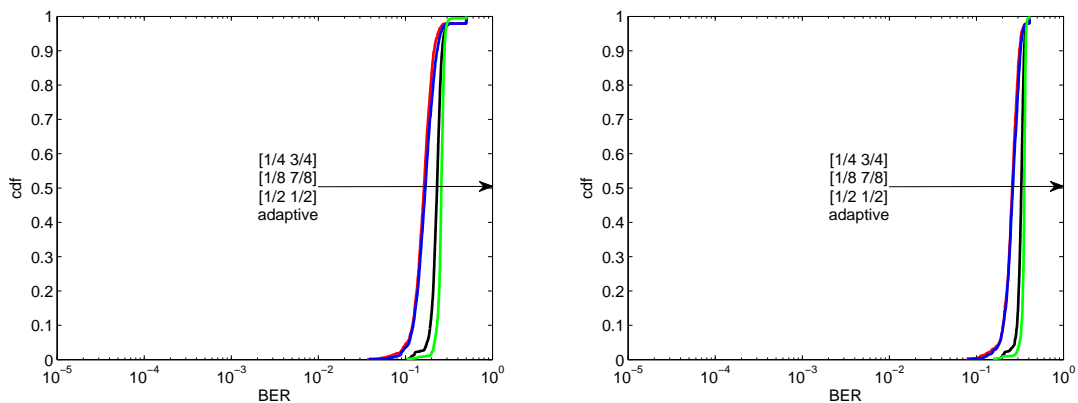


Fig. 5.11: The BER performances of MS1 and MS2 (left) as well as MS3 (right) along route 2 based on the BS6 measurement data

Figure 5.11 shows the cdf curves of the BER performances of MS1 and MS2 as well as MS3 along route 2 with power allocation scheme as parameter. As a comparison, the performance with an

equal power allocation is shown in the same figure. It can be found that the schemes with a fix power allocation ratio being $[\frac{1}{4} \frac{3}{4}]$ and $[\frac{1}{8} \frac{7}{8}]$ have almost the same performance which is better than the performance with an equal power allocation. Since more power is allocated to the R-D channel than to the S-R channel with the power allocation ratios being $[\frac{1}{4} \frac{3}{4}]$ and $[\frac{1}{8} \frac{7}{8}]$, the SNR_{rd} value is increased. Therefore, their performance outperforms the performance with an equal power allocation. However, compared the $[\frac{1}{8} \frac{7}{8}]$ scheme with the $[\frac{1}{4} \frac{3}{4}]$ scheme, no further performance improvement can be expected, even though more power is allocated to the RS to improve the SNR_{rd} value. The reason is that the SNR_{rd} value is limited by the maximum value 10 [dB] which happens when the total power is allocated to the RS. With the $[\frac{1}{2} \frac{1}{2}]$ scheme, the maximal SNR_{rd} value is 6.9 [dB] while with the $[\frac{1}{4} \frac{3}{4}]$ and $[\frac{1}{8} \frac{7}{8}]$ schemes, it is 8.7 [dB] and 9.4 [dB], respectively. From the $[\frac{1}{2} \frac{1}{2}]$ scheme to the $[\frac{1}{4} \frac{3}{4}]$ scheme, 1.6 [dB] gain can be achieved for the R-D channel while only 0.7 [dB] gain can be achieved from the $[\frac{1}{4} \frac{3}{4}]$ scheme to the $[\frac{1}{8} \frac{7}{8}]$ scheme. However, in both cases, the SNR_{sr} value is reduced with 3 [dB]. The reduction of the SNR_{sr} value indicates an increased amplify factor β as shown in Eqn. 4.9 in Chapter 4 and consequently an increased noise level. Because the improvement of the SNR_{rd} value from the $[\frac{1}{2} \frac{1}{2}]$ scheme to the $[\frac{1}{4} \frac{3}{4}]$ scheme is larger than that from the $[\frac{1}{4} \frac{3}{4}]$ scheme to the $[\frac{1}{8} \frac{7}{8}]$ scheme, an obvious performance improvement can be observed with the $[\frac{1}{4} \frac{3}{4}]$ and $[\frac{1}{8} \frac{7}{8}]$ schemes. However, after the trade off between the improvement of the SNR_{rd} value and the increased noise level, the schemes, $[\frac{1}{4} \frac{3}{4}]$ and $[\frac{1}{8} \frac{7}{8}]$, have almost the same performance.

Furthermore, it can be observed that the scheme with an adaptive power allocation has worse performance than other schemes in 98% case. As stated above, the scheme with an adaptive power allocation aims at returning equal SNR_{sr} and SNR_{rd} values. Due to the fact that the SNR_{rd} value is limited by the maximum value 10 [dB], this scheme tries to reduce the SNR_{sr} value to 10 [dB] in the case when $SNR_{sr} > SNR_{rd}$. As explained above, the system noise level will be increased with a reduced SNR_{sr} value. However, almost no SNR_{rd} gain can be achieved simultaneously. This is the reason why the scheme with an adaptive power allocation has worst performance in 98% case. The probability 98% depends on the occurrence that $SNR_{sr} > SNR_{rd}$ which can be observed in the right subplot in Fig. 5.9. In the rest 2% case, the scheme with an adaptive power allocation outperforms the other schemes with a fix power allocation ratio. In the rest 2% case, $SNR_{sr} < SNR_{rd}$. The scheme with an adaptive power allocation allocates more power to the S-R channel than to the R-D channel, by which the end-to-end performance of the relay transmission can be improved. However, the schemes with a fix power allocation ratio allocate more power to the the R-D channel than to the S-R channel which further impairs the end-to-end performance if $SNR_{sr} < SNR_{rd}$.

It can be concluded from the above observations that the power allocation schemes can improve the system performance in some sense. However, the performance of the relay transmission is still limited by the R-D channel. A possible solution could be exploiting more than 2 antenna elements at the BS to improve the link quality of the R-D channel, for example, through diversity gain. Therefore, keeping the balance between the tandem links of a relay channel is crucial for the relay system design.

5.4 Relay channel model based performance verification

As stated in Subsection 5.2.3, the distance between the BS and MSs is fixed to 500 [m] while the RS is positioned between the BS and the MSs. Therefore, different positioning schemes of the RS will be investigated in Sub-subsection 5.4.1.

5.4.1 Positioning of the RS

Three RS positioning schemes are considered: the RS is placed 125 [m] ($\frac{1}{4}$), 250 [m] ($\frac{1}{2}$), and 375 [m] ($\frac{3}{4}$) from the MSs. After simulations, the SNR values of each positioning scheme are listed as follows:

- $\frac{1}{4}$ positioning: $SNR_{sd} = 0$ [dB], $SNR_{sr} = 7$, [dB] $SNR_{rd} = 1$ [dB];
- $\frac{1}{2}$ positioning: $SNR_{sd} = 0$ [dB], $SNR_{sr} = 4$, [dB] $SNR_{rd} = 6$ [dB];
- $\frac{3}{4}$ positioning: $SNR_{sd} = 0$ [dB], $SNR_{sr} = 2$, [dB] $SNR_{rd} = 13$ [dB];

Two cases, *case: direct*) and *case: relay*), are considered in simulating the BER performance. Figure

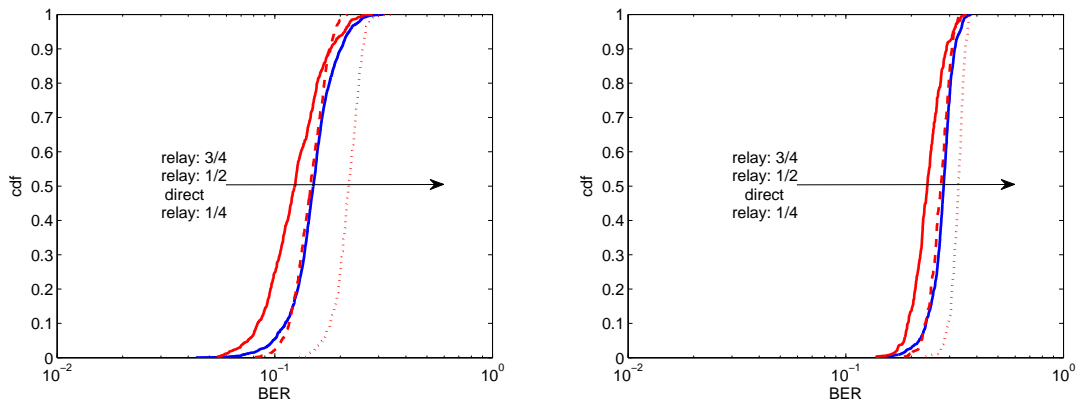


Fig. 5.12: The cdf curves of the BER performances of MS1 and MS2 (left) as well as MS3 (right) with different RS positioning schemes

5.12 shows the cdf curves of the BER performances of MS1 and MS2 as well as MS3 with different RS positioning schemes. It can be observed from Fig. 5.12 that, for all three MSs, $\frac{3}{4}$ positioning of the RS provides the best performance, which is followed by $\frac{1}{2}$ positioning and $\frac{1}{4}$ positioning sequentially. Furthermore, $\frac{3}{4}$ positioning has a better performance than the direct transmission. It is due to the SNR gain achieved by the tandem links of a relay channel. Even though $\frac{1}{2}$ positioning provides a better SNR balance between the tandem links of a relay channel than the other two positioning schemes, its performance is a little bit worse than that of $\frac{3}{4}$ positioning. The reason is that, SNR_{rd} of $\frac{3}{4}$ positioning is 7 [dB] higher than SNR_{rd} of $\frac{1}{2}$ positioning. However, SNR_{sr} of $\frac{3}{4}$ positioning is only 2 [dB] lower than SNR_{sr} of $\frac{1}{2}$ positioning. This 2 [dB] difference contributes almost no difference to the final channel amplitudes of two positioning schemes. This means, both $\frac{3}{4}$ positioning scheme and $\frac{1}{2}$ positioning scheme have almost the same S-R channel gain. But, the

R-D channel gain of $\frac{3}{4}$ positioning is much higher than that of $\frac{1}{2}$ positioning. As a consequence, the BER performance of $\frac{3}{4}$ positioning is better than that of $\frac{1}{2}$ positioning.

6. CONCLUSIONS

The primary goal of this dissertations has been: *propagation measurement based study on relay networks*. The study includes channel modeling, performance evaluation and verification. First of all, an experimental channel model of relay networks has been proposed based on the measurement data. By exploiting both this experimental channel model and raw measurement data, the performance of relay networks has been verified. For the verification purpose, MARN have been introduced as an example of the relay network. Various advanced techniques have been proposed for the performance improvement of MARN. The main contributions of this work are summarized as follows:

Due to the meshed topology of relay networks, the key idea of the relay channel modeling is to model the long-term correlation properties between the meshed-links. The correlation properties include both the intra-site correlation and the inter-site correlation. LSP, capturing the long-term variational characteristics of propagation channels in the spatial, temporal, frequency, and power domains, are the channel parameters in the correlation modeling. Through analyzing real-field relay measurement data, the experimental results of the correlation properties of LSP have been highlighted for both the urban and the indoor scenarios. Furthermore, these correlation properties have been fully introduced into the WIM framework for relay channel simulations.

For the purpose of performance evaluation and verification, MARN have been considered due to the fact that they may be suitable for the infrastructure based networks with dedicated RSs. Various techniques,

- MAC for the signal separability at the receiver and throughput improvement
- relay protocol design for high system resource efficiency
- the JU MMSE algorithm for the UKIF cancellation while keeping the multiple MSs' MAC-encoded signal structure
- an error detection aided signal selection technique for diversity increasing,

have been proposed for MARN in the presence of UKIF. An exemple system, 3 desired MSs with 1 UKIF MS and 1 RS, has been exploited for the performance evaluation. The performance enhancement has been proven by system simulations over Rayleigh channels. Furthermore, two forwarding strategies have been considered at the RS: the AF relaying and the DF relaying. The simulation results have shown that the DF relaying provides better performance than the AF relaying at the expense of an additional signal processing complexity at the RS.

Instead Rayleigh channels, realistic channels have been embedded in the simulation chain. The same example system but with a RS having an AF functionality has been considered for the performance verification. Channel realizations have been derived from raw measurement data and from the above mentioned experimental channel model. The simulation results have revealed that

- The simplified Rayleigh channels based simulation results overestimate the system performance.
- No further performance improvement can be expected in the practical applications in the similar urban environments considered, by the excessive use of space for BS antenna mounting, necessary to make antenna element spacing larger than $\frac{3}{2}\lambda_{WL}$.
- The performance of a relay transmission is limited by the worst of the tandem links of a relay channel. Therefore, keeping the balance between them is crucial for the relay system design.
- The relay transmission is especially important in the case when the direct transmission is blocked. As far as the direct transmission is available, the relay transmission can outperform the direct transmission if the SNR value of a relay link is higher than that of a direct link.
- In the realistic deployment, a careful selection of the RS position can further improve the system performance.

In Summary, this dissertation provides basic concepts and important experimental results on channel modeling for relay networks, and further addresses a common framework on theoretical and realistic performance evaluations.

Future works

1. Validate the proposed experimental relay channel model

The last step of the channel modeling process is system simulation and model validation. System simulation has been already discussed in this dissertation. However, model validation is still an open issue which could be one of the future works.

The validation can be performed by comparing channel parameters. The one is derived directly from raw measurement data. The other is extracted from the channel realizations simulated from the experimental relay channel model which is proposed based on the same raw data. The match level between them indicates the quality of a channel model.

2. Extend MARN to MIMO

In the MARN considered, both the desired MSs and the RS have a single antenna element. Therefore, it is possible in this dissertation to investigate the dependence of the system performance on the large scale correlation properties of LSF. If all stations have multiple antenna elements, the study can be extended to the channel parameters capturing various MIMO performances and limits, such as AS and NPCG.

Appendices

Appendix A

COMPARISON AMONG THE STATE-OF-THE-ART MIMO CHANNEL MODELS

	3GPP SCM [34]	802.11n [35]	COST273 [36]	WIM [145]
Frequency range	2GHz	2 & 5 GHz	2 & 5 GHz	2-6GHz
Bandwidth	5 MHz	100 MHz	Not stated	100MHz
Scenario	Outdoor	Indoor	Indoor, Outdoor	Indoor, Outdoor
Basic modeling principle	Ray-based	Cluster-structured and correlation based Kronecker model	Geometric clusters based	Ray-based
cluster	Zero-DS	Mean AOA, AOD	Mean angles and delays	Zero-DS
Model in delay domain	6-tapped delay line model, sum-of-20sinus for each tap	Tapped delay line model, each cluster has exponential PDP	Exponential decaying PDP	Clustered delay line model, sum-of-20sinus for each cluster
Statistical parameters	LSF, DS, AS	DS, AS	LSF, DS, AS@Tx, AS@Rx	LSF, DS, AS@Tx, AS@Rx, K-factor
Their distribution	Log-normal	Not stated	Log-normal	Log-normal/exponential/ Wrapped Gaussian
Intra-site auto-correlation	no	Not stated	De-correlation distance for outdoor	De-correlation distance
Intra-site cross-correlation	cross-correlation	cross-correlation	cross-correlation only for outdoor	cross-correlation
Inter-site correlation	0.5 for LSF	Not stated	0.5 for LSF in outdoor	No
Antenna independent	yes	no	no	yes

Continued on next page

TableA.1 – continued from previous page

	3GPP SCM	802.11n	COST273	WIM
Separate LOS/NLOS	No	LOS or NLOS	LOS occurrence	Yes
Inter-cell interference	no	no	no	no
Link-level modeling	yes	yes	yes	yes
System-level modeling	yes	no	Not stated	yes
Software implementation	yes [146]	matlab	n.a.	yes [44]
Relay support	no	no	no but ad-hoc peer to peer	yes

Appendix B

EXAMPLES OF MAC

Provided in Table B.1 and Table B.2

Tab. B.1: Examples of MAC for 4-MS case after computer searching.

N	N = 4										
User	#1	#2	#3	#4							
Elements	$\xi_1=4$	$\xi_2=4$	$\xi_3=4$	$\xi_4=169$							
	0000	0003	0030	0000	0112	0222	1000	1200	2002	2112	3010
	1111	1112	1121	0001	0113	0223	1001	1201	2003	2113	3011
	2222	2221	2212	0002	0120	0230	1002	1202	2010	2120	3012
	3333	3330	3303	0003	0121	0231	1003	1203	2011	2121	3013
				0010	0122	0232	1010	1210	2012	2122	3020
				0011	0123	0233	1011	1211	2013	2123	3021
				0012	0130	0300	1012	1212	2020	2130	3022
				0013	0131	0301	1013	1213	2021	2131	3023
				0020	0132	0302	1020	1220	2022	2132	3030
				0021	0133	0303	1021	1221	2023	2133	3031
				0022	0200	0310	1022	1222	2030	2200	3032
				0023	0201	0311	1023	1223	2031	2201	3033
				0030	0202	0312	1030	1230	2032	2210	3100
				0031	0203	0313	1031	1231	2033	2211	3102
				0032	0210	0320	1032	1232	2100	2300	3120
				0033	0211	0321	1033	1233	2101	2301	3122
				0100	0212	0322	1100	1300	2102	2310	3200
				0101	0213	0323	1102	1302	2103	2311	3201
				0102	0220	0330	1120	1320	2110	3000	3210
				0103	0221	0331	1122	1322	2111	3001	3211
				0110		0332		2000		3002	3300
				0111		0333		2001		3003	

Tab. B.2: Examples of MAC for 2-MS case and 3-MS case after computer searching.

N	N = 2		N = 3					
MS	#1	#2	#1	#2	#3			
Elements	$\xi_1=4$	$\xi_2=9$	$\xi_1=4$	$\xi_2=4$	$\xi_3=36$			
	00*	00	000	003	000	122	021	102
	11	01	111	112	001	123	022	103
	22	02	222	221	002	200	023	120
	33	03	333	330	003	201	030	121
		10			010	202	031	213
		12			011	203	032	300
		20			012	210	033	301
		21			013	211	100	302
		30			020	212	101	303
	* "0" = $(1+j)/\sqrt{2}$; "1" = $(-1+j)/\sqrt{2}$; "2" = $(1-j)/\sqrt{2}$; "3" = $(-1-j)/\sqrt{2}$							

Appendix C

SOLUTION OF THE MMSE CRITERION

For the simplicity in notation, we remove the subscript ^(k). For the optimal solution pairs $[\mathcal{W}_A, \mathcal{A}]$ and $[\mathcal{W}_H, \mathbf{H}]$, adding different subscript ^(k) distinguishes the final results for the first and second time-slots.

- \mathcal{A} -criterion

The cost function can be expressed as

$$\begin{aligned} |e_{\mathcal{A}}|^2 &= |\mathcal{W}_{\mathcal{A}}^H \mathbf{Y} - \mathcal{A}^H \mathbf{X}_d|^2 \\ &= (\mathcal{W}_{\mathcal{A}}^H \mathbf{Y} - \mathcal{A}^H \mathbf{X}_d) (\mathcal{W}_{\mathcal{A}}^H \mathbf{Y} - \mathcal{A}^H \mathbf{X}_d)^H \\ &= \mathcal{W}_{\mathcal{A}}^H \mathbf{Y} \mathbf{Y}^H \mathcal{W}_{\mathcal{A}} - \mathcal{W}_{\mathcal{A}}^H \mathbf{Y} \mathbf{X}_d^H \mathcal{A} - \mathcal{A}^H \mathbf{X}_d \mathbf{Y}^H \mathcal{W}_{\mathcal{A}} + \mathcal{A}^H \mathbf{X}_d \mathbf{X}_d^H \mathcal{A}. \end{aligned} \quad (\text{C.1})$$

Setting the partial derivative with respect to $\mathcal{W}_{\mathcal{A}}$ at zero in Eqn. C.1, we obtain

$$\mathcal{W}_{\mathcal{A}}^H \mathbf{Y} \mathbf{Y}^H = \mathcal{A}^H \mathbf{X}_d \mathbf{Y}^H. \quad (\text{C.2})$$

Now, in order to avoid the trivial solution $[\mathcal{W}_{\mathcal{A}}, \mathcal{A}] = [\mathbf{0}, \mathbf{0}]$, $\mathcal{A}_{i,i}$, $1 \leq i \leq n_{Rx}$, is set at 1. With the same method given in [38], we can easily obtain the i^{th} , $1 \leq i \leq n_{Rx}$, column of the optimal solution of matrix pair $\mathcal{W}_{\mathcal{A}}$ and \mathcal{A} as

$$\mathbf{w}_i = \left(\mathbf{M} - \sum_{j=1, j \neq i}^N \mathbf{h}_j \mathbf{h}_j^H \right)^{-1} \mathbf{h}_i, \quad (\text{C.3})$$

and

$$\mathbf{a}_i = [\mathbf{h}_1^H \mathbf{w}_i \cdots \mathbf{h}_{i-1}^H \mathbf{w}_i \ 1 \ \mathbf{h}_{i+1}^H \mathbf{w}_i \cdots \mathbf{h}_N^H \mathbf{w}_i]^T, \quad (\text{C.4})$$

where

$$\mathbf{M} = \mathcal{H} \mathcal{H}^H + \sigma_n^2 \mathbf{I}. \quad (\text{C.5})$$

and \mathbf{h}_i denotes the i^{th} column of channel matrix \mathbf{H}_d .

- \mathbf{H} -criterion

The cost function can be expressed as

$$\begin{aligned}
 |e_{\mathbf{H}}|^2 &= |\mathcal{W}_{\mathbf{H}}^H \mathbf{Y} - \mathbf{H}_D \mathbf{X}_d|^2 \\
 &= (\mathcal{W}_{\mathbf{H}}^H \mathbf{Y} - \mathbf{H}_D \mathbf{X}_d) (\mathcal{W}_{\mathbf{H}}^H \mathbf{Y} - \mathbf{H}_D \mathbf{X}_d)^H \\
 &= \mathcal{W}_{\mathbf{H}}^H \mathbf{Y} \mathbf{Y}^H \mathcal{W}_{\mathbf{H}} - \mathcal{W}_{\mathbf{H}}^H \mathbf{Y} \mathbf{X}_d^H \mathbf{H}_d - \mathbf{H}_D \mathbf{X}_d \mathbf{Y}^H \mathcal{W}_{\mathbf{H}} + \mathbf{H}_D \mathbf{X}_d \mathbf{X}_d^H \mathbf{H}_d. \quad (\text{C.6})
 \end{aligned}$$

Setting the partial derivative with respect to $\mathcal{W}_{\mathbf{H}}$ at zero in Eqn. C.6, we obtain

$$\mathcal{W}_{\mathbf{H}}^H = \mathbf{H}_d \mathbf{H}_d^H \mathbf{M}^{-1}. \quad (\text{C.7})$$

Appendix D

GLOSSARY OF OPERATORS, SYMBOLS, AND ACRONYMS

D.1 Mathematical operators

- $\text{vec}\{\mathbf{H}\}$ forms a column vector of the matrix \mathbf{H}
- $E\{\cdot\}$ the expectation operation
- \mathbf{H}^H the complex conjugate transpose of \mathbf{H}
- \mathbf{H}^T the complex transpose of \mathbf{H}
- $\mathbf{A} \otimes \mathbf{B}$ the Kronecker product of two matrices \mathbf{A} and \mathbf{B}
- $\det \mathbf{H}$ the determinant of \mathbf{H}
- $\min(n_{Tx}, n_{Rx})$ the smaller value from n_{Tx} and n_{Rx}
- $\max(\lambda_1^2, \dots, \lambda_{\min(n_{Tx}, n_{Rx})}^2)$ the maximal value from $\lambda_1^2, \dots, \lambda_{\min(n_{Tx}, n_{Rx})}^2$
- $\|\mathbf{X}\|_F$ Frobenius of a matrix \mathbf{X}

D.2 Acronym

3D	3-Dimension
AF	Amplify-and-Forward
ACK	Acknowledgment
AOA	Angle of Arrival
AOD	Angle of Departure
AP	Access Point
ARQ	Automatic Repeat-reQuest
AS	Angular Spread
AWGN	additive white Gaussian noise
BER	Bit Error Rate
BLER	Block Error Rate
BPSK	Binary Phase-Shifted Keying
BS	Base Station
cdf	Cumulative Distribution Function

CIR	Channel Impulse Response
COST	European Cooperation in the field of Scientific and Technical Research
CRC	Cyclic Redundancy Check
CSI	Channel State Information
CTF	Channel Transfer Function
DF	Decode-and-Forward
DoA	Direction of Arrival
DoD	Direction of Departure
DoF	Degree of Freedom
DS	Delay Spread
DW	Delay Window
ESPRIT	Estimation of Signal Parameters via Rotational Invariance Techniques
fft	Fast Fourier Transformation
GF	Galois field
GPP	Generation Partnership Project
GSM	Global System for Mobile Communications
IEEE	Institute of Electrical and Electronics Engineers
ifft	Inverse Fast Fourier Transformation
i.i.d	independent and identically distributed
JU	Joint User
LMSE	Least Mean Square Error
LOS	Line of Sight
LSA	Local Stationary Area
LSF	Large Scale Fading
LSP	Large Scale Parameters
MAC	Multiple Access Coding
MARN	Multiple Access Relay Networks
MCSSS	Multi-Carrier Spread Spectrum Signal
MIMO	Multiple-Input Multiple-Output
MISO	Multiple-Input Single-Output
ML	Maximum Likelihood
MMSE	Minimum Mean Square Error
MSE	Mean Square Error
MPC	Multipath Component
MS	Mobile Station
NAK	Negative Acknowledgment
NLOS	None Line of Sight
NPCG	Normalized Parallel Channel Gain
PAS	Power Angle Spectrum
PDF	Probability Density Function
PDP	Power Delay Profile
PL	Path Loss
PSD	Power Spectral Density
PUCPA	Polarimetric Uniform Circular Patch Array
PULA	Polarimetric Uniform Linear Array
QoS	Quality of Services
QPSK	Quadratur Phase Shift Keying
RIMAX	Gradient based ML Parameter estimation algorithm
RS	Relay Station
Rx	Receiver
SA	Service Area

SAGE	Space Alternating Generalized Expectation maximization
SCM	Spatial Channel Model
SIR	Signal-to-Interference Ratio
SISO	Single-Input Single-Output
SIMO	Single-Input Multiple-Output
SNR	Signal-to-Noise Ratio
SPUCPA	Stacked Polarimetric Uniform Circular Patch Array
SSF	Small Scale Fading
ST	Space Time
SVD	Single Value Decomposition
TDMA	Time Division Multiple Access
TDoA	Time Delay of Arrival
Tx	Transmitter
ULA	Uniform Linear Array
UMTS	Universal Mobile Telecommunications System
UKIF	Unknown Interference
WIM	WINNER channel Model
WINNER	Wireless World Initiative New Radio
WLAN	Wireless Local Area Networks
XPR	Cross-polarization Ratio

D.3 List of frequently used symbols

Symbol	Description	Chapter
n_{Rx}	The number of receive antenna elements	1
n_{Tx}	The number of transmit antenna elements	1
n_{hop}	The number of intermediate hops	1
H	A MIMO channel matrix in frequency domain	2.3
R	A correlation matrix	2.3
\mathcal{G}	A matrix with its elements being i.i.d zero mean complex Gaussian random variables	2.3
R_{Tx}	A correlation matrix at the transmitter side	2.3
h_i	The i th column of H	2.3
R_{Rx}	A correlation matrix at the receiver side	2.3
h^j	The j th row of H	2.3
B_c	Coherence bandwidth	2.5
τ_{rms}	DS	2.5
c_B	A selected coherence level	2.5
P_{Rx}	The received power	2.5
P_{Tx}	The transmit power	2.5
PL	PL	2.5
n_{PL}	The PL exponent	2.5
d	Distance between the transmitter and the receiver	2.5
B	The PL value when d is one meter	2.5

Continued on next page

TableD.1 – continued from previous page

Symbol	Description	Chapter
σ^2	The variance of LSF	2.5
λ_{WL}	Wavelength	2.5
G_{Tx}	Transmit antenna gain	2.5
G_{Rx}	Receiver antenna gain	2.5
$h_{i,j}$	The (i, j) element of \mathbf{H}	2.5
\mathbf{r}	Receive signal	2.5
\mathbf{s}	Transmit signal	2.5
\mathbf{n}	AWGN noise	2.5
\mathbf{U}	A unitary matrix with dimension $n_{Rx} \times n_{Rx}$	2.5
\mathbf{V}	A unitary matrix with dimension $n_{Tx} \times n_{Tx}$	2.5
λ_i	The i^{th} eigen value of a channel matrix \mathbf{H}	2.5
C_{MIMO}	The capacity of a MIMO channel	2.5
$\mathbf{I}_{\min(n_{Tx}, n_{Rx})}$	An identity matrix with dimension $\min(n_{Tx}, n_{Rx}) \times \min(n_{Tx}, n_{Rx})$	2.5
ρ_{SNR}	The SNR value of a MIMO channel	2.5
C_{AB}	the cross-covariance of A and B	2.5
ρ_{MS}	The intra-site auto-correlation	2.5
d_{MS}	Distance between two MSs	2.5
ρ_{AB}	The intra-site cross-correlation	2.5
d_{decorr}	De-correlation distance	2.5
θ_{s1}	The 3 dB beam width of sector 1 of a BS antenna array	2.5
θ_{s2}	The 3 dB beam width of sector 2 of a BS antenna array	2.5
θ_{OL}	The angle of overlapped main beam area of two sectors of the same BS	2.5
ρ_{AB}	The inter-sector correlation	2.5
ρ_{BS}	The inter-site correlation	2.5
d_{diff}	Distance difference between two links	2.5
d_1, d_2	Distance from a MS to two BSs/RSs, respectively	2.5
k_d	Coefficient between d_1 and d_2	2.5
θ	The angle seen from a MS to two BSs/RSs	2.5
d_{BS}	Distance between two BSs/RSs	2.5
h_{diff}	Height difference between two BSs/RSs	2.5
n_{BS}	The number of BSs	2.6
n_{MS}	The number of MSs	2.6
$n_l(i)$	The number of connections from MS i to BSs	2.6
n_{LSP}	The number of LSP	2.6
$m_x \times m_y$	A two-dimensional geometric grid	2.6

Continued on next page

TableD.1 – continued from previous page

Symbol	Description	Chapter
d_x	Distance along x-axis	2.6
d_y	Distance along y-axis	2.6
(x_1, y_1) and (x_2, y_2)	Positions of two MSs	2.6
$f(x, y)$	A two-dimensional filter function	2.6
$\zeta, \hat{\zeta}$	LSP at each MS location for one MS-BS link	2.6
v_{MS}	The moving speed of MS	3.2
h_{BS}	The height of a BS	3.2
h_{RS}	The height of a RS	3.2
h_{MS}	The height of a MS	3.2
τ_{max}	The time length of a SISO CIR	3.3.1
ss_i	The i^{th} snapshot	3.4.1
n_f	The number of frequency bins	3.4.1
n_{ss}	The number of snapshots within a LSA	3.4.1
\tilde{n}_{ss}	The number of valid snapshots within a LSA	3.4.1
AS_{Tx}	AS at the transmitter	3.4
AS_{Rx}	AS at the receiver	3.4
λ_{max}	The maximum singular value	3.4
τ_{DW}	DW	3.4
$p_{1 \times \tau_{max}}$	PDP after a ST averaging	3.4
$\tilde{p}_{1 \times \tau_{DW}}$	PDP after removing noise	3.4
$\bar{\tau}$	Mean delay	3.4
XPR_H	The power ratio between the HH co-polar and the HV cross-polar	3.4
XPR_V	The power ratio between the VV co-polar and the VH cross-polar	3.4
XPR	The power ratio between the $HH + VV$ co-polar and the $HV + VH$ cross-polar	3.4
\mathbf{h}	CIR	3.4
LSP	The LSP values from the measurement data	3.4.4
\widetilde{LSP}	The transformed Gaussian distributed LSP values	3.4.4
$f(LSP)$	The function transferring the LSP values from measurement data to be Gaussian distributed	3.4.4
$f^{-1}(\widetilde{LSP})$	The inverse function $f(LSP)$	3.4.4
$\sigma_{\widetilde{LSF}}^2$	The variance of a Gaussian distributed \widetilde{LSF}	3.4.4
$\mu_{\widetilde{LSF}}$	The mean(median) value of Gaussian distributed \widetilde{LSF}	3.4.4
σ^2	The variance	3.5.1.1
μ	The mean value	3.5.1.1
N	The number of the desired blocked MSs	4.2

Continued on next page

TableD.1 – continued from previous page

Symbol	Description	Chapter
L	The number of the UKIF MSs	4.2
$\mathbf{Y}_{s,d}$	The received signals at the BS from the MSs	4.2
$y_{s,r}$	The received signals at the RS	4.2
$\mathbf{H}_{s,d}$	The complex channel gain between the N desired MSs and the BS	4.2
$\mathbf{P}_{s,d}$	A diagonal matrix with the received power of the desired MSs-BS channels along the diagonal	4.2
\mathbf{X}	The transmit signal of the desired blocked MSs	4.2
$\mathbf{H}_{u,d}$	The complex channel gain between the L UKIF MSs and the BS	4.2
$\mathbf{P}_{u,d}$	A diagonal matrix with the received power of the UKIF MSs-BS channels along the diagonal	4.2
\mathbf{S}	The transmit signal of the UKIF MSs	4.2
\mathbf{n}	The AWGN vectors at the BS	4.2
$\mathbf{H}_{s,r}$	The complex channel gain between the N desired MSs and the RS	4.2
$\mathbf{P}_{s,r}$	A diagonal matrix with the received power of the desired MSs-RS channels along the diagonal	4.2
$n_{s,r}$	The AWGN vectors at the RS	4.2
$h_{i,r}$	The complex channel gain between the i^{th} desired MS and the RS	4.2
$p_{i,r}$	The received power of the i^{th} desired MS-RS channel	4.2
$h_{i,j}$	The complex channel gain between the j^{th} desired MS and the i^{th} BS antenna element	4.2
$p_{i,d}$	The received power of the i^{th} desired MS-BS channel	4.2
x_i	The transmit signal of the i^{th} desired MS	4.2
n_i	The AWGN noise at the BS i^{th} antenna element	4.2
$h_{i,j}$	The complex channel gain between the j^{th} UKIF MS and the i^{th} BS antenna element	4.2
$p_{i,d}$	The received power of the i^{th} UKIF MS-BS channel	4.2
s_i	The transmit signal of the i^{th} UKIF MS	4.2
$\mathbf{Y}_{r,d}$	The received signals at the BS from the RS	4.2
$\mathbf{H}_{r,d}$	The complex channel gain between the RS and the BS	4.2
$\mathbf{P}_{r,d}$	The received power of the RS-BS channel	4.2
$x_{r,d}$	The transmit signal from the RS	4.2

Continued on next page

TableD.1 – continued from previous page

Symbol	Description	Chapter
$h_{r,j}$	The complex channel gain between the RS and the j^{th} BS antenna element	4.2
$SIR^{(1)}$ or $SIR^{(2)}$	SIR at the first or second time-slot	4.2
β	The amplifying factor of the AF relay	4.3
\mathbf{Y}_d^{AF} or \mathbf{Y}_d^{DF}	The final output of the AF relaying or of the DF relay	4.3
\mathbf{H}_d^{AF} or \mathbf{H}_d^{DF}	The final desired channel gain of the AF relaying or of the DF relay	4.3
\mathbf{H}_u^{AF} or \mathbf{H}_u^{DF}	The final UKIF channel gain of the AF relaying or of the DF relay	4.3
\mathbf{n}_u^{AF} or \mathbf{n}_u^{DF}	The final AWGN noise of the AF relaying or of the DF relay at the BS	4.3
I^{AF}	The maximum mutual information of an AF relay	4.3
\mathbb{X} or $\bar{\mathbb{X}}$	A subset of $\left[x_1^{(1)} \ \dots \ x_N^{(1)} \right]$ and the corresponding complement	4.3
I^{DF}	The maximum mutual information of a DF relay	4.3
\hat{x}	The detected signal of x at the RS	4.3
$\hat{\hat{x}}$	The detected signal of x at the BS	4.3
p	A probability	4.3
\mathcal{C}_i	The MAC codebook of the i^{th} MS	4.4
ξ_i	The number of the i^{th} MAC codebook	4.4
\mathcal{X}	The set comprises all combinations of \mathbf{X}	4.4
\mathbf{Y}	The generalized received signal at the BS	4.4
\mathbf{H}_d	The generalized desired channel gain at the BS	4.4
\mathbf{X}_d	The generalized transmit signal of the desired MSs	4.4
\mathbf{H}_u	The generalized UKIF channel gain at the BS	4.4
\mathbf{S}_u	The generalized transmit signal of the UKIF MSs	4.4
\mathfrak{H}	The generalized total channel gain at the BS	4.4
\mathfrak{X}	The generalized total transmit signal of the MS	4.4
$\ e\ $	The error cost function of the JU MMSE detector	4.5.1.1
$\mathcal{W}_{\mathcal{A}}$ and \mathcal{A}	The spatial filtering weights of the \mathcal{A} -criterion	4.5.1.1
$\hat{\mathbf{Y}}$	The output of the JU MMSE detector	4.5.1.2
$\hat{\mathbf{H}}_d$	The equivalent channel matrix observed from the output of JU MMSE detector	4.5.1.2
$\hat{\mathbf{n}}$	The covariance matrix of the equivalent noise observed at the output of JU MMSE detector	4.5.1.2
\mathcal{R}_{cov}	The covariance matrix of UKIF-plus-noise	4.5.1.2
$\hat{\mathfrak{Y}}$	The N JU MMSE output vectors	4.5.2
SNR_{sd}	The SNR value of the S-D channel	5.1.2

Continued on next page

TableD.1 – continued from previous page

Symbol	Description	Chapter
SNR_{sr}	The SNR value of the S-R channel	5.1.2
SNR_{rd}	The SNR value of the R-D channel	5.1.2

BIBLIOGRAPHY

Own References

- [1] P. Kyösti et al., "Winner ii channel models," *IST-4-027756 WINNER II D1.1.2 V1.2*, 2007.
 - [2] Hong A., Sommerkorn G., Thomä R. S., and Zirwas W., "Considerations on the relationship between path loss and spatial characteristics based on mimo measurements," in *ITG Workshop on Smart Antennas*, Ulm, Germany, Mar. 2006.
 - [3] Hong A., Schneider C., Sommerkorn G., Milojević M., Thomä R. S., and Zirwas W., "Experimental evaluation of correlation properties of large scale parameters in indoor pico-cell environments," in *3rd International Symposium on Wireless Communication Systems (ISWCS)*, Valencia, Spain, Sep. 2006.
 - [4] Schneider C., Hong A., Sommerkorn G., Milojevic M., and Thomä R. S., "Path loss and wideband channel model parameters for winner link and system level evaluation," in *3rd International Symposium on Wireless Communication Systems (ISWCS)*, Valencia, Spain, Sep. 2006.
 - [5] Hong A., Narandzic M., Schneider C., and Thomä R. S., "Estimation of the correlation properties of large scale parameters from measurement data," in *IEEE International Symposium on Personal, Indoor and Mobile Radio Communications (PIMRC)*, Athens, Greece, Sep. 2007.
 - [6] Jalden N., Hong A., Zetterberg P., Ottersten P., , and Thomä R. S., "Correlation properties of large scale fading based on indoor measurements," in *IEEE Wireless Communication and Networking Conference*, Hongkong, China, Mar. 2007.
 - [7] Hong A. and Thomä R. S., "Experimental study on the impact of the base station height on the channel parameters," in *ITG Workshop on Smart Antennas*, Berlin, Germany, Feb. 2009.
 - [8] Schneider C., Sommerkorn G., Narandzic M., Käske M., Hong A., Algeier V., Kotterman W., Thomä R. S., and Jandura C., "Multi-user mimo channel reference data for channel modelling and system evaluation from measurements," in *ITG Workshop on Smart Antennas*, Berlin, Germany, Feb. 2009.
 - [9] Narandzic M., Kotterman W., Kaeske M., Schneider C., Sommerkorn G., Hong A., and Thomae R., "On a characterisation of large-scale channel parameters for distributed (multi-link) mimo - the impact of power level differences," in *The 4th European Conference on Antennas and Propagation*, Barcelona, Spain, Apr. 2010.
 - [10] Hong A., Matsumoto T., and Thomä R. S., "On the use of multiple access coding in cooperative space-time relay transmission and its measurement data based performance verification," in *ITG Workshop on Smart Antennas*, Vienna, Austria, Mar. 2007.
 - [11] Matsumoto T. and Hong A., "On the mmse criterion for space-time coded signaling in the presence of unknown interference," *EURASIP Research Letters in Communications*, vol. 2007, 2007.
-

- [12] Hong A. and Matsumoto T., "Preserving the coding structure in relay transmission in the presence of unknown interference," in *IEEE International Symposium on Spread Spectrum Techniques and Applications*, Bologna, Italy, Aug. 2008.

References by Other Authors

- [13] Rappaport T. S., Ed., *Wireless Communications. Principles and Practice*, 2nd ed. New Jersey, USA: Prentice Hall, 2002.
- [14] Kitao K. and Ichitsubo S., "Path loss prediction formula for microcell in 400 mhz to 8 ghz band," *Electronics Letters*, vol. 40, Nov. 2004.
- [15] Oda Y., Tsuchihashi R., Tsunekawa K., and Hata M., "Measured path loss and multipath propagation characteristics in uhf and microwave frequency band for urban mobile communications," in *IEEE Semiannual Vehicular Technology Conference*, vol. 1, Apr. 2001, pp. 337–341.
- [16] Sakawa K., Masui H., Ishii M., Shimizu H., and Kobayashi T., "Microwave path-loss characteristics in an urban area with base station antenna on top of a tall building," in *International Zurich Seminar on Broadband communications*, Feb. 2002, pp. 311–314.
- [17] Ralf Pabst et al., "relay based deployment concepts for wireless and mobile broadband radio," *IEEE Communication Magazine*, pp. 80–87, Sep. 2004.
- [18] Wijaya H., "Broadband multi-hop communication in homogeneous and heterogeneous wireless lan networks," Ph.D. dissertation, Technische Hochschule Aachen, Germany, Feb. 2005.
- [19] Redana et al. S., "Final assessment of relaying concepts for all cgs scenarios under consideration of related winner l1 and l2 protocol functions," *D3.5.3 v1.0, IST-4-027756 WINNER II*, 2007.
- [20] Schulz et al. D., "Relaying concepts and supporting actions in the context of cgs," *IST-4-027756 WINNER II D3.5.1 v1.0*, Oct. 2006.
- [21] Zirwas W., Li H., Lott M., Weckerle M., Schulz E., and Lampe M., "Radio resource management in cellular multihop networks," *European Transactions on Telecommunications*, vol. 15, no. 4, pp. 375–389, 2004.
- [22] Laneman J. N., "Cooperative diversity in wireless networks: Algorithms and architectures," PhD thesis, Massachusetts Institute of Technology (MIT), Sep. 2002.
- [23] Hunter Todd E. and Nosratinia A., "Coded cooperation under slow fading, fast fading, and power control," in *Asilomar Conference Signals, Systems and Computers*, Pacific Grove, California, Nov. 2002, pp. 118–122.
- [24] Hunter Todd E. and Nosratinia A., "Diversity through coded cooperation," *IEEE Transactions on wireless communications*, vol. 5, no. 2, pp. 283–289, Feb. 2006.
- [25] Nabar R., Bolcskei H., and Kneubuhler F. W., "Fading relay channels: performance limits and space-time signal design," *IEEE Journal on Selected Areas in Communications*, vol. 22, pp. 1099–1109, Aug. 2004.
- [26] Li S., Yeung R., and Cai N., "linear network coding," *IEEE Transaction on Information Theory*, vol. 49, pp. 371–381, Feb. 2003.
-

-
- [27] Dohler M., "Virtual antenna arrays," Ph.D. dissertation, University of London, United Kingdom, Strand, London, Nov. 2003.
- [28] Rankov R. and Wittneben A., "Spectral efficient signaling for half-duplex relay channels," in *Asilomar Conference on Signals, Systems, and Computers*, Nov. 2005.
- [29] Foschini G. J. and Gans M. J., "on the limit of wireless communications in a fading environment when using multiple antennas," *Wireless Personal Communications*, vol. 6, pp. 311–335, 1998.
- [30] Telatar I. E., "capacity of multi-antenna gaussian channels," *European Transactions on Telecommunications*, vol. 10, no. 6, pp. 585–595, Nov. 1999.
- [31] Pätzold M., *Mobile Fading Channels*. John Wiley & Sons, Jan. 2002.
- [32] Erceg V., Fortune Steven J. and Ling J., Rustako Jr. A. J., and Valenzuela Reinaldo A., "Comparisons of a computer-based propagation prediction tool with experimental data collected in urban microcellular environments," *IEEE Journal on Selected Areas in Communications*, vol. 15, no. 4, pp. 677–684, May 1997.
- [33] Suzuki H., "A statistical model of mobile radio reception," *IEEE transactions on Communications*, vol. COM-25, pp. 673–680, Jul. 1977.
- [34] "Spatial channel model for multiple input multiple output (mimo) simulations," *3GPP TR 25.996 V6.1.0*, Sep. 2003.
- [35] "Ieee p802.11 wireless lans, tgn channel models," *IEEE 802.11-03/940r2*, Jan. 2004.
- [36] Correia (ed) L., *mobile broadband multimedia networks: techniques, mobiles and tools for 4G. COST 273: European Cooperation in Mobile Radio Research*. Academic press, 2006.
- [37] Kasami T. and Lin S., "Coding for multiple-access channel," *IEEE Transaction on Information Theory*, vol. 22, no. 2, Mar. 1976.
- [38] Veselinovic N., Matsumoto T., and Juntti M., "Iterative mimo turbo multiuser detection and equalization for sttrc coded system with unknown interference," *EURASIP Journal on Wireless Communications and Networking, Special Issue on Multiuser MIMO Networks*, Dec. 2004.
- [39] Herhold P., Zimmermann E., and Fettweis G., "Cooperative multi-hop transmission in wireless networks," *Computer Networks*, vol. 49, no. 3, pp. 299–324, 2005.
- [40] Correia (ed) L., *Wireless Flexible Personalised Communications, COST 259: European Cooperation in Mobile Radio Research*. John Wiley & Sons, 2001.
- [41] J. Meinilä et al., "A set of channel and propagation models for early link and system level simulations," *WINNER D5.1 v1.0*.
- [42] J. Meinilä et al., "Determination of propagation scenarios," *WINNER D5.2 v1.0*.
- [43] Pätzold M., Killat U., and Laue F., "A deterministic digital simulation model for suzuki processes with application to a shadowed rayleigh land mobile radio channel," *IEEE Transactions on Vehicular Technology*, vol. 45, no. 2, p. 318.331, May 1996.
- [44] "www.ist-winner.org."
-

-
- [45] Yu K. and Ottersten B., "Models for mimo propagation channels, a review," *Special Issue on Adaptive Antennas and MIMO Systems Wiley Journal on Wireless Communications and Mobile Computing*, vol. 2, no. 7, pp. 653–666, Nov. 2002.
- [46] Schumacher L., Berger L., and Ramiro-Moreno J., "Recent advances in propagation characterisation and multiple antenna processing in the 3gpp framework," in *Union Radio Scientific Internationale Conference*, Maastricht, Netherlands, Aug. 2002.
- [47] "<http://www.awe-communications.com>."
- [48] Thomä R. S., Hampicke D., Landmann M., Richter A., and Sommerkorn G., "Measurement-based parametric channel modelling (mbpcm)," in *The International Conference on Electromagnetics in Advanced Applications*, Torino, Italy, Sep. 2003.
- [49] Steinbauer M., "The radio propagation channel - a non-directional, directional, and double-directional point-of-view," PhD thesis, Technische Universität wien (TUW), Sep. 2001.
- [50] Webb M., Watkins G., Williams C., Harrold T., Feng R., and Beach M., "Mobile multihop: Measurements vs. models," in *European Cooperation in The Field of Scientific and Technical Research COST2100*, no. COST 2100 TD(07) 322, Duisburg, Germany, Sept. 2007.
- [51] van der Meulen E. C., "Three-terminal communication channels," *Advances in Applied Probability*, vol. 3, pp. 120–154, 1971.
- [52] Cover T. M. and Gamal A. E., "Capacity theorems for the relay channel," *IEEE Transaction on Information Theory*, vol. IT-25, no. 5, pp. 572–584, Sep. 1979.
- [53] Kramer G., Gastpar M., and Gupta P., "Cooperative strategies and capacity theorems for relay networks," *IEEE Transactions on Information Theory*, vol. 51, no. 9, pp. 3037–3063, Sep. 2005.
- [54] Yin L., "Modelling and simulation of service area based ofdm air interfaces for beyond 3g mobile radio," Ph.D. dissertation, Technischen Universität Kaiserslautern, Germany, 2005.
- [55] Cover T. M. and Thomas J. A., *Elements of Information Theory*. New York, USA: John Wiley & Sons, Sep. 1991.
- [56] Fraile R., Monserrat J., Cardona N., and Nasreddine J., "Impact of shadowing modelling on td-cdma system-level simulations," in *3rd International Symposium on Wireless Communication Systems (ISWCS)*, Valencia, Spain, Sep. 2006.
- [57] Monserrat J., Gozalvez J., Fraile R., and Cardona N., "Effect of shadowing correlation modelling on the system level performance of adaptive radio resource management techniques," in *International Symposium on Wireless Personal Multimedia Communications*, Abano Terme, Italy, Sep. 2005.
- [58] Safak A., "Optimal channel reuse in cellular radio systems with multiple correlated log-normal interferers," *IEEE Transaction on Vehicular Technology*, vol. 43, pp. 304–312, May 1994.
- [59] Klingenbrunn T. and Mogensen P., "Model cross-correlated shadowing in network simulations," in *IEEE Semiannual Vehicular Technology Conference*, 1999, pp. 1407–1411.
- [60] Safak A. and Prasad R., "Effects of correlated shadowing signals on channel reuse in mobile radio systems," *IEEE Transactions on Vehicular Technology*, vol. 40, pp. 708–713, Nov. 1991.
- [61] Safak A., "Statistical analysis of the power sum of multiple correlated log-normal components," *IEEE Transactions on Vehicular Technology*, vol. 42, pp. 58–61, Feb. 1993.
-

-
- [62] Graziosi F., Pratesi M., Ruggieri M., and Santucci F., "Joint characterization of outage probability and handover performance in cellular mobile networks," in *IEEE Semiannual Vehicular Technology Conference*, May 1998, pp. 105–1058.
- [63] Saunders S., *Antenna and propagation for communication systems concept and design*. Wiley, 1999.
- [64] Algans A., Pedersen K. I., and Morgensen P. E., "Experimental analysis of the joint properties of azimuth spread, delay spread and shadowing fading," *IEEE Journal on Selected Areas in Communication*, vol. 20, no. 3, Apr. 2002.
- [65] Zetterberg P., Jaldén N., Bengtsson M., and Ottersten B., "Analysis of multi-cell measurements in an urban macro cell environment," in *Union Radio Scientific Internationale Conference*, Jun. 2005.
- [66] Jaldén N., Zetterberg P., Garcia L., and Ottersten B., "Inter and intra-site correlations of large-scale parameters from macrocellular measurements at 1800 mhz," *EURASIP Journal on Wireless Communications and Networking*, vol. 2007, Jul. 2007.
- [67] Zhao X., Hentilä L., Meinilä J., Jämsä T., Kyösti P., and Nuutinen J., "Correlations of wide-band channel parameters in street canyon at 2.45 and 5.25 ghz," *IEEE Antennas and Wireless Propagation Letter*, vol. 6, pp. 252–254, Jun. 2007.
- [68] Graziano V., "Propagation correlation at 900mhz," *IEEE Transaction on Vehicular Technology*, vol. VT-27, no. 4, pp. 182–189, Nov. 1978.
- [69] Mawira A., "Model for the spatial correlation functions of the log-normal component of the variability of the vhf/uhf field strength in urban environment," in *IEEE International Symposium on Personal, Indoor and Mobile Radio Communications*, 1992, pp. 436–440.
- [70] Sorensen T. B., "Slow fading cross-correlation against azimuth separation of base stations," *IEEE Electronics Letters*, vol. 35, no. 2, pp. 127–128, Jan. 1999.
- [71] Perahia E., Cox D., and Ho S., "Shadow fading cross-correlation between base stations," in *IEEE Semiannual Vehicular Technology Conference*, May. 2001, pp. 313–317.
- [72] Weitzen J. and Lowe T. J., "Measurement of angular and distance correlation properties of log-normal shadowing at 1900 mhz and its application to design of pcs systems," *IEEE Transactions on Vehicular Technology*, vol. 51, no. 2, Mar. 2002.
- [73] Jaldén N., "Analysis of radio channel measurements using multiple base stations," Ph.D. dissertation, KTH, May 2007.
- [74] Holma H. and Toskala A., *WCDMA for UMTS: radio access for third generation mobile communications*. John Wiley & Sons, 2001.
- [75] Jämsä T., Ylitalo J., Thomä R. S., and Alexiou A., "Wwrf white paper on multi-dimensional radio channel measurement and modelling for future mobile and short-range wireless systems," *Wireless World Research Forum (WWRF)*, Jul. 2005.
- [76] Kai Y., "Modeling of multiple-input multiple-output radio propagation channels," PhD thesis, Royal institute of Technology (KTH), Oct. 2002.
- [77] Weichselberger W., "Spatial structure of multiple antenna radio channels a signal processing viewpoint," Ph.D. dissertation, Technischen Universität Wien, Austria, Dec. 2003.
-

-
- [78] Pätzold M. and Hogstad B. O., “A wideband mimo channel model derived from the geometric elliptical scattering model,” in *International Symposium on Wireless Communication Systems (ISWCS)*, Valencia, Spain, Sep. 2006.
- [79] Maurer J., “Strahlenoptisches kanalmodell für die fahrzeug-fahrzeug-funkkommunikation,” Ph.D. dissertation, Universität Karlsruhe, Germany, Juli 2005.
- [80] Giovanni Del G., “Geometry-based channel modelling for multi-user mimo systems and applications,” Ph.D. dissertation, Technischen Universität Ilmenau, Germany, 2007.
- [81] Thomä R. S., Hampicke D., Landmann M., Richter A., and Sommerkorn G., “Measurement-based parametric channel modelling (mbpcm),” in *International Conference on Electromagnetics in Advanced Applications*, Torino, Italia, Sep 2003.
- [82] Richter A., “Estimation of radio channel parameters: Models and algorithms,” Ph.D. dissertation, Technischen Universität Ilmenau, Germany, 2005.
- [83] Trautwein U., Schneider C., and Thomä R. S., “Measurement based performance evaluation of advanced mimo transceiver design,” *EURASIP Journal on Applied Signal Processing*, 2005.
- [84] Narandzic M., Schneider C., Thomä R. S., Jämsä T., Kyäosti P., and Zhao X., “Comparison of scm, scme, and winner channel models,” in *IEEE Semiannual Vehicular Technology Conference*, Dublin, Irland, Apr. 2007.
- [85] Baum D., Salo J., Galdo G., Milojevic M., Ky”osti P., and Hansen J., “An interim channel model for beyond-3g systems,” in *IEEE Semiannual Vehicular Technology Conference*, vol. 5, Stockholm, Sweden, May 2005, pp. 3132–3136.
- [86] Jakes W. C., *Microwave Mobile Communications*. Piscataway, NJ: IEEE Press, 1994.
- [87] Fleury B. H., “An uncertainty relation for wss processes and its application to wssus systems.” *IEEE Transactions on Communications*, vol. 44, no. 12, Dec. 1996.
- [88] Gans M. J., “power-spectral theory of propagation in the mobile-radio environment,” *IEEE Transactions on Vehicular Technology*, vol. VT-21, no. 1, Feb. 1972.
- [89] Salo J., Vuokko L., and Vainikainen P., “why is shadow fading lognormal?” in *the 8th International Symposium on Wireless Personal Multimedia Communications*, Aalborg, Denmark, Sep. 2005, pp. 522–526.
- [90] Lee J. and Bertoni H. L., “coupling at cross, t, and l junctions in tunnels and urban street canyons,” *IEEE Transaction on Antennas and Propagation*, vol. 51, no. 5, May. 2003.
- [91] Ivrlac M. T. and Nossek J. A., “Quantifying diversity and correlation of rayleigh fading mimo channels,” in *IEEE International Symposium on Signal Processing and Information Technology*, Darmstadt, Germany, Dec. 2003, pp. 158–161.
- [92] Gudmundsonä M., “Correlation model for shadow fading in mobile radio systems,” *Electronic Letter*, vol. 27, pp. 2145–2146, Nov. 1991.
- [93] Fraile R., Monserrat J. F., Gozálviz J., and Cardonad N., “Wireless systems mobile radio bi-dimensional large-scale fading modelling with site-to-site cross-correlation,” *European Transactions on Telecommunications*, vol. 19, pp. 101–106, Feb. 2007.
- [94] Wang Z., Tameh E. K., and Nix A. R., “Joint shadowing process in urban peer-to-peer radio channels,” *IEEE Transactions on Vehicular Technology*, vol. 57, no. 1, pp. 52–64, Jan. 2008.
-

-
- [95] Cai X. and Giannakis G. B., "A two-dimensional channel simulation model for shadowing processes," *IEEE Transactions on Vehicular Technology*, vol. 52, no. 6, pp. 1558–1568, Nov. 2003.
- [96] "Selection procedures for the choice of radio transmission technologies of the umts," *European Telecommunications Standards Institute (ETSI)*, 1998.
- [97] "[http://www.channelsounder.de/.](http://www.channelsounder.de/)"
- [98] Landmann M., "Limitations of experimental channel characterisation," Ph.D. dissertation, Technischen Universität Ilmenau, Germany, 2008.
- [99] "[http://www.medav.de/.](http://www.medav.de/)"
- [100] Thomä R. S., Landmann M., and Richter A., "Rimax - a maximum likelihood framework for parameter estimation in multidimensional channel sounding," in *International Symposium on Antennas and Propagation*, Sendai, Japan, Aug. 2004.
- [101] Valenzuela R. A., Landron O., and Jacobs D. L., "Estimating local mean signal strength of indoor multipath propagation," *IEEE Transactions on Vehicular Technology*, vol. 46, Feb. 1997.
- [102] Zayana K. and Guisnet B., "Measurements and modelisation of shadowing cross-correlations between two base-stations," in *IEEE International Conference on Universal Personal Communications*, vol. 1, no. 10, Florence, Italy, Oct. 1998, pp. 101–105.
- [103] Greenstein L. J., Michelson D. G., and Erceg V., "Moment-method estimation of the rician k-factor," *IEEE Communication Letters*, vol. 3, no. 6, pp. 175–176, Jun. 1999.
- [104] Shiu D.-S., Foschini G. J., Gans M. J., and Kahn J. M., "Fading correlation and its effect on the capacity of multielement antenna systems," *IEEE Transactions on Communications*, vol. 48, no. 3, pp. 502–513, March 2000.
- [105] Marsan M. J., Hess G. C., and Gilbert S. S., "Shadowing variability in an urban land mobile environment at 900mhz," *IEEE Electronics Letters*, vol. 26, no. 10, pp. 646–647, May 1990.
- [106] Zhao X., Rautiainen T., Kalliola K., and Vainikainen P., "Path-loss models for urban micro-cells at 5.3 ghz," *IEEE Antenna and Wireless Propagation Letters*, vol. 5, Sep. 2006.
- [107] Kramer G. and Wijngaarden A. J. V., "On the white gaussian multiple-access relay channel," in *International Symposium on Information Theory*, Sorrento, Italy, June 2000.
- [108] Soldani D. and Dixit S., "Wireless relays for broadband access," *IEEE Communications Magazine*, vol. 46, pp. 58–66, March 2008.
- [109] Sankaranarayanan L., "Relay cooperation in multiaccess networks," Ph.D. dissertation, The State University of New Jersey, USA, 2007.
- [110] Sendonaris A., Erkip E., and Aazhang B., "User cooperation diversity^Upart i: System description," *IEEE Transactions on Communications*, vol. 51, no. 11, pp. 1927–1938, Nov. 2003.
- [111] Sendonaris A. Sand Erkip E. and Aazhang B., "User cooperation diversity^Upart ii: Implementation aspects and performance analysis," *IEEE Transactions on Communications*, vol. 51, no. 11, pp. 1939–1948, Nov. 2003.
-

-
- [112] Gupta P. and Kumar P. R., "Towards an information theory of large networks: An achievable rate region," *IEEE Transactions on Information Theory*, vol. 49, no. 8, pp. 1877–1895, Aug. 2003.
- [113] Schein B. and Gallager Robert G., "The gaussian parallel relay network," in *International Symposium on Information Theory*, Sorrento, Italy, June 2000, p. 22.
- [114] Janani M., Hedayat A., Hunter Todd E., and Nosratinia A., "Coded cooperation in wireless communications: Space-time transmission and iterative decoding," *IEEE Transaction on Signal Processing*, vol. 52, no. 2, pp. 362–371, Feb. 2004.
- [115] Zhao B. and Valenti M. C., "Distributed turbo coded diversity for relay channel," *IEE Electronics Letters*, vol. 39, no. 10, pp. 786–787, May 2003.
- [116] ten B. S., "Designing iterative decoding schemes with the extrinsic information transfer chart," *AEÜ Int. J. Electron. Commun.*, vol. 54, pp. 389–398, 2000.
- [117] Hausl C. and Dupraz P., "Joint network-channel coding for the multiple-access relay channel," in *International Workshop on Wireless Ad Hoc and Sensor Networks*, New York, USA, June 2006.
- [118] Chen Y., Kishore S., and Li J., "Wireless diversity through network coding," in *IEEE Wireless Communications and Networking Conference (WCNC)*, Las Vegas, USA, Mar. 2006.
- [119] Kambiz A., Hesham El G., and Philip S., "On the achievable diversity-multiplexing tradeoff in half-duplex cooperative channels," *IEEE Transactions on Information Theory*, vol. 51, no. 12, pp. 4152–4172, Dec. 2005.
- [120] Zheng L. and David Tse N. C., "Diversity and multiplexing: A fundamental tradeoff in multiple-antenna channels," *IEEE Transaction on Information Theory*, vol. 49, no. 5, pp. 1073–1096, May 2003.
- [121] Wyner A. D. and Ziv J., "The rate-distortion function for source coding with side information at the decoder," *IEEE Transactions on Information Theory*, vol. 22, no. 1, pp. 1–10, Jan. 1976.
- [122] Slepian D. and Wolf J. K., "Noiseless coding of correlated information sources," *IEEE Transaction on Information Theory*, vol. IT-19, no. 4, pp. 471–480, Jul. 1973.
- [123] Hu R. and Li J., "Exploiting slepian-wolf coding in wireless user cooperation," in *IEEE Workshop on Signal Processing Advances in Wireless Communications*, New York, USA, June 2005.
- [124] Li J. and Hu R., "Slepian-wolf cooperation: A practical and efficient compress-and-forward relay scheme," in *Allerton Conference on Communication, Control and Computing*, Sankt Louis, MO USA, Nov 2005.
- [125] Alamouti A. M., "A simple transmit diversity technique for wireless communication," *IEEE Journal on Select Areas in Communications*, vol. 16, no. 8, Oct. 1998.
- [126] Tarokh V., Seshadri N., and Calderbank A. R., "Space-time codes for high data rate wireless communication: Performance criterion and code construction," *IEEE Transactions on Information Theory*, vol. 44, no. 2, pp. 744–765, March 1998.
- [127] Unger T. and Klein A., "On the performance of distributed space-time block codes in cooperative relay networks," *IEEE Communications Letters*, vol. 11, no. 5, May. 2007.
-

-
- [128] Yiu S., Schober R., and Lampe L., "Distributed space-time block coding," *IEEE Transactions on Communications*, vol. 54 (7), pp. 1195–1206, 2006.
- [129] Oh J. E. and Yang K., "Space time codes with full antenna diversity using weighted nonbinary repeat-accumulate codes," *IEEE Transactions on Communications*, vol. 51, no. 11, pp. 1773–1779, Nov. 2003.
- [130] Yang S. and Belfiore J. C., "Optimal space-time codes for the mimo amplify-and-forward cooperative channel," *IEEE Transactions on Information Theory*, vol. 53, pp. 647 – 663, Feb. 2007.
- [131] Kim Y. and Liu H., "Infrastructure relay transmission with cooperative mimo," *IEEE Transactions on Vehicular Technology*, vol. 57, no. 4, pp. 2180–2188, Jul. 2008.
- [132] Karjalainen J., Kansane K., Veselinovic N., and Matsumoto T., "Antenna-by-antenna and joint-over-antenna mimo signal detection techniques for turbo-coded sc/mmse frequency domain equalization," in *IEEE Semiannual Vehicular Technology Conference*, Stockholm, Sweden, May. 2005, pp. 934–938.
- [133] Li J., Letaief K. B., and Cao Z., "Adaptive cochannel interference cancellation in space-time coded communication systems," *IEEE Transactions on Communication*, vol. 50, no. 10, Oct. 2002.
- [134] Sankaranarayanan L., Kramer G., and Mandayam N. B., "Capacity theorems for the multiple-access relay channel," in *Allerton Conference on Communications, Control and Computer.*, Monticello, USA, Sept. 29-Oct. 1 2004, pp. 1782–1791.
- [135] Veselinovic N., Matsumoto T., and Juntti M., "A pdf estimation-based iterative mimo signal detection with unknown interference," *IEEE Communications Letters*, pp. 422–424, Jul. 2004.
- [136] Haykin S., Ed., *Adaptive filter theory*, 2nd ed. Englewood Cliffs: Prentice Hall, 1991.
- [137] Yu M. and Li J., "Is amplify-and-forward practically better than decode-and-forward or vice versa?" in *IEEE International Conference on Acoustics, Speech, and Signal Processing*, vol. 3, Philadelphia, PA, USA, Mar. 2005.
- [138] Kyritsi P., Eggers P., Gall R., and Lourenco J. M., "Measurement based investigation of cooperative relaying," in *IEEE Semiannual Vehicular Technology Conference*, Montreal, Canada, September 2006, pp. 1–5.
- [139] Fan Y. and Thompson J., "Mimo configurations for relay channels: theory and practical," *IEEE transactions on Wireless Communications*, vol. 6, pp. 1774–1786, May 2007.
- [140] Kyritsi P., Popovski P., Eggers P., Wang Y., Khan D., Bouaziz A., Pietrarca B., and Sasso G., "Cooperative transmission: A reality check using experimental data," in *IEEE Semiannual Vehicular Technology Conference*, Dublin, Ireland, April 2007, pp. 2281–2285.
- [141] Haneda K., Riihonen T., Kolmonen V., Wichman R., Vainikainen P., and Takada J., "Measurement based analysis of gain-diversity tradeoff in relay transmission," in *European Cooperation in The field of Scientific and Technical Research COST 2100*, no. TD(08)549, Trondheim, Norway, June 2008.
- [142] Andersen J. B. and Kovacs I., "Power distributions revisited," in *COST 273 TD(02) 004*, Guildford, UK, Jan. 2002.
- [143] Andersen J. B., "A propagation overviewd," in *The 5th International Symposium on Wireless Personal Multimedia Communications*, vol. 1, Honolulu, Hawaii, Oct. 2002, pp. 1–6.
-

- [144] K. Kalliojärvi et a., “Intermediate concept proposal (metropolitan area) and evaluation,” *WINNER D6.13.4 v1.0*.
 - [145] Daniel Baum et a., “Final report on link level and system level channel models,” *WINNER D5.4 v1.4*.
 - [146] J. Salo et a., “Matlab implementation of the 3gpp channel model (3gpp tr 25.996),” <http://www.tkk.fi/Units/Radio/scm/>, Jan. 2005.
-

THESES TO "PROPAGATION MEASUREMENT BASED STUDY ON RELAY NETWORKS"

1. In the framework of the channel modeling for relay networks, the long-term correlation issues between links are the most crucial point due to the meshed-network topology.
 2. The correlation properties include both the intra-site correlation and the inter-site correlation.
 3. Large Scale Parameters (LSP), characterizing the long-term feature of propagation channels, are the key channel parameters for the correlation modeling.
 4. The experimental results of the correlation properties of LSP are presented through the analysis on the real-field measurement data for both the urban and indoor scenarios.
 5. The experimental results are fully introduced into the WINNER channel Model (WIM) for realistic relay channel simulations.
 6. For Multiple Access Relay Networks (MARN) with Unknown Interference (UKIF), an advanced coding technique, Multiple Access Coding (MAC), can improve the system sum rate; a relay protocol with adaptive transmission can further enhance the system resource efficiency; and a constructive combination of the direct transmission and the relay transmission provides additional diversity gain.
 7. Realistic channel realizations, used for the purpose of performance verification, can be extracted from raw measurement data and from the experimental channel model as well.
 8. A gap exists between the theoretical performance and the realistic performance due to the fact that the assumption, made to simplified Rayleigh channels, do not fully hold in reality.
 9. The relay transmission is of crucial importance in the case when the direct transmission is blocked. As far as the direct transmission is available, the relay transmission can outperform the direct transmission at the price of a higher Signal-to-Noise Ratio (SNR) value.
 10. Keeping the balance between the tandem links of a relay channel is crucial for the relay system design.
 11. In the realistic deployment, a careful selection of the Relay Station (RS) position can further improve the system performance.
-

ERKLÄRUNG

Ich versichere, dass ich die vorliegende Arbeit ohne unzulässige Hilfe Dritter und ohne Benutzung anderer als der angegebenen Hilfsmittel angefertigt habe. Die aus anderen Quellen direkt oder indirekt übernommenen Daten und Konzepte sind unter Angabe der Quelle gekennzeichnet.

Weitere Personen waren an der inhaltlich-materiellen Erstellung der vorliegenden Arbeit nicht beteiligt. Insbesondere habe ich hierfür nicht die entgeltliche Hilfe von Vermittlungs- bzw. Beratungsdiensten (Promotionsberater oder anderer Personen) in Anspruch genommen. Niemand hat von mir unmittelbar oder mittelbar geldwerte Leistungen für Arbeiten erhalten, die im Zusammenhang mit dem Inhalte der vorgelegten Dissertation stehen.

Die Arbeit wurde bisher weder im In- noch im Ausland in gleichere oder ähnlichen Form einer Prüfungsbehörde vorgelegt.

Ich bin darauf hingewiesen worden, dass die Unrichtigkeit der vorstehenden Erklärung als Täuschungsversuch angesehen wird und den erfolglosen Abbruch des Promotionsverfahrens zu Folge hat.

Ilmenau, 27.03.2010
